

UNIVERSITAT POLITÈCNICA DE VALÈNCIA
DEPARTAMENTO DE MÁQUINAS Y MOTORES TÉRMICOS



UNIVERSITAT
POLITÈCNICA
DE VALÈNCIA

IN-CYLINDER PRESSURE-BASED CONTROL OF
PREMIXED DUAL-FUEL COMBUSTION

PhD Dissertation

Presented by
Alvin Barbier

Supervised by
Prof. Carlos Guardiola
Dr. Pau Bares

Valencia, April 2022

IN-CYLINDER PRESSURE-BASED CONTROL OF PREMIXED DUAL-FUEL COMBUSTION

PhD Dissertation

Author: Alvin Barbier

Thesis supervisors: Prof. Carlos Guardiola
Dr. Pau Bares

Examination committee:

President: Prof. Jesús Benajes
Secretary: Prof. Francisco Vera
Examiner: Prof. Bengt Johansson

Reviewing committee:

Prof. Bengt Johansson
Prof. Leonor Hernández López
Dr. Carlos Jorques Moreno

Valencia, April 2022

This thesis was financially supported by the *Programa Operativo del Fondo Social Europeo (FSE) de la Comunitat Valenciana 2014-2020* through grant ACIF/2018/141.

*I don't get anxious about stuff I can't deal with because I know
we are doing the right thing to make the best possible plan.*

Dr. John C. Mather on the James Webb Space Telescope

Abstract

The current climate crisis has urged the research community and manufacturers to provide solutions to make the transportation sector cleaner. Among the various technologies proposed, low temperature combustion has undergone extensive investigation. Premixed dual-fuel combustion is one of the concepts addressing the NO_x -soot trade-off in compression ignited engines, while maintaining high thermal efficiency. This combustion makes use of two fuels with different reactivities in order to improve the controllability of this combustion mode over a wide range of operation.

Similarly to all premixed combustion modes, this combustion is nevertheless sensitive to the operating conditions and traditionally exhibits cycle-to-cycle variability with significant pressure gradients. Consequently, advanced control strategies to ensure a safe and accurate operation of the engine are required. Feedback control is a powerful approach to address the challenges raised by the premixed dual-fuel combustion. By measuring the output signals from the engine, strategies can be developed to adapt and correct the control actions to maintain the desired operation.

This thesis presents control strategies, based on the in-cylinder pressure signal measurement, applied to premixed dual-fuel combustion engines. Various objectives were addressed by designing dedicated controllers, where a special emphasis was made towards analyzing and implementing these solutions to the different levels of mixture stratification considered in these engines (i.e., fully, highly and partially premixed). At first, feedback control strategies based on the in-cylinder pressure signal processing were designed. Proportional-integral actions were selected to ensure the desired engine performance without exceeding the mechanical constraints of the engine. Extremum seeking was evaluated to track efficient combustion phasing and NO_x emissions reduction. The in-cylinder pressure resonance was then analyzed and a knock-like controller was implemented to ensure safe operation of the engine. Finally, mathematical models were used to design a control-oriented model and a state observer that aimed to leverage the signals measured in the engine to improve the prediction and diagnostic capabilities in such engine configuration.

The results from this work highlighted the importance of considering feedback control to address the limitations encountered in premixed combustion modes. Particularly, the use of the in-cylinder pressure measurement showed the relevance and potential of this signal to develop complex and accurate control strategies.

Resumen

La actual crisis climática ha instado a la comunidad investigadora y a los fabricantes a brindar soluciones para hacer que el sector del transporte sea más sostenible. De entre las diversas tecnologías propuestas, la combustión a baja temperatura ha sido objeto de una extensa investigación. La combustión premezclada *dual-fuel* es uno de los conceptos que abordan el compromiso de NO_x -hollín en motores de encendido por compresión manteniendo alta eficiencia térmica. Esta combustión hace uso de dos combustibles con diferentes reactividades para mejorar la controlabilidad de este modo de combustión en un amplio rango de funcionamiento.

De manera similar a todos los modos de combustión premezclados, esta combustión es sensible a las condiciones de operación y suele estar sujeta a variabilidad cíclica con gradientes de presión significativos. En consecuencia, se requieren estrategias de control avanzadas para garantizar un funcionamiento seguro y preciso del motor. El control en bucle cerrado es una herramienta eficaz para abordar los desafíos que plantea la combustión premezclada *dual-fuel*. En este tipo de control, para mantener el funcionamiento deseado, las acciones de control se adaptan y corrigen a partir de una retroalimentación con las señales de salida del motor.

Esta tesis presenta estrategias de control basadas en la medición de la señal de presión en el cilindro, aplicadas a motores de combustión premezclada *dual-fuel*. En ella se resuelven diversos aspectos del funcionamiento del motor mediante el diseño de controladores dedicados, haciéndose especial énfasis en analizar e implementar estas soluciones a los diferentes niveles de estratificación de mezcla considerados en estos motores (es decir, totalmente, altamente y parcialmente premezclada). Inicialmente, se diseñan estrategias de control basadas en el procesamiento de la señal de presión en el cilindro y se seleccionan acciones proporcionales-integrales para asegurar el rendimiento deseado del motor sin exceder las limitaciones mecánicas del motor. También se evalúa la técnica *extremum seeking* para realizar una supervisión de una combustión eficiente y la reducción de emisiones de NO_x . Luego se analiza la resonancia de la presión en el cilindro y se implementa un controlador similar a aquel usado para el control de *knock* para garantizar el funcionamiento seguro del motor. Finalmente, se utilizan modelos matemáticos para diseñar un modelo orientado a control y un observador que tiene como objetivo combinar las señales medidas en el motor para mejorar las capacidades de predicción y diagnóstico en dicha configuración de motor.

Los resultados de este trabajo destacan la importancia de considerar el control en bucle cerrado para abordar las limitaciones encontradas en los modos de combustión premezclada. En particular, el uso de la medición de presión en el cilindro muestra la relevancia y el potencial de esta señal para desarrollar estrategias de control complejas y precisas.

Resum

L'actual crisi climàtica ha instat a la comunitat investigadora i als fabricants a brindar solucions per a fer que el sector del transport siga més sostenible. D'entre les diverses tecnologies proposades, la combustió a baixa temperatura ha sigut objecte d'una extensa investigació. La combustió premesclada *dual-fuel* és un dels conceptes que aborden el compromís de NO_x -sutge en motors d'encesa per compressió mantenint alta eficiència tèrmica. Aquesta combustió fa ús de dos combustibles amb diferents reactivitats per a millorar la controlabilitat d'aquest tipus de combustió en un ampli rang de funcionament.

De manera similar a tots els tipus de combustió premesclada, aquesta combustió és sensible a les condicions d'operació i sol estar subjecta a variabilitat cíclica amb gradients de pressió significatius. En conseqüència, es requereixen estratègies de control avançades per a garantir un funcionament segur i precís del motor. El control en bucle tancat és una eina eficaç per a abordar els desafiaments que planteja la combustió premesclada *dual-fuel*. En aquesta mena de control, per a mantindre el funcionament desitjat, les accions de control s'adapten i corregeixen a partir d'una retroalimentació amb els senyals d'eixida del motor.

Aquesta tesi presenta estratègies de control basades en el mesurament del senyal de pressió en el cilindre, aplicades a motors de combustió premesclada *dual-fuel*. En ella es resolen diversos aspectes del funcionament del motor mitjançant el disseny de controladors dedicats, fent-se especial èmfasi a analitzar i implementar aquestes solucions als diferents nivells d'estratificació de mescla considerats en aquests motors (és a dir, totalment, altament i parcialment premesclada). Inicialment, es dissenyen estratègies de control basades en el processament del senyal de pressió en el cilindre i se seleccionen accions proporcionals-integrals per a assegurar el rendiment desitjat del motor sense excedir les limitacions mecàniques del motor. També s'avalua la tècnica *extremum seeking* per a realitzar una supervisió d'una combustió eficient i la reducció d'emissions de NO_x . Després s'analitza la ressonància de la pressió en el cilindre i s'implementa un controlador similar a aquell usat per al control de *knock* per a garantir el funcionament segur del motor. Finalment, s'utilitzen models matemàtics per a dissenyar un model orientat a control i un observador que té com a objectiu combinar els senyals mesurats en el motor per a millorar les capacitats de predicció i diagnòstic en aquesta configuració de motor.

Els resultats d'aquest treball destaquen la importància de considerar el control en bucle tancat per a abordar les limitacions trobades en la combustió premesclada. En particular, l'ús del mesurament de pressió en el cilindre mostra la rellevància i el potencial d'aquest senyal per a desenvolupar estratègies de control complexes i precises.

Acknowledgements

I think it is hard to realize exactly what it represents to enroll into a PhD when you take the decision to do so, until you get to experience it for real. I have questioned myself many times, had ups and downs, learned many things, and above all I understood that I have even more to learn still! These years have probably been one of the biggest journeys in my life so far and I am for sure not ready to forget my time in Valencia. This journey would have not been possible without all the people who surrounded me during those years. Although words will never be enough to express my gratitude to them, I am going to try within these lines!

I would like to acknowledge the Universitat Politècnica de València, and especially the Instituto CMT-Motores Térmicos and its staff, for giving me this opportunity. I had the chance to work with qualified people and get access to experimental facilities without which I could have not achieved the work presented in this manuscript.

I wish to thank Carlos Guardiola and Pau Bares, my thesis supervisors, for their support and guidance during those years. Thanks for these talks, not only about work but also about life, and for your patience. The results of this thesis would have not been possible without you. I also would like to thank Benjamín Pla for his help and invaluable contribution to this team.

I met extraordinary people during those years in Valencia and I am very grateful to have shared so many moments with them. My first thoughts go to my coworkers with who I spent most of my days in the last years: Varun Pandey, Irina Jimenez, Alexandra Aramburu and Rodrigo Raggi. Thank you so much for your friendship, those talks, laughs, and great moments shared together! *A esas horas que habéis perdido ayudándome con los detalles de la tesis!* I also think of all the great colleagues I had the chance to meet there as well: Alberto, Javi, André, Rafa, David, Álvaro... A special thanks also goes to Gabriel Alcantarilla with who I shared all the experiments in the engine test cell, *gracias por tu profesionalidad, tu ayuda y tu apoyo en todos estos momentos!* I also have to particularly thank Kévin Thein without who my early spanish days would have been way more complicated, *merci pour tout ce que tu as fait pour moi, pour ces discussions et tous ces moments !* My life in Valencia would have also been less enjoyable without all the friends I made along the way. To all of you, I am so glad I have met you, *gracias por ser parte de mi vida!*

I cannot end these acknowledgements without thanking my lifetime friends, Michaël, Fabrice, Fabien, Damien, Charlotte, Ludivine... as well as all my friends from ISAT! *Oui, j'en suis enfin venu à bout... Il était temps ! Merci d'être encore là malgré la distance et les aléas de la vie. Je profite de ces quelques lignes pour vous remercier de ce que vous m'avez apporté pendant toutes ces années. Pas seulement ces années de thèse, mais aussi toutes les années antérieures qui m'ont permis d'en arriver là aujourd'hui.*

There would be so many people to thank that I just cannot do it here, I think there is already enough to read! I probably forgot too many of you, but if you read this and do not see your name here, be sure that you were as important and you already probably know it!

Finally, I would like to end by saying a huge *merci* to my parents and family for always being supportive at any moment of my life. *Sans vous, rien de cela n'aurait été possible. Je vous dois beaucoup. Je ne saurais comment vous remercier, ni vous démontrer à quel point vous avez joué un rôle dans tout cela et à quel point je vous en suis reconnaissant. Encore merci pour tout, je vous aime profondément !*

Hopefully, there is more to come!

Nomenclature

Acronyms and abbreviations

ACEA	European Automobile Manufacturers Association
AFR	Air-fuel equivalence ratio
aTDC	After top dead center
atm	Atmospheric
BDC	Bottom dead center
BEV	Battery electric vehicle
BMEP	Brake mean effective pressure
BP	Back pressure
BR	Blending ratio
BSFC	Brake specific fuel consumption
BSNO _x	Brake specific NO _x emissions
bTDC	Before top dead center
CAD	Crank angle degree
CAN	Controller area network
CDC	Conventional diesel combustion
CDF	Conventional dual-fuel
CE	Common era
CFD	Computational fluid dynamics
CH ₄	Methane
CI	Compression ignition
CL	Closed-loop
CN	Cetane number
CNG	Compressed natural gas
CO	Carbon monoxide
CO ₂	Carbon dioxide
COM	Control-oriented model
COV	Coefficient of variation

cyl	Cylinder
DAQ	Data acquisition
DFC	Dual-fuel combustion
DI	Direct injection
DMDF	Dual-mode dual-fuel
DOC	Diesel oxidation catalyst
DOI	Duration of injection
DPF	Diesel particulate filter
ECU	Engine control unit
EGR	Exhaust gas recirculation
EKF	Extended Kalman filter
EOC	End of combustion
eq	Equivalent
ES	Extremum seeking
est	Estimation
EU	European Union
EURO	European emissions standards
EVO	Exhaust valve opening
exh	Exhaust
exp	Experimental
FPGA	Field-programmable gate array
GHG	Greenhouse gases
HC	Hydrocarbons
HCCI	Homogeneous charge compression ignition
HEV	Hybrid electric vehicle
HP	High pressure
HRF	High reactivity fuel
HTHR	High temperature heat release
ICCT	International Council on Clean Transportation
ICE	Internal combustion engine
ICEV	Internal combustion engine vehicle
int	Intake
IPCC	Intergovernmental Panel on Climate Change
IVC	Intake valve closing
KF	Kalman filter
LCA	Life cycle assessment
LHV	Low heating value
lim	Limit
LNT	Lean NO _x trap

LP	Low pressure
LPG	Liquefied petroleum gas
LPV	Linear parameter-varying
LQG	Linear quadratic Gaussian
LQI	Linear quadratic integral
LRF	Low reactivity fuel
LTC	Low temperature combustion
LTHR	Low temperature heat release
MA	Moving average
MCE	Multi-cylinder engine
MIMO	Multi-input multi-output
MKIM	Modified knock integral model
MPC	Model predictive control
N ₂ O	Nitrous oxide
NEDC	New European Driving Cycle
NI	National Instruments
NO _x	Nitrogen oxides
O ₂	Oxygen
O ₃	Ozone
OL	Open-loop
OP	Operating point
PC	Personal computer
PCCI	Premixed charge compression ignition
PCI	Premixed compression ignition
PDF	Probability density function
PEV	Plug-in electric vehicle
PFI	Port fuel injection
PHEV	Plug-in hybrid electric vehicle
PI	Proportional-integral
PID	Proportional-integral-derivative
PM	Particulate matter
PPC	Partially premixed combustion
pre	Premixed
PSD	Power spectral density
RCCI	Reactivity controlled compression ignition
RT	Real-time
SCE	Single cylinder engine
SCR	Selective catalytic converter
SI	Spark ignition

SOC	Start of combustion
SOI	Start of injection
STFT	Short-time Fourier transform
str	Stroke
SUV	Sport utility vehicle
TDC	Top dead center
tot	Total
UEGO	Universal exhaust gas oxygen
VGT	Variable-geometry turbine

Symbols and variables

A	Frequency amplitude in the extremum seeking calibration
A_{ht}	Effective heat transfer area in the cylinder
$B_{i,j}$	Bessel constant
c	Speed of sound
CA_{10}	Crank angle at 10% of the combustion energy released
CA_{50}	Crank angle at 50% of the combustion energy released
CA_{90}	Crank angle at 90% of the combustion energy released
$CACG$	Crank Angle combustion Center of Gravity
$[CO_2]$	Carbon dioxide concentration
c_v	Heat capacity at constant volume
D	Cylinder bore
e	Error
E_a	Energy of activation
f	Frequency
f_{res}	Resonant frequency
f_s	Sampling frequency
GF	Gasoline fraction
$IMEP$	Indicated mean effective pressure
h_c	Heat transfer coefficient
J	Cost function
k	Engine cycle index
k_{adv}	Calibration constant in knock controller
KI	Knock index
k_{ret}	Calibration constant in knock controller
L_c	Connecting-rod length
L_r	Crankshaft radius
m	Masses

m_a	Fresh air mass
$MAPO$	Maximum amplitude of pressure oscillations
m_b	Burnt products mass
m_{cyl}	In-cylinder trapped mass
m_d	Injected diesel fuel mass
m_{di}	Direct injected fuel mass
m_f	Total injected fuel mass
m_{ff}	Fuel film mass
m_g	Injected gasoline fuel mass
m_{PFI}	Port fuel injected fuel mass
$MPRR$	Maximum pressure rise rate
N	Engine speed
n	Calibration constant
$[O_2]$	Oxygen concentration
p	Pressures, in-cylinder pressure in heat release model
p_{hp}	High-pass filtered in-cylinder pressure
P_{int}	Intake manifold pressure
p_{kc}	Knock controller probability
p_{ki}	Percentage of exceeding cycles above the defined limit
p_{lp}	Low-pass filtered in-cylinder pressure
p_m	Motored in-cylinder pressure
P_{rail}	Diesel rail pressure
Q	Energy supplied to the system
Q_{app}	Apparent heat released
Q_c	Chemical energy released (from fuel)
Q_{ht}	Heat transferred to the walls
R	Specific gas constant
r	Reference
r_c	Compression ratio
RI	Ringing intensity
r_s	Encoder resolution
SOI_m	Diesel main injection timing
SOI_p	Diesel pilot injection timing
SOI_{post}	Diesel late (post) injection timing
S_p	Mean piston speed
T	Temperatures
t	Time
T_w	Cylinder wall temperature
u	Input

U	System internal energy
V	Volume
V_{cc}	Combustion chamber volume
V_d	Cylinder displacement volume
W	Work done by the system
x	States
y	Output, measurement
α	Calibration constant
β	Calibration constant
η_c	Combustion efficiency
η_v	Volumetric efficiency
γ	Heat capacity ratio
κ	Polytropic coefficient
λ	Air-fuel ratio measurement
μ	Calibration constant
ω	Average cylinder gas velocity
ϕ	Fuel-air equivalence ratio
ψ_s	Air-to-fuel ratio in stoichiometric conditions
σ	Standard deviation
τ	Delay
τ_{id}	Ignition delay
θ	Crank angle degree
Θ_{cyl}	Energy level bias at each cylinder
θ_d	Combustion duration
ϑ_{PFI}	Port fuel quantity distribution factor

Contents

1	Introduction	1
1.1	Background	1
1.2	Internal combustion engines	6
1.2.1	Fundamentals	6
1.2.2	Challenges	7
1.2.3	Combustion engine control and modeling	11
1.3	Outline and contributions	12
	References	15
2	Premixed dual-fuel combustion	29
2.1	Introduction	29
2.2	Combustion concept	30
2.3	Modeling and control applications	33
2.4	Conclusions	39
	References	40
3	Experimental setup and data processing	49
3.1	Engines	49
3.2	Instrumentation and signals	51
3.3	In-cylinder pressure signal	55
3.3.1	Signal acquisition	56
3.3.2	Signal processing	59
3.4	Acquisition and control system layout	64
3.4.1	Data acquisition	65
3.4.2	Control actions	66
3.5	Combustion evaluation and modeling	68
3.5.1	Heat release	68
3.5.2	Combustion metrics	72
3.6	Combustion modes	78

References	80
4 Dual-fuel combustion control using in-cylinder pressure feedback	87
4.1 Introduction	87
4.2 Proportional-Integral combustion control	89
4.2.1 Controller design	90
4.2.2 Results and discussion	94
4.3 On-line combustion operation optimization	106
4.3.1 Problem formulation	108
4.3.2 Controller design	109
4.3.3 Results and discussion	115
4.4 Safe engine operation by combustion resonance measurement and control	120
4.4.1 Problem illustration	121
4.4.2 Definition of the limitation index	122
4.4.3 Controller design	125
4.4.4 Results and discussion	129
4.5 Conclusions	138
References	140
5 Model-based approach for dual-fuel combustion control	147
5.1 Introduction	147
5.2 Combustion phasing control-oriented model for RCCI engines	148
5.2.1 Model description	149
5.2.2 Results and discussion	153
5.3 Individual cylinder fuel blend estimation using a state observer	157
5.3.1 Fuel quantity estimation from heat release computation	159
5.3.2 Characterization of the fuel mass dispersion in multi-cylinder dual-fuel engines	162
5.3.3 Individual cylinder fuel distribution estimation method	167
5.3.4 Results and discussion	174
5.4 Conclusions	187
References	188
6 Conclusions and future work	197
References	203

Chapter 1

Introduction

1.1 Background

Modern society is facing one of its greatest challenges: climate change. The major concern in this climate crisis is the Earth's global warming. Human activity, substantially since the industrial revolution (from mid 18th to mid 19th century), was evidenced to have been the major contributor in this warming trend with unprecedented levels of carbon dioxide (CO_2) in the atmosphere in the human era history and beyond [1,2]. Figure 1.1 presents the various episodes of CO_2 increase and decrease estimated on Earth, showing that the current situation registers the highest recorded peak.

Carbon dioxide, alongside with methane (CH_4), nitrous oxide (N_2O), ozone (O_3) and water vapor, is a greenhouse gas (GHG) which absorbs and emits radiation within the thermal infrared range. By increasing the emission levels of these gases, more heat is trapped in the atmosphere and results in a higher average temperature on Earth, this is the *greenhouse effect* [4]. Relative to the temperature average in the 1961-1990 baseline period, an increase of approximately 0.7°C was measured over the last decades [3] (Figure 1.2a), where almost the entire globe suffered from surface warming [1] (Figure 1.2b). As shown in Figure 1.2a, a clear correlation between this increase in temperature and the CO_2 emitted is observed. Although water vapor accounts for the most abundant greenhouse gas in the atmosphere, its amount is mainly regulated by the atmosphere temperature and therefore only the regulation of GHG influenced by human activity, such as CO_2 , is considered as a mean to address the climate change [5]. According to various projection scenarios from the Intergovernmental Panel on Climate Change (IPCC), it is *very likely* that this trend will continue for the following decades caus-

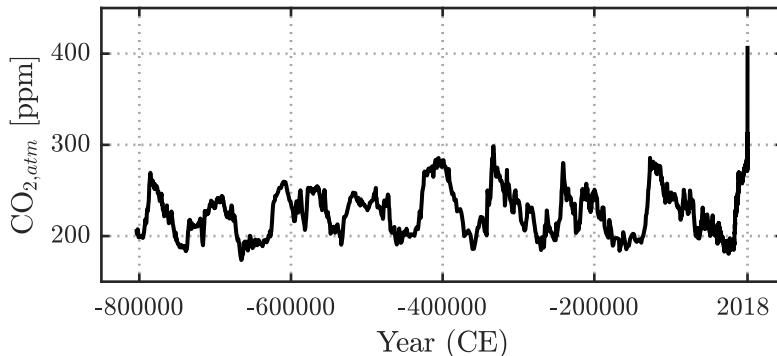
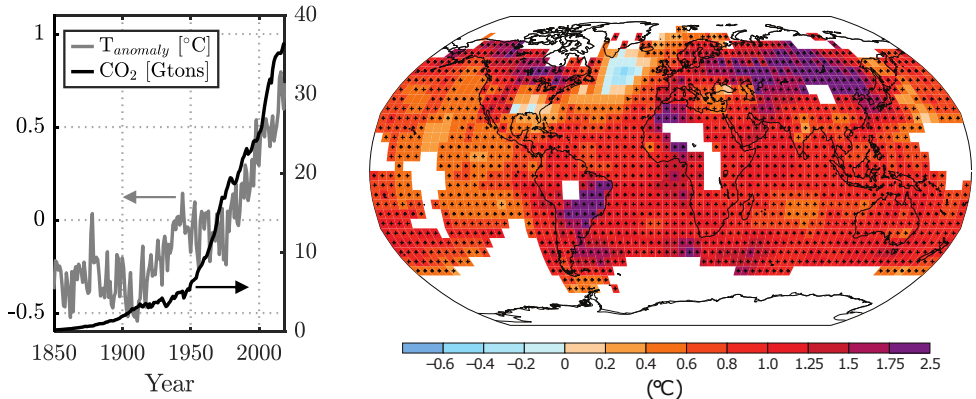


Figure 1.1: Atmospheric CO₂ concentration ($\text{CO}_{2,atm}$) over time in the Common Era (CE) year notation. *Data extracted from [3].*

ing long-term and irreversible consequences for people and ecosystems including, but not limited to: sea level rise, increased species extinction risk, marine organisms jeopardy due to ocean acidification, water and food supply repercussions, and impact on human health [1]. Against this alarming situation, important measures are needed more than ever to limit human-related GHG emissions.

The majority of the anthropogenic CO₂ emitted to the atmosphere comes from the combustion of fossil fuels (coal, oil, natural gas) [6], where the energy sector (electricity, heat and transportation) represents approximately 73% of the global greenhouse gases emissions (percentage based on the carbon dioxide equivalent CO_2eq distribution data for the year 2016 [3], Figure 1.3).

The transportation sector contribution (around 16% of the global GHG emissions), is composed of land, air and marine transportation emissions, where road transportation prevails. Over the world, more than 1 billion passenger vehicles are estimated to be in use on the road [7,8]. In 2020, despite the COVID-19 pandemic situation [9], according to a report from the European Automobile Manufacturers Association (ACEA) [10], almost 10 million new cars were registered in the European Union (EU). Current transportation market mostly includes internal combustion engine vehicles (ICEVs), where the engine is used to propel the vehicle by burning fuel (e.g. diesel, gasoline, compressed natural gas), battery electric vehicles (BEVs), which store the energy to move the vehicle in the form of electricity in batteries and deliver it when needed, and hybrid electric vehicles (HEVs), which use both ICEVs and BEVs technologies and exist in various configurations



(a) Global average temperature anomaly and CO₂ emissions (b) Observed change in surface temperature 1901-2012

Figure 1.2: (a) The CO₂ emissions, expressed in billion tons, come from the burning of fossil fuels for energy and cement production. Note that here only the CO₂ is shown and the other GHG were not accounted in the calculation. *Data extracted and adapted from [3].* (b) More information can be found in the source where the map has been extracted from [1].

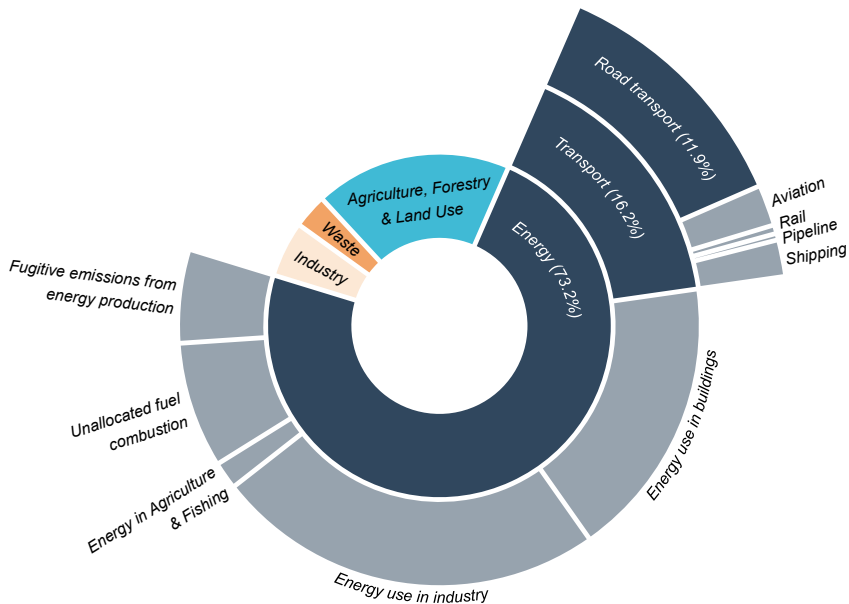


Figure 1.3: Global greenhouse gases emissions by sector in percentage based on the total emitted CO₂eq for the year 2016. *Adapted from [3].*

(i.e., mild, full, and plug-in hybrids). In 2020, in the European Union, around 92% of the cars sold were equipped with an internal combustion engine (i.e., gasoline, diesel and hybrid vehicles) and 5% were BEVs [10] (Figure 1.4a). In the recent years, ecological awareness, government policies and upcoming vehicle emissions restrictions (e.g., 95 g/km of CO₂ fleet-wide average emission for new cars in 2020-21 in the EU [11]) promoted the development and sales of plug-in vehicles around the world [12], see Figure 1.4b. Counter-intuitively, although the share of electric cars has been increasing over the past years [13], the average CO₂ emissions from new cars in the EU has been globally increasing since 2017 [14, 15] with a decrease in 2020 [16] (in the official New European Driving Cycle *NEDC* procedure). The reason to this increase is partly explained by the higher average vehicle weight, as reflected by the growing sport utility vehicles (SUVs) market [16]. These vehicles tend to be heavier and more powerful with larger frontal areas which all contribute to fuel consumption and, therefore, to carbon dioxide emissions [17]. As it was highlighted in a report of the European market from the International Council on Clean Transportation (ICCT) [16], since 2001, although the average vehicle weight increased by 12% and the engine power by 37%, a 29% CO₂ emissions reduction was obtained (in the NEDC test conditions) which shows that a further reduction might be possible by reducing vehicles weight and power output. Yet, it must be highlighted that the European restrictions are, currently, exclusively based on vehicle tailpipe emissions. Consequently, when the vehicles are using the electric mode, they are considered as emitting 0 g/km and therefore this is reflected by a decrease in the registered average CO₂ emissions. A life cycle assessment (LCA) could help to get a better *picture* of the real environmental impact of the different powertrain technologies [18] and various reports are being published in this sense recently [19–22].

The large number of vehicles in the world represents a substantial source of GHG emissions and the future of transportation must provide cleaner solutions in order to reach net-zero emissions by 2050 [23]. As demonstrates the target of 15% and 30% CO₂ emissions reduction set by the EU for 2025 and 2030 respectively [24], reducing the road transportation GHG footprint does not only consist into passenger cars, but concerns the road freight sector with heavy-duty vehicles as well (around 29% of the global CO₂ emissions from the whole transportation sector [25]). Although electrification is under intensive research and development in the transportation sector for its GHG emissions reduction potential, especially if combined with non-fossil energy sources for the electricity production [26], its market penetration is currently mainly limited to passenger cars. Heavy-duty applications such as long-haul trucks continue to mainly rely on diesel fuel as, lower

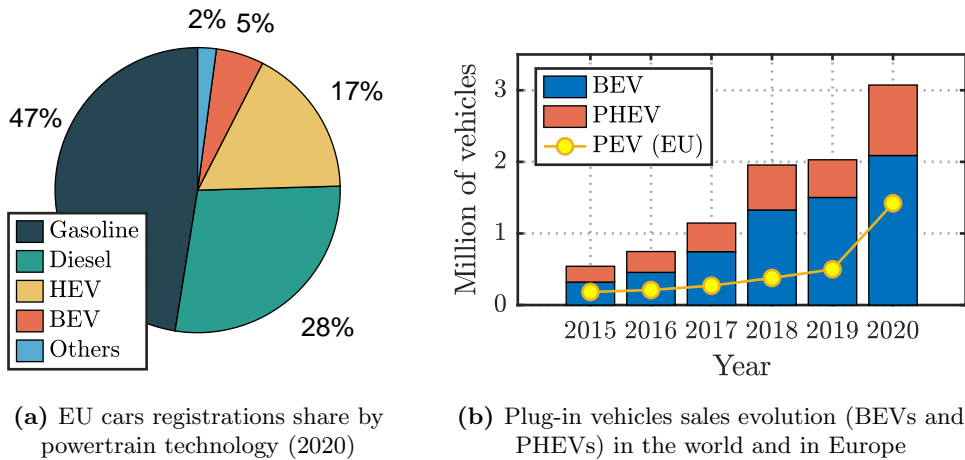


Figure 1.4: (a) Here *HEV* includes mild, full and plug-in hybrids (PHEV) and *Others* includes alternative propulsion technologies such as fuel cell, natural gas and E85. *Data extracted and adapted from [10]*. (b) Plug-in electric vehicles (PEV: BEV + PHEV) sales evolution. World sales are shown in bar graph where BEV and PHEV are detailed, while combined EU sales are shown by the solid line with dot markers. *Data extracted and adapted from [12]*.

energy density, shorter driving range, and adapted infrastructures are challenging their conversion to an all battery-based powertrain technology [27, 28]. Nonetheless, while the technology is not ready yet, this sector also requires a transition to low-carbon alternatives (e.g., biofuels) [29].

The future of internal combustion engines (ICE) in a sustainable world is a topical debate. Notwithstanding, the current readiness of electric powertrain technologies and corresponding infrastructures in some sectors such as heavy-duty vehicles, and the worldwide disparities in the access to low-carbon energy production [30], are challenging a worldwide and fast transition to such technology. Furthermore, considering that around 97% of the vehicles sold in 2020 were still provided with an ICE [31], it is believed that the ICE will continue to play a role in the near future of the transportation landscape where a mix of various powertrain technologies might coexist [32–35].

1.2 Internal combustion engines

Since its first appearance and application in the 19th century, high power density, long range, and low cost made the internal combustion engine a major player in the transportation and power generation sector [36]. From replacing steam machines with initial efficiency below 20% [37], to reaching thermal efficiency over 40% [38,39], and even as high as 50% in the power generation and maritime sector [40], the ICE has been part of an extensive and intensive investigation effort. These accomplishments were made possible by various technological improvements over the world from the 20th century [41], and by advanced techniques such as design optimization through computational fluid dynamics (CFD) [42, 43] and optical studies [44, 45].

1.2.1 Fundamentals

An internal combustion engine transforms chemical energy into useful work by burning fuel inside the combustion chamber. The leading engine configuration in the medium and heavy-duty sector, the one studied in this thesis, is the four stroke compression ignition engine. For the sake of simplicity, this section is centered on the compression ignition combustion and technologies found in conventional diesel combustion engines. Other engine architectures such as gasoline spark ignition engines [36] are therefore not described here.

The four stroke *engine cycle* is illustrated in Figure 1.5 and consists of the following steps: air is induced in the engine cylinder through the intake valves during the *intake* stroke with the downward movement of the piston towards the bottom dead center (BDC). The valves are then closed and the air is compressed at high pressure and temperature near the top dead center (TDC) during the *compression* stroke. At this moment, the fuel is injected in the combustion chamber via an injector. The high pressure and temperature conditions favor the auto-ignition of the fuel and the combustion starts. The pressure resulting from the combustion of the air-fuel mixture pushes the piston downward and produces the linear useful work which is converted into rotational work through the connecting-rod-crankshaft system, this is the *power* stroke. Finally, the exhaust valves are opened and the burnt products resulting from the combustion are expelled into the exhaust manifold with the upward movement of the piston during the *exhaust* stroke. Then, the complete cycle is repeated again.

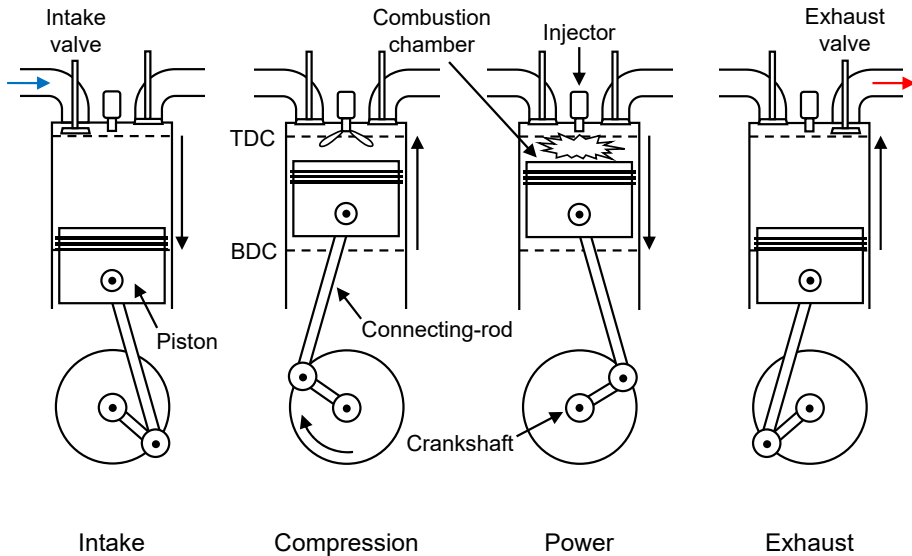


Figure 1.5: Illustration of the four stroke engine cycle.

1.2.2 Challenges

Along with the emissions of carbon dioxide resulting from the combustion of fossil fuels, internal combustion engines also emit various pollutants such as nitrogen oxides (NO_x), particulate matter (PM), carbon monoxide (CO) and hydrocarbons (HC). These pollutants result from many reactions and sources (e.g., incomplete combustion, high combustion temperature, local rich conditions) and were found to have a harmful impact on health [46,47]. As a result, exhaust emissions standards such as the European limits (EURO) were introduced to contribute into protecting the environment and reducing the air pollution [48]. Figure 1.6 illustrates the emissions standards evolution for the aforementioned pollutants in the heavy-duty sector from EURO I (1992) to EURO VI (2013). These standards provide pollutant emissions limitations for the different transportation sectors and have driven the research and development of solutions to face the stringent regulations over time (e.g., exhaust gas recirculation (EGR) [49], modern high-pressure common rail systems [50, 51]). A non-exhaustive list of the technologies that were, and are still, evaluated to tackle the challenges raised by these standards, and the urgent climate situation, is provided below [52].

After-treatment systems One of the solutions that was explored to limit the pollutants amount at the exhaust of the vehicles was to use after-treatment sys-

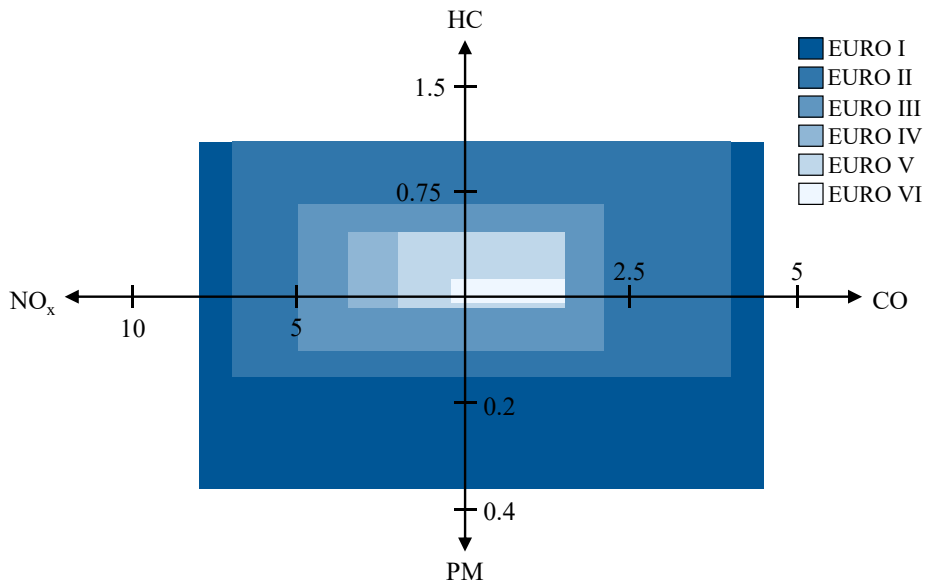


Figure 1.6: European emissions standards (CO, HC, NO_x and PM) for heavy-duty diesel vehicles (EURO I-VI) in g/kWh. *Data extracted and adapted from [53].*

tems [54–56]. These devices are installed directly on the exhaust line and aim to reduce the pollutants from the exhaust thanks to their design and internal reactions. As an example, the emissions of CO and HC can be reduced by oxidizing them with a diesel oxidation catalyst (DOC) [57]. In addition, NO_x and PM emissions can be respectively reduced by a selective catalytic converter (SCR), or lean NO_x trap (LNT) [58, 59], and a diesel particulate filter (DPF) [60]. Nevertheless, specific exhaust conditions, precise control of the reactions, and additional sensors, actuators and components (e.g., urea and its tank are required for the SCR technology) tend to increase the system complexity and cost [61].

Alternative fuels The main source of the life cycle GHG emissions of an ICE vehicle comes from its use phase due to the combustion of the fuel [62]. The major issue with this practice is that burning fossil fuels keeps adding carbon dioxide into the atmosphere. Faced with this situation, carbon-neutral fuels became an important area of combustion engine research, especially for biofuels and synthetic fuels (or e-fuels). Biofuels (e.g., ethanol, biodiesel) are made from plants or biological wastes, which are renewable sources, and were studied for their potential to balance the carbon dioxide emissions resulting from the combustion of these

fuels considering that a part of it is captured by the growing feedstock [63]. Although second- and third-generation biofuels addressed the main issues raised by the first-generation (i.e., availability, cost and sustainability of the feedstock, crop land competition with food production [64, 65]), life cycle GHG emissions benefits from biofuels remain uncertain. Indeed, the sustainability of their production, along with technical and economical challenges for their implementation, highlighted the need for further research to increase the sustainable potential of this solution [66–68]. On their side, synthetic fuels combine hydrogen extracted from water, and carbon extracted from CO₂ captured in the air, to produce new liquid fuels with similar properties to diesel or gasoline [69, 70]. By doing so, the combustion of these fuels would only emit back into the atmosphere the CO₂ that was used to create the fuel itself instead of adding new CO₂ such as with conventional combustion of fossil fuels. Nonetheless, in order to make this solution CO₂-neutral, the energy used to produce these fuels must come from renewable and clean sources such as wind or solar [71]. Although this solution is gaining more attention recently, and still requires further research in order to compare the impact of the various energy sources in powertrain technologies, it seems that expensive production and lower global efficiency compared to BEVs questioned this approach, particularly for passenger cars [72, 73]. Even though many challenges still have to be addressed, one of the greatest advantages of these fuels is that they keep a high energy density and could be applied on current combustion engines without the need to design new and complex technologies and infrastructures. These fuels could therefore participate quickly into the reduction of the transportation carbon footprint, especially for the heavy-duty vehicles, airplanes and ships [74–76]. Finally, considering that the carbon dioxide emitted from the combustion is due to the presence of carbon in the fuel composition, hydrogen, which is a carbon-free fuel, inherently received some interest [77, 78]. The hydrogen, similarly to gasoline or diesel, is injected inside the combustion chamber and is burned with the air, making this approach an attractive alternative as existing engine platforms knowledge and infrastructures could ease the transition to such a fuel [79]. Nevertheless, this solution raises some challenges as well, such as: the hydrogen storage in the vehicle due to low energy density by volume, uncontrolled and rapid combustion, the high temperature combustion responsible of an increase in NO_x emissions, and the need of clean energy sources for the hydrogen production to make this approach carbon-neutral [80–82]. Moreover, some studies suggested that using the same hydrogen directly into a fuel cell vehicle might, in the end, represent a more efficient solution, although more research is still necessary [83–85].

Low temperature combustion Instead of trying to reduce the pollutant emissions with dedicated devices in the exhaust line, which tends to increase the overall vehicle cost and complexity, another approach consists in mitigating these emissions directly at their formation source: the combustion. As an example, high combustion temperatures and lean mixture allow to reduce particulate matter emissions (soot). However, as a counterpart, this will tend to increase the emissions of NO_x [86,87]. To face this NO_x -soot trade-off, a combustion that simultaneously avoids both conditions is therefore desired. Such combustion concept was widely investigated over the years and it is referred to as low temperature combustion (LTC) [88]. This concept relies on a long air-fuel mixing time to avoid rich zones in the combustion chamber, and therefore soot formation, while ensuring combustion flame temperatures low enough for ultra-low NO_x emissions [89,90]. One of the former techniques to fall within this combustion category is the homogeneous charge compression ignition (HCCI) [91,92]. This combustion concept consists in the auto-ignition of a homogeneous air-fuel mixture, characterized by short combustion duration with high efficiency and low pollutant emissions thanks to lower combustion temperatures and reduced heat losses [93,94]. Because it is kinetically controlled (i.e., the ignition is highly dependent on the in-cylinder species concentration and temperature conditions), this concept raised some ignition timing control issues. Furthermore, although some works have succeeded to reach high load operation [95,96], the spontaneous ignition of the air-fuel mixture in the combustion chamber results in high combustion rates and is responsible of violent combustion with potential damage for the engine, which tends to limit the operating range of this combustion concept [97,98]. Various LTC concepts were proposed over the years to address the challenges faced by the HCCI combustion, such as premixed charge compression ignition (PCCI) or reactivity controlled compression ignition (RCCI). Similarly, these concepts keep the same goal of achieving high thermal efficiency and low pollutant emissions by avoiding high combustion temperatures and rich zones [99,100]. Figure 1.7 shows the regions of NO_x and soot formation with respect to local flame temperature and equivalence ratio. The operating regions of various combustion concepts are also illustrated with colored lines showing the path followed by LTC modes to avoid NO_x and soot emissions compared to conventional diesel combustion (CDC). Although some challenges such as controllability, load limitation, cold start capability or important cyclic and cylinder-to-cylinder variation are still to be tackled for their commercialization [101–103], low temperature combustion concepts have exhibited an attractive potential for future efficient propulsion technologies. Furthermore, these combustion concepts might also be combined with alternative fuels [104–106] or hybrid powertrains [107–109] to further contribute into providing clean transportation

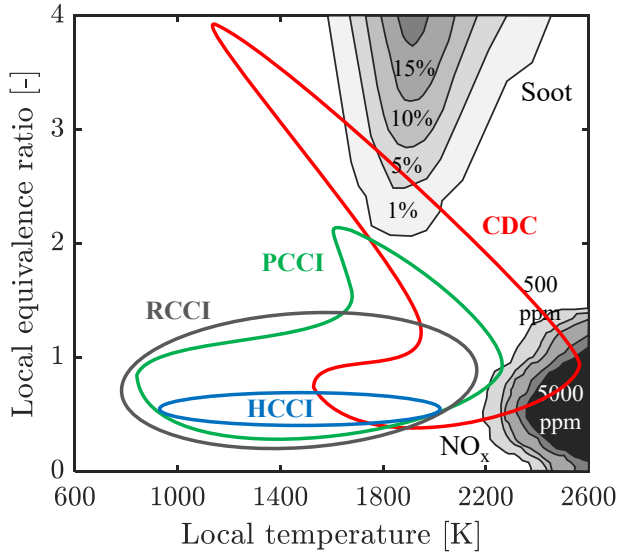


Figure 1.7: ϕ - T diagram, regions of NO_x and soot formation with respect to local flame temperature and equivalence ratio. Colored contours illustrate the operating regions of various combustion modes. Adapted from [90].

solutions.

1.2.3 Combustion engine control and modeling

No matter the powertrain technology, the combustion mode and its complexity, modeling and control have played a major role in the area of transportation and combustion engines development [110–112].

Thanks to the increasingly powerful electronic technologies, engine control units can embed elaborated multivariable strategies in order to set the control commands required to satisfy the driver demands [113]. Internal combustion engines are complex non-linear dynamic systems and traditionally rely on open-loop - *feedforward* - control. Open-loop is a straightforward solution where the controller output is a direct function of the controller input. Such relation might be expressed with mathematical equations or in the form of a two-input single-output look-up table where a calibrated map provides the value to apply [114]. Some controllers, on the other side, use a feedback from the engine, also known as closed-loop - *feedback* - control, to continuously correct the control variables in order to obtain the desired output. A common example of these two approaches can be found in

the control of the fuel injection in gasoline engines: the duration of injection is estimated based on the operating conditions (e.g. engine speed and intake manifold pressure), this is the open-loop mode. Meanwhile, the lambda sensor placed at the exhaust is used to evaluate the real equivalence ratio and correct the fuel injection to reach the stoichiometric conditions necessary for the high conversion efficiency at the three-way catalyst, this is the closed-loop mode [115].

Along with conventional open and closed-loop strategies, modeling represents a cost-effective approach to ease the design and the calibration of advanced control strategies in both feedforward and feedback configurations [116]. Indeed, as they provide an insight of the engine operation, the models are used to improve the controller definition and contribute to a more efficient operation. These models can be found with various levels of complexity depending on the desired approach and application, and can be applied in model-based controllers [117].

Stringent constraints on regulated pollutant emissions and evolving complexity of new combustion modes are pushing the research community to always keep improving and developing new controllers. Thanks to its improved effectiveness and accuracy against external disturbances and variations in the system's environment (e.g., aging, fuel properties), closed-loop combustion control is considered a way to enhance and ensure safe and efficient operation of combustion engines [118–121]; although particular attention has to be paid to sensors selection and signal processing to avoid control instabilities (e.g., noise) [122].

Thanks to its capacity to evaluate the in-cylinder process and obtain relevant information such as the indicated engine work, efficiency, and even NO_x formation [123], the in-cylinder pressure sensor is considered as the most powerful source of feedback information for internal combustion engines [124]. Although widely used in combustion research activities, this technology is still not broadly installed in on-road applications (some production engines equipped with such sensor can be found, such as the ones from VW [125] and Mazda [126]). Yet, an interest towards its implementation for closed-loop control was being evidenced [127–129], especially for the proper control of low temperature combustion concepts where many challenges are yet to be addressed [123, 130, 131]. Various combustion controllers based on such signal can be found in the literature such as cycle-to-cycle feedback control [132–134], in-cycle [135–137] or even model-predictive control strategies [138–140].

1.3 Outline and contributions

The present thesis describes the work conducted by the author in the area of cycle-to-cycle combustion control. The thesis is focused on the analysis, design and implementation of control strategies and models related to premixed dual-fuel combustion engines. Diesel medium-duty engines were converted to dual-fuel operation and instrumented with in-cylinder pressure sensors in order to develop closed-loop combustion controllers with special emphasis on providing strategies for various levels of mixture stratification in order to cover most of the engine operating range. The analysis and conclusions about the results obtained from the data acquired and presented in this dissertation are covered in the following chapters as specified below:

Chapter 2

First, an introduction to the premixed dual-fuel combustion is provided. It starts with a brief description of its history to address the challenges faced by other combustion modes such as the homogeneous charge compression ignition. The combustion concept with its applications and various injection strategies are mentioned. Then, a summary of the works found in the literature about the modeling and control of such combustion concept is given. Accordingly, the contributions of this thesis are finally highlighted.

Chapter 3

This chapter details the experimental setup and methods used throughout the investigation work conducted by the author. The engines, their respective instrumentation, as well as the signal acquisition and control layout are described. Given that this thesis is based on the in-cylinder pressure signal to develop the control strategies, a section is dedicated to its acquisition, processing and analysis. In particular, the resonant frequency range potential to provide relevant information about the combustion operation is highlighted.

Related publications

- Carlos Guardiola, Benjamín Pla, Pau Bares, Alvin Barbier. An analysis of the in-cylinder pressure resonance excitation in internal combustion engines. *Applied Energy*, Vol. 228, pp. 1272-1279, 2018.

Chapter 4

In this chapter, closed-loop combustion controllers are investigated. Based on the in-cylinder pressure signal, various approaches are evaluated. From maintaining the desired performance with PI controllers, to optimizing and ensuring the safe operation of the engine through extremum seeking and stochastic control, this chapter covers different control concepts and analyzes their outcomes when applied to the various injection strategies considered in this work.

Related publications

- Carlos Guardiola, Benjamín Pla, Pau Bares, Alvin Barbier. Closed-loop control of a dual-fuel engine working with different combustion modes using in-cylinder pressure feedback. *International Journal of Engine Research*, Vol. 21 n°3, pp. 484-496, 2020.
- Benjamín Pla, Pau Bares, Alvin Barbier, Carlos Guardiola. On-line Optimization of Dual-Fuel Combustion Operation by Extremum Seeking Techniques. *SAE Technical Paper*, 2021-01-0519, 2021.
- Carlos Guardiola, Benjamín Pla, Pau Bares, Alvin Barbier. Safe operation of dual-fuel engines using constrained stochastic control. *International Journal of Engine Research*, Vol. 23 n°2, pp. 285-299, 2022.

Chapter 5

Modeling offers a variety of benefits for control applications, either for its estimation or prediction capabilities. In this chapter, as a starting point, a control-oriented model dedicated to RCCI combustion is developed to estimate the combustion phasing. In a second step, combustion models are harnessed to estimate the fuel blend (i.e., the ratio between diesel and gasoline) in each cylinder through a state observer.

Related publications

- Carlos Guardiola, Benjamín Pla, Pau Bares, Alvin Barbier. A combustion phasing control-oriented model applied to an RCCI engine. *IFAC-PapersOnLine*, Vol. 51 n°31, pp. 119-124, 2018.
- Alireza Kakooee, Younes Bakhshan, Alvin Barbier, Pau Bares, Carlos Guardiola. Modeling combustion timing in an RCCI engine by means of a control-oriented model. *Control Engineering Practice*, Vol. 97, pp. 104321, 2020.

- Carlos Guardiola, Benjamín Pla, Pau Bares, Alvin Barbier. Individual cylinder fuel blend estimation in a dual-fuel engine using an in-cylinder pressure based observer. *Control Engineering Practice*, Vol. 109, pp. 104760, 2021.

Chapter 6

Finally, the last chapter summarizes the contributions of the present work in addressing the control of premixed dual-fuel engines and concludes about the potential paths towards an improved control architecture for real-world applications.

References

- [1] IPCC. IPCC, 2014: Climate Change 2014: Synthesis Report. Contribution of Working Groups I, II and III to the Fifth Assessment Report of the Intergovernmental Panel on Climate Change [Core Writing Team, R.K. Pachauri and L.A. Meyer (eds.)]. IPCC, Geneva, Switzerland, 151 pp. <https://www.ipcc.ch/report/ar5/syr/>.
(cited in pp. 1, 2, and 3)
- [2] IPCC. IPCC, 2021: Summary for Policymakers. In: Climate Change 2021: The Physical Science Basis. Contribution of Working Group I to the Sixth Assessment Report of the Intergovernmental Panel on Climate Change [Masson-Delmotte, V., P. Zhai, A. Pirani, S. L. Connors, C. Péan, S. Berger, N. Caud, Y. Chen, L. Goldfarb, M. I. Gomis, M. Huang, K. Leitzell, E. Lonnoy, J.B.R. Matthews, T. K. Maycock, T. Waterfield, O. Yelekçi, R. Yu and B. Zhou (eds.)]. Cambridge University Press. In Press. <https://www.ipcc.ch/report/ar6/wg1/>.
(cited in p. 1)
- [3] Ritchie Hannah and Roser Max. CO₂ and Greenhouse Gas Emissions. *Our World in Data*, 2020. <https://ourworldindata.org/co2-and-other-greenhouse-gas-emissions>.
(cited in pp. 1, 2, and 3)
- [4] IPCC. IPCC, 2007: Climate Change 2007: Synthesis Report. Contribution of Working Groups I, II and III to the Fourth Assessment Report of the Intergovernmental Panel on Climate Change [Core Writing Team, Pachauri, R.K and Reisinger, A. (eds.)]. IPCC, Geneva, Switzerland, 104 pp. <https://www.ipcc.ch/report/ar4/syr/>.
(cited in p. 1)
- [5] P. Forster, Ramaswamy V., Artaxo P., Berntsen T., Betts R., Fahey D.W., Haywood J., Lean J., Lowe D.C., Myhre G., Nganga J., Prinn R., Raga G., Schulz M. and Dorland R. Van. Changes in Atmospheric Constituents and in Radiative Forcing. In: Climate Change 2007: The Physical Science Basis. Contribution of Working Group I to the Fourth Assessment Report of the Intergovernmental Panel on Climate Change [Solomon, S., D. Qin, M. Manning, Z. Chen, M. Marquis, K.B. Averyt, M. Tignor and H.L. Miller (eds.)]. Cambridge University Press, Cambridge, United Kingdom and New York, NY, USA. <https://www.ipcc.ch/site/assets/uploads/2018/02/ar4-wg1-chapter2-1.pdf>.
(cited in p. 1)

References

- [6] IEA. IEA, Data and statistics: World CO2 emissions by energy source. <https://www.iea.org/data-and-statistics/data-browser/?country=WORLD&fuel=CO2%20emissions&indicator=CO2BySource>. Accessed 22 March 2022. (cited in p. 2)
- [7] Chesterton Andrew. How many cars are there in the world? <https://www.carsguide.com.au/car-advice/how-many-cars-are-there-in-the-world-70629>. Accessed 22 March 2022. (cited in p. 2)
- [8] OICA. OICA, retrieved from Statista: Number of passenger cars and commercial vehicles in use worldwide from 2006 to 2015 in (1,000 units). <https://www.statista.com/statistics/281134/number-of-vehicles-in-use-worldwide/>. Accessed 22 March 2022. (cited in p. 2)
- [9] WHO. World Health Organization (WHO), Coronavirus disease (COVID-19) pandemic. <https://www.who.int/emergencies/diseases/novel-coronavirus-2019>. Accessed 22 March 2022. (cited in p. 2)
- [10] ACEA. ACEA, Making the Transition to Zero-Emission Mobility - 2021 progress report, 2021. <https://www.acea.auto/publication/2021-progress-report-making-the-transition-to-zero-emission-mobility/>. (cited in pp. 2, 4, and 5)
- [11] European Commission. Reducing CO2 emissions from passenger cars - before 2020. https://ec.europa.eu/clima/policies/transport/vehicles/cars_en. Accessed 22 March 2022. (cited in p. 4)
- [12] IEA. IEA, Global electric passenger car stock, 2010-2020, IEA, Paris. <https://www.iea.org/data-and-statistics/charts/global-electric-passenger-car-stock-2010-2020>. Accessed 22 March 2022. (cited in pp. 4 and 5)
- [13] EEA. European Environment Agency, New registrations of electric vehicles in Europe. <https://www.eea.europa.eu/ims/new-registrations-of-electric-vehicles>. Accessed 22 March 2022. (cited in p. 4)
- [14] Tietge Uwe, Mock Peter and Dornoff Jan. CO2 emissions from new passenger cars in Europe: Car manufacturers' performance in 2019, 2020. <https://theicct.org/publications/co2-new-passenger-cars-europe-aug2020>. (cited in p. 4)
- [15] ACEA. ACEA, Making the Transition to Zero-Emission Mobility - 2020 progress report, 2020. <https://www.acea.auto/publication/making-the-transition-to-zero-emission-mobility-2020-progress-report/>. (cited in p. 4)
- [16] Díaz Sonsoles, Bernard Marie Rajon, Bernard Yoann, Bieker Georg, Lee Kaylin, Mock Peter, Mulholland Eamonn, Ragon Pierre-Louis, Rodriguez Felipe, Tietge Uwe and Wappelhorst Sandra. European vehicle market statistics 2021/22, 2021. <https://theicct.org/wp-content/uploads/2021/12/ICCT-EU-Pocketbook-2021-Web-Dec21.pdf>. (cited in p. 4)

-
- [17] EEA. European Environment Agency, Average CO₂ emissions from new cars and new vans increased again in 2019. <https://www.eea.europa.eu/highlights/average-co2-emissions-from-new-cars-vans-2019>. Accessed 22 March 2022. (cited in p. 4)
- [18] Hellweg Stefanie and Mila i Canals L. Emerging approaches, challenges and opportunities in life cycle assessment. *Science*, Vol. 344 n° 6188, pp. 1109–1113, jun 2014. (cited in p. 4)
- [19] Bouter Anne, Hache Emmanuel, Ternel Cyprien and Beauchet Sandra. Comparative environmental life cycle assessment of several powertrain types for cars and buses in France for two driving cycles: “worldwide harmonized light vehicle test procedure” cycle and urban cycle. *The International Journal of Life Cycle Assessment*, Vol. 25 n° 8, pp. 1545–1565, aug 2020. (cited in p. 4)
- [20] Egeskog Andrea, Hagdahl Karl-Henrik, Krewer Christoffer, Råde Ingrid and Bolin Lisa. Volvo Cars, with the participation of the IVL Swedish Environmental Research Institute - Carbon footprint report: Battery electric XC40 Recharge and the XC40 ICE, 2020. <https://group.volvocars.com/news/sustainability/2020/ /media/ccs/Volvo-carbonfootprintreport.pdf>. (cited in p. 4)
- [21] Bieker Georg. A global comparison of the life-cycle greenhouse gas emissions of combustion engine and electric passenger cars, 2021. <https://theicct.org/publications/global-LCA-passenger-cars-jul2021>. (cited in p. 4)
- [22] Burul Dora and Algesten David. Scania - Life cycle assessment of distribution vehicles: Battery electric vs diesel driven, 2021. <https://www.scania.com/group/en/home/newsroom/press-releases/press-release-detail-page.html/3999115-scania-publishes-life-cycle-assessment-of-battery-electric-vehicles>. (cited in p. 4)
- [23] IEA. IEA, World Energy Outlook 2020, Achieving net-zero emissions by 2050, IEA, Paris. <https://www.iea.org/reports/world-energy-outlook-2020/achieving-net-zero-emissions-by-2050>. Accessed 22 March 2022. (cited in p. 4)
- [24] EUR-Lex. Regulation (EU) 2019/1242 of the European Parliament and of the Council of 20 June 2019 setting CO₂ emission performance standards for new heavy-duty vehicles and amending Regulations (EC) No 595/2009 and (EU) 2018/956 of the European Parliament and of the Council and Council Directive 96/53/EC. <https://eur-lex.europa.eu/eli/reg/2019/1242/oj>. Accessed 22 March 2022. (cited in p. 4)
- [25] Ritchie Hannah. Cars, planes, trains: where do CO₂ emissions from transport come from? <https://ourworldindata.org/co2-emissions-from-transport#licence>. Accessed 22 March 2022. (cited in p. 4)

- [26] Bauer Christian, Hofer Johannes, Althaus Hans-Jörg, Del Duce Andrea and Simons Andrew. The environmental performance of current and future passenger vehicles: Life cycle assessment based on a novel scenario analysis framework. *Applied Energy*, Vol. 157, pp. 871–883, nov 2015. (cited in p. 4)
- [27] Guzzella Lino and Sciarretta Antonio. *Vehicle Propulsion Systems*, volume 91. Springer Berlin Heidelberg, Berlin, Heidelberg, 2013. (cited in p. 5)
- [28] IEA. IEA (2021), Global EV Outlook 2021, IEA, Paris. <https://www.iea.org/reports/global-ev-outlook-2021>. Accessed 22 March 2022. (cited in p. 5)
- [29] IEA. IEA (2020), Trucks and Buses, IEA, Paris. <https://www.iea.org/reports/trucks-and-buses>. Accessed 22 March 2022. (cited in p. 5)
- [30] Ritchie Hannah and Roser Max. Energy. *Our World in Data*, 2020. <https://ourworldindata.org/energy>. (cited in p. 5)
- [31] Conway Graham, Joshi Ameya, Leach Felix, García Antonio and Senecal Peter Kelly. A review of current and future powertrain technologies and trends in 2020. *Transportation Engineering*, Vol. 5 n° June, pp. 100080, sep 2021. (cited in p. 5)
- [32] Abdul-Manan Amir F.N. Uncertainty and differences in GHG emissions between electric and conventional gasoline vehicles with implications for transport policy making. *Energy Policy*, Vol. 87, pp. 1–7, dec 2015. (cited in p. 5)
- [33] Kalghatgi Gautam. Is it really the end of internal combustion engines and petroleum in transport? *Applied Energy*, Vol. 225 n° February, pp. 965–974, sep 2018. (cited in p. 5)
- [34] Senecal P.K. and Leach Felix. Diversity in transportation: Why a mix of propulsion technologies is the way forward for the future fleet. *Results in Engineering*, Vol. 4 n° October, pp. 100060, dec 2019. (cited in p. 5)
- [35] Lešnik Luka, Kegl Breda, Torres-Jiménez Eloísa and Cruz-Peragón Fernando. Why we should invest further in the development of internal combustion engines for road applications. *Oil & Gas Science and Technology – Revue d’IFP Energies nouvelles*, Vol. 75 n° 1, sep 2020. (cited in p. 5)
- [36] Heywood J.B. *Internal Combustion Engine Fundamentals*. Automotive technology series. McGraw-Hill, 1988. (cited in pp. 6, 71, 118, 119, 150, and 158)
- [37] Cummins C. Lyle. Early IC and Automotive Engines. In *SAE Technical Papers*, pp. 1960–1971, feb 1976. (cited in p. 6)
- [38] Lee Byeongsoek, Oh Heechang, Han Seungkook, Woo Soohyung and Son Jinwook. Development of High Efficiency Gasoline Engine with Thermal Efficiency over 42%. In *SAE Technical Papers*, volume 2017-October, oct 2017. (cited in p. 6)
- [39] Johnson Timothy and Joshi Ameya. Review of Vehicle Engine Efficiency and Emissions. *SAE International Journal of Engines*, Vol. 11 n° 6, pp. 1307–1330, apr 2018. (cited in p. 6)

-
- [40] Wärtsilä. Wärtsilä 31SG, the world's most efficient 4-stroke engine. <https://www.wartsila.com/insights/article/wartsila-31sg-the-worlds-most-efficient-4-stroke-engine>. Accessed 22 March 2022. (cited in p. 6)
- [41] Hempson J. G. G. The Automobile Engine 1920-1950. In *SAE Technical Papers*, feb 1976. (cited in p. 6)
- [42] Payri F., Benajes J., Margot X. and Gil A. CFD modeling of the in-cylinder flow in direct-injection Diesel engines. *Computers & Fluids*, Vol. 33 n° 8, pp. 995–1021, sep 2004. (cited in p. 6)
- [43] Li Yu, Li Hailin, Guo Hongsheng, Li Yongzhi and Yao Mingfa. A numerical investigation on methane combustion and emissions from a natural gas-diesel dual fuel engine using CFD model. *Applied Energy*, Vol. 205 n° February, pp. 153–162, nov 2017. (cited in p. 6)
- [44] Zhao H. and Ladommatos N. Optical diagnostics for soot and temperature measurement in diesel engines. *Progress in Energy and Combustion Science*, Vol. 24 n° 3, pp. 221–255, jan 1998. (cited in p. 6)
- [45] Tang Qinglong, Liu Haifeng, Li Mingkun, Yao Mingfa and Li Zhongshan. Study on ignition and flame development in gasoline partially premixed combustion using multiple optical diagnostics. *Combustion and Flame*, Vol. 177, pp. 98–108, mar 2017. (cited in p. 6)
- [46] Munawer Muhammad Ehsan. Human health and environmental impacts of coal combustion and post-combustion wastes. *Journal of Sustainable Mining*, Vol. 17 n° 2, pp. 87–96, 2018. (cited in p. 7)
- [47] Michał Krzyżanowski, Birgit Kuna-Dibbert and Jürgen Schneider. *Health effects of transport-related air pollution*. WHO Regional Office Europe, 2005. (cited in p. 7)
- [48] European Commission. Emissions in the automotive sector. https://ec.europa.eu/growth/sectors/automotive/environment-protection/emissions_en. Accessed 22 March 2022. (cited in p. 7)
- [49] Zheng Ming, Reader Graham T. and Hawley J.Gary. Diesel engine exhaust gas recirculation—a review on advanced and novel concepts. *Energy Conversion and Management*, Vol. 45 n° 6, pp. 883–900, apr 2004. (cited in p. 7)
- [50] Badami M., Mallamo F., Millo F. and Rossi E. E. Influence of Multiple Injection Strategies on Emissions, Combustion Noise and BSFC of a DI Common Rail Diesel Engine. In *SAE Technical Papers*, volume 2002, mar 2002. (cited in p. 7)
- [51] Mohan Balaji, Yang Wenming and Chou Siaw Kiang. Fuel injection strategies for performance improvement and emissions reduction in compression ignition engines—A review. *Renewable and Sustainable Energy Reviews*, Vol. 28 n° x, pp. 664–676, dec 2013. (cited in p. 7)

- [52] Brijesh P. and Sreedhara S. Exhaust emissions and its control methods in compression ignition engines: A review. *International Journal of Automotive Technology*, Vol. 14 n° 2, pp. 195–206, apr 2013. (cited in p. 7)
- [53] TransportPolicy. EU: Heavy-duty: Emissions. <https://www.transportpolicy.net/standard/eu-heavy-duty-emissions/>. Accessed 22 March 2022. (cited in p. 8)
- [54] Alkemade Ulrich G. and Schumann Bernd. Engines and exhaust after treatment systems for future automotive applications. *Solid State Ionics*, Vol. 177 n° 26-32 SPEC. ISS., pp. 2291–2296, 2006. (cited in p. 8)
- [55] Twigg Martyn V. Progress and future challenges in controlling automotive exhaust gas emissions. *Applied Catalysis B: Environmental*, Vol. 70 n° 1-4, pp. 2–15, jan 2007. (cited in p. 8)
- [56] Reşitoğlu İbrahim Aslan, Altinişik Kemal and Keskin Ali. The pollutant emissions from diesel-engine vehicles and exhaust aftertreatment systems. *Clean Technologies and Environmental Policy*, Vol. 17 n° 1, pp. 15–27, jan 2015. (cited in p. 8)
- [57] Russell April and Epling William S. Diesel Oxidation Catalysts. *Catalysis Reviews*, Vol. 53 n° 4, pp. 337–423, oct 2011. (cited in p. 8)
- [58] Guan Bin, Zhan Reggie, Lin He and Huang Zhen. Review of state of the art technologies of selective catalytic reduction of NOx from diesel engine exhaust. *Applied Thermal Engineering*, Vol. 66 n° 1-2, pp. 395–414, may 2014. (cited in p. 8)
- [59] Praveena V. and Martin M. Leenus Jesu. A review on various after treatment techniques to reduce NOx emissions in a CI engine. *Journal of the Energy Institute*, Vol. 91 n° 5, pp. 704–720, oct 2018. (cited in p. 8)
- [60] Adler Joerg. Ceramic Diesel Particulate Filters. *International Journal of Applied Ceramic Technology*, Vol. 2 n° 6, pp. 429–439, nov 2005. (cited in p. 8)
- [61] Cloudt Robert and Willems Frank. Integrated Emission Management strategy for cost-optimal engine-aftertreatment operation. *SAE International Journal of Engines*, Vol. 4 n° 1, pp. 1784–1797, apr 2011. (cited in p. 8)
- [62] Wu Zhixin, Wang Michael, Zheng Jihu, Sun Xin, Zhao Mingnan and Wang Xue. Life cycle greenhouse gas emission reduction potential of battery electric vehicle. *Journal of Cleaner Production*, Vol. 190, pp. 462–470, jul 2018. (cited in p. 8)
- [63] Nigam Poonam Singh and Singh Anoop. Production of liquid biofuels from renewable resources. *Progress in Energy and Combustion Science*, Vol. 37 n° 1, pp. 52–68, feb 2011. (cited in p. 9)
- [64] Jambo Siti Azmah, Abdulla Rahmath, Mohd Azhar Siti Hajar, Marbawi Hartinie, Gansau Jualang Azlan and Ravindra Pogaku. A review on third generation bioethanol feedstock. *Renewable and Sustainable Energy Reviews*, Vol. 65, pp. 756–769, nov 2016. (cited in p. 9)

-
- [65] Oumer A.N., Hasan M.M., Baheta Aklilu Tesfamichael, Mamat Rizalman and Abdullah A.A. Bio-based liquid fuels as a source of renewable energy: A review. *Renewable and Sustainable Energy Reviews*, Vol. 88 n° October 2017, pp. 82–98, may 2018. (cited in p. 9)
- [66] Whitaker Jeanette, Ludley Katherine E., Rowe Rebecca, Taylor Gail and Howard David C. Sources of variability in greenhouse gas and energy balances for biofuel production: A systematic review. *GCB Bioenergy*, Vol. 2 n° 3, pp. 99–112, jun 2010. (cited in p. 9)
- [67] IEA. IEA (2020), Transport Biofuels, IEA, Paris. <https://www.iea.org/reports/transport-biofuels>. Accessed 22 March 2022. (cited in p. 9)
- [68] Ambaye Teklit Gebregiorgis, Vaccari Mentore, Bonilla-Petriciolet Adrián, Prasad Shiv, van Hullebusch Eric D. and Rtimi Sami. Emerging technologies for biofuel production: A critical review on recent progress, challenges and perspectives. *Journal of Environmental Management*, Vol. 290 n° March, pp. 112627, jul 2021. (cited in p. 9)
- [69] Pearson Richard J., Eisaman Matthew D., Turner James W. G., Edwards Peter P., Jiang Zheng, Kuznetsov Vladimir L., Littau Karl A., di Marco Leon and Taylor S. R. Gordon. Energy Storage via Carbon-Neutral Fuels Made From CO₂, Water, and Renewable Energy. *Proceedings of the IEEE*, Vol. 100 n° 2, pp. 440–460, feb 2012. (cited in p. 9)
- [70] Lehtveer Mariliis, Brynolf Selma and Grahn Maria. What Future for Electrofuels in Transport? Analysis of Cost Competitiveness in Global Climate Mitigation. *Environmental Science & Technology*, Vol. 53 n° 3, pp. 1690–1697, feb 2019. (cited in p. 9)
- [71] Li Xuping, Anderson Paul, Jhong Huei-Ru Molly, Paster Mark, Stubbins James F. and Kenis Paul J. A. Greenhouse Gas Emissions, Energy Efficiency, and Cost of Synthetic Fuel Production Using Electrochemical CO₂ Conversion and the Fischer–Tropsch Process. *Energy & Fuels*, Vol. 30 n° 7, pp. 5980–5989, jul 2016. (cited in p. 9)
- [72] Brynolf Selma, Taljegard Maria, Grahn Maria and Hansson Julia. Electrofuels for the transport sector: A review of production costs. *Renewable and Sustainable Energy Reviews*, Vol. 81 n° February 2017, pp. 1887–1905, jan 2018. (cited in p. 9)
- [73] Freire Ordóñez Diego, Shah Nilay and Guillén-Gosálbez Gonzalo. Economic and full environmental assessment of electrofuels via electrolysis and co-electrolysis considering externalities. *Applied Energy*, Vol. 286 n° July 2020, pp. 116488, mar 2021. (cited in p. 9)
- [74] Schemme Steffen, Samsun Remzi Can, Peters Ralf and Stolten Detlef. Power-to-fuel as a key to sustainable transport systems – An analysis of diesel fuels produced from CO₂ and renewable electricity. *Fuel*, Vol. 205, pp. 198–221, oct 2017. (cited in p. 9)

- [75] Hänggi Severin, Elbert Philipp, Bütler Thomas, Cabalzar Urs, Teske Sinan, Bach Christian and Onder Christopher. A review of synthetic fuels for passenger vehicles. *Energy Reports*, Vol. 5, pp. 555–569, nov 2019. (cited in p. 9)
- [76] Hannula Ilkka and Reiner David M. Near-Term Potential of Biofuels, Electrofuels, and Battery Electric Vehicles in Decarbonizing Road Transport. *Joule*, Vol. 3 n° 10, pp. 2390–2402, oct 2019. (cited in p. 9)
- [77] Eichlseder Helmut, Wallner Thomas, Freymann Raymond and Ringler Jürgen. The Potential of Hydrogen Internal Combustion Engines in a Future Mobility Scenario. In *SAE Technical Papers*, number 724, jun 2003. (cited in p. 9)
- [78] Dimitriou Pavlos and Tsujimura Taku. A review of hydrogen as a compression ignition engine fuel. *International Journal of Hydrogen Energy*, Vol. 42 n° 38, pp. 24470–24486, sep 2017. (cited in p. 9)
- [79] Verhelst S. Recent progress in the use of hydrogen as a fuel for internal combustion engines. *International Journal of Hydrogen Energy*, Vol. 39 n° 2, pp. 1071–1085, jan 2014. (cited in p. 9)
- [80] Fayaz H., Saidur R., Razali N., Anuar F.S., Saleman A.R. and Islam M.R. An overview of hydrogen as a vehicle fuel. *Renewable and Sustainable Energy Reviews*, Vol. 16 n° 8, pp. 5511–5528, oct 2012. (cited in p. 9)
- [81] Sinigaglia Tiago, Lewiski Felipe, Santos Martins Mario Eduardo and Mairesse Siluk Julio Cezar. Production, storage, fuel stations of hydrogen and its utilization in automotive applications-a review. *International Journal of Hydrogen Energy*, Vol. 42 n° 39, pp. 24597–24611, sep 2017. (cited in p. 9)
- [82] Stępień Zbigniew. A Comprehensive Overview of Hydrogen-Fueled Internal Combustion Engines: Achievements and Future Challenges. *Energies*, Vol. 14 n° 20, oct 2021. (cited in p. 9)
- [83] Salvi B.L. and Subramanian K.A. Sustainable development of road transportation sector using hydrogen energy system. *Renewable and Sustainable Energy Reviews*, Vol. 51, pp. 1132–1155, nov 2015. (cited in p. 9)
- [84] Acar Canan and Dincer Ibrahim. The potential role of hydrogen as a sustainable transportation fuel to combat global warming. *International Journal of Hydrogen Energy*, Vol. 45 n° 5, pp. 3396–3406, jan 2020. (cited in p. 9)
- [85] Ahmadi Pouria, Torabi Seyed Hosein, Afsaneh Hadi, Sadegheih Yousef, Ganjehsarabi Hadi and Ashjaee Mehdi. The effects of driving patterns and PEM fuel cell degradation on the lifecycle assessment of hydrogen fuel cell vehicles. *International Journal of Hydrogen Energy*, Vol. 45 n° 5, pp. 3595–3608, jan 2020. (cited in p. 9)
- [86] Tree Dale R. and Svensson Kenth I. Soot processes in compression ignition engines. *Progress in Energy and Combustion Science*, Vol. 33 n° 3, pp. 272–309, jun 2007. (cited in p. 10)

-
- [87] Li Tie and Ogawa Hideyuki. Analysis of the trade-off between soot and nitrogen oxides in diesel-Like combustion by chemical kinetic calculation. *SAE International Journal of Engines*, Vol. 5 n° 2, pp. 94–101, aug 2012. (cited in p. 10)
- [88] Alriksson Malin, Rente Tanja and Denbratt Ingemar. Low Soot, Low NO_x in a Heavy Duty Diesel Engine Using High Levels of EGR. In *SAE Technical Papers*, volume 2006, pp. 75–2006, oct 2005. (cited in p. 10)
- [89] Krishnamoorthi M., Malayalamurthi R., He Zhixia and Kandasamy Sabariswaran. A review on low temperature combustion engines: Performance, combustion and emission characteristics. *Renewable and Sustainable Energy Reviews*, Vol. 116 n° September, pp. 109404, dec 2019. (cited in p. 10)
- [90] Pachiannan Tamilselvan, Zhong Wenjun, Rajkumar Sundararajan, He Zhixia, Leng Xianying and Wang Qian. A literature review of fuel effects on performance and emission characteristics of low-temperature combustion strategies. *Applied Energy*, Vol. 251 n° 301, pp. 113380, oct 2019. (cited in pp. 10 and 11)
- [91] Thring R. H. Homogeneous-Charge Compression-Ignition (HCCI) Engines. In *SAE Technical Paper Series*, sep 1989. (cited in p. 10)
- [92] Yao Mingfa, Zheng Zhaolei and Liu Haifeng. Progress and recent trends in homogeneous charge compression ignition (HCCI) engines. *Progress in Energy and Combustion Science*, Vol. 35 n° 5, pp. 398–437, 2009. (cited in pp. 10, 30, and 77)
- [93] Stanglmaier Rudolf H and Roberts Charles E. Homogeneous Charge Compression Ignition (HCCI): Benefits, Compromises, and Future Engine Applications. In *SAE Technical Paper*, number 724, 1999. (cited in pp. 10 and 30)
- [94] Epping Kathi, Aceves Salvador, Bechtold Richard and Dec John E. The Potential of HCCI Combustion for High Efficiency and Low Emissions. In *SAE Technical Papers*, number 724, jun 2002. (cited in pp. 10 and 30)
- [95] Olsson Jan-Ola, Tunestål Per, Haraldsson Göran and Johansson Bengt. A Turbo Charged Dual Fuel HCCI Engine. In *SAE Technical Papers*, number 724, may 2001. (cited in pp. 10 and 31)
- [96] Dec John E. and Yang Yi. Boosted HCCI for High Power without Engine Knock and with Ultra-Low NO_x Emissions - using Conventional Gasoline. *SAE International Journal of Engines*, Vol. 3 n° 1, apr 2010. (cited in p. 10)
- [97] Saxena Samveg and Bedoya Iván D. Fundamental phenomena affecting low temperature combustion and HCCI engines, high load limits and strategies for extending these limits. *Progress in Energy and Combustion Science*, Vol. 39 n° 5, pp. 457–488, oct 2013. (cited in p. 10)
- [98] Bendu Harisankar and Murugan S. Homogeneous charge compression ignition (HCCI) combustion: Mixture preparation and control strategies in diesel engines. *Renewable and Sustainable Energy Reviews*, Vol. 38, pp. 732–746, oct 2014. (cited in pp. 10, 30, and 87)

- [99] Imtenan S., Varman M., Masjuki H.H., Kalam M.A., Sajjad H., Arbab M.I. and Rizwanul Fattah I.M. Impact of low temperature combustion attaining strategies on diesel engine emissions for diesel and biodiesels: A review. *Energy Conversion and Management*, Vol. 80 n° x, pp. 329–356, apr 2014. (cited in p. 10)
- [100] Agarwal Avinash Kumar, Singh Akhilendra Pratap and Maurya Rakesh Kumar. Evolution, challenges and path forward for low temperature combustion engines. *Progress in Energy and Combustion Science*, Vol. 61, pp. 1–56, 2017. (cited in p. 10)
- [101] Dempsey Adam B., Walker N. Ryan, Gingrich Eric and Reitz Rolf D. Comparison of low temperature combustion strategies for advanced compression ignition engines with a focus on controllability. *Combustion Science and Technology*, Vol. 186 n° 2, pp. 210–241, 2014. (cited in pp. 10, 32, and 87)
- [102] Hasan M.M. and Rahman M.M. Homogeneous charge compression ignition combustion: Advantages over compression ignition combustion, challenges and solutions. *Renewable and Sustainable Energy Reviews*, Vol. 57, pp. 282–291, may 2016. (cited in p. 10)
- [103] Li Jing, Yang Wenming and Zhou Dezhi. Review on the management of RCCI engines. *Renewable and Sustainable Energy Reviews*, Vol. 69 n° May 2016, pp. 65–79, 2017. (cited in pp. 10, 32, and 155)
- [104] Kumar Pravin and Rehman A. Bio-diesel in homogeneous charge compression ignition (HCCI) combustion. *Renewable and Sustainable Energy Reviews*, Vol. 56, pp. 536–550, apr 2016. (cited in p. 10)
- [105] Khandal S.V., Banapurmath N.R. and Gaitonde V.N. Performance studies on homogeneous charge compression ignition (HCCI) engine powered with alternative fuels. *Renewable Energy*, Vol. 132 n° x, pp. 683–693, mar 2019. (cited in p. 10)
- [106] García Antonio, Monsalve-Serrano Javier, Villalta David and Guzmán-Mendoza María. Methanol and OME_x as fuel candidates to fulfill the potential EURO VII emissions regulation under dual-mode dual-fuel combustion. *Fuel*, Vol. 287 n° September 2020, pp. 119548, mar 2021. (cited in p. 10)
- [107] Solouk Ali and Shahbakhti Mahdi. Energy Optimization and Fuel Economy Investigation of a Series Hybrid Electric Vehicle Integrated with Diesel/RCCI Engines. *Energies*, Vol. 9 n° 12, pp. 1020, dec 2016. (cited in p. 10)
- [108] García Antonio, Monsalve-Serrano Javier, Sari Rafael, Dimitrakopoulos Nikolaos, Tunér Martin and Tunestål Per. Performance and emissions of a series hybrid vehicle powered by a gasoline partially premixed combustion engine. *Applied Thermal Engineering*, Vol. 150 n° January, pp. 564–575, mar 2019. (cited in p. 10)
- [109] García Antonio, Carlucci Paolo, Monsalve-Serrano Javier, Valletta Andrea and Martínez-Boggio Santiago. Energy management optimization for a power-split hybrid in a dual-mode RCCI-CDC engine. *Applied Energy*, Vol. 302 n° August, pp. 117525, nov 2021. (cited in p. 10)

-
- [110] Payri F., Luján JM, Guardiola C. and Pla B. A Challenging Future for the IC Engine: New Technologies and the Control Role. *Oil & Gas Science and Technology – Revue d'IFP Energies nouvelles*, Vol. 70 n° 1, pp. 15–30, jun 2015. (cited in p. 11)
- [111] Norouzi Armin, Heidarifar Hamed, Shahbakhti Mahdi, Koch Charles Robert and Borhan Hoseinali. Model Predictive Control of Internal Combustion Engines: A Review and Future Directions. *Energies*, Vol. 14 n° 19, pp. 6251, oct 2021. (cited in pp. 11 and 148)
- [112] Aliramezani Masoud, Koch Charles Robert and Shahbakhti Mahdi. Modeling, diagnostics, optimization, and control of internal combustion engines via modern machine learning techniques: A review and future directions. *Progress in Energy and Combustion Science*, Vol. 88, jan 2022. (cited in p. 11)
- [113] Guzzella Lino and Onder Christopher H. *Introduction to Modeling and Control of Internal Combustion Engine Systems*. Springer Berlin Heidelberg, Berlin, Heidelberg, 2010. (cited in p. 11)
- [114] Kiencke Uwe and Nielsen Lars. *Automotive Control Systems: For Engine, Driveline, and Vehicle*. Springer Berlin Heidelberg, Berlin, Heidelberg, 2005. (cited in pp. 11 and 128)
- [115] Eriksson Lars and Nielsen Lars. *Modeling and Control of Engines and Drivelines*. John Wiley & Sons, Ltd, Chichester, UK, feb 2014. (cited in p. 12)
- [116] Isermann Rolf. *Engine Modeling and Control*. Springer Berlin Heidelberg, Berlin, Heidelberg, 2014. (cited in p. 12)
- [117] Albin Thivaharan. *Nonlinear Model Predictive Control of Combustion Engines*. 2021. (cited in p. 12)
- [118] Thor Mikael, Egardt Bo, McKelvey Tomas and Andersson Ingemar. Closed-loop diesel engine combustion phasing control based on crankshaft torque measurements. *Control Engineering Practice*, Vol. 33, pp. 115–124, dec 2014. (cited in pp. 12 and 88)
- [119] Jung Insoo, Jin Jaemin, Lee Dongchul, Lee Seunghyun, Yang Seungwook and Min Kyoungdoug. Closed-Loop Control Method for Monitoring and Improving the Diesel Combustion Noise. In *SAE Technical Papers*, volume 2016-June, jun 2016. (cited in p. 12)
- [120] Yang Z., Winward E. and Stobart R.K. Improve Cylinder-to-Cylinder Consistency and Reduce Cycle-to-Cycle Variations of a Diesel Engine Using Closed-loop Control of Fuel Path Input Variables. *IFAC-PapersOnLine*, Vol. 49 n° 11, pp. 239–244, 2016. (cited in p. 12)
- [121] Ferrari A., Novara C., Paolucci E., Vento O., Violante M. and Zhang T. Design and rapid prototyping of a closed-loop control strategy of the injected mass for the reduction of CO₂, combustion noise and pollutant emissions in diesel engines. *Applied Energy*, Vol. 232 n° October, pp. 358–367, dec 2018. (cited in p. 12)

- [122] Docquier Nicolas and Candel Sébastien. Combustion control and sensors: a review. *Progress in Energy and Combustion Science*, Vol. 28 n° 2, pp. 107–150, jan 2002. (cited in p. 12)
- [123] Willems Frank. Is Cylinder Pressure-Based Control Required to Meet Future HD Legislation? *IFAC-PapersOnLine*, Vol. 51 n° 31, pp. 111–118, 2018. (cited in pp. 12, 34, 55, and 88)
- [124] Rogers David R. *Engine Combustion: Pressure Measurement and Analysis*. SAE international Warrendale, PA, 2010. (cited in pp. 12, 56, and 63)
- [125] Hadler Jens, Rudolph Falko, Dorenkamp Richard, Stehr Hartmut, Hilzendeger Juer-gen and Kranzusch Sebastian. Volkswagen’s new 2.0 l TDI engine for the most stringent emission standards - Part 1. *MTZ worldwide*, Vol. 69 n° 5, pp. 12–18, 2008. (cited in p. 12)
- [126] Kazuhiro Nagatsu, Atsushi Inoue, Kota Matsumoto, Takashi Kaminaga, Toru Miyamoto and Takashi Youso. Control device for compression ignition-type engine. U.S. Patent No. 9,719,441 B2., 2017. (cited in p. 12)
- [127] Powell J. David. Engine Control Using Cylinder Pressure: Past, Present, and Future. *Journal of Dynamic Systems, Measurement, and Control*, Vol. 115 n° 2B, pp. 343–350, jun 1993. (cited in p. 12)
- [128] Leonhardt Steffen, Muller N. and Isermann Rolf. Methods for engine supervision and control based on cylinder pressure information. *IEEE/ASME Transactions on Mechatronics*, Vol. 4 n° 3, pp. 235–245, 1999. (cited in p. 12)
- [129] Saracino Roberto, Gaballo Maria Rosaria, Mannal Soenke, Motz Stefan, Carlucci Antonio and Benegiamo Marco. Cylinder Pressure-Based Closed Loop Combustion Control: A Valid Support to Fulfill Current and Future Requirements of Diesel Powertrain Systems. In *SAE Technical Papers*, volume 2015, sep 2015. (cited in pp. 12 and 88)
- [130] Lu Xingcai, Han Dong and Huang Zhen. Fuel design and management for the control of advanced compression-ignition combustion modes. *Progress in Energy and Combustion Science*, Vol. 37 n° 6, pp. 741–783, 2011. (cited in pp. 12 and 30)
- [131] Fathi Morteza, Jahanian Omid and Shahbakhti Mahdi. Modeling and controller design architecture for cycle-by-cycle combustion control of homogeneous charge compression ignition (HCCI) engines – A comprehensive review. *Energy Conversion and Management*, Vol. 139, pp. 1–19, 2017. (cited in pp. 12 and 34)
- [132] Olsson Jan-ola, Tunestål Per and Johansson Bengt. Closed-Loop Control of an HCCI Engine. In *SAE Technical Paper*, mar 2001. (cited in pp. 12, 34, 35, and 37)
- [133] Carlucci A. P., Laforgia D., Motz S., Saracino R. and Wenzel S. P. Advanced closed loop combustion control of a LTC diesel engine based on in-cylinder pressure signals. *Energy Conversion and Management*, Vol. 77, pp. 193–207, 2014. (cited in p. 12)

-
- [134] Fang Cheng, Ouyang Minggao, Tunestal Per, Yang Fuyuan and Yang Xiaofan. Closed-loop combustion phase control for multiple combustion modes by multiple injections in a compression ignition engine fueled by gasoline-diesel mixture. *Applied Energy*, Vol. 231 n° May, pp. 816–825, dec 2018. (cited in pp. 12 and 89)
- [135] Yang Fuyuan, Wang Jinli, Gao Guojing and Ouyang Minggao. In-cycle diesel low temperature combustion control based on SOC detection. *Applied Energy*, Vol. 136, pp. 77–88, dec 2014. (cited in p. 12)
- [136] Lehrheuer Bastian, Pischinger Stefan, Wick Maximilian, Andert Jakob, Berneck Dirk, Ritter Dennis, Albin Thivaharan and Thewes Matthias. A Study on In-Cycle Combustion Control for Gasoline Controlled Autoignition. In *SAE Technical Papers*, volume 2016-April, apr 2016. (cited in p. 12)
- [137] Jorques Moreno Carlos, Stenlaas Ola and Tunestal Per. In-Cycle Closed-Loop Combustion Control for Pilot Misfire Compensation. In *SAE Technical Papers*, number 2020, pp. 1–13, sep 2020. (cited in p. 12)
- [138] Bengtsson Johan, Strandh Petter, Johansson Rolf, Tunestal Per and Johansson Bengt. Model predictive control of homogeneous charge compression ignition (HCCI) engine dynamics. *Computer Aided Control System Design, 2006 IEEE International Conference on Control Applications, 2006 IEEE International Symposium on Intelligent Control, 2006 IEEE*, pp. 1675–1680, 2006. (cited in pp. 12, 34, and 37)
- [139] Ebrahimi Khashayar and Koch Charles. Model Predictive Control for Combustion Timing and Load Control in HCCI Engines. In *SAE Technical Papers*, volume 2015-April, apr 2015. (cited in p. 12)
- [140] Ingesson Gabriel, Yin Lianhao, Johansson Rolf and Tunestal Per. Simultaneous Control of Combustion Timing and Ignition Delay in Multi-Cylinder Partially Premixed Combustion. *SAE International Journal of Engines*, Vol. 8 n° 5, pp. 2089–2098, 2015. (cited in p. 12)

Chapter 2

Premixed dual-fuel combustion

As introduced in Chapter 1, with the introduction of more stringent emissions restrictions for internal combustion engines, premixed low temperature combustion (LTC) modes were evaluated. These concepts aim to mitigate the issues encountered in conventional diesel combustion engines, such as the NO_x -soot trade-off, by decreasing the combustion temperatures and reducing the local equivalence ratio [1, 2]. Homogeneous charge compression ignition (HCCI) was one of the first concepts to be investigated. Nevertheless, many challenges were encountered and led to the development of various new strategies, such as partially premixed combustion (PPC) [3–5], premixed charge compression ignition (PCCI) [6–8], or reactivity controlled compression ignition (RCCI). This dissertation is focused on the premixed dual-fuel combustion in which the RCCI concept is included. In this chapter, first, an introduction to the premixed dual-fuel concept, its benefits and its challenges, is provided. Then, an attempt to summarize the research activities dedicated to the control strategies of this combustion concept is proposed.

2.1 Introduction

Homogeneous charge compression ignition combustion was proposed as a promising solution to address the challenges raised by conventional combustion modes. The HCCI combustion consists in injecting the fuel during the intake stroke in order to create a homogeneous air-fuel mixture in the cylinder, similarly to spark ignition engines, and therefore lower the local equivalence ratio. This mixture is then compressed and, once favorable pressure-temperature conditions are reached in the cylinder, the mixture is auto-ignited, similarly to compression ignited engines. The diluted charge operated in this combustion concept thanks to the lean mixtures, and/or high levels of exhaust gas recirculation, lowers the combustion

temperatures which, together with shorter combustion, contributes to minimize the heat transfer losses [9–11]. Accordingly, the main benefits observed were high thermal efficiency, a significant reduction in NO_x emissions thanks to the low temperature conditions, and a decrease in soot production as a result of the lean operation [12]. Nevertheless, the HCCI concept is usually limited to narrow zones of the engine operating map as a consequence of the high pressure gradients resulting from the fast combustion in the cylinder which represent a risk of damage for the engine [13]. Furthermore, being a kinetically controlled combustion, the proper ignition timing of the combustion is highly dependent on the in-cylinder conditions and species, which is inherently more challenging in terms of controllability [14]. Poor fuel conversion efficiency with excessive unburned products, and high cyclic variability were therefore observed, especially at low load conditions [15, 16]. Over the years, several solutions were explored to extend the range of operation and to improve the combustion controllability of this concept. Techniques such as air heating control and compression ratio adjustment [17, 18], or fuel properties variations, were proposed and it was suggested that a proper HCCI operation could be made possible with the use of a fuel that would exhibit characteristics between a gasoline and a diesel fuel [19, 20].

Dual-fuel combustion was intuitively proposed to address the aforementioned issues by creating a mixture of a low reactivity fuel (e.g., iso-octane, gasoline) and a high reactivity fuel (e.g., n-heptane, diesel) to alter the mixture reactivity. Works such as the one presented by Inagaki et al. [21] were dedicated to demonstrate the benefits of such implementation to extend the operation range of premixed combustion modes over the engine map while ensuring low levels of NO_x and soot emissions. Further investigations were subsequently carried out to optimize and extend this concept, which led to the RCCI combustion mode.

2.2 Combustion concept

Investigations about dual-fuel combustion can already be found since the last century [22]. Traditionally, these engines were compression ignited engines operated essentially with a homogeneous mixture of air and natural gas as the main contributor to the engine power output, and a small amount of diesel as the ignition source by injecting it near the top dead center, similarly to conventional diesel combustion [23]. These engines exhibited the benefits of: reducing the NO_x and soot emission levels thanks to the homogeneous air-gas mixture, and being able to either run on dual-fuel or pure diesel conditions depending on the fuel availability. However, higher CO and HC concentrations, especially at low loads, and signifi-

cant pressure rise rates, were encountered [24].

Given the issues raised by the homogeneous charge compression ignition concept (note that some of these concerns were already found in the aforementioned dual-fuel engines as they were mostly composed of a homogeneous charge), especially regarding its timing control, the use of a mixture reactivity resulting from the injection of two fuels with different properties was explored. The use of the mixing ratio between two fuels to control the combustion onset was already suggested in works such as the one proposed by Olsson et al. [25]. A blending of n-heptane and ethanol was used as a mean to control the combustion timing with two separate port fuel injection systems in a HCCI combustion engine. The objective of this work was, however, not to demonstrate the potential of the dual-fuel operation itself, but essentially to show the potential of high load HCCI combustion where the fuel blending was used as a substitute to air temperature for controlling the timing of the combustion. By contrast, Inagaki et al. [21] analyzed further the effect and outcomes from a dual-fuel combustion at different stratification levels. It was observed that, in HCCI combustion, the blending ratio of the two fuels was able to control the combustion timing but had no control authority over the burning rate which is responsible of the high load operation limitation of such concept. Consequently, a dual-fuel premixed compression ignition (PCI) combustion mode consisting in iso-octane port fuel injection, and diesel direct injection, was evaluated. It was observed that, not only the mixing ratio was able to control the combustion, but also that the stratification levels achieved in the cylinder thanks to the direct injection timings were able to mitigate the burning rate. Moreover, a significant reduction in NO_x and soot emissions under an extensive range of load operation was appreciated. These promising results have encouraged the research community to deepen the understanding of this combustion concept and to evaluate its potential implementation for commercial applications. Works such as the ones presented by Kokjohn et al. [26] and Hanson et al. [27] followed the early stages of the premixed dual-fuel concept by enhancing its understanding and operation through experimental and numerical analyses. It was highlighted that the combustion evolution of this dual-fuel PCCI strategy was dictated by the mixture reactivity stratification, from the most to the least reactive zones, leading to the known name of reactivity controlled compression ignition (RCCI) combustion [28].

Subsequently, the RCCI combustion was extensively investigated over the years with works dedicated to: improving the understanding of the operating conditions [29–31], injection strategies [32–35], and fuel properties [36–38] effects to improve the engine’s efficiency; performing combustion chamber optimization with

different piston geometries [39, 40]; or to assess the combustion operational limits and evaluate its potential for current engine platforms and applications [41–44]. It was found that the RCCI concept was able to enhance the combustion controllability against other LTC concepts thanks to the control of the mixture reactivity with the fraction of the low reactivity fuel, and the mixture stratification with the injection timing of the high reactivity fuel [45, 46]. It was thereby noticed that an increase in the low reactivity fuel resulted in a more delayed combustion due to the decrease in the mixture reactivity [47]. The effect of the high reactivity fuel injection timing was, however, less straightforward as it was observed to cause a change in the combustion regime (from kinetically controlled to mixing controlled) when approaching the top dead center vicinity [48]. Especially appealing for medium and heavy-duty engines [49, 50], in combination with high dilution levels, this concept was successfully extended to high load operation while maintaining reasonably low NO_x and soot emission levels [51]. However, due to its highly premixed conditions, the RCCI combustion was observed to not be exempted from significant pressure gradients due to the spontaneous ignition of the mixture in the combustion chamber, especially at high loads [52, 53]. Although reducing the compression ratio allows to reduce these pressure levels, this technique promotes CO and HC emissions at low loads due to poor fuel conversion efficiency [54]. It was therefore concluded that limitations to the application of the RCCI combustion over the entire engine operating map still remained.

In order to overcome these challenges, while leveraging the benefits of the RCCI combustion, new approaches such as the dual-mode dual-fuel (DMDF) concept were proposed [55]. In this concept, the RCCI operation is maintained until the pressure gradients are about to exceed the safe operation levels of the engine. Then, the combustion is progressively switched towards a more mixing controlled combustion by reducing the amount of premixed charge in the cylinder with later injections of the high reactivity fuel [56]. This combustion concept is therefore composed of fully and highly premixed charge conditions up to medium load operation, which ensures low NO_x and soot emissions, and switches to a partially premixed combustion, which could exhibit some diffusive-like reactions, to reach high load operation while respecting the mechanical constraints of the engine. However, these late injection timings promote the formation of rich zones which consequently result in an increase of the soot emissions. Furthermore, the increase in combustion temperature induced by the diffusive-like behavior of the high load operation penalizes the NO_x emissions as well. Despite such observation, this modification of the premixing levels in the dual-fuel combustion concept appeared to be a promising way to extend the benefits of this low temperature combustion

mode to the entire engine operating map (after-treatment systems might be used to compensate the emissions increase in these specific operating regions). Many challenges are yet to be tackled in order to comply with the upcoming restrictions on exhaust gas emissions and a substantial effort is currently carried out to adapt this technology to on-road applications, such as presented in the work conducted by Lago Sari [57].

In summary, premixed dual-fuel combustion has demonstrated to be a promising approach to face the actual concerns about the emissions caused by the transportation sector [58]. Yet, this combustion concept represents a challenging environment to ensure a proper engine operation while leveraging the benefits of this combustion (e.g., pressure gradients, cyclic variability, various injection strategies, different fuel properties).

2.3 Modeling and control applications

Combustion optimization is traditionally carried out in a controlled environment (i.e., engine test bench) in steady-state conditions where the engine is calibrated at the optimal setpoint for each given operating condition. Once encountered, the corresponding settings are generally saved within open-loop look-up tables which are then used to control the engine. Nevertheless, an extensive calibration effort on these maps is traditionally required for the readiness of such open-loop control in real-world conditions. Indeed, a particular attention has to be paid to transient conditions where a certain operation smoothness is expected for the user, and where the engine dynamics (e.g., air path response, temperature effect) might worsen the engine outcomes (performance and emissions) compared to the steady-state calibration alone.

In the case of premixed combustion modes, in addition, many challenges need to be tackled to operate the engine to its full potential. A proper understanding of the inputs-outputs pairing and further investigation about advanced control strategies are therefore required. Dual-fuel combustion concepts, such as RCCI combustion, were proposed to deal with some of the combustion control instabilities encountered in HCCI combustion [59], and to improve the LTC operation over the engine operating map. To this end, an efficient control system is key to harness the benefits from these concepts while handling the remaining challenges:

- Controllability and stability of the combustion operation, especially at highly premixed conditions where the combustion ignition is triggered by the in-cylinder conditions (i.e., species concentration and temperature).

- Mechanical and operating limitations to ensure a safe operation of the engine due to high pressure gradients resulting from this type of combustion.
- Transient operation with eventual combustion switching-mode to deliver the required performance in the most efficient and safest way.

Similarly to HCCI combustion, which has been undergoing extensive research activities in control applications in order to evaluate solutions for reliable operation [60–66], several control applications can be found in the literature for premixed dual-fuel combustion engines [67]. Due to the challenging aspects of such premixed combustion strategy (e.g., high cyclic variability, large pressure gradients, lack of robust combustion timing control, various combustion modes [68]), most of them use a feedback signal from the engine to ensure safe and stable operation. This signal is traditionally provided by an in-cylinder pressure sensor [69] but it is worth mentioning that some works are dedicated to evaluate the potential of cost effective and non-intrusive methods for estimating the engine combustion metrics such as with an accelerometer [70].

When investigating combustion control applications, two main families of control strategies can be established: those relying on conventional closed-loop controllers such as with proportional-integral-derivative (PID) actions, and the ones using physical equations to describe the engine behavior, the model-based controllers.

At the time where Olsson et al. were investigating the potential of the HCCI combustion in a heavy duty engine equipped with a double port fuel injection system, a closed-loop control of the combustion was proposed [71]. This controller was based on the in-cylinder pressure signal feedback to estimate the combustion phasing (represented by the crank angle where 50% of the heat has been released, CA50) and the indicated mean effective pressure (IMEP) which were then individually controlled in each cylinder by PID controllers. The load (IMEP) was controlled by modulating the total fuel quantity injected inside the cylinder, while the combustion timing was controlled by the mixing ratio of the two iso-octane and n-heptane fuels. This work preceded further investigations performed by the same group of researchers to evaluate and compare different control architectures such as with linear quadratic Gaussian (LQG) and model-predictive control (MPC), exhibiting their potential to control a HCCI engine [62, 72, 73]. Another investigation on model-based control of a dual-fuel HCCI engine was also proposed by Bidarvatan et al. [74]. Closed-loop controllers can also be found in natural gas-diesel engines such as the one proposed by Ott et al. [75]. In this case, as the diesel was

used as the ignition source by injecting it directly in the combustion chamber at the top dead center, the diesel injection timing and quantity were chosen as the control variables to regulate the combustion phasing and the maximum pressure rise rate (MPRR) with a PI controller.

With the introduction of the RCCI combustion concept, a special attention was paid regarding its controllability, especially for transient operation. Hanson and Reitz [76] compared a load change from 1 to 4 bar brake mean effective pressure (BMEP) from conventional diesel combustion and RCCI operation. In the RCCI combustion case, two control strategies were compared: open-loop based on steady-state operation tables, and closed-loop control of the combustion phasing by modulating the blending ratio (BR) of the two fuels (gasoline and diesel). It was observed that the engine was able to perform the load step in RCCI combustion in both control approaches. Nonetheless, the benefits of the closed-loop controller were appreciated with a faster response to reach the desired CA50 set-point. The authors finally concluded and highlighted that this combustion concept would certainly require more advanced control techniques to improve its operation in real-world conditions.

More recently, Arora and Shahbakhti [77] successfully implemented a closed-loop PI controller for controlling the load (IMEP) and the combustion phasing (CA50) in a 2-liter RCCI engine with port fuel injected iso-octane and direct injected n-heptane. In this case, the load was controlled by the total fuel amount, while the CA50 was controlled by either the blending ratio, or the injection timing of the high reactivity fuel. Indeed, unlike in HCCI combustion such as in [71], here the injection timing acts on the mixture stratification and can be used as a control variable. Arora and Shahbakhti therefore characterized the sensitivity of the CA50 to the BR and to the injection timing. Then, whichever had higher sensitivity (i.e., controllability) for the corresponding operating conditions was chosen to drive the CA50. The results showed that this strategy was able to reach the desired load under transient operation while maintaining the CA50 to its target value.

As a result of the need for advanced control strategies, models that could encompass the physics of premixed dual-fuel combustion with low computational cost started to be investigated. These computationally efficient models, also known as control-oriented models (COMs), aim to describe the combustion phenomena and to estimate variables such as the start of combustion (SOC), or the combustion phasing, by means of physical equations. These models address various purposes. As an example, they can be devoted to characterize the combustion itself (e.g., see

the models proposed by Khodadadi Sadabadi et al. [78] and Sui et al. [79]). These models can then substitute the real engine in the process of designing control strategies off-line in a simulation approach, which allows to reduce the experimental calibration effort. Bekdemir et al. [80] developed a multi-zone model of a natural gas-diesel heavy-duty RCCI engine to capture the response of the engine to a change in control variables such as the injection timing or the blending ratio of the fuels. The model was then used to compute a map-based model of the RCCI engine which enabled the fast analysis and development of PI controllers on the combustion phasing, engine load and blending ratio. This same model was also used by Indrajana et al. [81] to develop a multi-input multi-output (MIMO) feedback controller for RCCI combustion. The model was then completed by a conventional dual-fuel (CDF) combustion model (similar to the aforementioned DMDF concept) to design a closed-loop controller in [82]. Combined to PI control actions, this controller was based on decoupling the effect of each control variable on the engine outputs. A controller for combustion mode-switching, which is of great interest to implement such combustion concept into real-world applications, was also designed and evaluated (see another example with conventional diesel in [83]). Based on a similar strategy, the control approach was further demonstrated with a complete air-fuel path control which, this time, was experimentally validated by Willems et al. [84]. Khodadadi Sadabadi and Shahbakhti [85] designed a controller to track the desired CA50 by modulating the blending ratio of the two fuels using a simulated RCCI engine (i.e., its physical model representation was used instead to evaluate the controller). Kondipati et al. [86] followed a similar approach but in this case the designed controller was validated experimentally. First, the engine model was used to design and tune a PI controller aiming to track the combustion phasing. Then, the resulting calibration was tested on a real RCCI engine showing and validating the performance of the controller.

Compared to the aforementioned applications, control-oriented models can also be directly applied at the core of the controller such as in the model predictive control investigations performed by Raut et al. [87, 88]. Such implementation was chosen due to the MPC capability to handle input and output constraints. By doing so, the proposed controller was able to track the reference IMEP and CA50 under variations of the blending ratio, while maintaining the coefficient of variation of the IMEP (COV_{IMEP}) below a predefined threshold. Similarly, Irdmousa et al. [89] and Basina et al. [90] managed to implement a MPC in a RCCI engine. In [89], the MPC aimed to control the combustion phasing under varying operating conditions, while in [90], IMEP and CA50 tracking with pressure rise rate levels limitation were performed.

Table 2.1 summarizes and provides details about the control strategies for premixed dual-fuel combustion presented in this chapter. According to this table, it is seen that the majority of the works were dedicated to track the load (IMEP) and the combustion phasing (CA50), traditionally by adjusting the total injected fuel quantity in the cylinder, the blending ratio of the two fuels, and the injection timing of the direct injected high reactivity fuel. Moreover, it is noticed that few works were dedicated to explicitly address the significant pressure gradients resulting from this combustion in the controller definition, which is a critical constraint for an eventual implementation of this concept in real-world applications. It is therefore highlighted that there is still room for improvement in control investigations to enhance and bring this concept towards on-road implementation. Also, it can be noticed that unlike HCCI combustion, the control and sensitivity of the combustion timing to temperature dynamics and residual gases fraction modulation was not widely explored in concepts such as RCCI and late premixed dual-fuel combustion [91–93].

Table 2.1: Summary of the premixed dual-fuel control applications studies.

Authors	Controller	Control strategy
Olsson et al. [71]	PID	The load (IMEP) is driven by the total fuel amount, and the combustion timing (CA50) by the ratio of the two fuels. Peak pressure and maximum pressure rate are monitored to set alarms that modify IMEP or CA50 setpoint to avoid engine damage
Strandh et al. [72]	PID and LQG	Comparison of PID and LQG control of the combustion timing (CA50) using the fuel ratio as the control input
Bengtsson et al. [73]	MPC	Variable valve actuation (VVA) and fuel ratio were compared for controlling the combustion timing, which was delayed to avoid exceeding the pressure rise rate constraint
Bidarvatan et al. [74]	Sliding mode control	The desired combustion phasing (CA50) is obtained by adjusting the ratio of the two fuels
Ott et al. [75]	PI	Pressure rise rate and combustion timing are controlled by the diesel injection quantity and timing

(continued on next page)

Table 2.1 (*continued*)

Authors	Controller	Control strategy
Hanson and Reitz [76]	PID	Control of the combustion phasing using the blending ratio of the two fuels
Arora and Shahbakhti [77]	PI	Control of the IMEP with the total fuel quantity, and control of the combustion phasing (CA50) using either the high reactivity fuel injection timing or the blending ratio (according to a sensitivity map)
Bekdemir et al. [80]	PI	Control of the IMEP using the diesel quantity and the combustion timing with its injection timing. The blending ratio is also closed-loop controlled varying the quantity of natural gas
Indrajuana et al. [81]	MIMO feedback control	Control of the combustion timing, load and blending ratio with the diesel injection quantity and timing, and the natural gas quantity
Indrajuana et al. [82]	Combined decoupling matrix and PI control actions	Control of the air-path (EGR and pressure difference across the engine) with the EGR valve and the variable geometry turbine. Control of the CA50, IMEP, and BR with the diesel injection quantity and timing, and natural gas quantity
Willems et al. [84]	Combined decoupling matrix and PI control	Similar to Indrajuana et al. [82] with the addition of the control of the air-to-fuel ratio λ
Khodadadi Sadabadi and Shahbakhti [85]	Linear quadratic integral (LQI)	Control of the combustion phasing by modulating the blending ratio
Kondipati et al. [86]	PI	Combustion phasing tracking using either the blending ratio or the injection timing of the direct injected fuel
Raut et al. [88]	MPC	Control of the IMEP using the total fuel quantity, and control of the CA50 by adjusting either the injection timing or BR (similarly to Arora and Shahbakhti [77]) with BR used as a scheduling variable to switch from one MPC to another depending on the operating conditions

(continued on next page)

Table 2.1 (*continued*)

Authors	Controller	Control strategy
Irdmoussa et al. [89]	MPC	A linear parameter-varying (LPV) model was implemented into a MPC for tracking the CA50 with the n-heptane injection timing
Basina et al. [90]	MPC	The LPV model was implemented into the MPC to track IMEP and CA50 while limiting the MPRR. The load was controlled by the total fuel quantity and the injection timing was adjusted to comply with both the combustion phasing and the pressure rise rate target/constraint

2.4 Conclusions

This chapter summarized the numerous works carried out for the investigation of the premixed dual-fuel combustion concept. It was first concluded that this combustion strategy shows promising results to address the concerns related to the emissions levels of internal combustion engines. Nonetheless, many challenges are yet to be faced, especially regarding the potential implementation of this concept in current on-road applications. Various levels of mixture reactivity and stratification were proposed for this concept as a way to extend its benefits over the entire engine operating map. However, this raised at the same time new challenges and control requirements to provide an efficient combustion operation. Implementation of advanced combustion control strategies to ensure the correct, safe and stable operation of this combustion concept at any operating condition is therefore necessary.

Several works were dedicated to this aspect, from traditional closed-loop controllers, to more advanced model-based strategies. From the studies identified in the literature, it was observed that various works were intended to develop controllers to meet the required performance of the engine (i.e., load and combustion phasing), but few of them considered its operation constraints. Furthermore, some of these investigations were based on simulation results, and most of the results experimentally validated were presented from a single cylinder point of view, thus not exhibiting the cylinder-to-cylinder behavior of the control strategy.

In the following chapters, this work attempts to propose control strategies that could be applied on premixed dual-fuel engines in order to address some issues

raised by this concept and participate in the global effort to bring this combustion mode closer to real-world conditions implementation. In particular, for the most part, this investigation is oriented to a multi-cylinder engine configuration and also tries to tackle all the levels of mixture stratification found in this combustion concept in order to analyze the potential of each control approach in a wider operating range. By doing so, this work seeks to evaluate control strategies in a system, and in conditions, that could be encountered in an on-road vehicle.

References

- [1] Dec John E. Advanced compression-ignition engines—understanding the in-cylinder processes. *Proceedings of the Combustion Institute*, Vol. 32 n° 2, pp. 2727–2742, 2009. (cited in p. 29)
- [2] Reitz Rolf D. Directions in internal combustion engine research. *Combustion and Flame*, Vol. 160 n° 1, pp. 1–8, 2013. (cited in p. 29)
- [3] Noehre Christof, Andersson Magnus, Johansson Bengt and Hultqvist Anders. Characterization of Partially Premixed Combustion. In *SAE Technical Papers*, number 724, pp. 776–790, oct 2006. (cited in p. 29)
- [4] Lewander Magnus, Ekholm Kent, Johansson Bengt, Tunestål Per, Milovanovic Nebojsa, Keeler Nathan, Harcombe Tony and Bergstrand Pär. Investigation of the combustion characteristics with focus on partially premixed combustion in a heavy duty engine. *SAE International Journal of Fuels and Lubricants*, Vol. 1 n° 1, pp. 1063–1074, jun 2009. (cited in p. 29)
- [5] Benajes J., Novella R., De Lima D. and Thein K. Impact of injection settings operating with the gasoline Partially Premixed Combustion concept in a 2-stroke HSDI compression ignition engine. *Applied Energy*, Vol. 193 n° x, pp. 515–530, may 2017. (cited in p. 29)
- [6] Kanda Tomohiro, Hakozaki Takazo, Uchimoto Tatsuya, Hatano Jyunichi, Kitayama Naoto and Sono Hiroshi. PCCI Operation with Early Injection of Conventional Diesel Fuel. In *SAE Technical Papers*, volume 2005, apr 2005. (cited in p. 29)
- [7] de Ojeda William, Zoldak Philip, Espinosa Raul and Kumar Raj. Development of a Fuel Injection Strategy for Partially Premixed Compression Ignition Combustion. *SAE International Journal of Engines*, Vol. 2 n° 1, apr 2009. (cited in p. 29)
- [8] Torregrosa A.J., Broatch A., Novella R., Gomez-Soriano J. and Mónico L.F. Impact of gasoline and Diesel blends on combustion noise and pollutant emissions in Premixed Charge Compression Ignition engines. *Energy*, Vol. 137, pp. 58–68, oct 2017. (cited in p. 29)
- [9] Christensen Magnus, Johansson Bengt, Amnéus Per and Mauss Fabian. Supercharged Homogeneous Charge Compression Ignition. In *SAE Technical Paper Series*, number 724, feb 1998. (cited in p. 30)

-
- [10] Lu Xingcai, Han Dong and Huang Zhen. Fuel design and management for the control of advanced compression-ignition combustion modes. *Progress in Energy and Combustion Science*, Vol. 37 n° 6, pp. 741–783, 2011. (cited in pp. 12 and 30)
- [11] Bendu Harisankar and Murugan S. Homogeneous charge compression ignition (HCCI) combustion: Mixture preparation and control strategies in diesel engines. *Renewable and Sustainable Energy Reviews*, Vol. 38, pp. 732–746, oct 2014. (cited in pp. 10, 30, and 87)
- [12] Stanglmaier Rudolf H and Roberts Charles E. Homogeneous Charge Compression Ignition (HCCI): Benefits, Compromises, and Future Engine Applications. In *SAE Technical Paper*, number 724, 1999. (cited in pp. 10 and 30)
- [13] Eng J. A. Characterization of Pressure Waves in HCCI Combustion. In *SAE Technical Papers*, number 724, oct 2002. (cited in pp. 30, 62, and 76)
- [14] Epping Kathi, Aceves Salvador, Bechtold Richard and Dec John E. The Potential of HCCI Combustion for High Efficiency and Low Emissions. In *SAE Technical Papers*, number 724, jun 2002. (cited in pp. 10 and 30)
- [15] Persson H, Pfeiffer R, Hultqvist A, Johansson B and Ström H. Cylinder-to-Cylinder and Cycle-to-Cycle Variations at HCCI Operation With Trapped Residuals. In *SAE Technical Paper Series*, volume 2005, apr 2005. (cited in p. 30)
- [16] Yao Mingfa, Zheng Zhaolei and Liu Haifeng. Progress and recent trends in homogeneous charge compression ignition (HCCI) engines. *Progress in Energy and Combustion Science*, Vol. 35 n° 5, pp. 398–437, 2009. (cited in pp. 10, 30, and 77)
- [17] Haraldsson Göran, Tunestål Per, Johansson Bengt and Hyvönen Jari. HCCI Combustion Phasing in a Multi Cylinder Engine Using Variable Compression Ratio. In *SAE Technical Papers*, number 724, oct 2002. (cited in p. 30)
- [18] Gan Suyin, Ng Hoon Kiat and Pang Kar Mun. Homogeneous Charge Compression Ignition (HCCI) combustion: Implementation and effects on pollutants in direct injection diesel engines. *Applied Energy*, Vol. 88 n° 3, pp. 559–567, mar 2011. (cited in p. 30)
- [19] Dec John E. and Sjöberg Magnus. Isolating the Effects of Fuel Chemistry on Combustion Phasing in an HCCI Engine and the Potential of Fuel Stratification for Ignition Control. In *SAE Technical Papers*, volume 2004, mar 2004. (cited in p. 30)
- [20] Bessonette Paul W., Schleyer Charles H., Duffy Kevin P., Hardy William L. and Liechty Michael P. Effects of Fuel Property Changes on Heavy-Duty HCCI Combustion. In *SAE Technical Papers*, volume 2007, pp. 776–790, apr 2007. (cited in p. 30)
- [21] Inagaki Kazuhisa, Fuyuto Takayuki, Nishikawa Kazuaki, Nakakita Kiyomi and Sakata Ichiro. Dual-Fuel PCI Combustion Controlled by In-Cylinder Stratification of Ignitability. In *SAE Technical Paper Series*, volume 1, apr 2006. (cited in pp. 30 and 31)

- [22] Karim Ghazi A. A review of combustion processes in the dual fuel engine—The gas diesel engine. *Progress in Energy and Combustion Science*, Vol. 6 n° 3, pp. 277–285, jan 1980. (cited in p. 30)
- [23] Weaver Christopher S and Turner Sean H. Dual Fuel Natural Gas/Diesel Engines: Technology, Performance, and Emissions. In *SAE Technical Papers*, mar 1994. (cited in p. 30)
- [24] Kubesh John and Brehob Diana D. Analysis of Knock in a Dual-Fuel Engine. In *SAE Technical Papers*, oct 1992. (cited in p. 31)
- [25] Olsson Jan-Ola, Tunestål Per, Haraldsson Göran and Johansson Bengt. A Turbo Charged Dual Fuel HCCI Engine. In *SAE Technical Papers*, number 724, may 2001. (cited in pp. 10 and 31)
- [26] Kokjohn Sage L., Hanson Reed M., Splitter Derek A. and Reitz Rolf D. Experiments and modeling of dual-fuel HCCI and PCCI combustion using in-cylinder fuel blending. *SAE International Journal of Engines*, Vol. 2 n° 2, pp. 24–39, nov 2010. (cited in pp. 31, 96, and 151)
- [27] Hanson Reed M., Kokjohn Sage L., Splitter Derek A. and Reitz Rolf D. An experimental investigation of fuel reactivity controlled PCCI combustion in a heavy-duty engine. *SAE Technical Papers*, Vol. 3 n° 1, pp. 700–716, 2010. (cited in p. 31)
- [28] Kokjohn S L, Hanson R M, Splitter D A and Reitz R D. Fuel reactivity controlled compression ignition (RCCI): a pathway to controlled high-efficiency clean combustion. *International Journal of Engine Research*, Vol. 12 n° 3, pp. 209–226, 2011. (cited in pp. 31, 77, and 184)
- [29] Desantes José M., Benajes Jesús, García Antonio and Monsalve-Serrano Javier. The role of the in-cylinder gas temperature and oxygen concentration over low load reactivity controlled compression ignition combustion efficiency. *Energy*, Vol. 78, pp. 854–868, 2014. (cited in pp. 31, 96, 151, and 157)
- [30] Wu Yifeng and Reitz Rolf D. Effects of Exhaust Gas Recirculation and Boost Pressure on Reactivity Controlled Compression Ignition Engine at High Load Operating Conditions. *Journal of Energy Resources Technology*, Vol. 137 n° 3, pp. 032210, may 2015. (cited in p. 31)
- [31] Li Yaopeng, Jia Ming, Chang Yachao, Xu Zhen, Xu Guangfu, Liu Hong and Wang Tianyou. Principle of determining the optimal operating parameters based on fuel properties and initial conditions for RCCI engines. *Fuel*, Vol. 216 n° October 2017, pp. 284–295, mar 2018. (cited in p. 31)
- [32] Splitter Derek, Hanson Reed, Kokjohn Sage, Wissink Martin and Reitz Rolf D. Injection Effects in Low Load RCCI Dual-Fuel Combustion. In *SAE Technical Paper*, sep 2011. (cited in p. 31)
- [33] Wissink Martin L, Lim Jae Hyung, Splitter Derek A, Hanson Reed M. and Reitz Rolf D. Investigation of Injection Strategies To Improve High Efficiency RCCI combustion with diesel and gasoline direct injection. *Asme Icef2012-92107*, pp. 1–12, 2012. (cited in p. 31)

-
- [34] Nazemi M. and Shahbakhti M. Modeling and analysis of fuel injection parameters for combustion and performance of an RCCI engine. *Applied Energy*, Vol. 165, pp. 135–150, mar 2016. (cited in p. 31)
- [35] Li Jing, Ling Xiang, Liu Deng, Yang Wenming and Zhou Dezhi. Numerical study on double injection techniques in a gasoline and biodiesel fueled RCCI (reactivity controlled compression ignition) engine. *Applied Energy*, Vol. 211 n° August 2017, pp. 382–392, feb 2018. (cited in p. 31)
- [36] Hanson Reed, Kokjohn Sage, Splitter Derek and Reitz Rolf D. Fuel Effects on Reactivity Controlled Compression Ignition (RCCI) Combustion at Low Load. *SAE International Journal of Engines*, Vol. 4 n° 1, pp. 394–411, 2011. (cited in pp. 31 and 185)
- [37] Splitter Derek, Hanson Reed, Kokjohn Sage and Reitz Rolf D. Reactivity Controlled Compression Ignition (RCCI) Heavy-Duty Engine Operation at Mid-and High-Loads with Conventional and Alternative Fuels. In *SAE 2011 World Congress and Exhibition*, volume 1, apr 2011. (cited in p. 31)
- [38] Benajes Jesús, Molina Santiago, García Antonio and Monsalve-Serrano Javier. Effects of low reactivity fuel characteristics and blending ratio on low load RCCI (reactivity controlled compression ignition) performance and emissions in a heavy-duty diesel engine. *Energy*, Vol. 90, pp. 1261–1271, 2015. (cited in p. 31)
- [39] Hanson Reed, Curran Scott, Wagner Robert, Kokjohn Sage, Splitter Derek and Reitz Rolf D. Piston Bowl Optimization for RCCI Combustion in a Light-Duty Multi-Cylinder Engine. *SAE International Journal of Engines*, Vol. 5 n° 2, pp. 286–299, 2012. (cited in p. 32)
- [40] Splitter Derek, Wissink Martin, Kokjohn Sage and Reitz Rolf D. Effect of Compression Ratio and Piston Geometry on RCCI Load Limits and Efficiency. *SAE Technical Paper*, 2012. (cited in p. 32)
- [41] Kokjohn Sage, Hanson Reed, Splitter Derek, Kaddatz John and Reitz Rolf. Fuel Reactivity Controlled Compression Ignition (RCCI) Combustion in Light- and Heavy-Duty Engines. *SAE International Journal of Engines*, Vol. 4 n° 1, pp. 360–374, apr 2011. (cited in p. 32)
- [42] Doosje Erik, Willems Frank and Baert Rik. Experimental demonstration of RCCI in heavy-duty engines using diesel and natural gas. *SAE Technical Papers*, Vol. 1, 2014. (cited in p. 32)
- [43] Lim Jae Hyung and Reitz Rolf D. High Load (21 Bar IMEP) Dual Fuel RCCI Combustion Using Dual Direct Injection. *Journal of Engineering for Gas Turbines and Power*, Vol. 136 n° 10, pp. 101514, 2014. (cited in p. 32)
- [44] Benajes Jesús, Pastor José V., García Antonio and Boronat Vicente. A RCCI operational limits assessment in a medium duty compression ignition engine using an adapted compression ratio. *Energy Conversion and Management*, Vol. 126, pp. 497–508, 2016. (cited in pp. 32 and 49)

- [45] Dempsey Adam B., Walker N. Ryan, Gingrich Eric and Reitz Rolf D. Comparison of low temperature combustion strategies for advanced compression ignition engines with a focus on controllability. *Combustion Science and Technology*, Vol. 186 n° 2, pp. 210–241, 2014. (cited in pp. 10, 32, and 87)
- [46] Li Jing, Yang Wenming and Zhou Dezhi. Review on the management of RCCI engines. *Renewable and Sustainable Energy Reviews*, Vol. 69 n° May 2016, pp. 65–79, 2017. (cited in pp. 10, 32, and 155)
- [47] Benajes Jesús, Molina Santiago, García Antonio and Monsalve-Serrano Javier. Effects of direct injection timing and blending ratio on RCCI combustion with different low reactivity fuels. *Energy Conversion and Management*, Vol. 99, pp. 193–209, 2015. (cited in pp. 32, 109, 157, and 185)
- [48] DelVescovo Dan, Kokjohn Sage and Reitz Rolf. The Effects of Charge Preparation, Fuel Stratification, and Premixed Fuel Chemistry on Reactivity Controlled Compression Ignition (RCCI) Combustion. *SAE International Journal of Engines*, Vol. 10 n° 4, pp. 1491–1505, 2017. (cited in pp. 32, 96, 112, 127, and 157)
- [49] Splitter Derek, Wissink Martin, DelVescovo Dan and Reitz Rolf D. RCCI Engine Operation Towards 60% Thermal Efficiency. *SAE Technical Paper Series*, Vol. 1 n° X, 2013. (cited in p. 32)
- [50] Benajes Jesús, Molina Santiago, García Antonio, Belarte Eduardo and Vanvolsem Michel. An investigation on RCCI combustion in a heavy duty diesel engine using in-cylinder blending of diesel and gasoline fuels. *Applied Thermal Engineering*, Vol. 63 n° 1, pp. 66–76, 2014. (cited in pp. 32 and 184)
- [51] Molina S., Garcia A., Pastor J. M., Belarte E. and Balloul I. Operating range extension of RCCI combustion concept from low to full load in a heavy-duty engine. *Applied Energy*, Vol. 143, pp. 211–227, 2015. (cited in p. 32)
- [52] Benajes Jesús, Pastor José V., García Antonio and Monsalve-Serrano Javier. The potential of RCCI concept to meet EURO VI NO_x limitation and ultra-low soot emissions in a heavy-duty engine over the whole engine map. *Fuel*, Vol. 159, pp. 952–961, 2015. (cited in p. 32)
- [53] Wang Yifeng, Yao Mingfa, Li Tie, Zhang Weijing and Zheng Zunqing. A parametric study for enabling reactivity controlled compression ignition (RCCI) operation in diesel engines at various engine loads. *Applied Energy*, Vol. 175, pp. 389–402, 2016. (cited in pp. 32 and 157)
- [54] Reitz Rolf D. and Duraisamy Ganesh. Review of high efficiency and clean reactivity controlled compression ignition (RCCI) combustion in internal combustion engines. *Progress in Energy and Combustion Science*, Vol. 46, pp. 12–71, 2015. (cited in p. 32)
- [55] Boronat Colomer Vicente. *Dual-Fuel Dual-Mode combustion strategy to achieve high thermal efficiency, low NO_x and smoke emissions in compression ignition engines*. PhD Thesis, Universitat Politècnica de València, 2018. (cited in pp. 32 and 51)

-
- [56] Benajes Jesus, Garcia Antonio, Monsalve-Serrano Javier and Boronat Vicente. Achieving clean and efficient engine operation up to full load by combining optimized RCCI and dual-fuel diesel-gasoline combustion strategies. *Energy Conversion and Management*, Vol. 136, pp. 142–151, 2017. (cited in pp. 32 and 155)
- [57] Lago Sari Rafael. *Dual Mode Dual Fuel Combustion: Implementation on a Real Medium Duty Engine Platform*. PhD Thesis, Universitat Politècnica de València, 2021. (cited in pp. 33 and 51)
- [58] Paykani Amin, Garcia Antonio, Shahbakhti Mahdi, Rahnama Pourya and Reitz Rolf D. Reactivity controlled compression ignition engine: Pathways towards commercial viability. *Applied Energy*, Vol. 282 n° PA, pp. 116174, jan 2021. (cited in pp. 33 and 168)
- [59] Chiang C. J. and Stefanopoulou A. G. Dynamics of homogeneous charge compression ignition (HCCI) engines with high dilution. *Proceedings of the American Control Conference*, Vol. 15 n° 2, pp. 2979–2984, 2007. (cited in p. 33)
- [60] Haraldsson Göran, Tunestål Per, Johansson Bengt and Hyvönen Jari. HCCI Closed-Loop Combustion Control Using Fast Thermal Management. In *SAE Technical Paper Series*. SAE International, mar 2004. (cited in p. 34)
- [61] Haraldsson Göran, Tunestål Per, Johansson Bengt and Hyvönen Jari. Transient Control of a Multi Cylinder HCCI Engine During a Drive Cycle. In *SAE Technical Paper Series*, apr 2005. (cited in p. 34)
- [62] Bengtsson Johan, Strandh Petter, Johansson Rolf, Tunestål Per and Johansson Bengt. Multi-Output Control of a Heavy Duty HCCI Engine Using Variable Valve Actuation and Model Predictive Control. In *SAE Technical Paper Series*, apr 2006. (cited in p. 34)
- [63] Shahbakhti Mahdi and Koch Charles Robert. Control oriented modeling of combustion phasing for an HCCI engine. *Proceedings of the American Control Conference*, n° Ivc, pp. 3694–3699, 2007. (cited in pp. 34 and 152)
- [64] Shahbakhti Mahdi and Koch Charles Robert. Physics Based Control Oriented Model for HCCI Combustion Timing. *Journal of Dynamic Systems, Measurement, and Control*, Vol. 132 n° 2, pp. 021010, 2010. (cited in pp. 34 and 148)
- [65] Ebrahimi Khashayar and Koch Charles Robert. HCCI combustion timing control with Variable Valve Timing. In *2013 American Control Conference*, pp. 4429–4434. IEEE, jun 2013. (cited in p. 34)
- [66] Fathi Morteza, Jahanian Omid and Shahbakhti Mahdi. Modeling and controller design architecture for cycle-by-cycle combustion control of homogeneous charge compression ignition (HCCI) engines – A comprehensive review. *Energy Conversion and Management*, Vol. 139, pp. 1–19, 2017. (cited in pp. 12 and 34)
- [67] Hall Carrie and Kassa Mateos. Advances in combustion control for natural gas–diesel dual fuel compression ignition engines in automotive applications: A review. *Renewable and Sustainable Energy Reviews*, Vol. 148 n° August 2020, sep 2021. (cited in p. 34)

- [68] Martin Jonathan and Boehman André. Mapping the combustion modes of a dual-fuel compression ignition engine. *International Journal of Engine Research*, may 2021. (cited in p. 34)
- [69] Willems Frank. Is Cylinder Pressure-Based Control Required to Meet Future HD Legislation? *IFAC-PapersOnLine*, Vol. 51 n° 31, pp. 111–118, 2018. (cited in pp. 12, 34, 55, and 88)
- [70] Ravaglioli Vittorio, Carra Filippo, Moro Davide, De Cesare Matteo and Stola Federico. Remote Sensing Methodology for the Closed-Loop Control of RCCI Dual Fuel Combustion. In *SAE Technical Papers*, volume 2018-April, pp. 1–10, apr 2018. (cited in pp. 34 and 88)
- [71] Olsson Jan-ola, Tunestål Per and Johansson Bengt. Closed-Loop Control of an HCCI Engine. In *SAE Technical Paper*, mar 2001. (cited in pp. 12, 34, 35, and 37)
- [72] Strandh Petter, Bengtsson Johan, Johansson Rolf, Tunestål Per and Johansson Bengt. Cycle-to-Cycle Control of a Dual-Fuel HCCI Engine. In *SAE Technical Paper*, volume 2004, mar 2004. (cited in pp. 34, 37, and 148)
- [73] Bengtsson Johan, Strandh Petter, Johansson Rolf, Tunestål Per and Johansson Bengt. Model predictive control of homogeneous charge compression ignition (HCCI) engine dynamics. *Computer Aided Control System Design, 2006 IEEE International Conference on Control Applications, 2006 IEEE International Symposium on Intelligent Control, 2006 IEEE*, pp. 1675–1680, 2006. (cited in pp. 12, 34, and 37)
- [74] Bidarvatan M., Shahbakhti M., Jazayeri S. A. and Koch C. R. Cycle-to-cycle modeling and sliding mode control of blended-fuel HCCI engine. *Control Engineering Practice*, Vol. 24 n° 1, pp. 79–91, 2014. (cited in pp. 34 and 37)
- [75] Ott T., Zurbriggen F., Onder C. and Guzzella L. Cylinder Individual Feedback Control of Combustion in a Dual Fuel Engine. *IFAC Proceedings Volumes*, Vol. 46 n° 21, pp. 600–605, 2013. (cited in pp. 34, 37, and 121)
- [76] Hanson Reed and Reitz Rolf. Transient RCCI Operation in a Light-Duty Multi-Cylinder Engine. *SAE International Journal of Engines*, Vol. 6 n° 3, pp. 1694–1705, 2013. (cited in pp. 35 and 38)
- [77] Arora Jayant Kumar and Shahbakhti Mahdi. Real-Time Closed-Loop Control of a Light-Duty RCCI Engine During Transient Operations. In *SAE Technical Paper*, mar 2017. (cited in pp. 35, 38, 55, and 89)
- [78] Khodadadi Sadabadi K., Shahbakhti M., Bharath A. N. and Reitz R. D. Modeling of combustion phasing of a reactivity-controlled compression ignition engine for control applications. *International Journal of Engine Research*, Vol. 17 n° 4, pp. 421–435, 2016. (cited in pp. 36, 150, 151, and 152)
- [79] Sui Wenbo, González Jorge Pulpeiro and Hall Carrie M. Combustion Phasing Modelling of Dual Fuel Engines. *IFAC-PapersOnLine*, Vol. 51 n° 31, pp. 319–324, 2018. (cited in p. 36)

-
- [80] Bekdemir Cemil, Baert Rik, Willems Frank and Somers Bart. Towards Control-Oriented Modeling of Natural Gas-Diesel RCCI Combustion. In *SAE Technical Paper*, apr 2015. (cited in pp. 36 and 38)
- [81] Indrajuna Armando, Bekdemir Cemil, Luo Xi and Willems Frank. Robust Multivariable Feedback Control of Natural Gas-Diesel RCCI Combustion. *IFAC-PapersOnLine*, Vol. 49 n° 11, pp. 217–222, 2016. (cited in pp. 36 and 38)
- [82] Indrajuna Armando, Bekdemir Cemil, Feru Emanuel and Willems Frank. Towards Model-Based Control of RCCI-CDF Mode-Switching in Dual Fuel Engines. In *SAE Technical Paper*, pp. 1–13, apr 2018. (cited in pp. 36 and 38)
- [83] Divekar Prasad, Han Xiaoye, Tan Qingyuan, Asad Usman, Yanai Tadanori, Chen Xiang, Tjong Jimi and Zheng Ming. Mode Switching to Improve Low Load Efficiency of an Ethanol-Diesel Dual-Fuel Engine. *SAE Technical Paper*, 2017. (cited in p. 36)
- [84] Willems Frank, Kupper Frank, Ramesh Sudarshan, Indrajuna Armando and Doosje Erik. Coordinated Air-Fuel Path Control in a Diesel-E85 RCCI Engine. In *SAE Technical Paper*, pp. 1–11, apr 2019. (cited in pp. 36, 38, and 148)
- [85] Khodadadi Sadabadi Kaveh and Shahbakhti Mahdi. Dynamic Modelling and Controller Design of Combustion Phasing for an RCCI Engine. In *Volume 2: Mechatronics; Mechatronics and Controls in Advanced Manufacturing; Modeling and Control of Automotive Systems and Combustion Engines; Modeling and Validation; Motion and Vibration Control Applications; Multi-Agent and Networked Systems; Path Pla.* American Society of Mechanical Engineers, oct 2016. (cited in pp. 36, 38, and 106)
- [86] Kondipati Naga Nithin Teja, Arora Jayant Kumar, Bidarvatan Mehran and Shahbakhti Mahdi. Modeling, design and implementation of a closed-loop combustion controller for an RCCI engine. In *2017 American Control Conference (ACC)*, pp. 4747–4752. IEEE, may 2017. (cited in pp. 36, 38, 147, and 150)
- [87] Raut Akshat, Bidarvatan Mehran, Borhan Hoseinali and Shahbakhti Mahdi. Model Predictive Control of an RCCI Engine. In *2018 Annual American Control Conference (ACC)*, pp. 1604–1609. IEEE, jun 2018. (cited in pp. 36, 106, 148, and 157)
- [88] Raut A., Irdmoussa B.K. and Shahbakhti M. Dynamic modeling and model predictive control of an RCCI engine. *Control Engineering Practice*, Vol. 81 n° June, pp. 129–144, dec 2018. (cited in pp. 36 and 38)
- [89] Irdmoussa B K, Rizvi Syed Z, Velni J Mohammadpour, Naber J D and Shahbakhti M. Data-driven Modeling and Predictive Control of Combustion Phasing for RCCI Engines. *2019 American Control Conference (ACC)*, pp. 1617–1622, 2019. (cited in pp. 36 and 39)
- [90] Basina L. N. Aditya, Irdmoussa Behrouz K., Velni Javad Mohammadpour, Borhan Hoseinali, Naber Jeffrey D. and Shahbakhti Mahdi. Data-driven Modeling and Predictive Control of Maximum Pressure Rise Rate in RCCI Engines. In *2020 IEEE*

- Conference on Control Technology and Applications (CCTA)*, pp. 94–99. IEEE, aug 2020. (cited in pp. 36 and 39)
- [91] Chang Kyoungjoon, Lavoie George A., Babajimopoulos Aristotelis, Filipi Zoran and Assanis Dennis N. Control of a Multi-Cylinder HCCI Engine During Transient Operation by Modulating Residual Gas Fraction to Compensate for Wall Temperature Effects. In *SAE Technical Papers*, apr 2007. (cited in p. 37)
- [92] Chiang Cha Jui, Stefanopoulou Anna G. and Janković Mrdjan. Nonlinear observer-based control of load transitions in homogeneous charge compression ignition engines. *IEEE Transactions on Control Systems Technology*, Vol. 15 n° 3, pp. 438–448, 2007. (cited in p. 37)
- [93] Batool Sadaf, Naber Jeffrey D. and Shahbakhti Mahdi. Multi-mode Low Temperature Combustion (LTC) and Mode Switching Control. In *Energy, Environment, and Sustainability*, pp. 43–93. Springer Nature, 2022. (cited in p. 37)

Chapter 3

Experimental setup and data processing

The experiments presented in this thesis were carried out on medium-duty engines in test cells from the CMT-Motores Térmicos research and development laboratory in the Universitat Politècnica de València. These engines were modified to run in dual-fuel operation and various mixture stratification levels were explored. In order to provide a better understanding of the tools used in this work, this chapter details the engines, the measured signals, the acquisition instruments and the devices used for controlling the engines, as well as a more detailed description of the in-cylinder pressure signal, from its acquisition to its processing and analysis.

3.1 Engines

Two compression ignited (CI) engines, which specifications can be found in Table 3.1, were used in this work. These two engines shared a common cylinder architecture and only the number of cylinders was initially differing. Both engines, originally designed to run on conventional diesel combustion (CDC), were equipped with additional port fuel injectors in the intake manifold runners in order to perform dual-fuel combustion operation. Aiming at extending the operating range of the dual-fuel concept, the pistons were machined to lower the compression ratio (the nominal value being 17.5:1) [1]. Hereafter, further details about engine A and B, thereby identified in this manuscript, are provided.

Engine A In order to evaluate the dual-fuel combustion concept in a controlled and precise environment, engine A was modified in a hybrid single-cylinder engine

Table 3.1: Engines specifications.

Engine		A	B
Bore	[mm]	110	
Stroke	[mm]	135	
Connecting-rod length	[mm]	212.5	
Number of cylinders	[-]	4	6
Total displacement	[dm ³]	5.1	7.7
Compression ratio	[-]	15.3:1	12.2:1

(SCE) by isolating one cylinder for dual-fuel combustion operation, hence avoiding cylinder-to-cylinder dispersion effect on the combustion metrics and emissions measurement. Only this specific cylinder received therefore dedicated equipment to carry out dual-fuel combustion investigation (e.g., machined piston, port fuel injector, diesel fuel supply), while the rest of the cylinders were kept with the stock configuration and control (e.g., common-rail, turbocharger). This design approach, between a multi-cylinder engine (MCE) and a SCE, provides a cost effective solution to conventional SCE research, although it does not allow to obtain brake (torque-based) results as the dynamometer measures the whole engine performance. Indeed, in this case, the three other cylinders were controlled in CDC by the stock engine control unit (ECU) to compensate forces on the crankshaft by balancing the cylinder-to-cylinder load. Nonetheless, indicated quantities, obtained from the in-cylinder pressure signal measurement, allowed to study the combustion concept.

To achieve stable operation of the gas-exchange system, the air-loop used for the single-cylinder part of engine A was separated from the stock engine. The original high-pressure (HP) exhaust gas recirculation (EGR) loop was removed from the stock engine to compensate the flow loss from the isolated cylinder (each part of the engine has its own exhaust line). A dedicated air supply line was used for the dual-fuel single-cylinder, and an EGR line was installed between its exhaust and intake manifolds to provide the desired air dilution.

Engine B Engine B was used to evaluate the dual-fuel combustion concept in a multi-cylinder engine configuration. Each cylinder was therefore equipped with a port fuel injector, and the air management was ensured by the stock configuration which includes a variable-geometry turbine (VGT) turbocharger, to provide the required boost pressure, and a cooled high-pressure exhaust gas recirculation

Table 3.2: Fuel properties.

		Diesel	Gasoline
Research octane number (RON)	[-]	-	95
Motor octane number (MON)	[-]	-	85
Cetane number (CN)	[-]	51	-
Low heating value (LHV)	[MJ/kg]	42.8	42.4

loop. To further expand the air dilution capabilities for this engine, and evaluate various EGR scenarios, a low-pressure EGR (LP-EGR) path was added between the turbine outlet and the compressor inlet. The direct injection was assigned to the original common rail configuration.

Fuels In the present study, the fuels used by both engines were regular gasoline as the port fuel injected low reactivity fuel (LRF), and diesel as the high reactivity fuel (HRF) for the direct injection, whose main properties are listed in Table 3.2.

3.2 Instrumentation and signals

Both engines were installed in a fully instrumented test cell and equipped with various sensors and actuators to run the engines under a wide range of operating conditions. From now on, unless specified, *engine A* refers to the SCE part of this same engine, and the instrumentation and equipment are therefore detailed for the dual-fuel SCE application. Figure 3.1 and figure 3.2 illustrate the respective engine layout. Details about the instrumentation and signals are provided hereinafter, and additional information about the sensors is listed in Table 3.3. Note that these figures only give an overview of the engines instrumentation and implementation. More details can be found in [2] and [3] for engine A and B, respectively.

Dynamometer The engines were connected to an ELIN INDY 44/4Z dynamometer which has an engine speed range from 0 to 4200 rpm and can handle up to 440 kW of load. This dynamometer maintains the engine at the desired engine speed and provides a measurement of the torque delivered by the engine as well.

Gas-exchange The desired boosted air was supplied to engine A by a dedicated screw compressor, while the VGT was used for engine B. For the air dilution, the EGR flow rate was regulated by a valve placed between the inlet and the outlet of

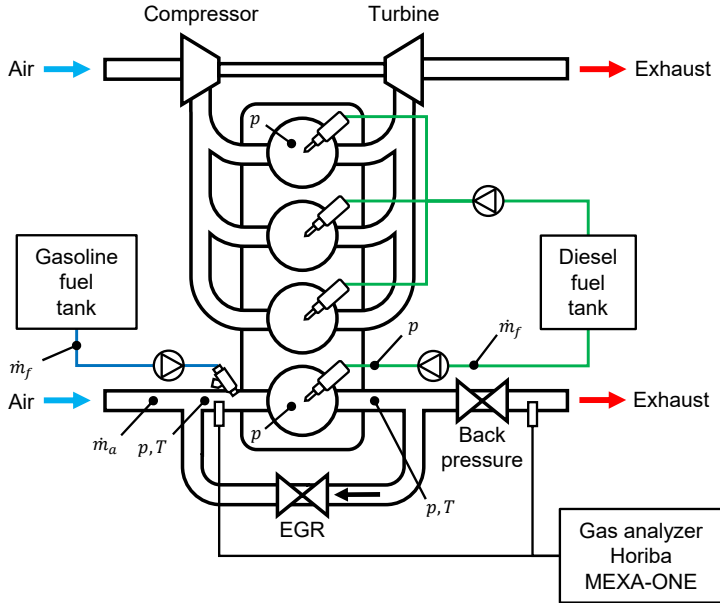


Figure 3.1: Scheme of the engine A layout with equipment and measurements indication: pressures p , temperatures T , air mass flow \dot{m}_a , and fuel consumption \dot{m}_f . A valve is used for the back pressure, and another one for the exhaust gas recirculation (EGR). The in-cylinder pressure in the cylinder from the MCE part of this engine is used to measure the combustion evolution and for balancing the cylinder-to-cylinder load with the SCE part.

Table 3.3: Sensors specifications summary.

Sensor	Model	Measurement range	Accuracy
Air flow meter	Eng. A: Elster RVG G100	1-160 m ³ /h	±1-2%
	Eng. B: Sensycon	0-2400 kg/h	n/a
Fuel flow meter	AVL 733S fuel balance	0-150 kg/h	0.12%
Lambda	Bosch LSU 4.9	0.65 to air	±0.01-0.05
Pressure	Kistler 4045A10	0-10 bar	≤ ±0.1%FSO*
Temperature	Type K thermocouples	0-1100°C	±2.5°C
	PT100 thermoresistances	-200°C to +650°C	±0.3°C
In-cylinder pressure	Kistler 6125C	0-300 bar	≤ ±0.4%FSO*

* Full scale output linearity

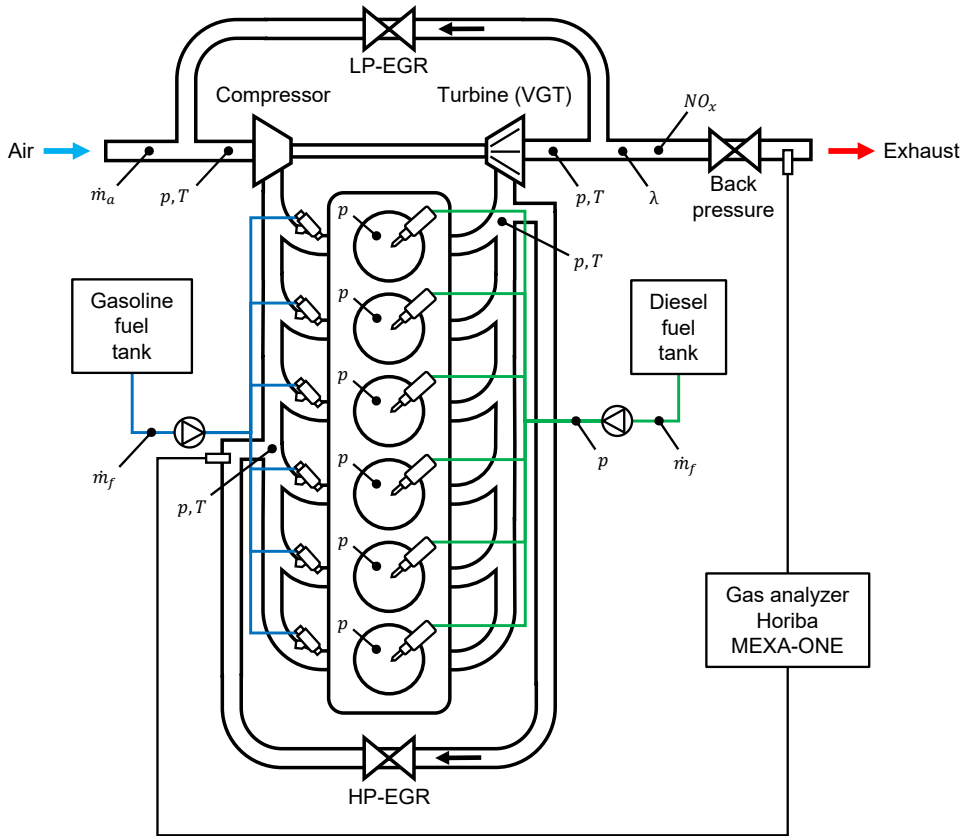


Figure 3.2: Scheme of the engine B layout with equipment and measurements indication: pressures p , temperatures T , air mass flow \dot{m}_a , fuel consumption \dot{m}_f , air-fuel ratio λ , and nitrogen oxides NO_x . A valve is used for the back pressure, and two other for the low-pressure (LP) and high-pressure (HP) exhaust gas recirculation (EGR).

the recirculation line. In the case of engine A, one valve was used for the EGR, and two valves were installed for engine B (LP and HP-EGR). Both engines had an additional back pressure (BP) valve at the exhaust line mounted after the exhaust gas recirculation line. In the case of engine A, this valve was used to replicate the counter pressure created by the turbine in a conventional configuration, while in engine B, it aimed to create further back pressure to force the exhaust gases to flow through the LP-EGR line.

Fuel injection Both engines were supplied with solenoid direct injection (DI) injectors in all the cylinders, which were coupled to the high pressure diesel common-rail, with the exception of engine A where a separated fuel supply was installed

for the SCE diesel direct injector. An additional fuel pump, fuel tank, fuel consumption balance, and fuel filter were added to the engine test cell facilities for the gasoline port fuel injection system to undertake the dual-fuel investigation. As previously mentioned, only one cylinder was equipped with an injector for port fuel injection (PFI) in engine A, while each cylinder intake runner received a PFI injector in engine B. Both diesel and gasoline fuel lines were mounted with pressure sensors to monitor the fuel pressure applied to the injectors.

Air flow The air mass flow in engine A was measured using the air pressure and temperature together with the volumetric flow rate provided by an Elster RVG G100 meter. In the case of engine B, a Sensycon mass flow meter with a measuring range from 0 to 2400 kg/h was placed before the compressor.

Fuel flow Gasoline and diesel fuel flows were measured by two AVL 733S dynamic fuel meter.

Air-fuel equivalence ratio In both engines, the air-fuel equivalence ratio (AFR) was evaluated from the ratio of the measured air to fuel mass flows, and from the value provided by the exhaust gas analyzer which is based on the emissions monitoring. Engine B embedded an additional lambda (λ) sensor after the turbine outlet.

In-cylinder pressure sensor In both engines, the in-cylinder pressure signal was measured by a Kistler 6125C piezoelectric transducer which was connected to a Kistler type 5011 charge amplifier. Engine A had one sensor for the SCE cylinder and another one in one of the three cylinders from the MCE part. The latter was used to help the manual balancing of the cylinder-to-cylinder load dispersion when performing the experiments, as previously mentioned. By modifying the injection settings in the MCE, thanks to its ECU, similar maximum cylinder pressure, load and combustion phasing than in the dual-fuel single cylinder were obtained. In the case of engine B, the six cylinders were equipped with a pressure transducer. Next section provides a description of this signal as its acquisition and processing are at the core of the presented work.

Pressure and temperature sensors Various pressure and temperature sensors were placed along the intake and exhaust lines to measure the engine operating conditions. The pressure evaluation consisted in Kistler type 4045A10 piezoresistive absolute pressure sensors connected to Kistler type 4603 charge amplifiers,

while the temperature measurement was assigned to type K thermocouples and PT100 thermoresistances.

Exhaust emissions A MEXA-ONE-D1-EGR exhaust gas analyzer from HORIBA was used to measure the HC, CO, NO_x, O₂ and CO₂ levels at the exhaust. An additional CO₂ probe was placed in the intake manifold to evaluate the EGR rate as:

$$EGR = \frac{[CO_2]_{int} - [CO_2]_{atm}}{[CO_2]_{exh} - [CO_2]_{atm}} \quad (3.1)$$

where *int*, *exh* and *atm* stand for *intake*, *exhaust* and *atmospheric*, respectively, and $[CO_2]_{atm}$ was considered equal to 0.04%. Due to the slow gas analyzer response, in the case of engine B, a NO_x sensor was added after the turbine to enhance the nitrogen oxides monitoring under transient conditions.

3.3 In-cylinder pressure signal

With the increasing complexity of the combustion concepts introduced in the recent years as a response to the stringent emissions regulations, a proper evaluation of the combustion process is more than ever crucial to properly understand the outcomes and leverage their potential. While the majority of the traditional sensors such as manifolds pressure and temperature, or exhaust probes such as the lambda sensor, allow to evaluate the engine operating conditions, they fail to accurately characterize the combustion reactions inside the cylinder. One way to overcome this barrier is to use an in-cylinder pressure sensor.

The in-cylinder pressure signal is among the most important signals in combustion engines research and development. Indeed, this signal allows to get a direct insight into what is happening inside the cylinder, which explains why it is traditionally measured in research applications. Commonly used for off-line processing, this signal is gaining more interest in series applications for its potential to enhance on-line combustion engines operation. Furthermore, in the case of low temperature combustion, where low controllability was encountered and high resonance levels detected, in-cylinder pressure measurement could improve the implementation of such concepts [4, 5]. The in-cylinder pressure signal has found its place in many applications and is still widely used in present investigation: from providing a direct feedback of the engine operation for cycle-to-cycle [6–8] and in-cycle [9, 10] closed-loop controllers, knock detection and control [11–13], to emissions estimation [14–16].

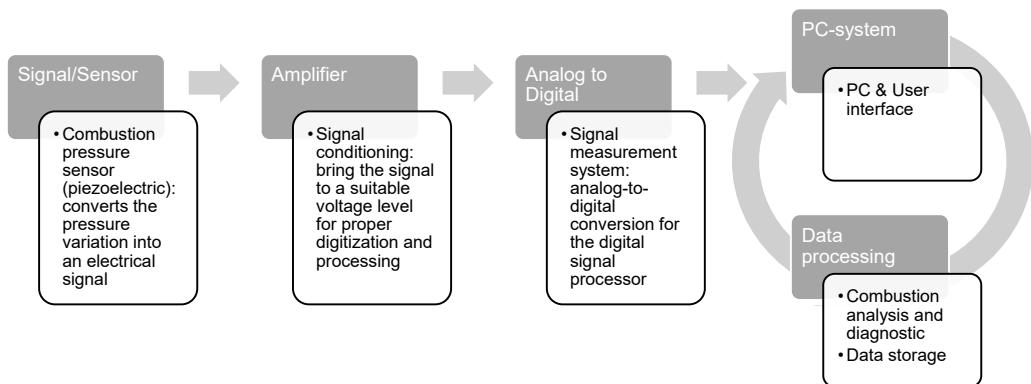


Figure 3.3: Conventional workflow of the in-cylinder pressure signal acquisition and processing.

3.3.1 Signal acquisition

The in-cylinder pressure signal is traditionally measured by a piezoelectric pressure transducer which converts the mechanical force created from the pressure variation in the cylinder into an electrical signal that can be measured. This analog signal must then be digitized in order to be processed by the data acquisition hardware. The typical workflow of the combustion measurement can be summarized by the process shown in Figure 3.3 (the reader is invited to refer to the book *Engine Combustion: Pressure Measurement and Analysis* from David Rogers [17] for a detailed and comprehensive description of the pressure measurement technology in combustion engines). A modification was made in the right part of this figure according to the configuration used in this thesis. When implemented into a real-time application, the data processing and the display through the personal computer (PC) user interface enter into a loop where the in-cylinder pressure signal might be processed on-line (and not simply stored and analyzed later), and the combustion diagnostic and metrics are therefore displayed in real-time.

The two most important features in the in-cylinder pressure acquisition are the analog-to-digital converter resolution, i.e., the number of bits per measurement, and the sampling frequency, i.e., the number of samples (measurements) per second. While the former participates to the signal measurement accuracy and is fixed by the hardware characteristics, the latter can be tuned according to the desired acquisition application, and the hardware specifications. In the case of the in-cylinder pressure acquisition, two approaches can be mentioned for the sampling frequency: time-based and crank angle-based.

Most of the combustion engines investigation make use of the crank angle-based solution with an angular encoder in order to phase the in-cylinder pressure signal with the crank position (i.e., piston position and cylinder volume) throughout the engine cycle. In this case, the encoder is used as an external digital clock which, in the end, provides the sampling frequency f_s (in Hz) according to its resolution r_s (in samples/crank angle degree), i.e., the number of encoder signal edges within one crank angle degree (CAD), and the engine speed N (in rpm) such as:

$$f_s = 6Nr_s \quad (3.2)$$

where the encoder resolution r_s is an important factor that affects the observable frequency range of the in-cylinder pressure signal and should therefore be set accordingly (i.e., Nyquist–Shannon sampling theorem). In addition, a triggering edge from a once-per-cycle trigger signal should also be provided to acquire the in-cylinder pressure signal at the same position from one experiment to the other and to reference the top dead center (TDC) position. For detailed combustion analysis, the proper TDC determination from the acquired in-cylinder pressure signal is an important aspect of the data processing in order to phase it with the volume evolution, as most of the calculations depend on these two quantities (see section 3.5). The thermodynamic TDC offset should therefore also be taken into account when processing the cylinder pressure signal [18–20]. Figure 3.4 illustrates the principle behind the in-cylinder pressure acquisition where the in-cylinder pressure and volume signals are already in phase. Once the top dead center position is known, a once-per-cycle signal, or similar, is also used to reference the position of the piston in the cylinder according to the combustion TDC to differentiate it from scavenging (similarly to the crankshaft and camshaft position signals in series applications [21]). This position, illustrated in Figure 3.4 by *TDC position*, is then used to physically phase the injection settings in the cylinder (e.g., injection timings).

Thereafter, events and metrics are referred to as *after* or *before* the combustion TDC, respectively aTDC and bTDC. By convention in this thesis, aTDC and bTDC are preceded by the symbol $^\circ$ to refer to the crank angle *degree*. Injection settings and combustion phasing, for instance, are reported this way. When referring to a crank angle degree value that is not referenced to the top dead center (e.g., a standard deviation) then the acronym CAD is used instead.

When performing frequency analysis (e.g., short-time Fourier transform) of the in-cylinder pressure signal, the time-based approach is preferred due to the constant time elapsed between two samples. Nonetheless, one can neglect the engine

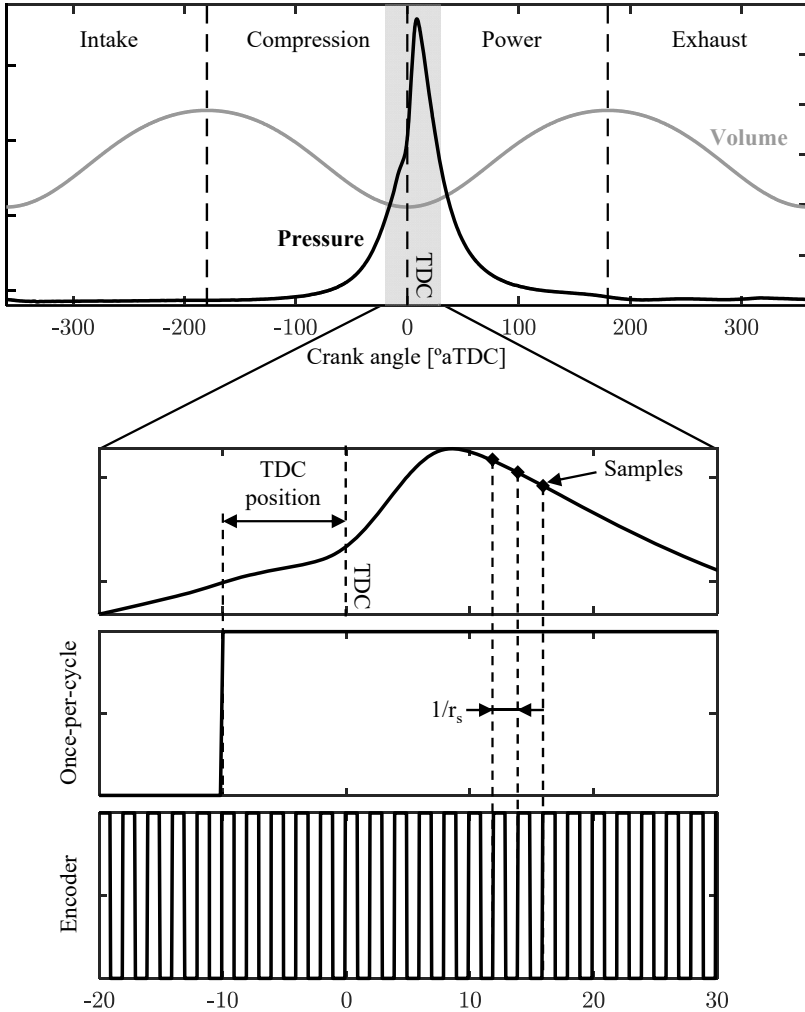


Figure 3.4: Illustration of the in-cylinder pressure signal acquisition in the crank angle domain. The research encoder signal edges provide the sampling frequency and the once-per-cycle signal allows to reference the pressure evolution according to the piston position in the cylinder.

speed fluctuations during the engine cycle [22] and therefore facilitate the time-frequency analysis of crank angle-based signals.

In this thesis, all the in-cylinder pressure traces were recorded in the crank angle domain and more information about the encoder resolution is provided later.

3.3.2 Signal processing

As it is acquired, the in-cylinder pressure signal requires to be processed to be valid for combustion analysis [23, 24]. Two main steps are required before performing combustion calculations:

- **Pegging:** by design, the piezoelectric sensor measures a change in pressure during the engine cycle inside the cylinder but does not provide an absolute pressure reading. Consequently, a zero-level correction, or *pegging*, is required. Many techniques exist to correct the pressure curve, such as referencing it with an absolute pressure sensor at the intake considering that the value measured in the cylinder at a certain crank angle (e.g., bottom dead center) is equal to the level measured by this intake pressure sensor, or by applying a thermodynamic offset fitting during the compression [25, 26]. In this thesis, the intake manifold referencing technique was selected.
- **Filtering:** the in-cylinder pressure signal decomposition through filtering is a key feature in combustion analysis [27, 28]. Figure 3.5 shows the in-cylinder pressure frequency components in three different areas of the engine cycle: compression, combustion and expansion. In the left plot, the in-cylinder pressure trace (1800 rpm and 50% load from engine B in RCCI combustion) is shown in black, and the windows of interest are illustrated in grey scale. The resulting Fourier transform for each window are shown in the right plot in a log-log scale. From this figure, it can be observed that in the compression and expansion phase, the frequencies above 200 Hz (left vertical black line) decay rapidly, compared to the combustion window where the frequency components below 3000 Hz (right vertical black line) are still representative. Above 3 kHz, the signal is characterized by peaks in the high frequency range, particularly representative between 3 and 10 kHz, associated to resonance at different modes excited by the combustion. Such observation provides a first insight into the calibration of the low-pass filter of the in-cylinder pressure signal for combustion analysis. Most of the time, the high frequency components associated to resonance are considered as noise and are removed. Nonetheless, the resonance components might also gather important information about the combustion and could therefore be processed. Hereinafter

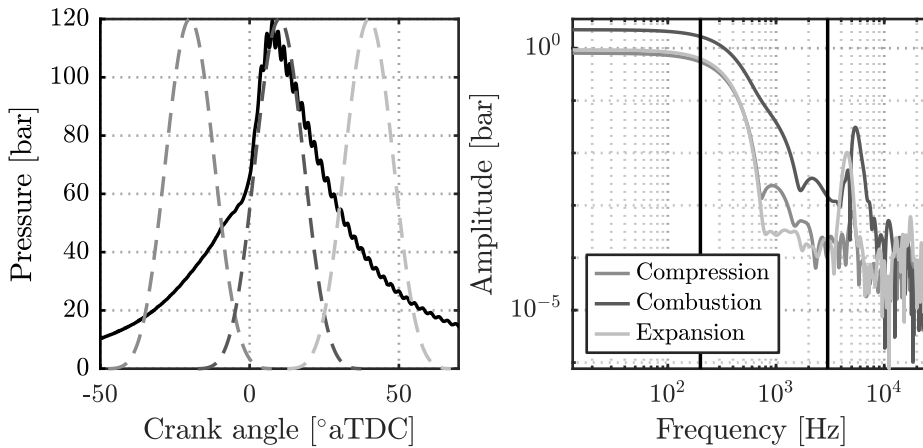


Figure 3.5: In-cylinder pressure of a conventional RCCI combustion cycle in engine B: crank-angle domain (left) and frequency domain (right) at three signal windows, namely compression, combustion, and expansion.

is provided a brief description of the resonance analysis and its contribution to the global definition of the in-cylinder pressure evaluation.

Resonance analysis

Pressure waves resulting from the combustion can be measured in the cylinder and observed in the high frequency range of the in-cylinder pressure signal. Figure 3.6 shows the decomposition of the pressure signal illustrated in Figure 3.5 into the low-pass (p_{lp}) and high-pass (p_{hp}) filtered signals tuned at 3 kHz. Pressure oscillations induced by combustion up to more than 3 bar amplitude can be observed in p_{hp} . The high-pass filtered signal is a direct representation of the pressure resonance and is therefore the main source of information for its analysis.

The resonant modes from the in-cylinder pressure in a cylindrical combustion chamber were characterized by Draper who stated that the frequency of each mode was a function of the cylinder geometry and the speed of sound such as [29]:

$$f_{i,j,g} = c \sqrt{\frac{B_{i,j}^2}{(\pi D)^2} + \frac{g^2}{2h^2}} \quad (3.3)$$

where $B_{i,j}$ and g are constants characterizing each mode, D and h are the combustion chamber bore and height, and c is the speed of sound. As the combustion

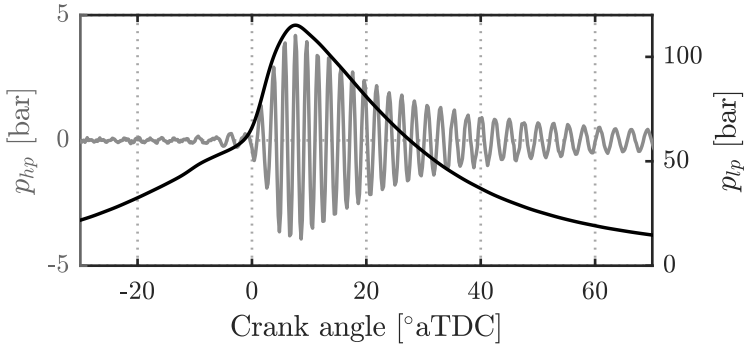


Figure 3.6: Decomposition of the in-cylinder pressure signal shown in Figure 3.5 into low-pass (p_{tp} , combustion) and high-pass (p_{hp} , pressure oscillations) signals.

Table 3.4: Bessel constants for each resonant modes: i corresponds to the circumferential modes and j to the radial modes.

$B_{i,j}$	$B_{i,0}$	$B_{i,1}$
$B_{0,j}$	3.83	7.02
$B_{1,j}$	1.84	5.33
$B_{2,j}$	3.00	6.75

occurs near the top dead center, h becomes really small and the axial modes used to be neglected [30], leading to the commonly used form of the resonant frequency calculation:

$$f_{res} = c \frac{B_{i,j}}{\pi D} \quad (3.4)$$

where the speed of sound can be calculated using the in-cylinder conditions:

$$c = \sqrt{\gamma RT} \quad (3.5)$$

and the Bessel constant $B_{i,j}$ is chosen according to the selected resonant mode (a non-exhaustive list is provided in Table 3.4 [29]).

In spark ignition (SI) engines, this resonance is traditionally associated to knock [31]. Knock corresponds to the auto-ignition of the end gas, before the flame front reaches all the combustion chamber, which excites heavily the resonant frequencies inside the cylinder. Knock can result in a thermal efficiency drop and can be responsible of engine damage [32]. Various indexes based on the analysis of the in-cylinder pressure oscillations signal were proposed over time to detect and characterize such phenomena [33–36] (note that in commercial applications,

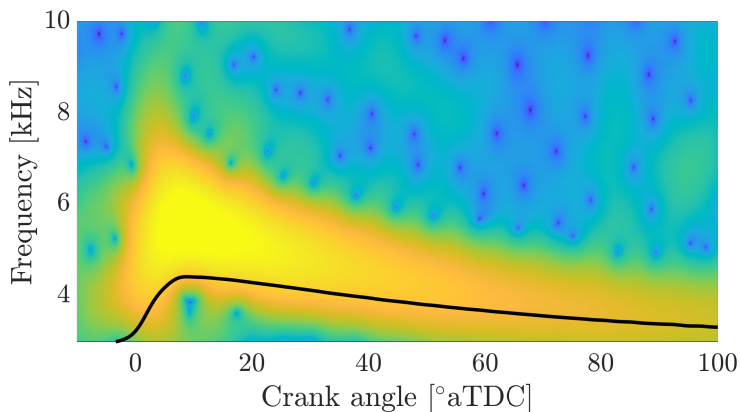


Figure 3.7: Short-time Fourier transform of a RCCI combustion cycle. The black line represents the theoretical resonant frequency of the first mode in a cylindrical combustion chamber.

such detection is traditionally performed by an accelerometer, also known as knock sensor, placed on the engine block, and not by an in-cylinder pressure sensor [37]).

Similarly, compression ignition engines with high degree of premixed charge exhibit high frequency components due to the rapid auto-ignition of the mixture, showing the importance of addressing this aspect on new combustion modes as well [38]. Most of the resonance content released by the combustion pressure oscillations was found to be well characterized by the first two circumferential modes [39–41], where the first one tend to be more relevant and persistent along the combustion evolution. Figure 3.7 shows the short-time Fourier transform of the cycle analyzed in Figures 3.5 and 3.6. The black line represents the theoretical resonant frequency of the first mode calculated from (3.4) as expressed by Draper in a cylindrical combustion chamber [29]. It is observed that the resonant frequency follows the cylindrical theory only far from the TDC, at the end of the combustion (crank angle $> 60^\circ\text{aTDC}$). This observation was explained by the in-bowl piston geometry in the engine. As it was studied by Broatch et al. [42], it was found that in the case of such piston geometry, discrepancies exist near the TDC compared to the cylindrical theory, while a convergence is observed when the effect of the bowl becomes negligible. Yet, as previously mentioned, it can be appreciated that the first mode is slowly damped and therefore observable throughout the combustion evolution.

The proper measurement of the resonant modes is sensitive to the combustion

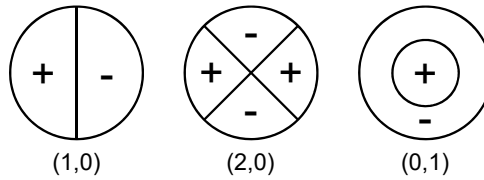


Figure 3.8: Resonant modes in a cylindrical chamber where circumferential (i) and radial (j) modes are indicated in the form (i, j)

chamber geometry and the pressure sensor location [43]. As an example, it is not recommended to use centrally mounted pressure transducers when investigating phenomena with high circumferential modes excitation because such configuration would mainly detect the first radial mode [17]. Such statement can be further understood in Figure 3.8. In this figure, the first two circumferential (i) and the first radial modes (j) in a cylindrical chamber are illustrated from left to right, respectively [29]. The lines represent the nodes where the pressure is constant, hence, if the pressure transducer is located in one of these nodal lines, the corresponding resonant mode detection becomes more challenging [44]. A proper implementation of the in-cylinder pressure sensor with identical sensor properties and position in all the cylinders is therefore advised for multi-cylinder engines applications.

The in-cylinder pressure resonance is a rich source of information and might be addressed, especially for the evaluation of potential engine damage. In this dissertation, Chapter 4 makes use of the high-pass filtered signal to evaluate the maximum pressure oscillation in the cylinder and control its value to a desired threshold, with a defined probability, in order to limit the risk of high amplitude cycles.

Trapped mass estimation Apart from its potential to address engine noise and prevent engine damage, the analysis of the resonance can provide useful information for the in-cylinder trapped mass estimation as well. Indeed, by inverting the calculation formulated in (3.4), with the definition of the speed of sound and the ideal gas equation, one might estimate the overall in-cylinder mass m_{cyl} through:

$$m_{cyl} = \frac{B_{i,j}^2 \gamma p V}{(f_{res} \pi D)^2} \quad (3.6)$$

Such approach was explored by Bares [45] by computing the short-time Fourier transform (STFT) of the in-cylinder pressure signal to obtain f_{res} , and by proposing a variation of the Fourier transform to correlate virtual masses with the reso-

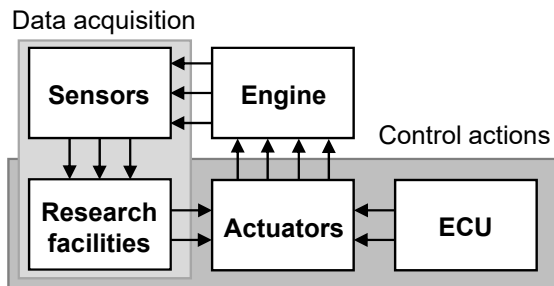


Figure 3.9: System layout implementation used in this work for the control actions (dark grey) and the data acquisition (light grey) during the experiments.

nant modes in order to avoid incorrect identification of f_{res} . The results showed the potential of this method for diagnosis and control, including in premixed combustion modes such as HCCI which exhibit high resonance excitation.

3.4 Acquisition and control system layout

In commercial on-road applications, the ECU is in charge of acquiring and processing the signals coming from the set of sensors installed on the engine, and to send the command to the different actuators to control the engine operation with pre-calibrated strategies. In a research environment, many degrees of freedom are needed, in both terms of acquisition and control, in order to evaluate new concepts such as the one presented in this work, i.e., premixed dual-fuel combustion. Although open-ECUs could allow to take control over the present actuators, some systems might require dedicated platforms if no other device has been yet developed, e.g., in the present case the ECUs supplied with the engines were not developed to integrate additional port fuel injectors control. Furthermore, the signal acquisition must be addressed according to various properties such as the measurement range, or the expected signal resolution, where different sampling rates might coexist as well. For these reasons, various devices and layouts were implemented in order to acquire all the signals and control all the systems used in this work. Figure 3.9 shows the global layout used to perform the dual-fuel combustion investigation, where the control actions and the data acquisition are delimited by grey areas. In this figure, *Research facilities* includes the rapid prototyping systems, and conventional devices and software for test bed applications.

3.4.1 Data acquisition

The data acquisition (DAQ) layout was composed of two main systems: the AVL PUMA test bed workstation, and the rapid prototyping platform developed using National Instruments (NI) devices, in which all the features described in this work were programmed in the visual programming language LabVIEW using the built-in functions and libraries.

The acquisition of the analog signals on a crank angle basis, and some additional cycle-based signals, was carried out by dedicated devices: the PXIe-6356 (engine A) and PXIe-6358 (engine B) modules from NI which offer simultaneous acquisition up to 1.25 MS/s/channel with a 16 bits resolution to 8 and 16 analog inputs, respectively. In order to coordinate and transmit the data to the host personal computer, the PXIe-8135 controller was used as the real-time (RT) core of the developed DAQ system. This controller embeds an Intel Core i7 processor, a hard drive in order to save the data, and several communication ports in which the Ethernet one was used to communicate with the host PC. This controller was also in charge of executing the processing of the data and the computation of the models. These equipment were connected to a PXIe-1071 chassis in order to transmit data and control sequences from one module to the other.

The sensors installed on the engine were transmitting the signals to the AVL PUMA and/or to the analog acquisition module PXIe-635x (x being either 6 or 8 depending on the module used). The emissions measurement was done using exhaust probes connected to the HORIBA exhaust analyzer and the registered values were transmitted to the AVL PUMA and the rapid prototyping platform using an Ethernet port (TCP/IP communication protocol). Furthermore, in engine B, the additional NO_x sensor signal was connected to a PXI-8512 high-speed Controller Area Network (CAN) interface module, whose acquisition was programmed using CAN (XNET) library within LabVIEW.

Sampling The AVL PUMA testbed software was set with a fixed sampling frequency of 10 Hz for all the signals registered. On the other hand, the signal acquisition from the National Instruments devices offered a higher degree of freedom and allowed to tune the desired sampling frequency for each signal within the same platform. Accordingly, all the mean variables measured with the DAQ devices from NI (e.g., intake pressure, emissions, air mass flow) were sampled every engine cycle. On the other hand, the instantaneous analog signals, such as the in-cylinder pressure traces, were recorded in the crank angle domain using a research encoder mounted on the crankshaft with a sampling resolution r_s of

5 samples/CAD, which corresponds to a 0.2 crank angle degree resolution (see section 3.3 for more details about the sampling frequency in crank angle-based applications).

In-cylinder pressure acquisition The in-cylinder pressure signal was acquired in the crank angle domain using the sampling frequency driven by the research encoder f_s . The *pegging* was based on the intake manifold pressure correction in the area of the bottom dead center, and the filters applied to the signal were tuned at 2.5 kHz to separate the combustion signal from the resonant components, as discussed in the previous section.

3.4.2 Control actions

The control of the actuators was shared between the devices from National Instruments, the provided ECUs using CAN protocol, and dedicated devices for some specific systems. The main features of the control architecture are described below.

Engine speed The engine speed was controlled and maintained by the ELIN INDY dynamometer according to the setpoint provided by the AVL PUMA engine test system.

Gas-exchange In engine A, the screw compressor used to provide the desired air at the intake was controlled by a dedicated system which used PID control actions to reach the target air boost pressure. For the exhaust loop, the back pressure and EGR were managed by 4-20 mA control valves.

In the case of engine B, except for the back pressure valve which was controlled using an analog signal, the EGR valves (both low-pressure and high-pressure) were connected to the PXI-8512 module and controlled through CAN protocol. In this engine, the air boost was performed using the VGT which was controlled by the provided ECU.

Injection control The injection control was performed by dedicated modules from National Instruments: the NI-9758 for the port fuel injection, and the NI-9751 for the direct injection. These modules are provided with injection duration and timing settings, and send the signals to the injectors accordingly. In order to phase the injections, a NI-9752 was in charge of acquiring both the crankshaft and camshaft position to synchronize the injection settings during the engine cycle. All of these modules were connected to a cRIO-9024 real-time controller in engine A,

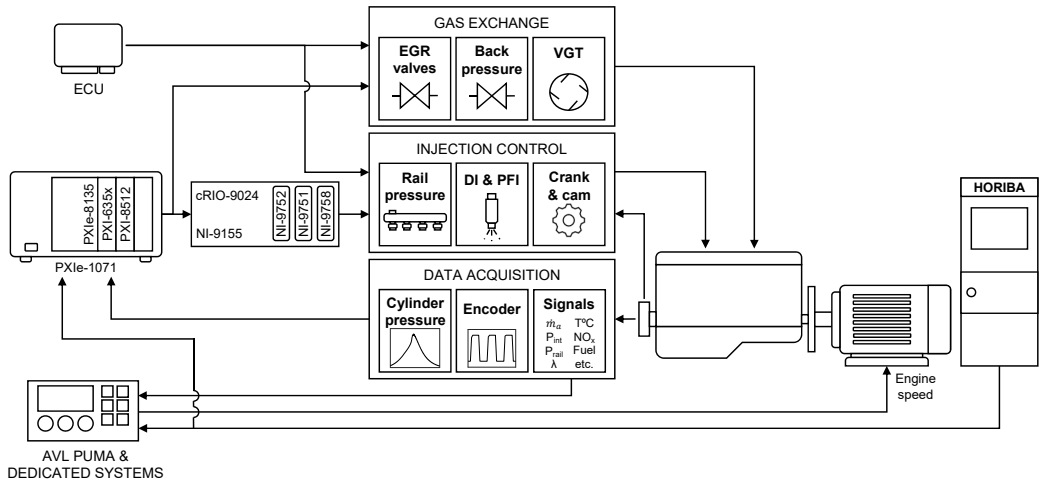


Figure 3.10: Summary of the data acquisition and control system layout. Note that this figure is a general illustration and more details about the specific equipment used in engines A and B can be found in sections 3.2 and 3.4.

and a MXI-Express NI-9155 CompactRIO chassis for engine B. In the first case, the cRIO was connected through an Ethernet port to the host PC and was dedicated to the injection system by communicating with the PXIe-8135 controller, in charge of the control strategies, through network shared variables. In the second case, the NI-9155 chassis was directly connected to the PXIe-8135 controller, hence acting as an extension of the RT controller. This configuration allowed to simplify the layout and to avoid time delay between the control requirement and the resulting actuation. In both cases, the injection control was programmed in the field-programmable gate array (FPGA) embedded in each chassis using LabVIEW. The port fuel injection pressure was manually regulated and fixed at a constant level, while the diesel injection pressure was regulated and controlled with an in-house common-rail control system in engine A, and by the ECU in the case of engine B.

Figure 3.10 summarizes the flow of data and control actions in the implemented system to investigate the dual-fuel combustion concept in both engines A and B.

3.5 Combustion evaluation and modeling

Although a significant quantity of information about the combustion can be obtained from the in-cylinder pressure signal alone, many models leverage this signal to get a better understanding about what is happening inside the cylinder. This section presents the main tools used in combustion analysis and describes the variables that will be used throughout this dissertation.

3.5.1 Heat release

One of the main tools to analyze the combustion evolution is the heat release computation. This calculation considers the cylinder as a closed system and is based on the first law of thermodynamics which, if neglecting mass transfer (i.e., the valves are closed, and the injected fuel quantity and potential blow-by are considered negligible), states that:

$$dU = dQ - dW \quad (3.7)$$

where the change in internal energy dU is expressed as the subtraction of the work done by the system dW from the energy supplied to the system dQ . Given the definitions of the change in internal energy and work, the following expression is obtained:

$$m c_v dT = dQ - p dV \quad (3.8)$$

where m is the mass in the system, c_v is the heat capacity at constant volume, T the temperature, and p and V are the pressure and the volume of the system, respectively. By considering a constant mass and the ideal gas equation of state ($pV = mRT$) to express the change in temperature dT , this leads to:

$$\frac{c_v}{R} d(pV) = dQ - p dV \quad (3.9)$$

where the specific gas constant R is here assumed constant. Replacing the gas constant by its relation with the heat capacity ratio:

$$R = c_v(\gamma - 1) \quad (3.10)$$

and considering that the heat supplied to the system corresponds to the difference between the chemical energy released by the fuel (dQ_c) and the heat transferred to the walls (dQ_{ht}), the description of the total heat released by the combustion of the fuel in the cylinder can be described by the following expression:

$$dQ_c = \frac{\gamma}{\gamma - 1} p dV + \frac{1}{\gamma - 1} V dp + dQ_{ht} \quad (3.11)$$

The calculations considered in this work for each element of the heat release rate model in (3.11) are provided below.

Cylinder volume While the in-cylinder pressure p is directly measured by the pressure transducer, as described in section 3.3, the instantaneous cylinder volume V is computed from the cylinder geometry with the connecting-rod length L_c , the crankshaft radius L_r , and the cylinder bore D , for every crank angle θ :

$$V(\theta) = V_{cc} + \frac{\pi D^2}{4} \left(L_c + L_r(1 - \cos(\theta)) - \sqrt{L_c^2 - L_r^2 \sin^2(\theta)} \right) \quad (3.12)$$

where the minimum combustion chamber volume V_{cc} (at the top dead center) is calculated from the compression ratio r_c :

$$V_{cc} = \frac{V_d}{r_c - 1} \quad (3.13)$$

with V_d the cylinder displacement volume.

Heat capacity ratio The heat capacity ratio γ depends on the species concentration and temperature of the system and may thus vary during the engine cycle. Its value may be estimated through equations based on thermodynamics properties of individual species [46], but in this work it was decided to evaluate it at each crank angle degree using the approach provided in [47]. First, the gas constant R_c of the in-cylinder gas is estimated using the gas constants and the mass fractions of the species contained in the cylinder, being air (m_a), fuel (m_f) and burnt products (m_b):

$$R_a = 287 \text{ J/kg.K} \quad (3.14)$$

$$R_f = 55.95 \text{ J/kg.K} \quad (3.15)$$

$$R_b = 285.4 \text{ J/kg.K} \quad (3.16)$$

$$R_c = \frac{1}{m_{cyl}} (R_a m_a + R_f m_f + R_b m_b) \quad (3.17)$$

where m_a , m_f and m_b are the instantaneous mass of each species at each crank angle degree, and m_{cyl} is the total in-cylinder trapped mass. Then, the instantaneous in-cylinder temperature is calculated:

$$T = \frac{pV}{m_{cyl} R_c} \quad (3.18)$$

The temperature is then used to determine the specific heat at constant volume c_v of the three considered species using polynomial correlations, in which the

Table 3.5: Coefficients k_{ij} used in the polynomial correlations for the heat capacity calculation in equations (3.19) to (3.21) from [47].

k_{ij}	k_{i1}	k_{i2}	k_{i3}	k_{i4}	k_{i5}
k_{1j}	-1.04×10^1	2.52×10^3	-6.72×10^4	9.17×10^5	-4.18×10^6
k_{2j}	-2.01×10^2	0.69×10^1	-4.05×10^{-3}	9.10×10^{-7}	1.46×10^6
k_{3j}	6.41×10^2	4.31×10^{-1}	-1.13×10^{-4}	8.98×10^{-9}	

coefficients are listed in Table 3.5, and finally obtain the global c_v :

$$c_{v,a} = k_{11}T^{0.5} + k_{12} + k_{13}T^{-0.5} + k_{14}T^{-1} + k_{15}T^{-1.5} \quad (3.19)$$

$$c_{v,f} = k_{21} + k_{22}T + k_{23}T^2 + k_{24}T^3 + k_{25}T^{-2} \quad (3.20)$$

$$c_{v,b} = k_{31} + k_{32}T + k_{33}T^2 + k_{34}T^3 \quad (3.21)$$

$$c_v = \frac{1}{m_{cyl}} (c_{v_a}m_a + c_{v_f}m_f + c_{v_b}m_b) \quad (3.22)$$

Finally, using (3.17) and (3.22), the instantaneous γ can be estimated by:

$$\gamma = \frac{R_c + c_v}{c_v} \quad (3.23)$$

As introduced in (3.17), (3.18) and (3.22), the computation of the energy released by the fuel combustion depends on the estimation of the in-cylinder charge m_{cyl} . A common way to estimate the total trapped mass is by applying the speed density method. This method relies on the pressure and the temperature measurement at the intake port, and uses a pre-calibrated volumetric efficiency map, function of the engine speed and the intake pressure, to estimate the total mass inducted in the cylinder [48]. However, apart from the possible error coming from the volumetric efficiency estimation, such methodology might not be able to deal with the cylinder-to-cylinder variability if based on a single intake runner measurement. In that case, the trapped mass estimation based on the in-cylinder pressure resonance (see section 3.3) might address this aspect if all the cylinders are equipped with an in-cylinder pressure transducer. In this work, such method was selected to estimate the trapped mass at each cylinder in the evaluation of the individual fuel blend concentration in Chapter 5.

Heat transfer The heat transferred to the cylinder walls can be modeled using Newton's law of cooling, which is based on the effective heat transfer area A_{ht}

obtained from the geometry of the cylinder and the piston's position, and the thermal gradient between the system and the environment:

$$\frac{dQ_{ht}}{d\theta} = \frac{h_c A_{ht}}{6N} (T - T_w) \quad (3.24)$$

where the engine speed N (in rpm) is used to convert this quantity to the crank angle domain (θ), T_w is the temperature of the cylinder walls, and h_c is the heat transfer coefficient which is approximated with the Woschni correlation [49, 50] using the cylinder bore D , the in-cylinder pressure and temperature (p and T), and the average cylinder gas velocity ω :

$$h_c = 0.013D^{-0.2}p^{0.8}T^{-0.53}\omega^{0.8} \quad (3.25)$$

where ω is estimated by:

$$\omega = C_1 S_p + C_2 \frac{V_d T_{ivc}}{p_{ivc} V_{ivc}} (p - p_m) \quad (3.26)$$

with the mean piston speed S_p , the cylinder conditions at intake valve closure (IVC), the instantaneous in-cylinder pressure p , the motored cylinder pressure p_m , and C_1 and C_2 being two empirical constants [51].

Apparent heat release

In many control applications, where the heat release rate computation is performed in real-time within a cycle delay and where a high degree of accuracy of the heat release calculation might not be required, the heat transfer calculation is often removed [52]. In this case, this quantity, named the net apparent heat release rate, is defined as follows:

$$dQ_{app} = \frac{\kappa}{\kappa - 1} p dV + \frac{1}{\kappa - 1} V dp \quad (3.27)$$

where κ is a polytropic coefficient traditionally set to a constant value ranging from 1.30 to 1.35 [51], or fitted at the compression and the expansion stroke and linearly interpolated in-between during the combustion phase [53].

The heat release rate can then be integrated to obtain the accumulated heat release $Q(\theta)$:

$$Q(\theta) = \int_{\theta_{ivc}}^{\theta_{evo}} \frac{dQ}{d\theta} d\theta \quad (3.28)$$

where the same calculation applies to any heat release rate model, e.g., dQ_c or dQ_{app} , hence indicated simply as Q here. The integration is naturally performed

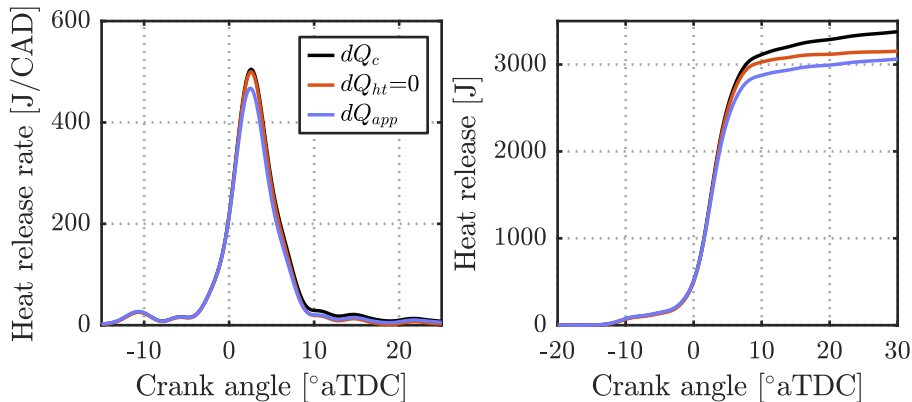


Figure 3.11: Illustration and comparison of the heat release rate (left) and heat release (right) calculation from the model definition in (3.11) with the heat capacity ratio obtained as in (3.23), the same model but without the heat transfer ($dQ_{ht} = 0$), and the apparent heat release approach presented in (3.27) with a constant κ set to 1.3.

in the closed part of the engine cycle between intake valve closing (θ_{ivc}) and exhaust valve opening (θ_{evo}). Figure 3.11 shows the difference between different heat release computations for the same engine cycle. The complete model definition in (3.11) with the heat capacity ratio computed from (3.23), the same model but without the heat transfer ($dQ_{ht} = 0$), and the apparent heat release in (3.27) with a constant κ set to 1.3, are compared. Especially in the right plot, it can be observed the effect of removing the calculation of the heat transferred to the cylinder walls that leads to a reduction of the total heat released amount. In the left plot, considering a constant heat capacity ratio shows a modification of the maximum heat release rate peak value.

3.5.2 Combustion metrics

Aside from the crank angle-based signals, such as the in-cylinder pressure and the heat release rate, cycle-to-cycle metrics can be computed from these signals in order to evaluate the engine operation. In this thesis, most of the following metrics are used as a feedback to develop closed-loop controllers applied to premixed dual-fuel combustion.

Engine load The engine metrics were exclusively computed from the in-cylinder pressure signal. Consequently, the measurements were limited to the indicated parameters, i.e., torque-based (brake) values were not measured for feedback application in this work. Here, the gross indicated mean effective pressure (*IMEP*)

was considered to evaluate the engine load. This value is a normalized quantity that represents the work done by the gas on the piston during the closed part of the cycle:

$$IMEP = \frac{1}{V_d} \int_{\theta_{ivc}}^{\theta_{evo}} p dV \quad (3.29)$$

An example of the use of such value can be found in Chapter 4 where it was selected to evaluate the engine load for developing a closed-loop controller that ensures to maintain the load level to a desired threshold against external disturbances.

Combustion phasing The main objective during the combustion is to obtain the maximum work from the heat released in the cylinder with the minimum heat losses through the cylinder walls in order to improve the fuel conversion efficiency. The combustion phasing plays therefore an important role in the amount of work transferred to the piston: a too early combustion is counterproductive as the piston is moving towards the top dead center against the combustion pressure evolution, while if the combustion starts too late, the volume has increased, the peak pressure is consequently reduced and less work is obtained [54, 55].

The combustion phasing is commonly used as an indicator of the combustion efficiency and is traditionally estimated with the crank angle where 50% of the energy released by the fuel is encountered, the CA50. This value is determined by finding the crank angle CAx where the sought amount of the total energy released is reached:

$$CAx = \theta_i \quad \text{when} \quad x = 100 \frac{Q(\theta_i)}{\max(Q(\theta))} \quad (3.30)$$

where i denotes the index iteration on the crank angle vector, Q is defined in (3.28), and x would be equal to 50 in this case to find the CA50.

Other indicators such as the CA10 and the CA90 are commonly used respectively as the start of combustion (SOC) and the end of combustion (EOC) to evaluate the burn duration, particularly for premixed combustion modes where the combustion of the cylinder mixture is mostly initiated at once. Figure 3.12 illustrates the accumulated heat release from one cycle showing the corresponding combustion timing events. In this thesis, and in the majority of the investigated applications, the combustion phasing metrics were evaluated using the apparent heat release model in (3.27), and then computing similarly the accumulated heat release (3.28) to obtain the combustion phasing (3.30). Indeed, compared to a more detailed model, no significant deviation was observed in estimating the combustion phasing.

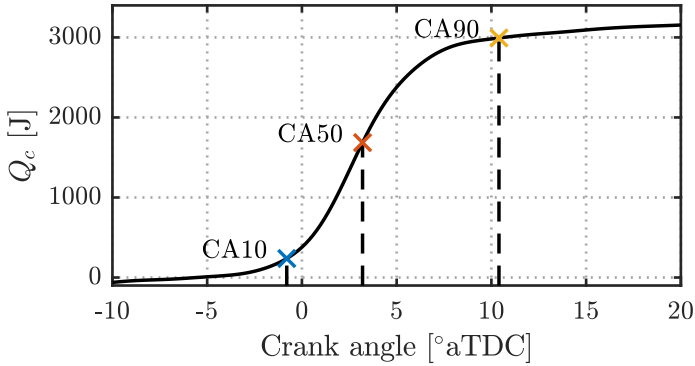


Figure 3.12: Illustration of the accumulated heat release signal showing the CA_{10} , CA_{50} and CA_{90} positions which are common metrics used in combustion analysis to evaluate the combustion evolution.

ing with a simpler heat release calculation approach [56].

Nonetheless, in some operating conditions, control instabilities were found when using the CA_{50} as the reference for the combustion phasing evaluation, as illustrated in the right plot from Figure 3.13. When using a late diesel injection (close to the TDC, in partially premixed combustion as detailed in the following section), the CA_{50} estimation could correspond to the exact transition between the premixed and the late combustion phase (see the heat release traces in the left plot). In the case shown in the left plot, the first heat release rise represents around 50% of the total fuel mixture energy and is mainly composed of premixed gasoline (about 85%) and a small part of premixed diesel, while the second part is only composed by the late diesel injected fuel (the diesel fuel injection timings are shown with colored crosses in the left plot of Figure 3.13, the gasoline injection was injected at 340°bTDC and is not shown in this graph). It can be observed that in these conditions, the premixed diesel auto-ignited the whole premixed mixture and thus made that charge to burn early in the cycle. Consequently, when the post diesel injection is performed, the previous premixed combustion is about to end and, therefore, the late injection (start of injection at 5°bTDC) creates a second combustion phase. For this reason, in order to adapt the combustion phasing control to combustion operation with late diesel injections, it was decided to use a different parameter here named the Crank Angle combustion Center of Gravity (CACG), also known as the combustion centroid [57]. This value consists in an

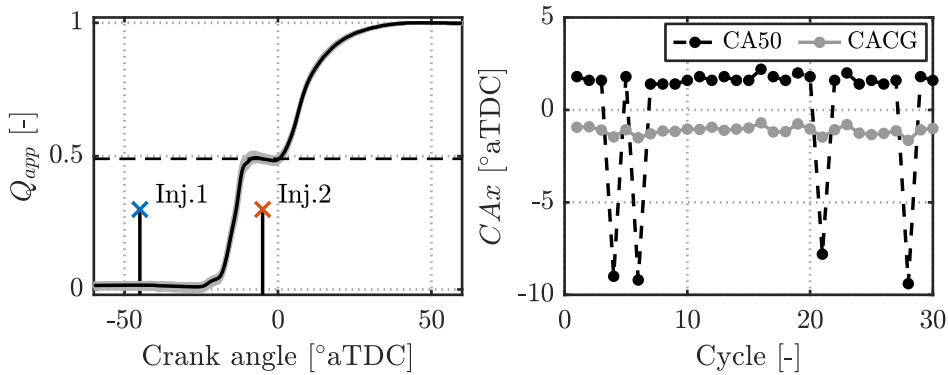


Figure 3.13: CA50 dispersion (1200 rpm-15 bar IMEP) and corresponding CACG metric. The left plot shows the cumulative apparent heat release traces Q_{app} used to estimate the combustion phasing (grey: cycle-to-cycle, black: mean) with the 50% level shown in black dashed line. The diesel injection (Inj.) timings are also represented with colored crosses, and the gasoline is not illustrated here. The resulting CA50 (black dash-dotted line) and CACG (solid-dotted grey line) estimation are shown in the right plot.

energy balance from the apparent heat release rate dQ_{app} as detailed in (3.31):

$$CACG = \frac{\int_{SOC}^{EOC} \theta dQ_{app} d\theta}{\int_{SOC}^{EOC} dQ_{app} d\theta} \quad (3.31)$$

As it can be seen in a grey line in the right plot of Figure 3.13, the CACG shows a more stable behavior for a closed-loop control application than the CA50 in these operating conditions.

Both the CA50 and the CACG are used in the control strategies described in the following chapters depending on the intended control objective and combustion operation.

Operating condition constraints At any given operating condition, the engine must not exceed its mechanical constraints [58]. To evaluate the harmful potential of the combustion, the in-cylinder pressure is commonly used as the principal source of information. The main features that are considered are: how large is the combustion pressure, how fast it occurs, and how large is the pressure resonance excited. While the first one can be easily monitored by measuring directly the maximum in-cylinder pressure, the latter have been widely studied for

various combustion modes and different indexes were proposed.

Among the indexes found in literature for evaluating the harmfulness of the combustion, it is worth mentioning three that are typically used in combustion analysis: the maximum pressure rise rate (MPRR), the ringing intensity (RI), and the maximum amplitude of pressure oscillations (MAPO). While the first one characterizes how fast the combustion pressure evolves, the last two aim to describe the pressure oscillations generated by the combustion.

The MPRR, expressed in bar/CAD, is obtained with the maximum value of the first derivative of the filtered pressure signal p_{lp} :

$$MPRR = \max(dp_{lp}(\theta)) \quad (3.32)$$

This index is traditionally considered as a mechanical and combustion noise constraint limitation thanks to its easy calculation and implementation in real-time applications [59–61]. In this thesis, Chapter 4 makes use of the MPRR as the limitation factor in a closed-loop combustion controller for dual-fuel operation. Nonetheless, being based on the low-pass filtered pressure trace, this index alone fails to capture the combustion pressure oscillations, as it was highlighted by Wissink et al. [40].

Assuming that high pressure rise rates stimulate pressure oscillations in the combustion chamber, the ringing intensity, expressed in MW/m², was proposed by Eng [38] to approximate the intensity of the pressure waves with the following correlation:

$$RI \approx \frac{1}{2\gamma} \frac{\left(\beta \left(\frac{dp}{dt}\right)_{max}\right)^2}{p_{max}} \sqrt{\gamma RT_{max}} \quad (3.33)$$

where $(dp/dt)_{max}$, p_{max} and T_{max} are the maximum pressure rise rate (kPa/ms), cylinder pressure (kPa) and temperature (K), respectively. The adjustable term β aims to relate the pressure oscillations amplitude to the pressure rise rate and is often considered to be 0.05, while γ is the heat capacity ratio, and R the gas constant. Note that $(dp/dt)_{max}$ is the time-based equivalent of the crank angle-based MPRR mentioned above in (3.32). The ringing intensity was initially proposed for homogeneous charge compression ignition. Similarly to knock in SI engines, the resulting pressure waves might represent a source of potential damage for the engine and must be limited and controlled [62]. The ringing intensity is a commonly adopted index for low temperature combustion concepts where a criterion of 5 MW/m² is often considered to differentiate knocking (i.e., above this criterion)

from non-knocking cycles [63, 64]. This method was found to be more robust but sensitive to the calibration of β and, as pointed out by Dernette et al. [41], this correlation was originally designed to be implemented in zero- and one-dimensional engine models which do not account for any information of the pressure waves. The ringing intensity shares therefore similar limitations with the MPRR.

Lastly, the MAPO directly measures the maximum absolute value of the pressure oscillations amplitude in the p_{hp} signal and is expressed in bar:

$$MAPO = \max(|p_{hp}(\theta)|) \quad (3.34)$$

This index has been especially used in knock detection for spark ignition engines [37], where a cycle is considered as knocking when the MAPO is detected above a predefined threshold [65]. Although this index addresses explicitly the measured pressure waves, it is implicitly sensitive to the pressure trace measurement conditions, e.g., pressure transducer location (see section 3.3).

It must be noted that these three indexes share the common attributes of being sensitive to the filter definition and requiring a threshold definition to separate knocking from non-knocking cycles, which is function of the application and the engine, and is traditionally empirically set.

New low temperature combustion (LTC) modes such as HCCI, or reactivity controlled compression ignition (RCCI), are limited by their MPRR levels due to the rapid auto-ignition of the mixture [66–68] and traditionally exhibit high resonance excitation. Shahlari et al. [69], Wissink et al. [40] and Dernette et al. [41] studied the pressure oscillations in various combustion modes using the MPRR and the RI, and characterized the combustion noise generated by the pressure waves using power spectral density (PSD) analysis. It was highlighted that the magnitude of the three indexes are not always correlated and that the levels of MPRR and RI are highly dependent on the processing of the cylinder pressure signal. The raw data is subject to noise amplification when calculating its gradient and this might bias the detection of ringing event, while filtering may remove some information and provide noticeably different values of MPRR and RI. Consequently, it is important to clearly state the filter characteristics along with the results. In this thesis, Chapter 4 compares and discusses the three aforementioned indexes in premixed dual-fuel combustion with different stratification levels. A knock-like controller is then proposed to ensure that these indexes do not exceed a predefined threshold to ensure safe operation of the engine.

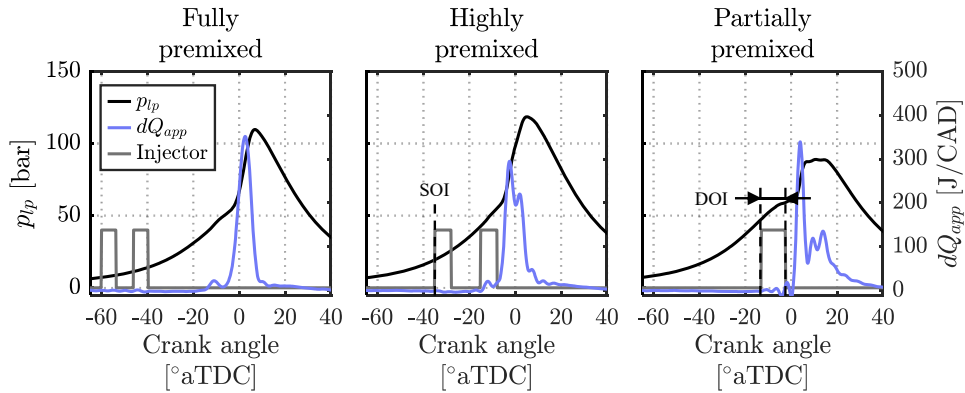


Figure 3.14: Illustration of the in-cylinder pressure (p_{lp}), apparent heat release rate (dQ_{app}), and injector signals (diesel injection, the gasoline is injected during the intake stroke) in the three dual-fuel combustion modes evaluated in this work: fully premixed (left), highly premixed (middle) and partially premixed (right). The start of injection (SOI) and the duration of injection (DOI) are also represented.

3.6 Combustion modes

As it was mentioned in Chapter 2, dual-fuel combustion can be controlled by various injection strategies. Particularly in this work, these strategies are referred to their corresponding premixing levels of the mixture, and are characterized within three combustion modes: fully premixed, highly premixed and partially premixed.

Figure 3.14 shows the low-pass filtered in-cylinder pressure p_{lp} signal, the apparent heat release rate dQ_{app} , and the direct diesel injector signal of a typical cycle at each combustion mode. For comparison and illustration purposes, these three conditions were performed at the same load. Together with the injector signal, the start of injection (SOI) and the duration of injection (DOI) are indicated. Here, the gasoline injection signal is not shown because its timing was the same for the three combustion modes, i.e., during the intake stroke. Finally, note that the diesel injector signals shown in this figure are here chosen for illustration purposes only and do not represent the real shape of the signal applied to the injector.

These combustion modes are commonly associated to a specific area of the engine operating map, as illustrated in Figure 3.15, and can be described as:

- At low/medium loads, fully or highly premixed conditions are used depending on the hardware setup. In engine A, while the air requirement was ful-

filled with the screw compressor, fully premixed conditions were used at low loads. However, with commercial hardware implementation such as in engine B, the highly premixed mode was used instead, as shown in Figure 3.15, and the fully premixed strategy was performed at higher loads when the conditions allowed to advance the diesel injections and maintain an efficient combustion. In these combustion modes, which fall into the RCCI combustion concept, the combustion phasing is mainly driven by the mixture reactivity, and the high mixing times ensure low NO_x and soot emissions. These strategies are characterized by single peak combustion corresponding to the auto-ignition of the mixture in the cylinder, as illustrated by the heat release rate dQ_{app} in the left and middle plots of Figure 3.14.

- At high loads, the rapid auto-ignition of the mixture becomes critical and only partially premixed combustion can be safely achieved. To this aim, a single diesel injection, which triggers the combustion, is moved in the vicinity of the top dead center to reduce the amount of premixed charge. In these conditions, the combustion might show some diffusive-like behavior, as shown in the right plot of Figure 3.14, where an abrupt peak due to the combustion of the premixed mixture is followed by a long diesel-like combustion during the power stroke. Such combustion mode penalizes the total NO_x emissions but allows to extend the operating range of the dual-fuel combustion.

These combustion modes were addressed and used in both engines throughout the investigation described in this manuscript.

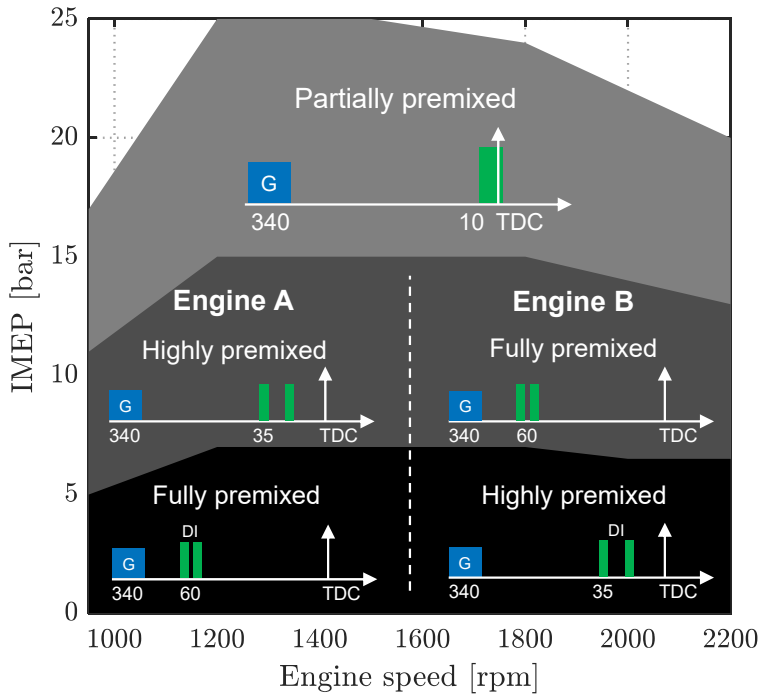


Figure 3.15: Injection strategy in every combustion mode in the engine operating map. The gasoline injection (G, blue) and the diesel injections (DI, green) are illustrated and the numbers under the injections representation stand for the injection timings indicated in °bTDC (note that these values are only given as examples to describe the common area of injection timing). The difference in injection strategy between engine A and B at low and medium loads is explained by hardware limitations (more details in the description of the combustion modes).

References

- [1] Benajes Jesús, Pastor José V., García Antonio and Boronat Vicente. A RCCI operational limits assessment in a medium duty compression ignition engine using an adapted compression ratio. *Energy Conversion and Management*, Vol. 126, pp. 497–508, 2016. (cited in pp. 32 and 49)
- [2] Boronat Colomer Vicente. *Dual-Fuel Dual-Mode combustion strategy to achieve high thermal efficiency, low NO_x and smoke emissions in compression ignition engines*. PhD Thesis, Universitat Politècnica de València, 2018. (cited in pp. 32 and 51)
- [3] Lago Sari Rafael. *Dual Mode Dual Fuel Combustion: Implementation on a Real Medium Duty Engine Platform*. PhD Thesis, Universitat Politècnica de València, 2021. (cited in pp. 33 and 51)

-
- [4] Eriksson Lars and Thomasson Andreas. Cylinder state estimation from measured cylinder pressure traces - A Survey. *IFAC-PapersOnLine*, Vol. 50 n° 1, pp. 11029–11039, jul 2017. (cited in p. 55)
- [5] Willems Frank. Is Cylinder Pressure-Based Control Required to Meet Future HD Legislation? *IFAC-PapersOnLine*, Vol. 51 n° 31, pp. 111–118, 2018. (cited in pp. 12, 34, 55, and 88)
- [6] Haraldsson Goran, Tunestal Per, Johansson Bengt and Hyvonen Jari. HCCI Combustion Phasing with Closed-Loop Combustion Control Using Variable Compression Ratio in a Multi Cylinder Engine. In *SAE Technical Papers*, may 2003. (cited in p. 55)
- [7] Husted H., Kruger D., Fattic G., Ripley G. and Kelly E. Cylinder Pressure-Based Control of Pre-Mixed Diesel Combustion. In *SAE Technical Papers*, volume 2007, apr 2007. (cited in p. 55)
- [8] Arora Jayant Kumar and Shahbakhti Mahdi. Real-Time Closed-Loop Control of a Light-Duty RCCI Engine During Transient Operations. In *SAE Technical Paper*, mar 2017. (cited in pp. 35, 38, 55, and 89)
- [9] Jorques Moreno Carlos, Stenlaas Ola and Tunestal Per. Cylinder Pressure-Based Virtual Sensor for In-Cycle Pilot Mass Estimation. *SAE International Journal of Engines*, Vol. 11 n° 6, pp. 1167–1182, apr 2018. (cited in p. 55)
- [10] Wick Maximilian, Bedei Julian, Gordon David, Wouters Christian, Lehrheuer Bastian, Nuss Eugen, Andert Jakob and Koch Charles Robert. In-cycle control for stabilization of homogeneous charge compression ignition combustion using direct water injection. *Applied Energy*, Vol. 240 n° January, pp. 1061–1074, apr 2019. (cited in p. 55)
- [11] Worret R., Bernhardt S., Schwarz F. and Spicher U. Application of Different Cylinder Pressure Based Knock Detection Methods in Spark Ignition Engines. In *SAE Technical Papers*, number 724, may 2002. (cited in p. 55)
- [12] Taglialatela F., Moselli G. and Lavorgna M. Engine knock detection and control using in-cylinder pressure signal and soft computing techniques. In *SAE Technical Papers*, volume 2005-Septe, sep 2005. (cited in p. 55)
- [13] Siano Daniela, Panza Maria Antonietta and D’Agostino Danilo. Knock detection based on MAPO analysis, AR model and discrete wavelet transform applied to the in-cylinder pressure data: Results and comparison. *SAE International Journal of Engines*, Vol. 8 n° 1, pp. 1–13, oct 2015. (cited in p. 55)
- [14] Çebi Emrah Cihan, Rottenkolber Gregor and Uyar Erol. In-Cylinder Pressure Based Real-Time Estimation of Engine-Out Particulate Matter Emissions of a Diesel Engine. In *SAE 2011 World Congress and Exhibition*, apr 2011. (cited in p. 55)
- [15] Formentin Simone, Corno Matteo, Waschl Harald, Alberer Daniel and Savaresi Sergio M. NO_x Estimation in Diesel Engines via In-Cylinder Pressure Measurement. *IEEE Transactions on Control Systems Technology*, Vol. 22 n° 1, pp. 396–403, jan 2014. (cited in p. 55)

- [16] Guardiola C., Martín J., Pla B. and Bares P. Cycle by cycle NOx model for diesel engine control. *Applied Thermal Engineering*, Vol. 110, pp. 1–2, 2017. (cited in p. 55)
- [17] Rogers David R. *Engine Combustion: Pressure Measurement and Analysis*. SAE international Warrendale, PA, 2010. (cited in pp. 12, 56, and 63)
- [18] Díaz Jaime Martín. *Aportación al diagnóstico de la combustión en motores diesel de inyección directa*. PhD Thesis, Universitat Politècnica de València, 2007. (cited in p. 57)
- [19] Tunestål Per. Model Based TDC Offset Estimation from Motored Cylinder Pressure Data. *IFAC Proceedings Volumes*, Vol. 42 n° 26, pp. 241–247, 2009. (cited in p. 57)
- [20] Pipitone Emiliano and Beccari Alberto. Determination of TDC in internal combustion engines by a newly developed thermodynamic approach. *Applied Thermal Engineering*, Vol. 30 n° 14-15, pp. 1914–1926, oct 2010. (cited in p. 57)
- [21] Reif Konrad. *Diesel Engine Management*. Springer Fachmedien Wiesbaden, Wiesbaden, 2014. (cited in p. 57)
- [22] Antonopoulos Antonis and Hountalas Dimitrios. Identification and Correction of the Error Induced by the Sampling Method Used to Monitor Cylinder Pressure of Reciprocating Internal Combustion Engines. In *SAE Technical Papers*, apr 2012. (cited in p. 59)
- [23] Ponti Fabrizio. In-Cylinder Pressure Measurement: Requirements for On-Board Engine Control. *Journal of Engineering for Gas Turbines and Power*, Vol. 130 n° 3, pp. 032803, 2008. (cited in p. 59)
- [24] Payri F., Luján J. M., Martín J. and Abbad A. Digital signal processing of in-cylinder pressure for combustion diagnosis of internal combustion engines. *Mechanical Systems and Signal Processing*, Vol. 24 n° 6, pp. 1767–1784, 2010. (cited in p. 59)
- [25] Brunt Michael F. J. and Pond Christopher R. Evaluation of Techniques for Absolute Cylinder Pressure Correction. *SAE Technical Paper*, n° 412, 1997. (cited in p. 59)
- [26] Lee Kangyoon, Kwon Minsu, Sunwoo Myounggho and Yoon Maru. An in-cylinder pressure referencing method based on a variable polytropic coefficient. *SAE Technical Papers*, n° 2007-01-3535, 2007. (cited in p. 59)
- [27] Payri F., Broatch A., Tormos B. and Marant V. New methodology for in-cylinder pressure analysis in direct injection diesel engines - Application to combustion noise. *Measurement Science and Technology*, Vol. 16 n° 2, pp. 540–547, 2005. (cited in p. 59)
- [28] Payri F., Olmeda P., Guardiola C. and Martín J. Adaptive determination of cut-off frequencies for filtering the in-cylinder pressure in diesel engines combustion analysis. *Applied Thermal Engineering*, Vol. 31 n° 14-15, pp. 2869–2876, oct 2011. (cited in p. 59)

-
- [29] Draper C.S. The physical effects of detonation in a closed cylindrical chamber. *NACA Report*, n° 493, 1935. (cited in pp. 60, 61, 62, and 63)
- [30] Vressner Andreas, Lundin Andreas, Christensen Magnus, Tunestål Per and Johansson Bengt. Pressure Oscillations During Rapid HCCI Combustion. In *SAE Technical Papers*, volume 2003, oct 2003. (cited in p. 61)
- [31] Wang Zhi, Liu Hui and Reitz Rolf D. Knocking combustion in spark-ignition engines. *Progress in Energy and Combustion Science*, Vol. 61, pp. 78–112, jul 2017. (cited in p. 61)
- [32] Nates R.J. and Yates A. D. B. Knock Damage Mechanisms in Spark-Ignition Engines. In *SAE Technical Papers*, number 412, oct 1994. (cited in p. 61)
- [33] Millo F. and Ferraro C. V. Knock in S.I. Engines: A Comparison between Different Techniques for Detection and Control. In *SAE Technical Papers*, number 724, oct 1998. (cited in p. 61)
- [34] Galloni Enzo. Dynamic knock detection and quantification in a spark ignition engine by means of a pressure based method. *Energy Conversion and Management*, Vol. 64, pp. 256–262, dec 2012. (cited in p. 61)
- [35] Bares P., Selmanaj D., Guardiola C. and Onder C. A new knock event definition for knock detection and control optimization. *Applied Thermal Engineering*, Vol. 131, pp. 80–88, feb 2018. (cited in p. 61)
- [36] Pla Benjamin, De La Morena Joaquin, Bares Pau and Jiménez Irina. Knock Analysis in the Crank Angle Domain for Low-Knocking Cycles Detection. In *SAE Technical Papers*, volume 2020-April, pp. 1–11, apr 2020. (cited in p. 61)
- [37] Zhen Xudong, Wang Yang, Xu Shuaiqing, Zhu Yongsheng, Tao Chengjun, Xu Tao and Song Mingzhi. The engine knock analysis – An overview. *Applied Energy*, Vol. 92, pp. 628–636, apr 2012. (cited in pp. 62 and 77)
- [38] Eng J. A. Characterization of Pressure Waves in HCCI Combustion. In *SAE Technical Papers*, number 724, oct 2002. (cited in pp. 30, 62, and 76)
- [39] Scholl David, Davis Craig, Russ Stephen and Barash Terry. The Volume Acoustic Modes of Spark-Ignited Internal Combustion Chambers. In *SAE Technical Papers*, number 724, feb 1998. (cited in p. 62)
- [40] Wissink Martin, Wang Zhi, Splitter Derek, Shahlari Arsham and Reitz Rolf D. Investigation of Pressure Oscillation Modes and Audible Noise in RCCI, HCCI, and CDC. In *SAE Technical Papers*, volume 2, apr 2013. (cited in pp. 62, 76, and 77)
- [41] Dernotte Jeremie, Dec John and Ji Chunsheng. Investigation of the Sources of Combustion Noise in HCCI Engines. *SAE International Journal of Engines*, Vol. 7 n° 2, pp. 730–761, apr 2014. (cited in pp. 62 and 77)
- [42] Broatch Alberto, Guardiola Carlos, Bares Pau and Denia Francisco D. Determination of the resonance response in an engine cylinder with a bowl-in-piston geometry by the finite element method for inferring the trapped mass. *International Journal of Engine Research*, Vol. 17 n° 5, pp. 534–542, jun 2016. (cited in p. 62)

- [43] Brunt Michael F.J., Pond Christopher R. and Biundo John. Gasoline Engine Knock Analysis using Cylinder Pressure Data. In *SAE Technical Papers*, number 724, feb 1998. (cited in p. 63)
- [44] Dahl Daniel, Andersson Mats and Denbratt Ingemar. The Origin of Pressure Waves in High Load HCCI Combustion: A High-Speed Video Analysis. *Combustion Science and Technology*, Vol. 183 n° 11, pp. 1266–1281, nov 2011. (cited in p. 63)
- [45] Bares Moreno Pau. *In-cylinder pressure resonance analysis for trapped mass estimation in automotive engines*. PhD Thesis, Universitat Politècnica de València, 2017. (cited in p. 63)
- [46] McBride Bonnie J. *NASA Glenn coefficients for calculating thermodynamic properties of individual species*. National Aeronautics and Space Administration, John H. Glenn Research Center, 2002. (cited in p. 69)
- [47] Lapuerta M., Armas O. and Hernández J.J. Diagnosis of DI Diesel combustion from in-cylinder pressure signal by estimation of mean thermodynamic properties of the gas. *Applied Thermal Engineering*, Vol. 19 n° 5, pp. 513–529, may 1999. (cited in pp. 69 and 70)
- [48] Wang Zhe, Zhu Qilun and Prucka Robert. A Review of Spark-Ignition Engine Air Charge Estimation Methods. In *SAE Technical Papers*, volume 2016-April, apr 2016. (cited in p. 70)
- [49] Woschni G. A Universally Applicable Equation for the Instantaneous Heat Transfer Coefficient in the Internal Combustion Engine. *SAE Technical Paper*, 1967. (cited in p. 71)
- [50] Payri F., Molina S., Martín J. and Armas O. Influence of measurement errors and estimated parameters on combustion diagnosis. *Applied Thermal Engineering*, Vol. 26 n° 2-3, pp. 226–236, 2006. (cited in p. 71)
- [51] Heywood J.B. *Internal Combustion Engine Fundamentals*. Automotive technology series. McGraw-Hill, 1988. (cited in pp. 6, 71, 118, 119, 150, and 158)
- [52] Asad Usman and Zheng Ming. Fast heat release characterization of a diesel engine. *International Journal of Thermal Sciences*, Vol. 47 n° 12, pp. 1688–1700, 2008. (cited in pp. 71 and 158)
- [53] Tunestål Per. Self-tuning gross heat release computation for internal combustion engines. *Control Engineering Practice*, Vol. 17 n° 4, pp. 518–524, 2009. (cited in pp. 71 and 158)
- [54] Ma Fanhua, Wang Yu, Wang Junjun, Ding Shangfen, Wang Yefu and Zhao Shuli. Effects of Combustion Phasing, Combustion Duration, and Their Cyclic Variations on Spark-Ignition (SI) Engine Efficiency. *Energy & Fuels*, Vol. 22 n° 5, pp. 3022–3028, sep 2008. (cited in p. 73)
- [55] Caton Jerald A. Combustion phasing for maximum efficiency for conventional and high efficiency engines. *Energy Conversion and Management*, Vol. 77, pp. 564–576, jan 2014. (cited in p. 73)

-
- [56] Bengtsson J., Strandh P., Johansson R., Tunestål P. and Johansson B. Closed-loop combustion control of homogeneous charge compression ignition(HCCI) engine dynamics. *International Journal of Adaptive Control and Signal Processing*, Vol. 18 n° 2, pp. 167–179, mar 2004. (cited in p. 74)
- [57] Payri F., Broatch A., Salavert J. M. and Martín J. Investigation of diesel combustion using multiple injection strategies for idling after cold start of passenger-car engines. *Experimental Thermal and Fluid Science*, Vol. 34 n° 7, pp. 857–865, 2010. (cited in pp. 74 and 90)
- [58] Johansson Thomas, Johansson Bengt, Tunestål Per and Aulin Hans. HCCI Operating Range in a Turbo-charged Multi Cylinder Engine with VVT and Spray-Guided DI. In *SAE Technical Paper Series*, apr 2009. (cited in p. 75)
- [59] Ingesson Gabriel, Yin Lianhao, Johansson Rolf and Tunestål Per. A Double-Injection Control Strategy For Partially Premixed Combustion. *IFAC-PapersOnLine*, Vol. 49 n° 11, pp. 353–360, 2016. (cited in pp. 76 and 121)
- [60] Yang Tianhao, Yin Lianhao, Ingesson Gabriel, Tunestål Per, Johansson Rolf and Long Wuqiang. Simultaneous control of soot emissions and pressure rise rate in gasoline PPC engine. In *1st Annual IEEE Conference on Control Technology and Applications, CCTA 2017*, volume 2017-Janua, pp. 572–577. IEEE, aug 2017. (cited in p. 76)
- [61] Haskara Ibrahim and Wang Yue-Yun. Closed-Loop Combustion Noise Limit Control for Modern Diesel Combustion Modes. *IEEE Transactions on Control Systems Technology*, Vol. 25 n° 4, pp. 1168–1179, jul 2017. (cited in pp. 76 and 121)
- [62] Blumreiter Julie and Edwards Chris. Overcoming Pressure Waves to Achieve High Load HCCI Combustion. In *SAE Technical Papers*, volume 1. SAE International, apr 2014. (cited in p. 76)
- [63] Kokjohn S L, Hanson R M, Splitter D A and Reitz R D. Fuel reactivity controlled compression ignition (RCCI): a pathway to controlled high-efficiency clean combustion. *International Journal of Engine Research*, Vol. 12 n° 3, pp. 209–226, 2011. (cited in pp. 31, 77, and 184)
- [64] Bahri Bahram, Shahbakhti Mahdi, Kannan Kaushik and Aziz Azhar Abdul. Identification of ringing operation for low temperature combustion engines. *Applied Energy*, Vol. 171, pp. 142–152, jun 2016. (cited in p. 77)
- [65] Li Ruixue C. and Zhu Guoming G. A real-time pressure wave model for knock prediction and control. *International Journal of Engine Research*, Vol. 22 n° 3, pp. 986–1000, mar 2021. (cited in p. 77)
- [66] Yao Mingfa, Zheng Zhaolei and Liu Haifeng. Progress and recent trends in homogeneous charge compression ignition (HCCI) engines. *Progress in Energy and Combustion Science*, Vol. 35 n° 5, pp. 398–437, 2009. (cited in pp. 10, 30, and 77)
- [67] Asad Usman, Divekar Prasad, Zheng Ming and Tjong Jimi. Low Temperature Combustion Strategies for Compression Ignition Engines: Operability limits and Challenges. *SAE Technical Paper Series*, Vol. 1, 2013. (cited in p. 77)

- [68] Paykani Amin, Kakaee Amir-Hasan, Rahnama Pourya and Reitz Rolf D. Progress and recent trends in reactivity-controlled compression ignition engines. *International Journal of Engine Research*, Vol. 17 n° 5, pp. 481–524, jun 2016. (cited in p. 77)
- [69] Shahlari Arsham J., Hocking Chris, Kurtz Eric and Ghandhi Jaal. Comparison of compression ignition engine noise metrics in low-temperature combustion regimes. *SAE International Journal of Engines*, Vol. 6 n° 1, pp. 541–552, apr 2013. (cited in p. 77)

Chapter 4

Dual-fuel combustion control using in-cylinder pressure feedback

4.1 Introduction

Every combustion concept has its own control requirements to be addressed in the controller-design process. In general, the combustion engine controller aims to provide the performance required by the user while ensuring to not exceed operational constraints (e.g., maximum cylinder pressure, unstable operation, emissions).

Advanced combustion concepts such as highly premixed low temperature combustion (LTC) represent a challenging environment when attempting to ensure safe and stable operation. The more the air-fuel mixture gets premixed, the more the combustion gets kinetically driven and consequently raises controllability issues as it was experienced with the homogeneous charge compression ignition (HCCI) concept [1, 2]. Load limitation due to high pressure gradients, significant cycle-to-cycle variation, or excessive unburned products are all examples of obstacles that were encountered and that the developed controllers should tackle [3]. Although the premixed dual-fuel combustion concept helped to improve the controllability capabilities by adding a control over the mixture reactivity [4], this strategy is nonetheless still subject to excessive pressure rise rates in highly premixed conditions. Also, this combustion concept was found to be sensitive to variations in the operating conditions and fuel properties where cylinder balancing is required to achieve optimal efficiency [5, 6]. These challenges should therefore be addressed

in the design of the engine control implementation, especially when dealing with transient operation where non-linear dynamics might lead to unstable operation.

In order to develop control strategies with the aforementioned features, a feedback of the various combustion metrics to be supervised is required. Although actual sensors configuration might already be mature for air-path control, they are nevertheless limited when trying to evaluate what is happening inside the combustion chamber. Some studies aimed for instance to estimate the combustion metrics in each cylinder (e.g., load, combustion phasing, knock) by measuring the crankshaft position [7–9], or the engine block vibration with accelerometers [10–12]. While these solutions are indeed attractive as they take advantage of the sensors currently available on an engine, they used to lack of precision and might require extensive calibration effort.

The in-cylinder pressure sensor has traditionally been adopted for combustion research purposes. Nonetheless, thanks to its direct feedback from the combustion chamber, it was evidenced for its potential to enhance the development of advanced control strategies [13, 14]. Furthermore, once developed, these strategies could be adapted to engines with a competitive cylinder pressure measurement technique, such as ion current sensors, or non-intrusive estimation approach [15–20].

This chapter explores the use of the in-cylinder pressure signal as a feedback in different control scenarios applied to various dual-fuel combustion strategies in order to cover the whole engine operation map, from fully to partially premixed as presented in Chapter 3. First, a closed-loop controller based on proportional-integral control actions is developed to reject external disturbances such as intake pressure or EGR variations in steady operation. The controller effectiveness is also validated in transient conditions where the controller is able to change the combustion mode in order to fulfill the required load, as well as limiting the maximum pressure rise rate to a predefined threshold. The results are provided in section 4.2. Then, the results of an on-line combustion operation optimization using extremum seeking techniques are shown in section 4.3. In this case, the monitoring of the combustion phasing and the NO_x sensor signal were used and, thanks to the controller, the combustion was maintained to a fuel efficient operating area while the nitrogen oxide levels were substantially decreased. Finally, section 4.4 studies the resonance content of the cylinder pressure signal and presents the results of a strategy based on the conventional SI engine knock controller applied to a dual-fuel combustion to limit the harmful potential of heavily excited combustion conditions. Note that, although some control authority was available over the

air-path (see Chapter 3), this work presents results from controllers based on the control of the fuel injection settings only.

4.2 Proportional-Integral combustion control

Conventional combustion control relies mainly on open-loop control strategies which are based on look-up tables storing the control variables values, traditionally function of the load and the engine speed. The main drawback of such method is that the control input is set regardless of the system output response and consequently external disturbances might cause the output to deviate from its desired setpoint. In the case of an engine, if the operating conditions (e.g., intake pressure or exhaust gas recirculation) differ from the expected ones, undesired performance and emissions might be obtained. In order to mitigate such unintended effect, a closed-loop controller can be applied to correct the control inputs. One of the most common and practical solutions is the proportional-integral (PI) controller [21,22]. This type of controller provides corrections to apply to the plant control inputs according to the error measured between a reference setpoint and the actual plant output with the aim to reduce the error to zero. Its discrete form approximation is expressed as:

$$u_{k+1} = K_p e_k + K_i \sum_{j=1}^k e_j \quad \text{with} \quad e_k = r_k - y_k \quad (4.1)$$

where u is the controller output, k the cycle index, e the error between the setpoint r and the system output y , and K_p and K_i are the controller gains for the proportional and the integral actions, respectively. In the case where the considered system embeds open-loop (OL) control inputs, these might be used as feedforward values where the PI actions provide the corrections to apply (Δu) in order to reach the desired plant output setpoint as it is illustrated in Figure 4.1. In this figure, the area delimited by the grey rectangle shows the PI control introduced in (4.1), and the complete closed-loop controller embeds the feedforward control input from the open-loop process whose value is added to the PI control corrections. Such control layout is broadly used in combustion engine control [23–25].

This section presents a real-time closed-loop combustion controller based on the in-cylinder pressure signal applied to engine A, whose specifications can be found in Chapter 3. A control concept is designed for controlling the load and the combustion phasing at a desired value while keeping the pressure rise rate under a defined and safe threshold in all the combustion modes used over the engine

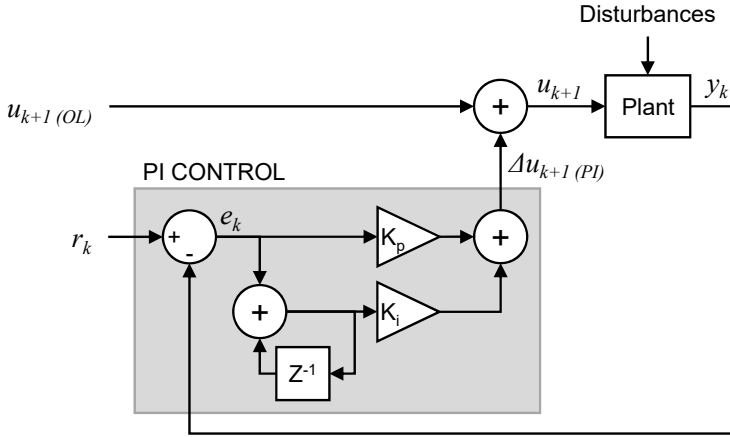


Figure 4.1: Closed-loop control layout based on feedforward and proportional-integral (PI) corrections. The reference r is compared with the output y to estimate the error e . Based on this error, the proportional-integral controller, tuned by K_p and K_i gains, provides the corrections to apply to the control input u .

map. Both steady state and transient conditions were evaluated and the results are provided hereinafter.

4.2.1 Controller design

The controller-design objective was based on the following constraints:

- Regardless of the eventual external disturbances, the engine must provide the load required by the user.
- The combustion phasing is commonly associated to the engine’s efficiency and the controller should therefore be designed to track a reference setpoint.
- No matter the operating conditions, the engine must be kept away from harmful conditions that might be responsible of engine damage.

Here, the load was evaluated using the indicated mean effective pressure (IMEP) calculated from the cylinder pressure trace and the instantaneous volume computation (see Chapter 3). The maximum pressure rise rate (MPRR) was considered as the mechanical constraint limitation to avoid engine damage where a value of 15 bar/CAD was considered as the limit to not overcome in this engine. Finally, in this control application, instead of the common CA50, the combustion phasing was estimated through the parameter known as the combustion centroid [26],

hereinafter named the crank angle of the combustion center of gravity (CACG). This choice was justified by CA50 cycle-to-cycle variations observed in this engine under some conditions when using late diesel injection control (partially premixed mode). More details are provided in Chapter 3.

In order to fulfill the aforementioned objectives, the controller must be designed according to the system input-output pairing. The fuel injection provides a cycle-to-cycle control over the combustion and was therefore chosen as the core of the closed-loop control design. This responsiveness is essential to ensure a safe operation of the engine if harmful conditions are detected in order to respond from one cycle to the next one. The various fuel injection control variables were explored and selected for each control objective, as detailed below.

IMEP control The load is directly a function of the quantity of fuel burned during the combustion. Thus, the more the fuel injected and burned inside the cylinder, the larger the expected engine load. For this reason, the total fuel quantity m_f^{tot} was chosen as the control variable to control and correct the load in the closed-loop controller:

$$m_f^{tot} = m_f^{pre} + m_d^{post} \quad (4.2)$$

where m_f^{pre} corresponds to the fuel quantity injected in premixed conditions, and m_d^{post} refers to the quantity of diesel injected in the top dead center vicinity in the partially premixed combustion mode. The former is composed of the gasoline amount injected during the intake stroke (m_g) and the diesel injected in a premixed timing window before the TDC (m_d^{pre}), which might be injected at once or split into a *pilot* and *main* injections:

$$m_f^{pre} = m_g + m_d^{pre} \quad (4.3)$$

In this section, the name *post* is used to ease the interpretation of the area in which the diesel is injected (near the TDC). If present, this injection corresponds in reality to the *main* injection and does not represent a post injection as it is traditionally named in multiple injection strategies.

CACG control Dual-fuel combustion offers an additional degree of freedom to enhance the control of the combustion timing: the blending ratio of the low and the high reactivity fuels. Such control variable allows to act on the reactivity of the fuel mixture. In fully/highly premixed conditions, such as the RCCI concept, increasing the low reactivity fuel proportion was found to delay the combustion. Accordingly, the gasoline fraction was selected to act on the combustion timing.

Nonetheless, the designed controller aims to be applied in the various dual-fuel combustion modes, and the partially premixed conditions might exhibit lower sensitivity to a change in the gasoline fraction. Indeed, when reaching the TDC vicinity, the late diesel injection is used to ignite the premixed charge composed mainly of gasoline and is consequently more prone to trigger the combustion and have an effect on the resulting combustion timing (see Chapter 2 for more information and references). As a result, in this concept, although the CACG is controlled using a single PI controller, it is proposed to apply the corrections to two control parameters: the gasoline fraction of the premixed charge (GF_{pre}), described in (4.4), and the post diesel injection timing (SOI_{post}).

$$GF_{pre} = \frac{m_g}{m_{pre}^f} \quad (4.4)$$

Figure 4.2 describes the logic behind the CACG controller. The correction applied by the PI controller (Δu_{CACG}) is distributed to both the gasoline fraction and the injection timing. First, while the combustion phasing can be reached by using the premixed charge blending ratio only, GF_{pre} is controlled in order to modify the reactivity of the fuel mixture. However, when GF_{pre} approaches the unity, meaning that the premixed fuel quantity is exclusively composed of gasoline, such control parameter cannot be extended further and therefore SOI_{post} starts to control the CACG (note that here the gasoline fraction is a normalized value). In this case, the corrections were limited to $GF_{pre} = 1$ for Δ_{GF} (see upper part of Figure 4.2), and 0 for the injection timing correction Δ_{SOI} (see lower part of the figure). More precisely, the controller starts acting on the injection timing correction only once the gasoline fraction approaches the unity, represented by the value of 0.96 in Figure 4.2 which is used for a better transition between both control actions. Note that the injection timing is expressed in CAD before TDC (bTDC), which justifies why its correction (Δ_{SOI}) is oriented to the negative values in order to delay the combustion further. Here, it was decided to design the PI controller in such a way that its correction value was directly applied to GF_{pre} (Δ_{GF}). For this reason, the gain K_{SOI} was used for the scaling correction due to the difference in units between GF_{pre} and SOI_{post} , and consequently provide a suitable value to the injection timing correction (Δ_{SOI}). Note that the error used to calculate the PI correction corresponds to the error between the desired CACG value ($CACG_r$) and the measured feedback expressed in CAD after TDC (aTDC).

MPRR control The harmful potential of premixed combustion modes comes from the rapid auto-ignition of the air-fuel mixture, resulting from the early fuel injection. According to this statement, it was decided to use the premixed fuel

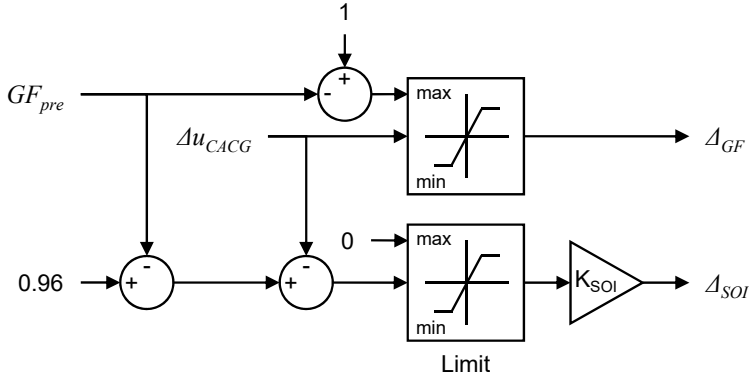


Figure 4.2: CACG control concept. A single PI correction (Δu_{CACG}) is used to estimate the correction to apply to both GF_{pre} and SOI_{post} . The correction is applied to the gasoline fraction first, either to advance or delay the combustion. Once its value is getting close to 1 (tuned by the constant here set at 0.96), and therefore cannot be increased anymore, the correction is performed by the injection timing whose value is determined by a calibration gain K_{SOI} to adapt the correction to this control variable.

quantity m_f^{pre} , as expressed in (4.3), to control the maximum pressure rise rate. When the MPRR is detected above a limit ($MPRR_{lim}$) the control starts to correct the premixed charge to maintain the MPRR level to the desired threshold according to:

$$\Delta m_{f(k+1)}^{pre} = K_p e_{MPRR(k)} + K_i \sum_{j=1}^k e_{MPRR(j)} \quad \text{when } e_{MPRR} > 0 \quad (4.5)$$

$$\Delta m_{f(k+1)}^{pre} = C_1 K_p e_{MPRR(k)} + C_2 K_i \sum_{j=1}^k e_{MPRR(j)} \quad \text{when } e_{MPRR} \leq 0 \quad (4.6)$$

where K_p and K_i are the proportional and the integral gains respectively, and C_1 and C_2 are calibration constants (higher than 1) in order to get a faster response from the controller when the MPRR is reaching a value above the limit. Such control embeds an hysteresis for avoiding control instabilities, that is: the pressure rise rate has to be detected above an upper limit to activate the control, and must comply with a safe operation for various cycles before switching back. This hysteresis is set around the desired MPRR limit which was here set to 12 bar/CAD in order to keep a safety margin from the considered engine limitation of 15 bar/CAD. According to this control design, as long as the load can be achieved in highly premixed conditions, the total fuel quantity m_f^{tot} equals the

premixed part m_f^{pre} . However, the latter will be limited when operating at the engine limit and, if a higher load has to be achieved, then the total fuel quantity has to be increased. When such situation occurs, the required difference will be injected in the post injection (m_d^{post}) at a predefined injection timing near the TDC.

The aforementioned control parameters (m_f^{pre} , m_f^{tot} , GF_{pre} , SOI_{post}) are stored in look-up tables as a function of the engine speed (N) and the IMEP for conventional open-loop control. These values are then closed-loop corrected in order to reach the desired performance. The rest of the control variables such as the gasoline and the premixed diesel injection timings are considered as calibration parameters (also stored in look-up tables), and are not varied by the controller. The closed-loop control system can be summarized by the following description where r , y and u are the *reference*, *output* and *input* vectors respectively:

$$r = \begin{pmatrix} IMEP_r \\ CACG_r \\ MPRR_{lim} \end{pmatrix}, y = \begin{pmatrix} IMEP \\ CACG \\ MPRR \end{pmatrix}, u = \begin{pmatrix} m_f^{tot} \\ GF_{pre} \\ m_f^{pre} \\ SOI_{post} \end{pmatrix} \quad (4.7)$$

Figure 4.3 presents the overall closed-loop control concept used in this work. Note that a low-pass filter was applied to the feedback values to calculate the error in order to avoid control instabilities that could be caused by normal cyclic variability. Finally, all the fuel injection variables were rearranged and transcribed into injection duration to be sent to the injectors thanks to injector models in the form of look-up tables, which are a function of the required mass and a pressure reference (intake manifold for PFI and rail for DI).

4.2.2 Results and discussion

Controller experiments were conducted to validate the proposed strategy in engine A. First, steady-state conditions were used to evaluate the ability of the controller to maintain the desired engine performance while rejecting external disturbances. Then, a load transient test was performed to evaluate the controller behavior against such conditions.

Steady-state validation

Table 4.1 lists the tests that were performed for the steady-state controller evaluation. These tests represent various conditions: tests 1, 2 and 3 were used to evaluate the controller capability to maintain the required performance under a variation, respectively, in EGR, intake pressure P_{int} and diesel rail pressure P_{rail} .

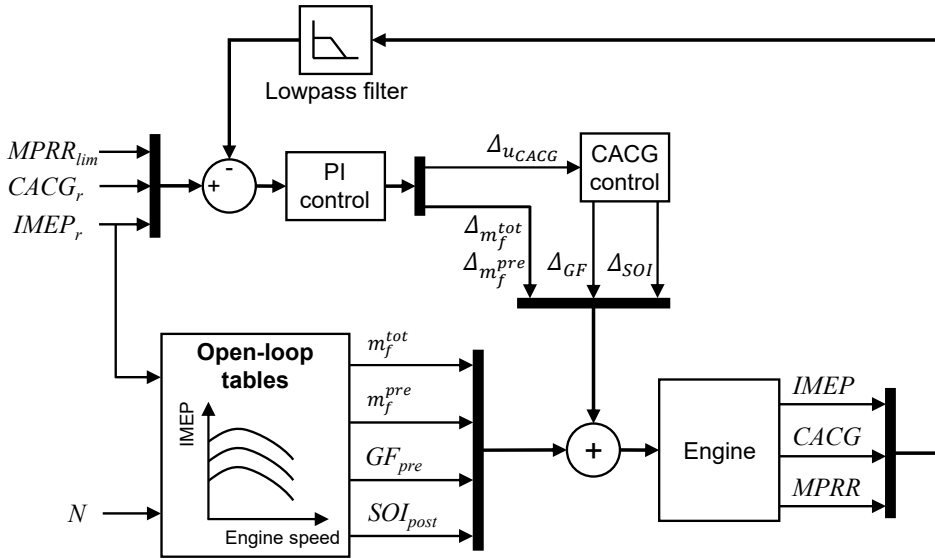


Figure 4.3: Closed-loop controller layout used for the control of the dual-fuel combustion in engine A. Note that for the CACG control (detailed in Figure 4.2), GF_{pre} is an input and should therefore be connected to this box as well from the open-loop tables output. However, for illustration purposes, this connection was not represented here.

Test 4 was used to observe the controller response under changes in the CACG reference setpoint ($CACG_r$). Each test was performed under a specific combustion mode where the test 2 represents a transition between fully premixed and highly premixed strategy due to its operating conditions (please refer to Chapter 3 for a description of the combustion modes used in this engine).

The control variables m_f^{tot} , m_f^{pre} , GF_{pre} and SOI_{post} were originally set by the open-loop look-up tables and then closed-loop corrected (see Figure 4.3) to reach the desired performance, i.e., ensure IMEP and CACG tracking and maintain the MPRR to a safe threshold when necessary. In the following figures, the control variables are shown in solid black lines, and the measured outputs in a solid grey line. The target values for IMEP and CACG, as well as the limit threshold for MPRR, are shown in a black dashed line. An additional graph shows the apparent heat release rate traces dQ_{app} of three selected cycles, shown in colored crosses, in order to illustrate the resulting combustion evolution at different conditions over the test. The injected fuel quantities are expressed in mg/str, where *str* refers to stroke, hence *per cycle per cylinder*.

Table 4.1: Operating conditions of the experimental tests used for the steady-state controller validation.

Test	Premixed combustion mode	N [rpm]	IMEP [bar]	P_{int} [bar]	P_{rail} [bar]	EGR [%]
1	Fully	1200	4	1.4	1200	0 to 58
2	Fully-Highly	1200	8	1.8 to 2.7	1200	24 to 38
3	Highly	1200	12	2.2	1000 to 1400	49
4	Partially	1200	16	2.4	1200	45

Figure 4.4 presents the EGR variation in test 1 where the EGR valve position was varied to modify the CO_2 concentration at the intake. The air dilution caused by the exhaust gas recirculation is responsible of increasing the ignition delay and delaying the combustion [27, 28]. In fully premixed conditions, it is thus expected that the longer ignition delay, resulting from the increase in EGR rate, should be compensated by the gasoline fraction in order to keep the combustion phasing constant [29, 30]. It can be observed that once the EGR was increased, GF_{pre} was corrected (decreased in this case) by the controller to maintain the combustion phasing at the desired target. No significant effect on the IMEP was observed as the controller was able to maintain its level by modulating the total injected fuel mass m_f^{tot} . In this case, the MPRR was not controlled due to the low levels obtained at this load. Consequently, the total fuel quantity m_f^{tot} was equal to the premixed amount m_f^{pre} because the premixed charge alone was able to provide the desired load. Over the complete experiment, the controller was able to control the IMEP and the CACG within a mean absolute error (between the setpoint and the actual value) of 0.09 bar and 0.28 CAD respectively. The respective error standard deviation for the IMEP and the CACG along the test were 0.11 bar and 0.36 CAD. The combustion evolution can be appreciated in the top right plot where the dQ_{app} traces from three selected cycles at different conditions show a very similar evolution, hence exhibiting an equivalent IMEP, CACG and MPRR. These apparent heat release rate traces show the typical combustion evolution of the RCCI combustion concept with a low temperature heat release (LTHR) preceding the main high temperature heat release (HTHR) [31].

The results from the intake manifold pressure variation along test 2 are shown in Figure 4.5. Note that the EGR valve opening was kept constant, hence justifying the variation in the EGR rate as indicated in Table 4.1. Increasing the

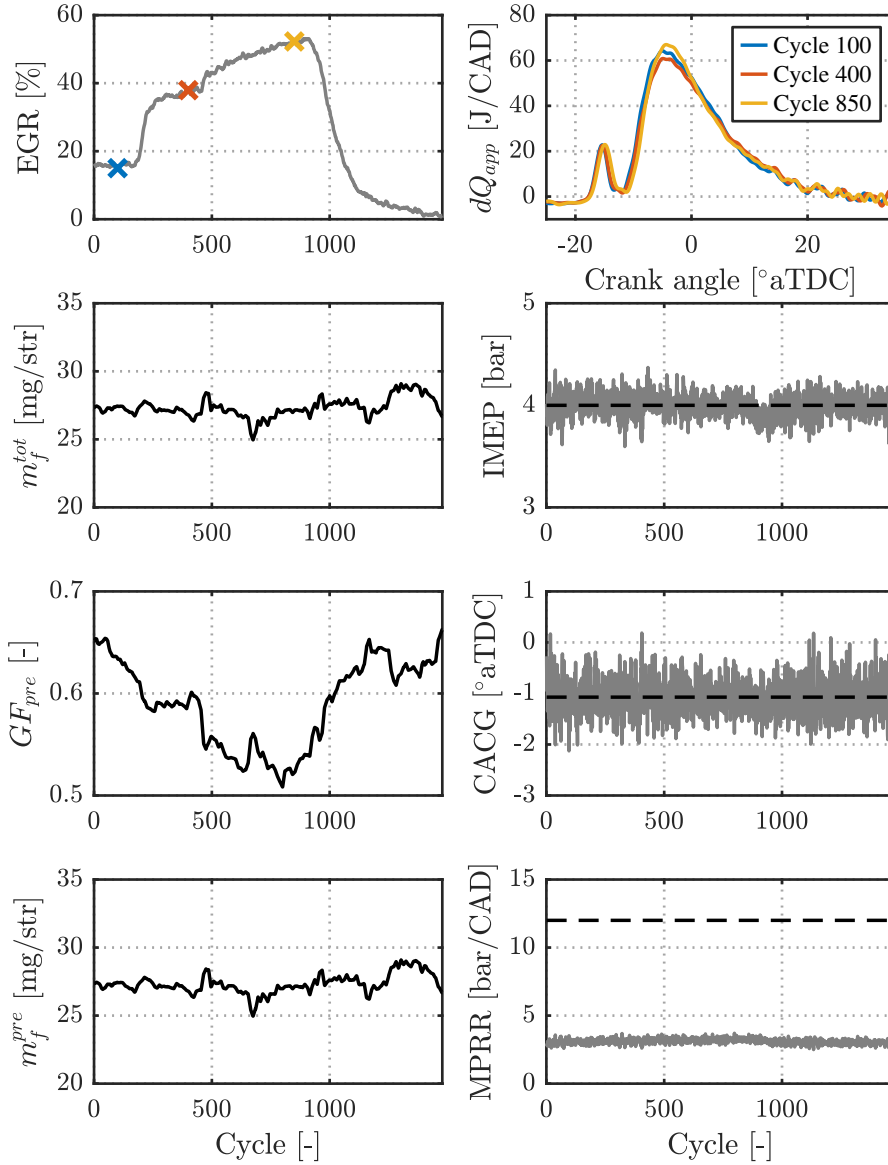


Figure 4.4: Closed-loop controller inputs (u) and outputs (y) from (4.7) during an EGR variation in test 1 (Table 4.1). Reference setpoints r are shown with a black dashed line. In this test m_f^{pre} and m_f^{tot} are equal as the MPRR is below its limit. Top right plot shows the heat release rate traces from three selected cycles shown in top left plot.

intake pressure was expected to advance the auto-ignition of the mixture, due to the rise of pressure and temperature during the compression stroke [32], and explains why the gasoline fraction was increased by the controller in order to maintain the combustion phasing to its setpoint. The increase in P_{int} also induced a faster combustion evolution which caused an increase of the MPRR level, followed by a transition between the fully premixed and the highly premixed combustion modes. Indeed, in this situation, the pressure rise rate level exceeds the limit and thus activates the control of the MPRR (grey shaded area in these plots). The premixed fuel m_f^{pre} is limited by the controller to keep the MPRR level to the limit threshold, while m_f^{tot} is controlled to fulfill the load requirement using the late diesel injection in the TDC area, i.e., the load is achieved through m_d^{post} . It was observed that the load was correctly controlled to its reference by the total fuel amount. Although a post diesel injection was used to maintain the required load, here the gasoline fraction alone was able to control the combustion phasing and the SOI_{post} control was therefore unnecessary. When the intake pressure decreased enough to come back into a safe engine operation, the MPRR control was deactivated and the load was again controlled only by the premixed fuel quantity m_f^{pre} . The cycle-to-cycle CACG variation was observed to be, overall, higher in fully premixed conditions (standard deviation of 0.46 CAD) than in highly premixed combustion (standard deviation of 0.30 CAD). This was attributed to the combustion mode as the fully premixed combustion is purely driven by the reaction rates of the in-cylinder species, while the highly premixed mode might have exhibited a better control over the combustion phasing thanks to the late diesel injection timing. However, the observed IMEP variation rise, when the pressure rise rate control was activated (0.36 bar standard deviation against 0.18 bar otherwise), was found to be caused by some bias in the injector models in this region, resulting in a higher variability. Despite such situation, the errors at the IMEP and the CACG control were found to be within a mean absolute error of 0.18 bar and 0.33 CAD, and error standard deviation of 0.25 bar and 0.43 CAD, respectively. Meanwhile, when the MPRR control was enabled (shaded area), around 30% of the cycles were observed above the 12 bar/CAD threshold with a maximum peak measured at 13.8 bar/CAD, showing that the controller was able to keep the engine in a safe operation area.

Figure 4.6 provides the results obtained in test 3 where the diesel rail pressure was varied between 1000 and 1400 bar in order to evaluate the controller ability to reject such variation while keeping IMEP, CACG and MPRR to their setpoint and limitation. This test was performed in the highly premixed combustion mode. In these load conditions, the MPRR level could be harmful for the engine and is

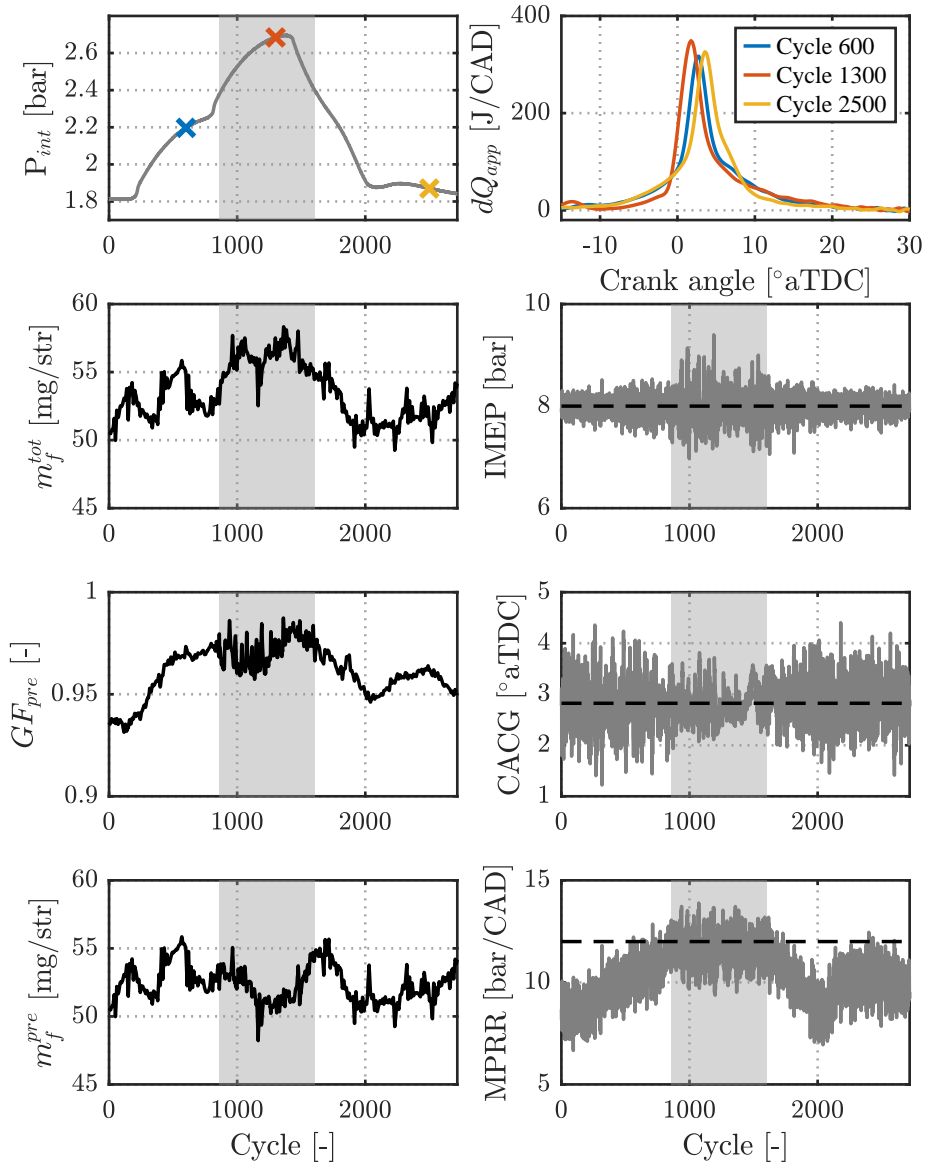


Figure 4.5: Closed-loop controller inputs (u) and outputs (y) from (4.7) during a P_{int} variation in test 2 (Table 4.1). Reference setpoints r are shown with a black dashed line. The shaded area from cycle 860 to cycle 1600 corresponds to the combustion switching-mode and MPRR control activation. In this area m_f^{pre} and m_f^{tot} differ as the former is limited (the load is fulfilled by m_d^{post}). Top right plot shows the heat release rate traces from three selected cycles shown in top left plot.

hence controlled near the limit, resulting in a different m_f^{pre} (limited) and m_f^{tot} (controlled to fulfill the load requirement). Similarly to the previous experiment, GF_{pre} alone was able to control the CACG to the desired value and the control of SOI_{post} was consequently not activated. The controller shows a global capacity to compensate P_{rail} variations although some spikes in the load and the combustion phasing control can be observed when changing suddenly the rail pressure from 1200 to 1400 bar, and opposite way. Such phenomena could be justified by some inaccuracies in the injector model and controller response time to tackle these spikes when they occur (about 30 to 40 cycles were necessary to recover the combustion phasing). These rapid changes represent a challenge for the controller as they induce a modification of the injection map operating area and might interfere with the previous corrections applied by the PI controller. A finer injector look-up table model and a more aggressive controller are believed to contribute to address these spikes more efficiently. Despite the stated spikes, the mean absolute error of the IMEP control was 0.13 bar, about 0.50 CAD for the CACG control, and the MPRR was maintained within a mean absolute difference to the limitation value of about 0.52 bar/CAD. In this experiment, the respective error/difference standard deviations for the IMEP, the CACG, and the MPRR, between the setpoint and the actual value, were 0.18 bar, 0.70 CAD and 0.60 bar/CAD. In this combustion mode, the beginning of a tail combustion induced by the late diesel injection can be noticed in the dQ_{app} plot compared to the single peak combustion observed previously in fully premixed conditions.

Finally, an experimental verification of the strategy presented in Figure 4.2, in a partially premixed combustion, is shown in Figure 4.7 (test 4). Here, the CACG setpoint value was varied throughout the test. In particular, the control strategy including the activation of the use of the post diesel injection timing to delay the combustion is evaluated. It can be observed that, as the combustion setpoint gets delayed, the first phase is undertaken by an increase in the gasoline fraction. Then, once this value approaches the unity saturation, the combustion needs to be phased by the help of adjusting SOI_{post} in order to reach the desired value. The resulting combustion evolution can be appreciated in the plot representing the apparent heat release rate dQ_{app} corresponding to the selected cycles (50, 240 and 380). However, it was found that the controller lasted several cycles to reach the target value. A rise time¹ of about 30 cycles for the gasoline fraction control (first setpoint variation) and about 90 cycles for the SOI control (second setpoint variation), with a settling time² of about 70 and 120 cycles, respectively, were

¹The time the system requires to go from 10% to 90% of the final value.

²The time required for the system to settle within a 5% range of the final value.

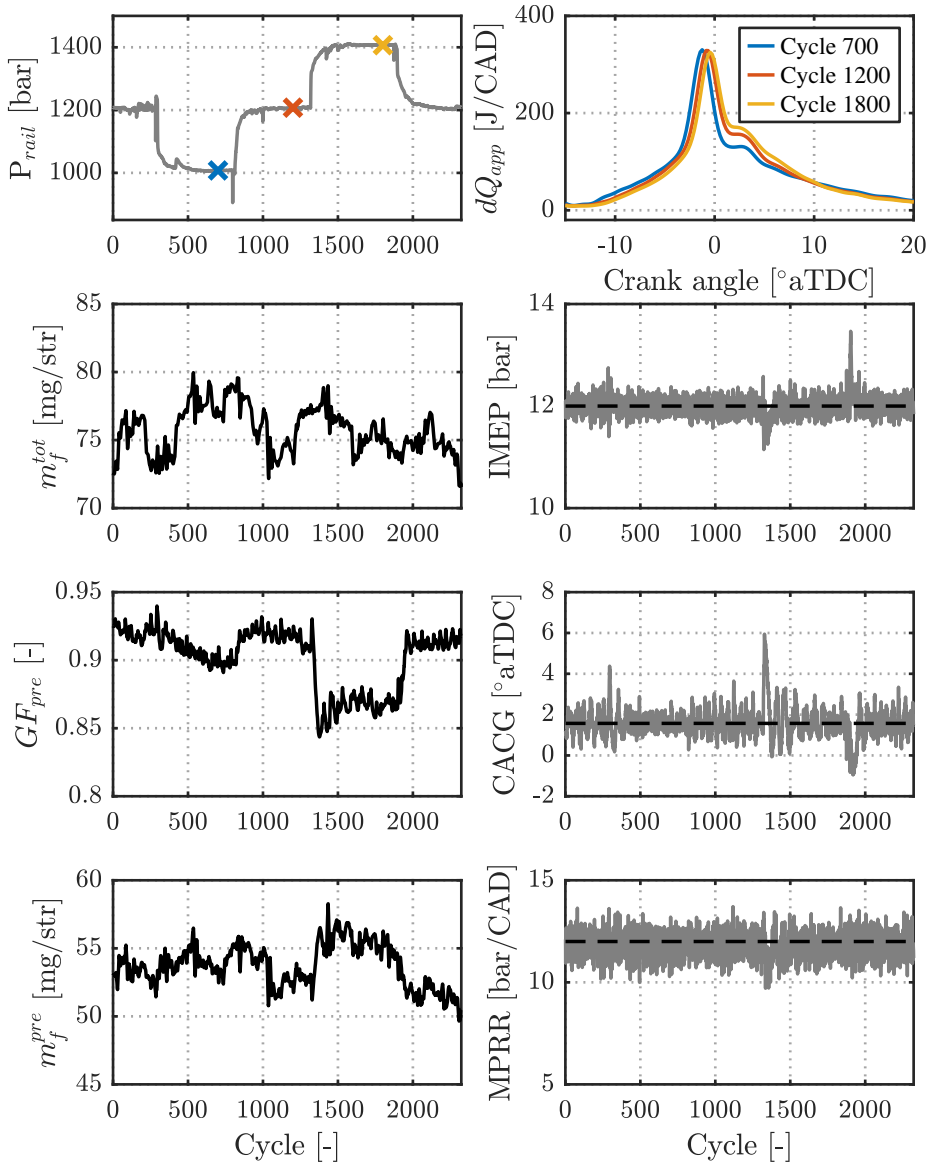


Figure 4.6: Closed-loop controller inputs (u) and outputs (y) from (4.7) during a P_{rail} variation in test 3 (Table 4.1). Reference setpoints r are shown with a black dashed line. In this test m_f^{pre} and m_f^{tot} differ as the former is limited for MPRR control (the load is fulfilled by m_d^{post}). Top right plot shows the heat release rate traces from three selected cycles shown in top left plot.

Table 4.2: Mean absolute value (MAE) and standard deviation (σ_e) of the error between the setpoint and the cycle-to-cycle value during the steady-state validation experiments.

Test	Disturbance		IMEP		CACG		MPRR	
			MAE	σ_e	MAE	σ_e	MAE	σ_e
1	EGR	(Fig. 4.4)	0.09	0.11	0.28	0.36	Not enabled	
2	P_{int}	(Fig. 4.5)	0.18	0.25	0.33	0.43	0.75*	0.38*
3	P_{rail}	(Fig. 4.6)	0.13	0.18	0.50	0.70	0.52	0.60
4	$CACG_r$	(Fig. 4.7)	0.13	0.17	0.20 [†]	0.22 [†]	0.47	0.56

* When the MPRR controller is enabled (shaded area in Figure 4.5)

[†] Once CACG is stabilized (after settling time)

observed. This observation is justified by the PI gains used in this application. Here, the priority was set to ensure a proper load and pressure rise rate control at the expense of the combustion phasing. Indeed, while the load and the MPRR represent the performance and the safe operation of the engine, the latter is traditionally associated to fuel consumption optimization, which was not considered as the first priority in this case. Nonetheless, improved rise and settling times should be obtained with a finer tuning of the controller PI gains. Regarding the IMEP and the MPRR control, as in the previous test, m_f^{pre} and m_f^{tot} differed for the same reason, and it was measured that both output values were correctly controlled to their target value within a mean absolute error of 0.13 bar and 0.47 bar/CAD, with an error standard deviation of 0.17 bar and 0.56 bar/CAD, respectively.

Table 4.2 summarizes the outcomes of the PI combustion controller developed in this section in the various steady-state experiments. Furthermore, in order to verify that the closed-loop controller was not leading into an additional source of cycle-to-cycle variation, the standard deviation σ from four operating points in steady-state conditions were compared between dual-fuel combustion (DFC) operation in open-loop (OL) and closed-loop (CL) control. Figure 4.8 presents the results obtained from 100 recorded cycles for IMEP, CACG and MPRR. The results are compared to similar operating points, in the same engine, with conventional diesel combustion (CDC) as reference. It can be observed that the closed-loop control tends to increase the standard deviation, although not significantly, for the IMEP and the CACG compared to DFC-OL. It is also noticed that the CACG cyclic variation tends to decrease as the load increases which is believed to be justified by the mixing controlled combustion at these load levels

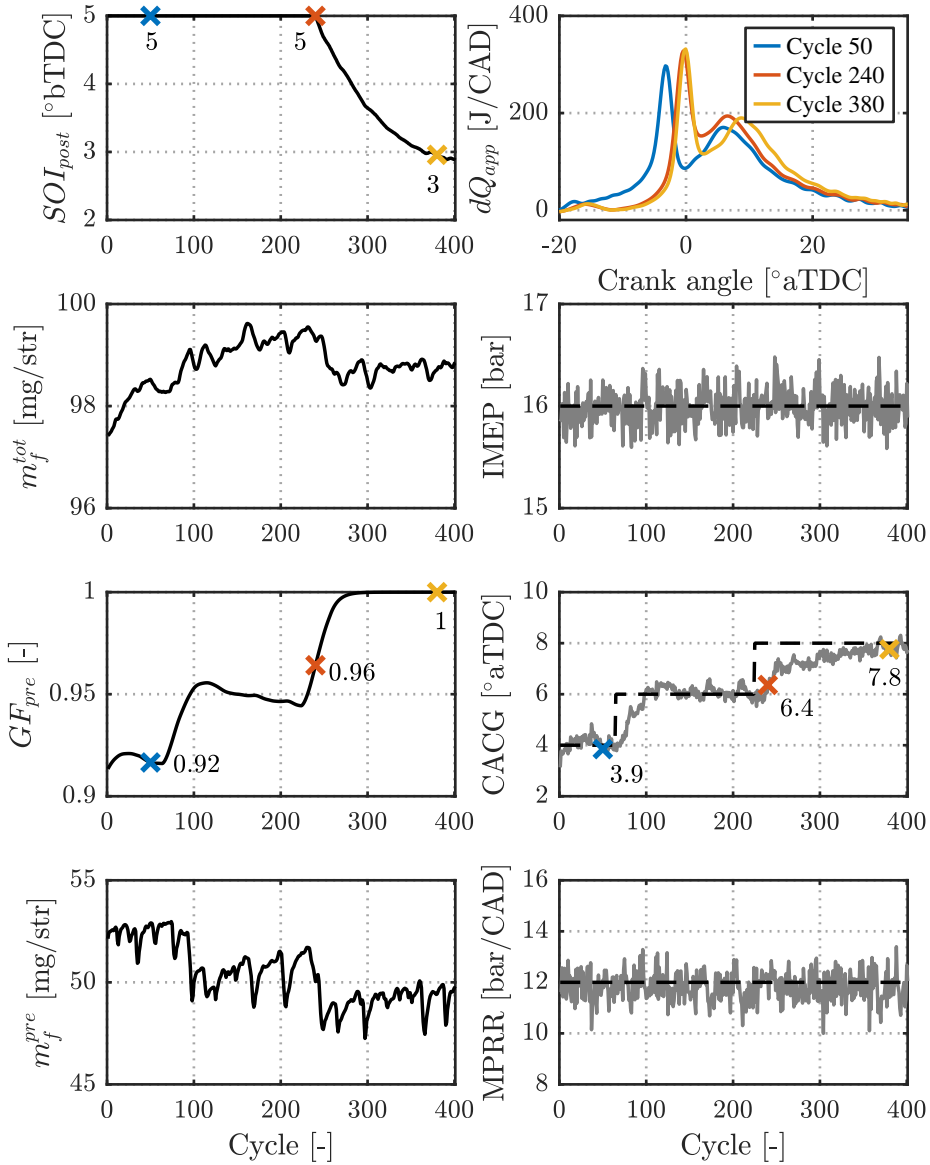


Figure 4.7: Closed-loop controller inputs (u) and outputs (y) from (4.7) during a CACG setpoint variation in test 4 (Table 4.1). Reference setpoints r are shown with a black dashed line. In this test m_f^{pre} and m_f^{tot} differ as the former is limited for MPRR control (the load is fulfilled by m_d^{post}). Top right plot shows the heat release rate traces from three selected cycles shown in top left plot.

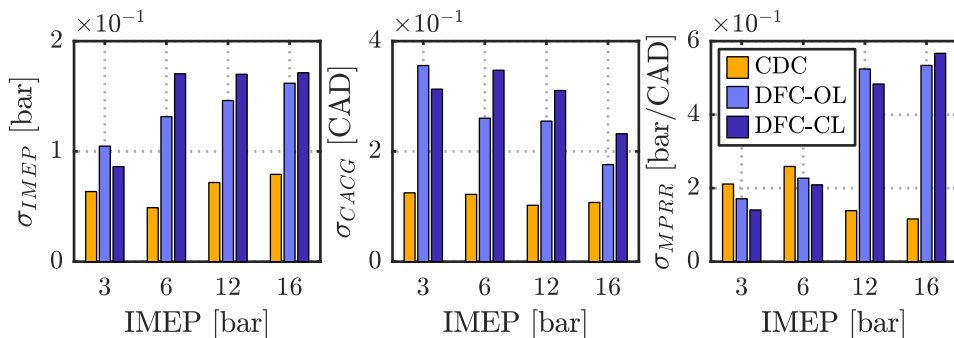


Figure 4.8: Cycle-to-cycle standard deviation comparison of IMEP (left), CACG (middle) and MPRR (right) at different loads between conventional diesel combustion (CDC) in open-loop control and dual-fuel combustion (DFC) in open-loop (OL) and closed-loop (CL) control.

(i.e., partially premixed with the use of a diesel injection in the TDC vicinity to trigger the combustion). Regarding the pressure derivative, at low load, the MPRR is not controlled because of its low level. However, at 12 and 16 bar IMEP, when the control is activated, DFC-CL shows a similar standard deviation value to DFC-OL. Finally, overall, it is noticed that the premixed dual-fuel combustion seems to exhibit more cycle-to-cycle variation than in CDC. This observation was also made by Klos et al. [33] where premixed combustion modes such as RCCI and HCCI were found to show more cyclic variation. This observation is mainly justified by the combustion sensitivity to the operating conditions (e.g., pressure, temperature, residual gases) for these types of combustion that feature a different mixture stratification (i.e., significant premixed charge) compared to conventional diesel combustion strategy [34].

Transient validation

The designed controller was evaluated in transient conditions and the results are provided in Figure 4.9. Here, the combustion phasing control was not evaluated as the priority was set to provide the required load at first while constantly ensuring a safe engine operation. In this test, a significant change in load was performed from 5 to 24 bar IMEP, resulting in a combustion switching-mode from fully to partially premixed. In this case, the switch in the combustion mode was directly applied by the controller using the feedforward open-loop settings, where an important fuel quantity is injected through a late diesel injection as it can be seen in the left plots of Figure 4.9 (i.e., the difference between m_f^{pre} and m_f^{tot}).

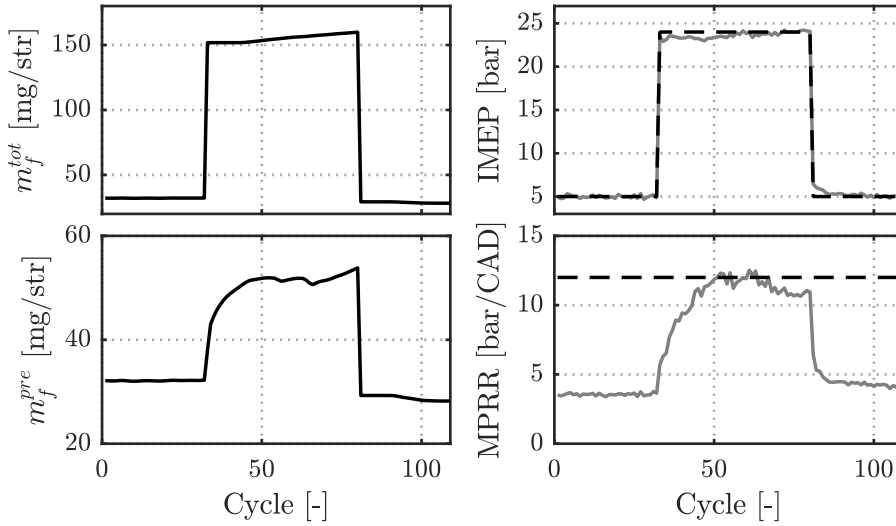


Figure 4.9: Controller validation under transient conditions at 1200 rpm. A significant change in the IMEP setpoint is performed and the resulting controller outputs are monitored. The total fuel quantity m_f^{tot} is controlled to provide the required load, while m_f^{pre} is limited to ensure a safe operation of the engine. Reference setpoints r are shown with a black dashed line.

In an important setpoint variation, such as the one presented here, the closed-loop corrections applied before the setpoint change might no longer be suitable for the new control region. For this reason, it was decided to reset the PI corrections and to rely on the open-loop settings only for a few cycles, right after the setpoint transient, before getting back to the closed-loop control strategy. Furthermore, in high and fast transient operation, if the operating conditions (e.g., intake pressure, oxygen concentration) are not satisfied quickly enough, the applied injection settings might result in non-desired operation (e.g., significant pressure rise rate) due to the difference with the conditions used for the open-loop look-up tables calibration. It was therefore decided to limit the premixed fuel quantity m_f^{pre} to a pre-calibrated value within a safe region for a few cycles at first before closed-loop correcting the value provided by the open-loop look-up table. The effect of the operating conditions can be observed in the last part of the high load transient region in the m_f^{pre} plot (around cycle 65) where, after some time due to the air-path dynamics, the conditions (EGR, pressure and temperature, etc.) led to a safer operation with a decrease in the MPRR level and allowed therefore to increase the premixed fuel quantity.

The controller was able to reach the desired IMEP within a rise time of 1-2 cycles and without overshoot. The settling time at 5% was found to be of 1 cycle, and about 20 cycles at 2%, which shows some margin for improvements. Also, it is important to note that in this strategy the fuel transport dynamics from the port fuel injection [35] at the intake were not considered because the main part of the load was provided by the late diesel injection (difference between m_f^{pre} and m_f^{tot}), which does not exhibit any fuel transport dynamics since it is direct injected. However, in a case where the gasoline fraction would represent an important part of the load charge, the port fuel injection transport dynamics effect might be included in the controller in order to improve its performance [36]. Furthermore, in transient conditions, the residual gases from the previous cycle can affect the combustion of the next cycle [37]. In this work, the change of the residual gases fraction from one cycle to the other was considered to be small enough to be directly corrected by the PI actions. Finally, as previously highlighted with steady-state conditions, the controller was able to maintain the MPRR at the desired limit value by modulating the premixed fuel quantity. The mean absolute error of the IMEP control over the complete transient test was 0.3 bar with a peak at 1.5 bar error, when decreasing the load around cycle 80, during 1 cycle.

Overall, the controller showed its ability to maintain the expected performance under an acceptable cyclic variability against external disturbances, in both steady-state and transient conditions, without significant overshoot and without getting over the mechanical constraints limitations. It was observed that the controller was able to switch from one combustion mode to another, to ensure the load requirement using a post injection, and to balance the gasoline fraction and the diesel injection timing control actions to track the CACG setpoint, although with some margin for improvement to get a faster response. A gain-scheduling approach [38] could contribute to improve the feedback controller ability to operate in a wider range of operating conditions and might assist in transient operation.

4.3 On-line combustion operation optimization

While conventional feedback controllers such as the one presented in the previous section are efficient to track and maintain the engine operation to the reference setpoint against external disturbances, they cannot ensure its optimal operation. Indeed, engine calibration prior to on-road application is traditionally performed in a controlled environment (e.g., engine test bench). During this calibration phase, a combustion phasing area might be chosen for the best efficiency and pollutant emissions trade-off under certain operating conditions, and be therefore considered

as the target to be achieved. However, in real-world operation, if these conditions deviate from the expected ones, enforcing the tracking of the pre-calibrated combustion phasing setpoint by closed-loop control might worsen the emissions because the setpoint is no longer optimal.

An efficient way to optimize the engine operation on-line is by means of extremum seeking technique. One of the main advantages of the extremum seeking (ES) strategy is that it is a powerful tool that does not require a model of the system. Instead, this model-free strategy finds the input that minimizes (or maximizes, depending on the definition) a function by perturbing the system with a known periodic input signal. By analyzing the output response, the corresponding gradient can be obtained and be used to seek for the extreme region (i.e., optimal). This approach was introduced in the 1920s [39] and has been since then investigated in many areas, e.g., from heat pumps to powered prostheses [40–42].

The system's output signal can be analyzed directly by the extremum seeking controller, or previously reordered in the form of a cost function. This signal (or function) is then, first, band-pass filtered to remove the low frequency content, associated to the mean amplitude, and the high frequency content, associated to noise, to capture the function response to the input perturbation. The gradient is then estimated by multiplying the band-pass filtered signal by the perturbation. The final correction is obtained by integrating the gradient multiplied by a calibrated gain. It is important to ensure that both the perturbation and the output of the band-pass filter signals are in phase. Indeed, in the case of sensor measurement delay, while the perturbation would be incremented at the instant t_0 , the sensor might provide the resulting system response only at $(t_0 + \delta t)$, which can result in an incorrect gradient estimation and lead to unstable operation [43]. If necessary, the perturbation might be shifted accordingly to get both signals in phase. The global extremum seeking principle architecture is shown in Figure 4.10 where the ES controller is delimited by the grey area. In this figure, u_0 corresponds to the initial control input value. More information about extremum seeking algorithms can be found in [44, 45].

Extremum seeking controllers can be found in spark ignition engines with control over the spark advance timing in order to optimize the engine efficiency [46–48]. Lewander et al. [49] applied an extremum seeking controller to a diesel engine where an optimal combustion phasing reference was evaluated and tracked to provide the best indicated efficiency. Van der Weijst et al. in [50] considered an ES controller for on-line fuel efficiency optimization in a diesel engine by adjusting the

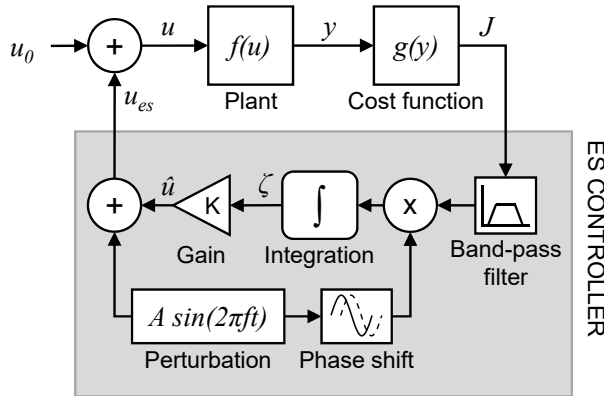


Figure 4.10: Conventional extremum seeking controller architecture for a single variable. A periodic perturbation of amplitude A and frequency f is applied to the original steady state input u_0 . The plant output y is restructured into a cost function J which serves as an input to the extremum seeking (ES) controller.

combustion phasing and pumping losses references. Both air and fuel-path were considered and a NO_x sensor placed at the engine exhaust was used to constrain the control actions. Due to the traditional sensor delay observed in NO_x sensors, Tan et al. [43] proposed to include the nitrogen oxides emissions in the cost function by taking advantage of their correlation with the combustion temperature. The ES controller aimed therefore to reduce the estimated in-cylinder temperature in order to reduce NO_x emissions.

In this section, a controller is designed based on the extremum seeking technique and is applied to engine B. In particular, the extremum seeking method was chosen to minimize a cost function consisting in the optimal combustion phasing tracking and the reduction of NO_x emissions.

4.3.1 Problem formulation

The overall objective of this investigation is to propose and verify an on-line optimization algorithm for dual-fuel engine operation. To this end, it is necessary to define the quantity to optimize and which control inputs can operate the system to do so.

The combustion phasing, usually expressed as the CA50, is a commonly adopted variable to track the highest engine brake efficiency. A reference setpoint $CA50_r$

might therefore be calibrated and tracked by the controller, similarly to the previous section. However, a trade-off exists between fuel consumption (i.e., brake efficiency) optimization and pollutant emissions reduction. In this work, it was therefore decided to also include the NO_x sensor measurement into the function to consider the pollutant emissions in the optimization problem. The performance function design resulted in the following cost function J :

$$J = |CA50 - CA50_r| + \beta NO_x \quad (4.8)$$

where the first part aims to operate the engine in an efficient area provided by a previously calibrated value of $CA50_r$, and the last part corresponds to the pollutant emissions criteria. The weighting factor β was used to emphasize the importance of the NO_x emissions in the final cost evaluation. When $\beta > 0$ the optimizer algorithm will attempt to reduce the NO_x level at the expense of an ideally phased combustion.

4.3.2 Controller design

In this work, the extremum seeking technique was designed to optimize the engine operation according to (4.8). The proposed controller must therefore be based on control variables able to drive both the combustion phasing ($CA50$), and the nitrogen oxides emissions (NO_x). The NO_x emissions are sensitive to the combustion temperature. Hence, to some extent, their level depends on the combustion evolution and phasing: conditions with high heat release peaks near the TDC might favor their formation and increase their amount [51].

When developing control strategies, this work focuses on the use of the injection settings actions only, i.e., the air-path control is not considered in the control system. Therefore, considering a dual-fuel combustion engine at constant load operation, two main control variables can be selected to handle the on-line optimization, the gasoline fraction and the diesel injection timing:

- The gasoline fraction (GF) represents the mixture reactivity and in this section is calculated as follows:

$$GF = \frac{m_g}{m_g + m_d} \quad (4.9)$$

where m_g and m_d are the injected gasoline and diesel masses, respectively. The gasoline fraction was found to delay the combustion as its value increases due to the difference in resistance to auto-ignition between gasoline and diesel.

- The injection timing, or start of injection (SOI), of the direct diesel injection drives the mixture stratification. At early timings, the mixture is close to homogeneous conditions, and when delayed, richer equivalence ratio distribution in the cylinder results in some control authority over the combustion evolution.

Combustion sensitivity

In order to design the controller, it is important to analyze the system's output response to the input perturbation. The perturbation frequency should be high enough to ensure a fast convergence to the optimal operation, but slow enough to properly observe the system response as well. Similarly, a high perturbation amplitude would reduce the optimization duration and ease the oscillation detection, but would also result in a too excessive variation around the optimal point at the end of the process. Methods to improve conventional extremum seeking operation, where the perturbation amplitude is decreased as the system is getting closer to the optimal region, were not evaluated here [52].

Each combustion mode introduced in Chapter 3 has a specific injection strategy, traditionally function of the engine load. The combustion sensitivity to a particular control variable might therefore depend on the operating conditions, e.g., the fully premixed case is expected to be less sensitive to a slight variation in the injection timing due to the mixture homogeneity with the long ignition delays resulting from the early timings.

Previously, CA_{50} and NO_x were selected to define the cost function, and GF and SOI were considered as possible control variables. In the three investigated combustion modes, the engine was exposed to a perturbation applied to the gasoline fraction and the injection timing in the form of a chirp signal, being up-chirp for GF and down-chirp for SOI . The starting operating conditions and settings that were exposed to the perturbation are listed in Table 4.3. Note that SOI_p refers to the pilot injection and SOI_m to the main injection timing. The injection timings are expressed in crank angle degree before top dead center (bTDC). In this work, only the use of the main injection was evaluated in the extremum seeking design, i.e., the pilot injection timing was kept constant because this injection is not used to trigger the combustion.

Table 4.4 summarizes the chirp signal calibration applied to the control inputs where the minimum and maximum frequencies f applied were 0.05 and 0.6 Hz, and the chosen amplitudes A were 0.02 for GF and 1.5 CAD for SOI_m . An illus-

Table 4.3: Operating conditions of the experimental data used in the combustion sensitivity analysis for each combustion mode.

Operating conditions		Fully premixed	Highly premixed	Partially premixed
Engine speed	[rpm]	1800	1800	1800
IMEP	[bar]	11.3	11.9	11.8
EGR	[%]	40	33	34
GF	[-]	0.73	0.66	0.60
SOI_p	[°bTDC]	60	35	None
SOI_m	[°bTDC]	46	15	13

Table 4.4: Chirp signal specifications applied on GF and SOI_m for the combustion sensitivity analysis.

Chirp signal		GF	SOI_m
Amplitude A	[-]/[CAD]	0.02	1.5
Frequency f	[Hz]	From 0.05 to 0.6	From 0.6 to 0.05

tration of the resulting signals is shown in Figure 4.11.

The combustion phasing (estimated from the heat release computation) and the NO_x emissions (measured by the sensor placed at the exhaust) response to the input perturbation were analyzed in the frequency domain. The results are provided in Figure 4.12, where the brightest regions show the highest frequency response amplitudes. Top and bottom plots show respectively the short-time Fourier transform (STFT) of the $CA50$ and NO_x signals. As expected, it is observed that the gasoline fraction has the highest control authority over the combustion in the fully premixed conditions because of the kinetically controlled combustion (GF is perturbed by the chirp signal from 0.05 to 0.6 Hz, see Table 4.4). Meanwhile, the injection timing has a larger controllability in the partially premixed combustion. The highly premixed condition represents an in-between configuration where both of the control variables had some authority over the combustion, especially from the $CA50$ signal. In the case of the NO_x emissions, it is observed that the NO_x sensor measurement signal tends to exhibit a higher response magnitude to lower frequencies (below 0.3 Hz), likely to be due to the system's dynamics (e.g., gas transport and sensor delay). More importantly, this figure shows that both $CA50$

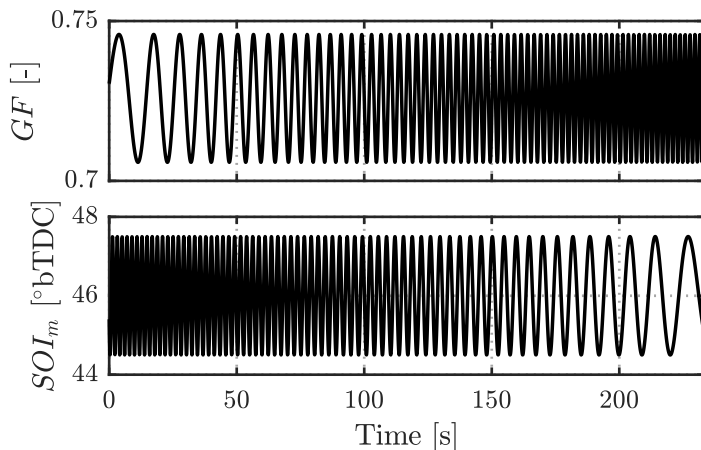


Figure 4.11: Representation of the chirp perturbation in GF (top) and SOI_m (bottom). Details about the original settings and the chirp calibration can be found in Table 4.3 and Table 4.4, respectively.

and NO_x respond to a perturbation in GF and SOI_m , verifying therefore that the extremum seeking controller should be able to find the optimal cost function area thanks to these two control variables, no matter the combustion mode operation.

It is important to highlight that such results can be obtained as long as the sensitivity of the combustion follows the same tendency. Indeed, as described by DelVescovo et al. [31], premixed dual-fuel combustion modes were observed to exhibit a stratification region where the mixing conditions led to a combustion phasing progression which was inversely correlated to the injection timing one. The same observation was made by Li when analyzing the combustion phasing sensitivity to the injection timing in the transition from HCCI to PPC combustion (*spoon shape*) [53]. Consequently, if the $CA50$ is to be exactly in the regime transition area, and that the perturbation amplitude of the controller covers this region, some control instability or inefficiency are to be expected. In the present case, the injection timings considered were found to either provide an almost null $CA50$ sensitivity (fully premixed) or some sensitivity but always of the same sign (highly and partially premixed).

Dual-fuel extremum seeking controller

The cost function J in (4.8) is composed of two distinct parts: the $CA50$ tracking error, and the NO_x emissions reduction. Consequently, each part should be

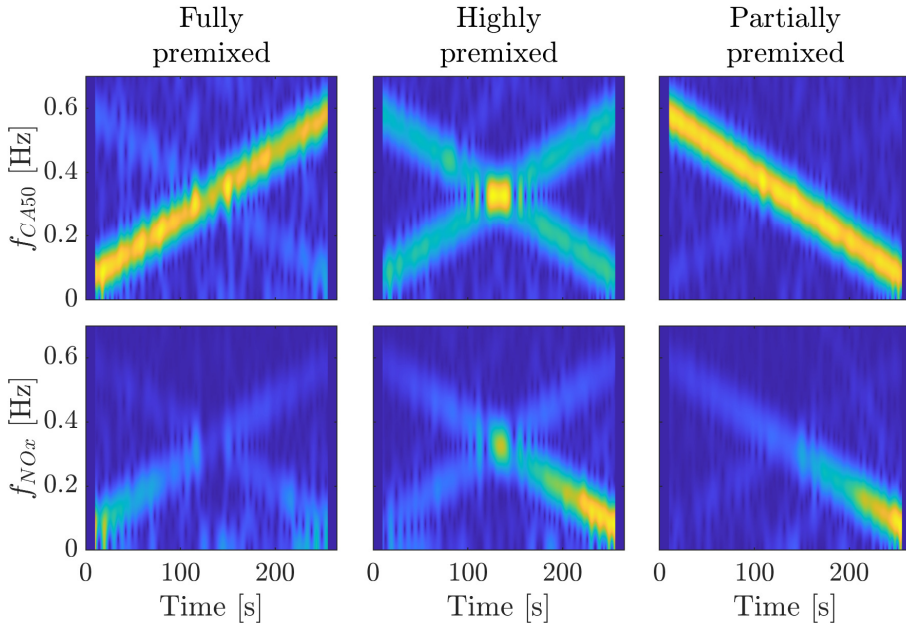


Figure 4.12: Short-time Fourier transform (STFT) of the $CA50$ (top) and the NO_x (bottom) response signals. The operating conditions are detailed in Table 4.3 and Table 4.4. It is observed that the gasoline fraction has a higher control authority in fully premixed conditions, while the injection timing has higher controllability in partially premixed mode.

individually processed by the extremum seeking controller to calculate their contribution to the final correction. The single input ES controller, such as the one shown in Figure 4.10, was therefore modified to integrate the multiple cost function inputs layout in the present application. Figure 4.13 shows the resulting ES controller structure where J_1 and J_2 are the components of the cost function in (4.8):

$$J_1 = J_{CA50} = |CA50 - CA50_r| \quad (4.10)$$

$$J_2 = J_{NO_x} = \beta NO_x \quad (4.11)$$

The NO_x measurement is subject to sensor and gas transport delay. Consequently, the sensor needs to be characterized in order to include its phase shift in the extremum seeking controller. Otherwise, the corresponding gradient might be incorrectly estimated and lead to unstable execution. One method consists in performing an input step and deriving the dynamics with a linear first order

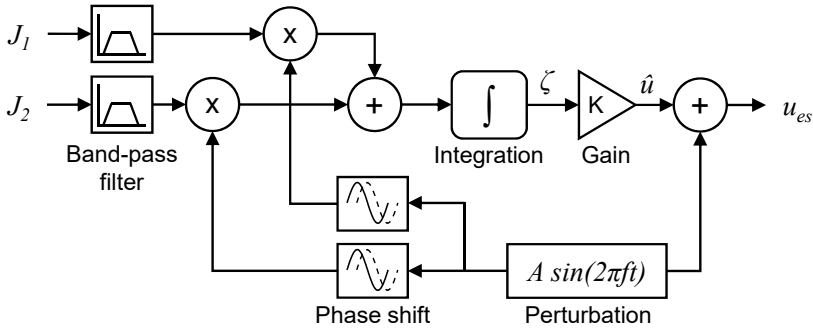


Figure 4.13: Multi-input extremum seeking controller layout used in this investigation that is repeated for each control input: GF and SOI_m .

model [54]. Here, it was decided to identify the NO_x dynamics by perturbing the injection timing as in Figure 4.11 in order to evaluate the response to be expected in the experiments. To ease the characterization, partially premixed conditions were selected to increase the NO_x emissions sensitivity to the injection timing. First, a simple linear static model was obtained by approximating the NO_x level as a function of the injection timing around the considered operating point. Then, the NO_x signal was assumed to follow a first order filter with a dead time τ (sensor delay) as follows:

$$NO_x^{signal}(t) = \mu NO_x^{signal}(t - \delta t) + (1 - \mu) NO_x^{model}(t - \tau) \quad (4.12)$$

where δt is the time step between two measurements, NO_x^{model} is the output of the aforementioned linear static model, and μ the filter calibration constant. The perturbation frequency at the injection timing was linearly increased (chirp signal), and a least mean squares fitting between the measurement (NO_x^{sensor}) and the resulting filtered signal (NO_x^{signal}) provided the following calibration constants: $\mu = 0.96$ and $\tau = 1$ s, where the response/dead time agreed with what can be found in the literature [54]. The respective signals are provided in the bottom plot of Figure 4.14, where the static model (NO_x^{model}) is directly phased with the injection timing in the top plot. It can be observed that by increasing the frequency, the sensor is not only characterized by its dead time, but the magnitude is decreased as well because not enough time is available to measure the real emissions. This statement agrees with and confirms the conclusions from Figure 4.12 where the highest magnitudes in the NO_x measurement response were observed at low frequencies.

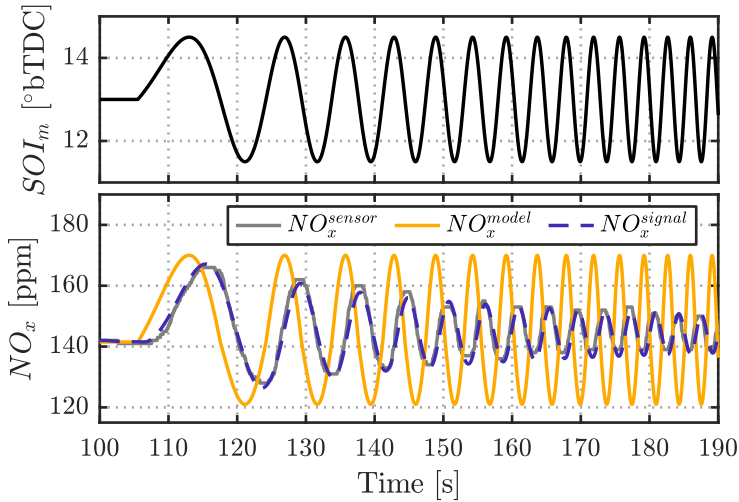


Figure 4.14: NO_x sensor characterization with the injection timing as the control input (top) and the resulting NO_x emissions from different sources (bottom): NO_x^{sensor} is the value measured by the sensor placed at the exhaust, NO_x^{model} is the linear static model $NO_x^{model} = f(SOI_m)$, and NO_x^{signal} is the modeled signal estimated by (4.12).

The final layout implementation of the extremum seeking controller is shown in Figure 4.15 where each ES controller includes the architecture shown in Figure 4.13. According to the operating conditions, correction limitations such as on the gasoline fraction might be considered in order to avoid unstable combustion operation where very high concentration might lead to misfire conditions due to low mixture reactivity and late combustion.

4.3.3 Results and discussion

The extremum seeking controller shown in Figure 4.15 was implemented in engine B. Highly premixed conditions were selected for its validation as they represent an in-between operation (compared to fully and partially premixed) where both GF and SOI_m should be driving the combustion to its optimal operation area. Table 4.5 summarizes the operating conditions used for the experiment while the perturbation settings are listed in Table 4.6. In this experiment, the perturbation for J_{NO_x} was shifted by a constant $\tau = 1$ s according to the previous observations, while it remained unshifted for J_{CA50} due to the cycle-to-cycle response from the combustion phasing to a change in the control input. Note that the eventual delay generated by the port fuel injection dynamics (wall wetting effect) [35] was con-

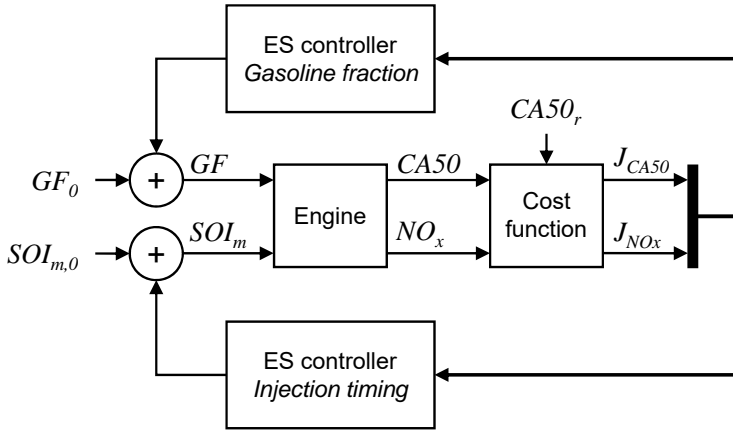


Figure 4.15: Dual-fuel extremum seeking controller layout using the gasoline fraction (GF) and the main diesel injection timing (SOI_m) as control variables. The subscript 0 refers to the initial condition. Each ES controller includes the architecture shown in Figure 4.13 where the $CA50$ and the NO_x signals are used to calculate each component of the cost function expressed in (4.8).

sidered insignificant according to the slow perturbation frequency chosen for the gasoline fraction and is, therefore, not modeled here. The results are illustrated in Figure 4.16 where each color corresponds to a cylinder, the grey line represents the NO_x sensor measurement, $CA50_r$ is shown with a black dashed line, and the solid black line represents the moving average of the variables over a 20 seconds window.

Two evaluation sections are shown in this figure: a first one during 314 s (white background), and from this time stamp till the end of the test (shaded background). In the first part, the ES controller is evaluated with the following

Table 4.5: Operating conditions of the experimental data used for the extremum seeking controller validation.

Engine speed	[rpm]	1800
IMEP	[bar]	10.3
EGR	[%]	35
SOI_p	[°bTDC]	60
GF	[-]	0.735
SOI_m	[°bTDC]	22

Table 4.6: Extremum seeking controller perturbation settings where $f_{bandpass}^{cutoff}$ corresponds to the calibration of the band-pass filter.

		GF	SOI_m
A	$[-]/[CAD]$	0.01	1.5
f	$[Hz]$	0.05	0.2
$f_{bandpass}^{cutoff}$	$[Hz]$	$[0.02 - 0.1]$	$[0.1 - 0.4]$
K	$[-]$	-0.05	-0.1

cost function calibration: $\beta = 0.1$ and $CA50_r = 4^\circ\text{aTDC}$. The controller aims therefore to minimize the NO_x emissions while reducing the setpoint tracking error of the $CA50$ at the same time. Finally, the second part delimited by the shaded grey area shows the system response when β was modified from 0.1 to 0. The objective of the overall validation is to evaluate the controller ability to respond to the cost function definition and calibration using the gasoline fraction and the injection timing as control inputs. By removing the NO_x weight from the cost function ($\beta = 0$), the controller is expected to track the combustion phasing reference and leave the NO_x emissions free of any control action.

In the first part of the test, according to the levels shown by the moving average over 20 seconds in the solid black line, the gasoline fraction was increased from 0.735 to around 0.78, and the injection timing was advanced from 22 to 25°bTDC. This resulted in a delayed combustion with the $CA50$ moving from 3.2 to 7°aTDC. Such observation shows that the final GF and SOI_m corrections particularly aimed at optimizing the NO_x emissions while maintaining a certain control authority over the required $CA50$ level. Indeed, as previously mentioned, when $\beta > 0$ the controller seeks to decrease the nitrogen oxides emissions at the expense of the combustion phasing tracking error. The combustion was therefore delayed, which resulted in less in-cylinder pressure and temperature and, consequently, lower NO_x emissions levels. Note that due to the actual definition of J in (4.8), and the original levels of NO_x in these conditions, even a small β value represents a significant weight amount in the cost function evaluation.

At the beginning of the test it is observed that the $CA50$ and NO_x signals are composed of two distinct frequency components (corresponding to GF and SOI_m actions), whereas after 150 seconds, GF seems to become predominant. Increasing the gasoline fraction not only delays the combustion and decreases the NO_x emissions, but it increases the homogeneous proportion of the mixture as

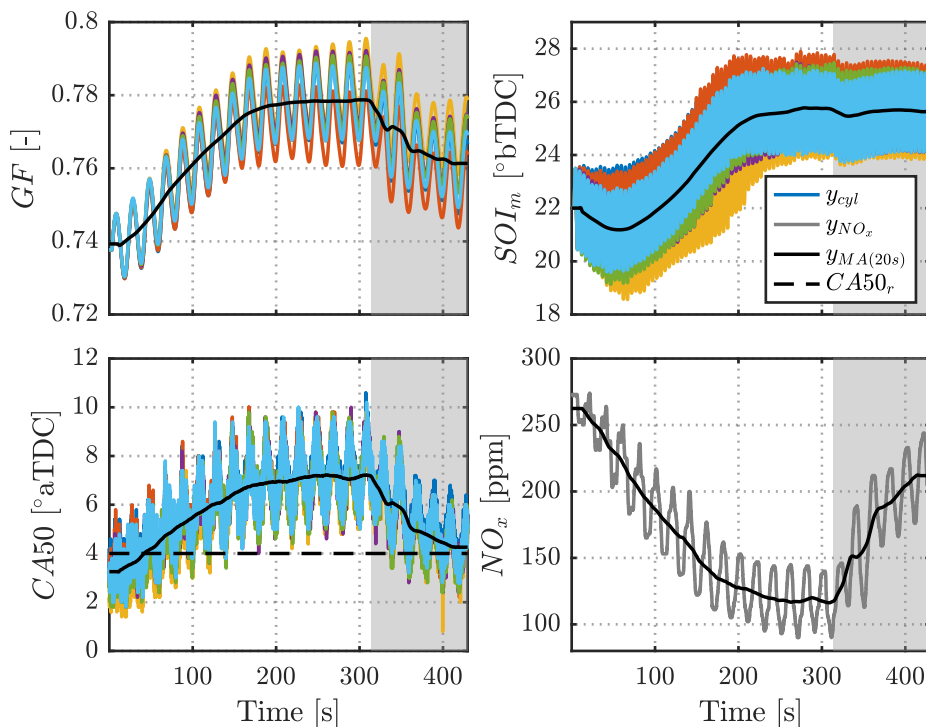


Figure 4.16: Dual-fuel extremum seeking controller results in highly premixed conditions. Each color represents a cylinder, the grey color is used for NO_x , and the black dashed line shows the $CA50$ reference setpoint. The moving average (MA) over 20 seconds is represented in black and the notation y stands for the representation of the variable on the y-axis in each plot. The shaded area on the right part shows the results when NO_x emissions are taken out of the optimization problem ($\beta = 0$).

well. Consequently, due to the simultaneous increase in the gasoline fraction and advance in the direct injection, bringing the mixture into higher levels of premixed conditions, the combustion is observed to exhibit a sensitivity predominantly to the gasoline fraction (see Figure 4.12).

As previously mentioned, the combustion phasing is traditionally used to track the maximum brake efficiency. In the first part of the experiment, since the combustion phasing was not driven to the desired level, an increase in the brake specific fuel consumption (BSFC) of 4% was observed (this quantity was chosen for evaluating the fuel conversion efficiency [55]). Nonetheless, a 54% reduction in the brake specific NO_x (BS NO_x) was measured thanks to the extremum seeking con-

Table 4.7: Extremum seeking outcomes at the start and at the end of the execution with CA50 and NO_x optimization (first part of the validation test).

		Start	End ($\sim 300s$)	Relative difference
σ_{CA50}	[CAD]	0.65	0.40	-38%
BSFC	[g/kWh]	202	210	+4%
BSNO _x	[g/kWh]	2	0.92	-54%

trol actions (this value was selected to compare the evolution of the NO_x emissions according to the performance of the engine [55,56]). A trade-off between fuel efficiency and pollutant emissions exists and the priority can be given to the desired feature through the cost function calibration. Finally, it must be noticed that the CA50 cylinder-to-cylinder dispersion was also reduced thanks to the use of the ES controller where a standard deviation σ of 0.40 CAD was measured at the end, compared to 0.65 at the beginning of the test (see Table 4.7).

In the last part of the test (grey area) the weighting factor β was set to 0 to remove the pollutant emissions from the optimization algorithm, see (4.8). With the current cost function definition, this results in a simple tracking strategy where the CA50 is therefore driven to the combustion phasing reference ($CA50_r$), at the expense of a NO_x emissions increase. Note that the gasoline fraction remains the principal variable to exhibit a control over the combustion in this case. This is believed to be justified by the highly premixed conditions reached at the end of the first part where the injection timing was found to already have less control authority.

The designed extremum seeking controller showed that this strategy was able to reduce the NO_x emissions by modifying the combustion operation, but at the expense of a slight increase in the BSFC. The experimental results show the potential of this technique to achieve optimal operation in such systems. Furthermore, the cost function might be designed to include more variables and consequently participate in improving the combustion operation. Future investigation on on-line optimization of the dual-fuel combustion operation could encompass an improved definition of the cost function with further calibration effort in order to enhance the trade-off between fuel consumption and pollutant emissions and therefore be able to track the combustion phasing while maintaining the NO_x emissions to the lowest level.

4.4 Safe engine operation by combustion resonance measurement and control

Previous sections were dedicated to the design of controllers that ensured the required engine performance and tracking of optimal operation in the best extent possible. However, engine safety should be brought to the foreground when developing control strategies as some operating conditions, even optimal, might represent a risk of damage for the engine. Section 4.2 addressed this matter proposing a control of the pressure rise rate by limiting the premixed fuel quantity injected in the cylinder. However, in premixed combustion, the combustion is initiated at several kernels which create high pressure gradients inside the cylinder. Similarly to knock in spark ignition engines, these gradients might be responsible of important pressure oscillations with a harmful potential for the engine. These oscillations might therefore be considered in the controller design in order to limit their impact on the engine operation, as it can be extensively found in knock control [57–59].

In dual-fuel combustion strategies, Selim [60] considered the maximum pressure rise rate (MPRR) as an index to study what was called *knock* in a dual-fuel engine using pure methane (CH_4), compressed natural gas (CNG) and liquefied petroleum gas (LPG) as the main fuels, and diesel as the ignition source. It was found that advancing the diesel injection resulted in higher ignition delays and thus increased the maximum cylinder pressure and MPRR levels. Kirsten et al [61] considered the pressure oscillations and proposed a knock event detection by separating the ringing oscillations due to the premixed combustion and the knocking combustion of the end-gas in a natural gas/diesel engine. A threshold was experimentally calibrated and was used to evaluate if the cycles were in knocking or non-knocking conditions. Lounici et al. [62] analyzed knock in a natural gas/diesel engine with the maximum amplitude of pressure oscillations (MAPO) and found that the brake thermal efficiency and the emissions were worsened under knocking conditions. In addition, as the knock intensity was increased, a higher cyclic variability of the index was noticed. The MAPO was also considered by Chen et al. [63] to study the cyclic knock variability in a methane/n-heptane CI combustion engine by varying the timing of the n-heptane injection. They optically observed the multipoint auto-ignition process of the combustion and stated that the pressure oscillations were induced by local fast burning rate.

While it is common to find studies about the definition of resonance, knock and combustion noise indexes in premixed combustion engines, as well as how

the control variables would affect them (some examples can be found in [64–66]), few of them were dedicated to real-time control implementation. Moreover, most of the works used the pressure rise rate as the limitation factor for the harmful potential of the combustion [67–69], but they did not address the pressure oscillations. Mashkournia et al. [70] implemented a controller in a HCCI engine where the knock was detected by a discrete wavelet transform of the pressure oscillations. A threshold was experimentally determined and the controller kept the knock index close to the desired value by regulating the fuel octane number of the mixture (dual injectors of n-heptane and iso-octane).

This section studies the in-cylinder pressure oscillations from the dual-fuel combustion concept and evaluates a control strategy for ensuring a safe operation of the engine in the three investigated combustion modes: fully, highly and partially premixed. After an analysis of the resonance excitation in each combustion mode, a knock-like controller using the gasoline fraction and the diesel injection timing to control the MAPO is proposed and validated in engine B. The results show the controller ability to control the number of cycles exceeding the resonance index limit in all the cylinders.

4.4.1 Problem illustration

Premixed combustion strategies are characterized by a rapid auto-ignition of the air-fuel mixture and, as a result, usually exhibit high pressure gradients. This fast combustion at multiple points in the combustion chamber is not only responsible of significant pressure rise rate, but causes a substantial resonance excitation as well, similarly to knock in SI engines.

To illustrate this phenomenon, a medium-low load point was selected where all the investigated combustion modes can be tested by applying the appropriate control inputs (i.e., EGR, gasoline fraction, diesel injection timings, etc.). Table 4.8 collects the operating conditions. Figure 4.17 shows the respective in-cylinder pressure (both low and high-pass filtered, p_{lp} and p_{hp}) and heat release rate (dQ_{app}) traces from 500 consecutive cycles at steady-state operation in grey, and an individual selected cycle is highlighted in black (please refer to Chapter 3 for the filter definition). The middle plots illustrate the in-cylinder pressure oscillations in each condition. The rapid combustion of the premixed charge heavily excites the in-cylinder pressure resonance leading to important pressure oscillations which might persist till the end of the power stroke. It can be observed that the combustion events and conditions influence the in-cylinder pressure oscillations. As an example, in the partially premixed case (OP 3), the premixed mixture with

Table 4.8: Operating conditions for each combustion mode. A medium-low load operating point was selected to be performed in all the combustion modes for comparison purposes.

Parameter	Unit	Fully premixed	Highly premixed	Partially premixed
Operating point	(OP)	1	2	3
Engine speed	[rpm]	1800	1800	1800
IMEP	[bar]	12.5	12.4	11.2
CA50	[°aTDC]	2.5	3	12
P_{int}	[bar]	2.05	2.15	2.15
T_{int}	[°C]	63	67	60
EGR	[%]	44	43	33
GF	[%]	63	62	62
SOI_p	[°bTDC]	60	34	none
SOI_m	[°bTDC]	46	19	10

low reactivity is suddenly burned by the reactions of the diesel injection combustion and significant inhomogeneities might lead to high pressure oscillations. It is also noticed that in fully and highly premixed combustion conditions (OP 1 and OP 2), the pressure oscillations exhibit a lower magnitude compared to the partially premixed case.

4.4.2 Definition of the limitation index

As mentioned and described in Chapter 3, various indexes can be found in the literature when addressing the limitation of the engine operation. However, these indexes might not address the same phenomena and not be correlated with each other. Here, the maximum pressure rise rate (MPRR), the ringing intensity (RI) and the maximum amplitude of pressure oscillations (MAPO) levels resulting from the operating points shown in Figure 4.17 (whose settings can be found in Table 4.8) are illustrated with box and whiskers plots in Figure 4.18. It is observed that, when reducing the premixing time of the mixture (from OP 1 to OP 3), a decrease in MPRR and RI levels is obtained. However, at the same time, it can be noticed that the MAPO level increases. Note that in this case, the detection of a decrease in the MPRR despite the increase in MAPO could occur because the MPRR is obtained from a low-pass filtered signal that aims to remove high frequency components, hence lacking of resonance content evaluation. The similar

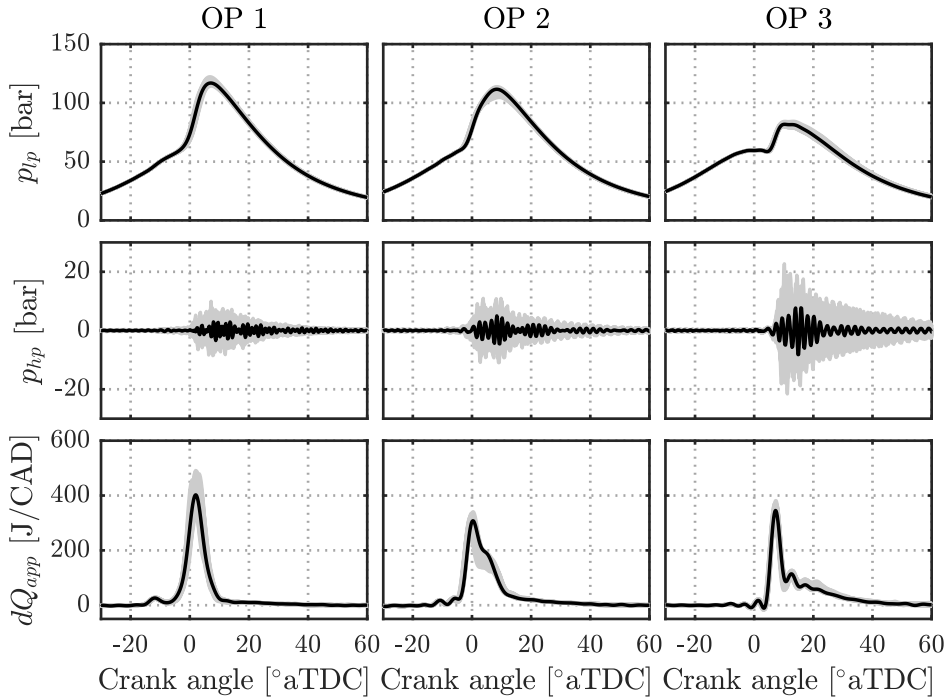


Figure 4.17: Low-pass filtered (top) and pressure oscillations from high-pass filtered (middle) in-cylinder pressure signals, and heat release rate traces (bottom) at each dual-fuel combustion strategy as detailed in Table 4.8 (grey: series of 500 consecutive cycles, black: individual selected cycle).

RI magnitude noticed in OP 2 and 3, although the MPRR was reduced, is likely to be justified by the maximum pressure and temperature compensation (please refer to equation (3.33) in Chapter 3 for the relation between these two indexes). Furthermore, it can be seen that the measured ringing intensity levels exceed the traditional limit of 5 MW/m^2 , although the MPRR is below the considered safety margin of 15 bar/CAD in this engine, showing the filter calibration and engine dependency of these indexes. Also, it must be noticed that the variability of the MPRR and RI decreases as it approaches partially premixed conditions, but the expected oscillations have, on the contrary, an important cycle-to-cycle variability (from 2.5 to more than 20 bar of MAPO), manifesting the stochastic nature of the resonance excitation.

Overall, this figure shows that an opposite trend may be detected when ad-

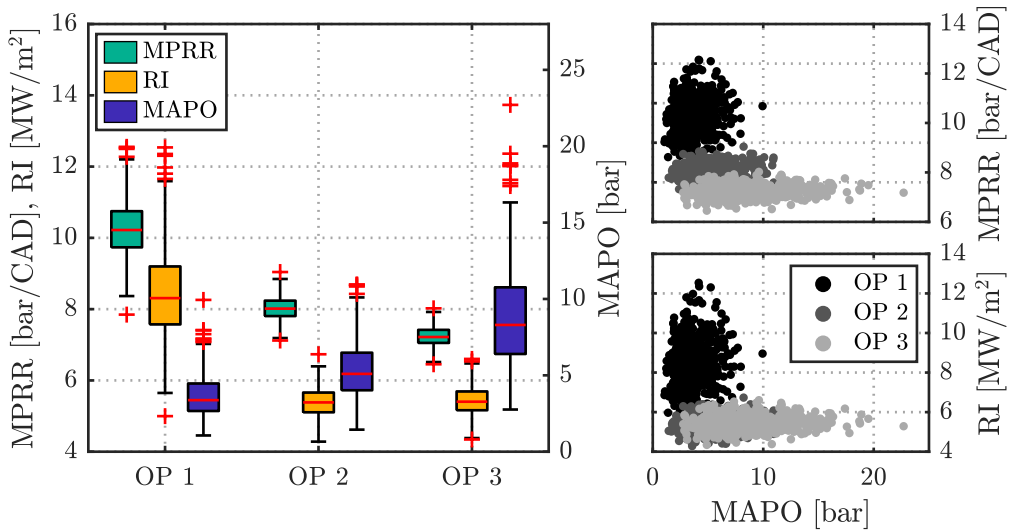


Figure 4.18: Comparison between MPRR, RI and MAPO levels in the three dual-fuel combustion modes at the conditions listed in Table 4.8 (left), and cycle-to-cycle variability relation between these three indexes (right).

addressing the harmful potential of the combustion with a direct measurement of the resonance excitation, such as with MAPO, compared to other indexes that characterize how rapid the combustion is, such as with MPRR. Accordingly, high resonance excitation might be identified although safer operation would be supposed by the pressure rise rate reading alone. Finally, as illustrated in the right part of this figure, the cycles with high levels of MPRR and RI do not necessarily correspond to the cycles with high pressure oscillations amplitude, verifying that these indexes deal with different phenomena and that they should be addressed independently.

Important combustion pressure oscillations might lead to thermal efficiency loss and possible damage for the engine and, therefore, require to be tracked. In the investigation described in this section, the resonance intensity level alone was considered, and in this sense, the MAPO was therefore selected as the resonance index and limitation factor when designing the controller. Nonetheless, a comparison with MPRR and RI is also provided in the controller results section to evaluate the differences and outcomes of the controller when applied to these other indexes.

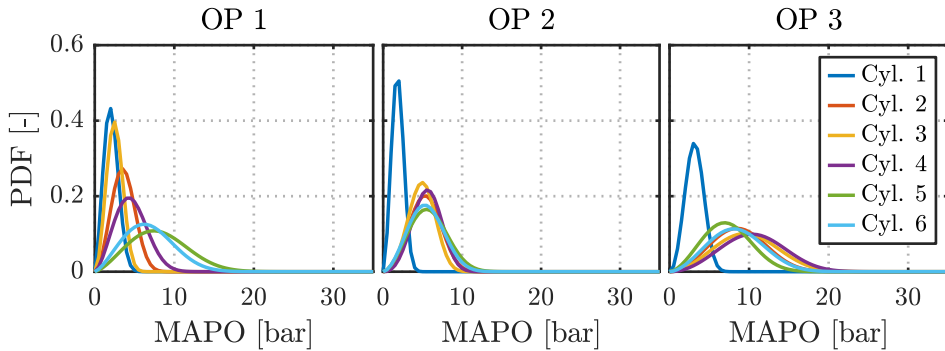


Figure 4.19: Individual cylinder MAPO probability density function in all the conditions listed in Table 4.8.

4.4.3 Controller design

Premixed conditions exhibit an important cyclic combustion variability due to the inhomogeneities at the combustion ignition (i.e., kinetically controlled combustion) [71]. Additionally, multi-cylinder engines might present uneven fuel distribution from the PFI system, direct injectors ageing, or EGR dispersion between cylinders under high pressure EGR operation [72, 73]. Henceforth, the resonance intensity of a given operating condition in a premixed combustion can be understood as a stochastic phenomena, in the same way that knock is understood in spark ignited engines.

The probability density functions (PDF) of the MAPO resulting from the operating conditions listed in Table 4.8 in each cylinder are illustrated in Figure 4.19. The resonance intensity distributions observed in Figure 4.19 show that: first, each cylinder should be controlled individually as they do not exhibit the same distribution (likely to be justified by the difference in in-cylinder conditions), and second, the resonance intensity is random in nature so its control should be addressed from this perspective. It was noticed that cylinder 1 used to exhibit a distinct amplitude distribution compared to the general trend measured in the other cylinders. This was attributed to the pressure sensor location in the cylinder where the pressure oscillations may be sensed differently [74]. Indeed, as shown in Figure 4.20, engine B was equipped with five pressure sensors positioned at the same location, for cylinder 2 to 6 (location 2), while cylinder 1 had a pressure sensor in a different location for engine geometry reasons (location 1), impacting consequently the way the pressure oscillations were sensed.

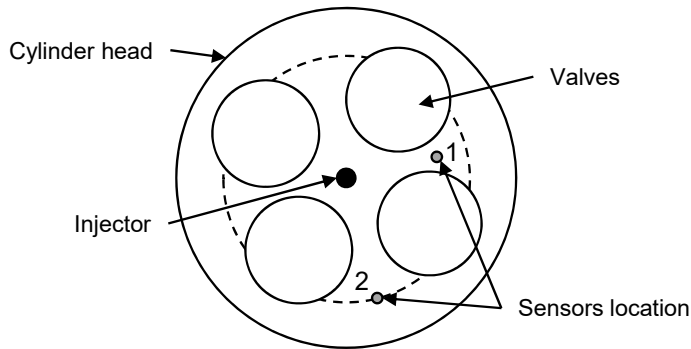


Figure 4.20: In-cylinder pressure sensors location layout. Location 1: cylinder 1, location 2: cylinder 2 to 6.

Combustion sensitivity

Ensuring a safe operation of the engine requires to determine which control variables drive the resonance intensity (MAPO in this case). Figure 4.17 showed that the combustion conditions (e.g., rate of energy released, start of combustion, mixture stratification) affect the pressure oscillations amplitude. Consequently, each combustion mode is expected to exhibit a different sensitivity to the control inputs depending on the considered strategy. This work focuses on the use of the injection settings only as control inputs. By doing so, the controller should provide a fast and safe control of the engine operation as this approach allows to influence the combustion within a cycle resolution compared to other methods with slower dynamics (e.g., air path, EGR control).

Similarly to section 4.3, it was decided to investigate the combustion sensitivity to a change in the gasoline fraction and the start of the main diesel injection for the three operating points discussed previously (see Table 4.8). The resulting probability density functions are shown in Figure 4.21 (note that for the sake of clarity this figure shows the results from only one cylinder). It was found that the resonance was mainly influenced by the gasoline fraction in the fully premixed mode (OP 1). This observation was expected as the combustion ignition is kinetically controlled in these conditions (similar observation was made in section 4.3). Higher gasoline rates reduced the average levels, while the injection timing effect was less explicit: only the case with a SOI_m of 49°bTDC seemed to have had an effect, though not following a clear tendency as with the gasoline fraction. Due to the early injection timings and high mixing times in this combustion mode, a slight

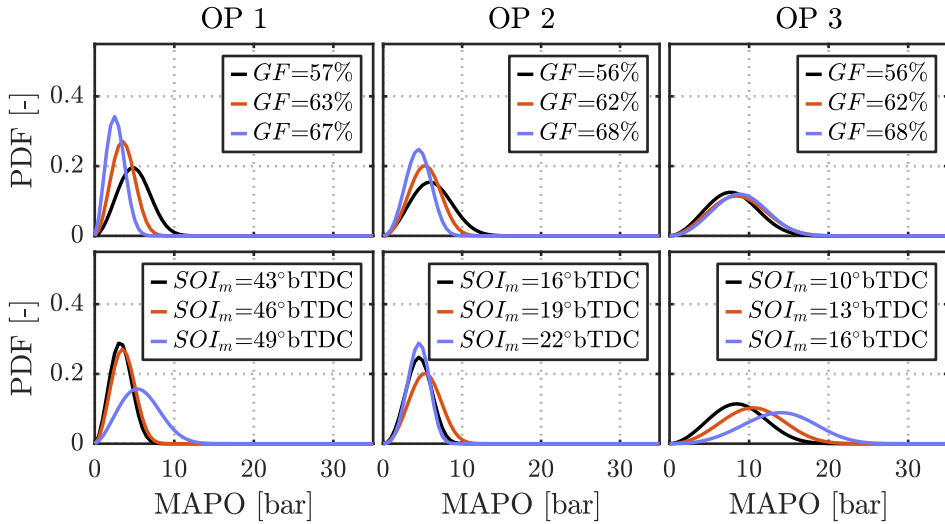


Figure 4.21: Probability density functions of MAPO in all the dual-fuel combustion modes to evaluate its sensitivity to the control inputs: gasoline fraction (top) and diesel injection timing (bottom). It is observed that the gasoline fraction has a higher control authority over the combustion in fully premixed conditions while the MAPO distribution is more sensitive to the injection timing in partially premixed combustion.

change in the injection timing is assumed to not affect drastically the combustion evolution. As the gasoline fraction modifies the in-cylinder mixture reactivity, this results in a modification of the combustion evolution where the resonance might be excited in a larger extent. For instance, the combustion energy might be released all at once closer to the top dead center by advancing the combustion. Once the diesel injection timing is getting closer to the top dead center, the effect of this control variable becomes more relevant in the resonance intensity distribution as it is shown in the partially premixed case (OP 3). This is justified by the mixture stratification modification resulting from the change in SOI. By approaching the TDC vicinity, the mixture becomes less homogeneous and richer local equivalence ratios appear, which enhance the combustion reactions. Unlike the fully premixed case, here, the gasoline fraction was observed to have no apparent impact on the MAPO distribution and the different blending ratios were found to excite the in-cylinder pressure resonance in a similar way. For its part, the highly premixed condition represents an in-between case where both gasoline fraction and injection timing have some control authority, and where a transition in the combustion regime might be observed [31].

Dual-fuel resonance controller

A control strategy is proposed to ensure a safe operation of the engine based on the stochastic nature of the resonance intensity in the combustion chamber. The probability distributions shown previously in Figure 4.21 can be used to set an index threshold not to be exceeded with a predefined probability. The controller should then always ensure that, independently of the combustion mode, the probability of having a cycle above the threshold will be maintained at a certain value. This threshold is defined for engine safety and durability and can be shared at each cylinder, considering that the pressure oscillations are equally measured and processed in all the cylinders (e.g., pressure sensor location).

A commonly used technique for such purpose is the conventional knock control, which continuously modifies a given input (u) at every engine cycle k by a certain amount k_{adv} until an event above the knock index (KI) threshold is detected [75]. Once such event appears, the input is modified in the opposite direction by a larger amount k_{ret} :

$$u_k = \begin{cases} u_{k-1} - k_{ret}, & \text{if } KI > KI_{lim} \\ u_{k-1} + k_{adv}, & \text{otherwise} \end{cases} \quad (4.13)$$

where the k_{adv} and k_{ret} calibration determines how fast the controller approaches the operation limit (KI_{lim}) and how the input is modified when an event is detected.

On average, under stable operation, it is assumed that both increments should cancel each other. Considering that k_{ret} (i.e., knock event) occurs with a probability p_{kc} , these two parameters are therefore linked by the following relation [76]:

$$k_{adv} = \frac{p_{kc}}{1 - p_{kc}} k_{ret} \quad (4.14)$$

Consequently, if the probability p_{kc} is considered as a design parameter, the definition of either k_{adv} or k_{ret} will fully characterize the controller, as they are linked by the knock probability p_{kc} . By adjusting these parameters, a trade-off can be found between a fast response to knocking events and a high control actions dispersion [57]. The controller layout is illustrated in Figure 4.22 where u_k corresponds to either GF or SOI_m , and KI is the resonance intensity level, MAPO in this case.

Finally, it is important to highlight that this work investigates the use of MAPO, evaluated from the in-cylinder pressure measurement, but the same strategy might be investigated evaluating the pressure oscillations intensity through

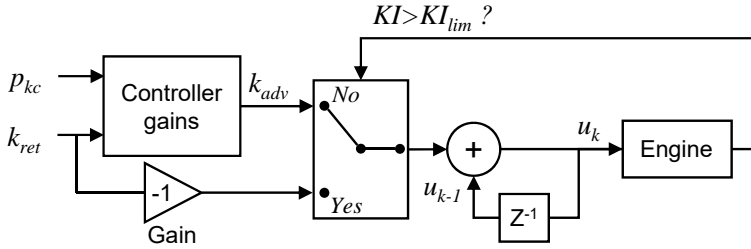


Figure 4.22: Knock-like controller layout applied to the dual-fuel combustion concept where u_k corresponds to either GF or SOI_m , and KI is MAPO in the presented case (another index might be used and the controller could still be similarly applied).

another index or technique, e.g., conventional knock sensor on the engine structure, to evaluate if similar results could be obtained [77,78]. The only requirement being that the proper control variables have to be selected, i.e., a sensitivity of the selected index to these inputs must exist.

4.4.4 Results and discussion

The previously described knock-like controller was evaluated at each combustion mode (from OP 1 to OP 3) using the gasoline fraction (tests referenced as a) and the injection timing (tests referenced as b) as the control variables according to the parameters listed in Table 4.9. The goal of the controller was to maintain the probability of the cycles with a MAPO above the limit ($MAPO_{lim}$) to a specified threshold (p_{kc}). Here, the percentage of events p_{kc} and k_{ret} were selected to characterize the proposed controller, and k_{adv} was therefore calculated on-line using (4.14). In this evaluation, it was considered that the combustion sensitivity sign was already known (e.g., the gasoline fraction should be increased in fully pre-mixed conditions to decrease the resonance levels), and each control variable was tested independently. Therefore, a control architecture where both control inputs would be actuated at the same time, and where an automatic transition from one mode to the other would be performed, was not evaluated here.

A summary of the results can be found in the lower part of Table 4.9, where the resulting percentage of exceeding cycles in each cylinder is named p_{ki} . In this table, $p_{ki,median}$ represents the median value from all the p_{ki} obtained at each cylinder, and $p_{ki,min}$ and $p_{ki,max}$ are the minimum and maximum measured values to show the dispersion between cylinders. That way, if the controller was able to control the high resonance intensity cycles probability, $p_{ki,median}$, $p_{ki,min}$, and

Table 4.9: Operating conditions and results from the tests performed to evaluate the knock-like controller at each combustion mode.

Test	OP 1		OP 2		OP 3		
	1a	1b	2a	2b	3a	3b	
u	GF	SOI_m	GF	SOI_m	GF	SOI_m	
u_{min}	[-]/[°bTDC]	0.30	35	0.30	6	0.30	8
u_{max}	[-]/[°bTDC]	0.92	49	0.92	23	0.85	20
$MAPO_{lim}$	[bar]	5.5	5.5	7	7	18	18
p_{kc}	[-]	0.030	0.030	0.030	0.030	0.030	0.030
k_{ret}	[-]/[CAD]	-0.03	1	-0.03	1	-0.03	1
$p_{ki,median}$	[-]	0.030	0.053	0.030	0.032	0.032	0.028
$p_{ki,min}$	[-]	0.028	0.028	0.028	0.028	0.005	0.027
$p_{ki,max}$	[-]	0.032	0.145	0.032	0.032	0.033	0.030

$p_{ki,max}$ should all be in the same range than p_{kc} . Due to the different levels obtained in cylinder 1 (see Figure 4.19), it was decided to not include this cylinder in the controller validation. Therefore, in this table are indicated the median, minimum and maximum probability from cylinder 2 to 6. When a control variable had no authority on the resonance intensity, the percentage of events could not be controlled, leading to undesired values as discussed in the following conclusions.

It is important to note that the objective of the following validation is to evaluate the potential of the selected control variables (GF and SOI_m) to maintain the combustion operation to its limit by means of a knock-like controller in all the combustion modes. For this reason, the resonance intensity limitation was defined according to each combustion conditions, i.e., the limit was set empirically and relatively close to the original levels, hence restricting the controller amplitude range of actuation. The definition of a global index limitation threshold for the whole engine map, similarly to some knock definition in SI engines, was not evaluated in this work. Therefore, in some cases, a more restrictive resonance intensity limitation might result in control restrictions and exhibit distinct outcomes, e.g., if a control variable reaches its limitations (u_{min} or u_{max}), then the resulting p_{ki} would inevitably be out of the desired range. Consequently, it must be highlighted that the results hereinafter described correspond, in some extent, to a narrow range of control actuation. Yet, this situation is to be expected if such control strategy is activated only in circumstances where the operating conditions are reaching the engine limitation and thus would ensure to not overcome it. The

control implementation for activation and deactivation as a function of the combustion operation, e.g., enabled only when harmful conditions are met until safer ones are expected, was however not considered here either.

Each control variable was constrained, as stated by the values u_{min} and u_{max} in Table 4.9, in order to avoid unstable engine operation. According to the previous combustion sensitivity analysis, it was found that the resonance level should be controlled by the gasoline fraction in fully and highly premixed conditions, where a higher quantity results in lower resonance levels. Therefore, the controller will first attempt to reduce the gasoline fraction until a cycle is detected to overcome the limit. Even though the resonance intensity should be detected above the limit before reaching really low GF levels, the lower limitation was set to avoid pure diesel operation in any circumstance. Meanwhile, the upper limit was set to avoid high gasoline concentration which could lead to misfire conditions and result in unstable combustion operation. In fully and highly premixed combustion modes, the injection timing upper limit was set to avoid injections merging with the pilot injection (i.e., dwell time limitation). In the partially premixed case, this value was chosen to leave some margin to the controller action and to avoid combustion regime modification as well. The lower injection timing limitation was chosen to avoid combustion mode transition in OP 1 and 2, and unstable operation and poor combustion efficiency in OP 3.

The left part of Figure 4.23 to Figure 4.25 shows the overall controller behavior in three selected cases from Table 4.9. In each of these plots, the white area represents the section of the test where the controller is enabled, while when it is not, the area is shaded in grey. The top plot shows the cycle-to-cycle resonance intensity level at each cylinder (i.e., MAPO), the middle plot the control actions, and the bottom plot the evolution of the probability of exceeding cycles in a moving buffer of 100 cycles, for illustration purposes. The dashed black lines represent the resonance intensity limit in the top plot, and the desired probability threshold in the bottom plot. A zoomed section of the outcomes when the controller is enabled is also shown in the right part of these figures. This zoom presents a 100 cycles window of one cylinder to illustrate the cycle-to-cycle controller actions. When a cycle is detected to exceed the index limitation threshold in the top plot, a response of the controller is expected in the middle plot by varying the control variable level.

Fully premixed case As suggested in Figure 4.21, and confirmed in the results from Table 4.9, only the gasoline fraction was able to drive the resonance excitation

to the desired threshold in fully premixed operation (test 1a). On the other hand, the injection timing control resulted in a percentage of cycles exceeding the limit out of the target range (test 1b, $p_{ki,median} = 0.053$) with high cylinder-to-cylinder probability dispersion, from a minimum of 0.028 in cylinder 3 to a maximum of 0.145 in cylinder 4. These results show that the injection timing is not able to control the resonance content in the cylinder under these conditions due to the early injection timings in this combustion mode. Figure 4.23 illustrates the controller response to the conditions in test 1a. It was observed that the controller was able to maintain the cycles exceeding the MAPO limit down to the desired probability threshold using the gasoline fraction as the control variable in all the cylinders. Once a cycle was detected above the MAPO limit (specified in Table 4.9), the gasoline fraction was reduced by an amount k_{ret} , as specified in (4.13), and slowly drove back to the limit operation (i.e., the gasoline fraction was increased in this case since its correction is negative, see Table 4.9). Note that in order to appreciate the final magnitude in the probability evolution, the bottom plot was cropped and some cylinders were therefore not fully represented. Moreover, this bottom plot also shows that not all the cylinders exhibit a similar probability of cycles exceeding the limit when the controller is not enabled (i.e., some cylinders have a probability level already below the desired threshold). This indicates that the control of each cylinder might be individually enabled or not according to their original resonance levels.

Highly premixed case Similarly to the fully premixed case, the gasoline fraction was able to maintain the combustion at its operation limit in the highly premixed case (test 2a). From its part, the injection timing controllability in test 2b was less noticeable in these conditions. Figure 4.24 shows the results obtained when the injection timing was used to control MAPO in OP 2. It was observed that the injection timing at each cylinder was individually controlled within u_{min} and u_{max} (represented by dash-dotted black lines) to drive the probability of the cycles exceeding the limit value towards the desired probability threshold, as shown in the bottom plot. Overall, the control actions in this case exhibited some authority but less than the gasoline fraction, which agreed with Figure 4.21, and might be explained by the in-between situation of the injection timing effect under these conditions (i.e., transition between kinetically and mixing controlled combustion).

Partially premixed case Finally, test 3a and test 3b were respectively performed to evaluate the gasoline fraction and the injection timing ability to control the MAPO distribution in partially premixed conditions. In these conditions, the gasoline fraction was unable to control the combustion to the desired operation

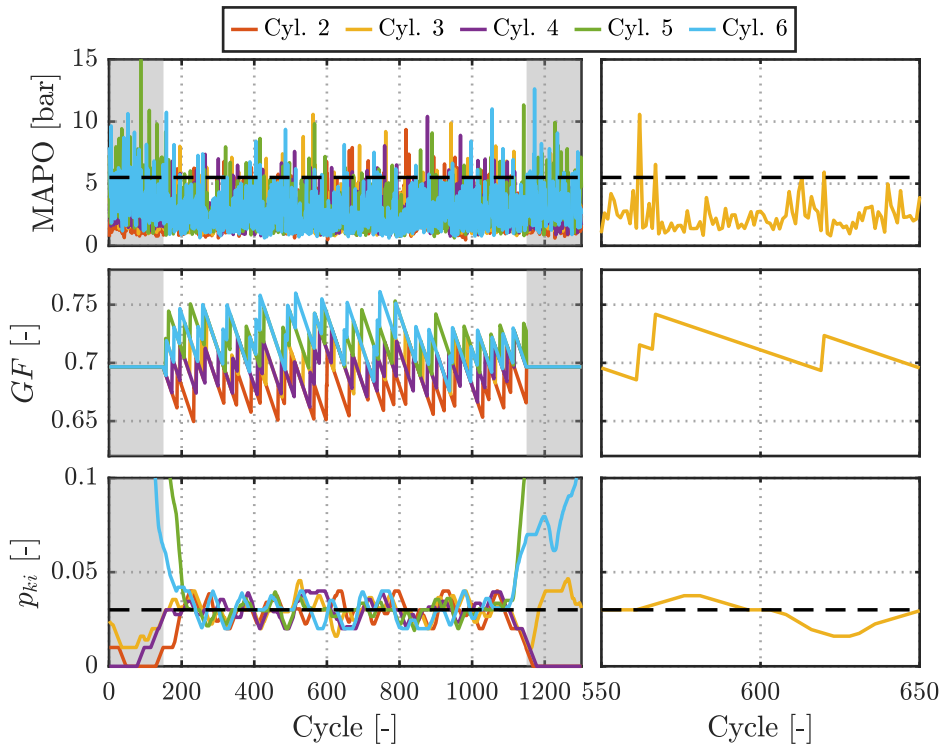


Figure 4.23: Test 1a: MAPO control (top) using the gasoline fraction (middle) to control the probability of cycles exceeding the desired threshold (bottom) in fully premixed conditions. A zoom on a cycles area is provided on the right part to show a detailed view of the controller actions. Dashed black line: MAPO limitation (top) and probability threshold (bottom). Note that cylinder 1 is omitted from this experiment.

limit in all the cylinders as indicated in Table 4.9 (test 3a). This was expected according to the very low sensitivity found previously (see Figure 4.21). Meanwhile, the injection timing was capable of moving and maintaining the MAPO probability towards the specified threshold as shown in Figure 4.25. In this case, the injection timing was advanced in almost all the cylinders because the starting MAPO levels were below the defined limitation.

Altogether, the results showed that in fully premixed conditions the controller was able to limit the pressure oscillations by regulating the mixture reactivity with the gasoline fraction. Similarly, the highly premixed condition was found to be efficiently controlled by the gasoline fraction, and the injection timing exhibited

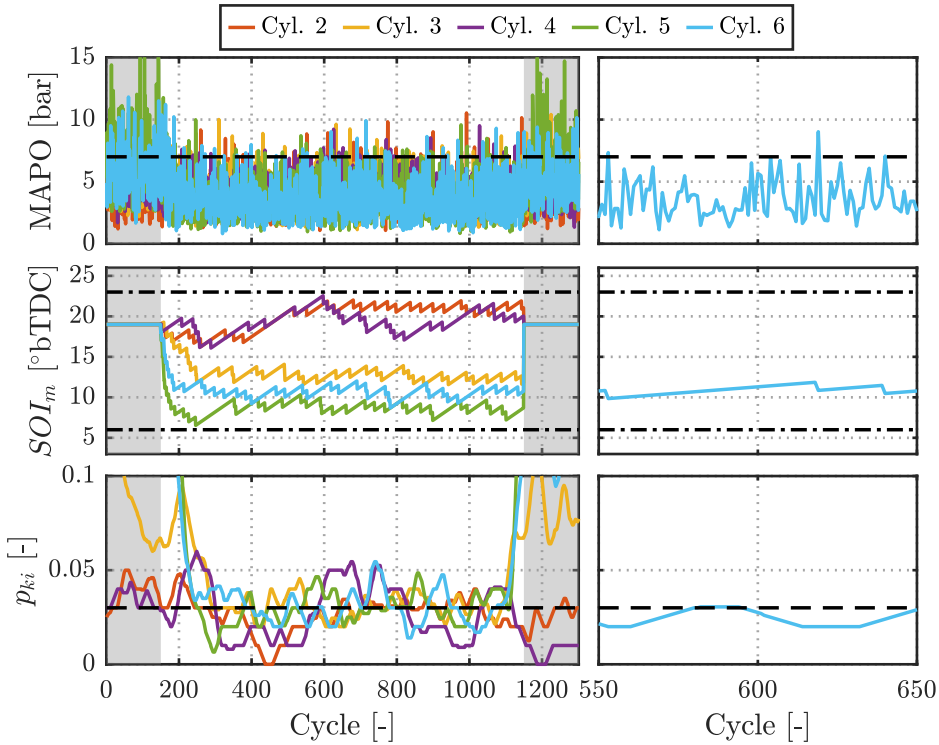


Figure 4.24: Test 2b: MAPO control (top) using the start of the main injection (middle) to control the probability of cycles exceeding the desired threshold (bottom) in highly premixed conditions. A zoom on a cycles area is provided on the right part to show a detailed view of the controller actions. Dashed black line: MAPO limitation (top) and probability threshold (bottom), dash-dotted black lines: control actions limitations (middle). Note that cylinder 1 is omitted from this experiment.

some control authority over the resulting amount of cycles exceeding the operation limit to some extent as well. At last, the probability of cycles exceeding the predefined limit in the partially premixed strategy was properly regulated by the injection timing. As a future improvement, a controller able to select the control variable with the highest control authority over the combustion in real-time could enable to cover a wider range of operation with a single controller.

Controller evaluation comparison with other indexes

Aiming at evaluating if the proposed controller could be implemented in a dual-fuel engine relying on more traditional limitation indexes, the same analysis was

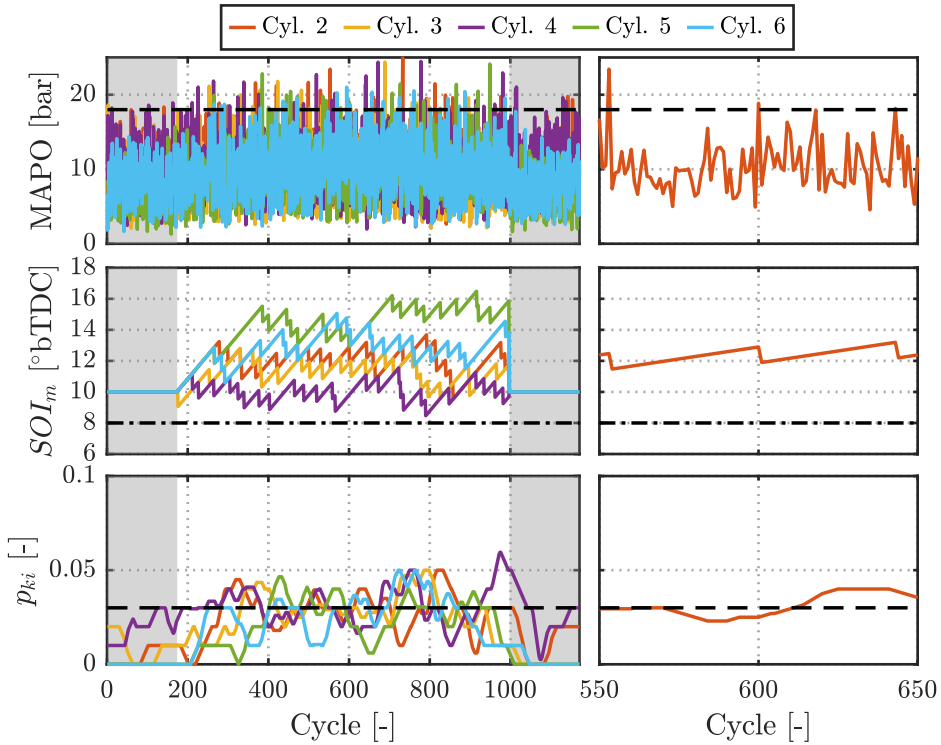


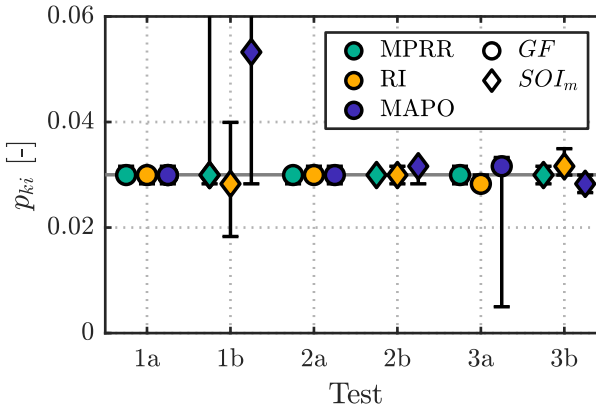
Figure 4.25: Test 3b: MAPO control (top) using the start of the main injection (middle) to control the probability of cycles exceeding the desired threshold (bottom) in partially premixed conditions. A zoom on a cycles area is provided on the right part to show a detailed view of the controller actions. Dashed black line: MAPO limitation (top) and probability threshold (bottom), dash-dotted black lines: control actions limitations (middle). Note that cylinder 1 is omitted from this experiment.

performed using the MPRR and the RI, and the results were compared with the ones obtained using the MAPO limitation. The conditions and controller calibration were the same than the ones presented in Table 4.9 with the exception of KI_{lim} (see Figure 4.22) which was modified according to the considered index and combustion mode as provided in Table 4.10.

Figure 4.26 shows the results for each index in all the tests in a similar way than indicated in Table 4.9: the median probability $p_{ki,median}$ for cylinders 2 to 6 is illustrated in a circle (GF actuation) or diamond shape (SOI_m actuation), and the boundaries ($p_{ki,min}$ and $p_{ki,max}$) are shown with errorbars. Similar results

Table 4.10: Operating conditions when using MPRR and RI as limitation factors in the knock-like controller proposed originally with MAPO.

Test		OP 1		OP 2		OP 3	
		1a	1b	2a	2b	3a	3b
u		GF	SOI_m	GF	SOI_m	GF	SOI_m
KI_{lim}	MPRR [bar/CAD]	9	9	7	7	8	8
	RI [MW/m ²]	7.5	7.5	4.5	4.5	5.5	5.5


Figure 4.26: Probability results of cycles exceeding the specified limitation with various indexes. The solid grey line shows the desired probability threshold ($p_{kc} = 0.03$).

were observed in fully premixed conditions (test 1a and 1b): the gasoline fraction was able to maintain the probability of exceeding cycles at the specified threshold for every index, while the injection timing resulted in high cylinder-to-cylinder dispersion with probabilities distant from the desired value. Same conclusions can be drawn when using MPRR and RI in test 2a, 2b and 3b compared to the MAPO results, while a greater responsiveness to the gasoline fraction was found in the partially premixed mode in test 3a. In this combustion mode, both MPRR and RI exhibited some sensitivity to GF as it is illustrated in Figure 4.27. Same observation was made for the SOI_m sensitivity in OP 2.

Figure 4.27 compares the distribution of the three indexes in the same cylinder against the control variables variations in all the combustion modes. It can be seen that, unlike the MAPO, an increase in the gasoline fraction resulted in a

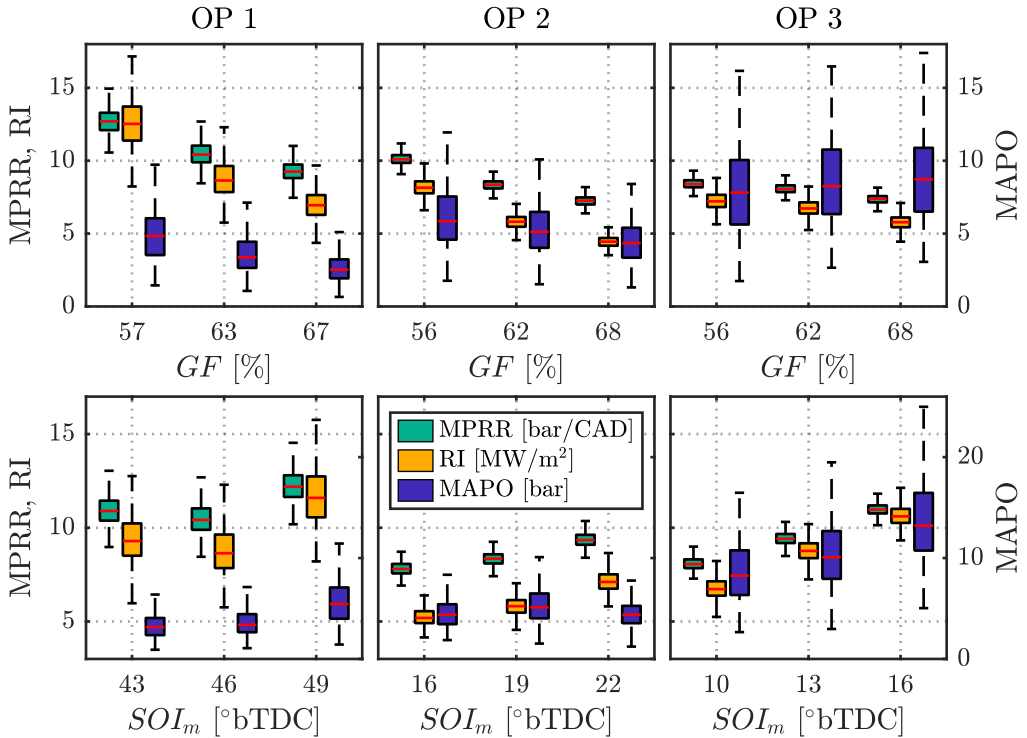


Figure 4.27: Combustion sensitivity of the MPRR, RI and MAPO to the gasoline fraction (top) and the diesel injection timing (bottom) in all the dual-fuel combustion modes.

slight, but distinct, decrease in the MPRR and the RI levels in OP 3. In this case, the mixture reactivity sweep was sufficient to cause a change in the combustion evolution measured with the low-pass filtered pressure trace (which is then used to obtain the pressure rise rate and the ringing intensity), but was not sufficient to appreciate an important change in the resonance excitation in the combustion chamber (i.e., pressure oscillations detection). Furthermore, it can be highlighted that in partially premixed conditions, the MAPO distribution exhibits high levels of cycle-to-cycle variability, representative of the stochastic nature of this index, which might therefore result in a more challenging environment for the controller to ensure complete control over the probability of exceeding cycles.

This analysis showed that although indexes based on the direct measurement of the pressure oscillations might be of greater interest to limit their intensity by means of stochastic control, more traditional indexes such as the MPRR or the

RI might also be used in the same controller architecture to limit the combustion operation, as long as a sensitivity to the control variables is demonstrated.

4.5 Conclusions

This chapter investigated the use of the in-cylinder pressure sensor signal for feedback control applied to dual-fuel combustion engines where various methods with different objectives were explored. Particularly, in order to propose the widest range of application possible, it was decided to expand the control investigation and design to all the considered and available combustion modes in dual-fuel engines: fully, highly and partially premixed.

First, a traditional proportional-integral closed-loop controller was proposed to track the load (IMEP), the combustion phasing (CACG) and ensure that the engine was not exceeding its mechanical constraints (MPRR). The control strategy was applied on the single cylinder engine A and the input-output pairing was analyzed to design the controller. As a result, the total fuel quantity, the premixed injected fuel, the gasoline fraction and the late diesel injection timing were selected. The results showed that the controller was able to reject disturbances in the operating conditions such as with EGR, intake and rail pressure variations, but also to track a change in the combustion phasing setpoint, no matter the operated combustion mode. The controller was designed to prioritize the load and safe operation achievement, at the expense of the combustion phasing tracking response time where further calibration effort could improve the controller response. A test at high load transient condition was also performed to evaluate the proper combustion switching-mode execution induced by the open-loop control and its correction by the closed-loop controller in order to track the desired load. The controller robustness-responsiveness trade-off was found to achieve the load within a few cycles while ensuring a safe control of the MPRR without overshoot in the control actions. These results suggested that this strategy might be applied individually to each cylinder in a multi-cylinder engine in order to compensate for the cylinder-to-cylinder dispersion and provide a more balanced engine operation.

Because a simple closed-loop controller based on proportional-integral actions could not ensure optimal operation of the combustion engine, it was decided to investigate the use of the feedback from the sensors installed on the engine to develop an on-line optimizer algorithm in engine B. It was decided to base the controller on the extremum seeking technique using a cost function that relies on combustion phasing tracking (CA50 in this case) and nitrogen oxides emissions

reduction. That way, the controller aimed, in the best extent possible, to keep the combustion phasing in a fuel efficient area while decreasing the exhaust emissions measured by the NO_x sensor placed at the exhaust. The gasoline fraction and the main diesel injection timing were selected as the control variables. A frequency analysis of the CA_{50} and the NO_x signals response to a perturbation to these inputs showed that each combustion mode exhibited a different sensitivity: the gasoline fraction was more prone to influence the combustion in fully premixed conditions, and the injection timing was more effective in partially premixed combustion. Based on these results, the extremum seeking controller was calibrated and applied on a highly premixed case. The results showed encouraging outcomes as a substantial reduction in the NO_x emissions was observed, at the expense of a slight increase in the fuel consumption. Such strategy might be enhanced with further calibration and by adding more variables into the cost function definition which could then be expanded to the whole engine map operation by selecting the proper control constraints.

Finally, it was decided to explore the use of a knock-like controller based on the measurement of the pressure oscillations in engine B in order to ensure a safe operation of the engine, which is of high importance when dealing with premixed combustion strategies. Due to the potential engine damage that could result from the pressure resonance excitation, the maximum amplitude of the pressure oscillations (MAPO) was considered as the limiting factor for the combustion operation. The gasoline fraction and the injection timing were again selected as the control variables. Similar sensitivity behavior as in the optimization investigation was found, where the gasoline fraction and the injection timing control authority over the combustion were respectively prevailing in fully and partially premixed conditions. The results showed that the designed strategy was able to keep the percentage of cycles exceeding the limit around the desired threshold within the control constraints in each combustion mode, exhibiting its potential to provide a safer engine operation. Further investigation in the dual-fuel combustion pressure oscillations formation and magnitude would be of high interest in order to better characterize the resonance in this kind of combustion mode, and therefore provide a global resonance intensity index definition. Furthermore, it is important to highlight that another detection index using cost effective pressure sensors or a conventional knock sensor placed on the engine structure could be used and the same control strategy might be applied to improve the pressure oscillations limitation.

The various control strategies explored in this chapter showed the potential

given by the in-cylinder pressure signal to comply with a commercial multi-cylinder application. From disturbances rejection to operation optimization, the feedback provided by such sensor can be coupled with the already existing set of sensors to enhance the control of dual-fuel engines in terms of performance, efficiency, safety operation, as well as pollutant emissions.

References

- [1] Singh Akhilendra Pratap and Agarwal Avinash Kumar. Combustion characteristics of diesel HCCI engine: An experimental investigation using external mixture formation technique. *Applied Energy*, Vol. 99, pp. 116–125, nov 2012. (cited in p. 87)
- [2] Bendu Harisankar and Murugan S. Homogeneous charge compression ignition (HCCI) combustion: Mixture preparation and control strategies in diesel engines. *Renewable and Sustainable Energy Reviews*, Vol. 38, pp. 732–746, oct 2014. (cited in pp. 10, 30, and 87)
- [3] Shim Euijoon, Park Hyunwook and Bae Choongsik. Comparisons of advanced combustion technologies (HCCI, PCCI, and dual-fuel PCCI) on engine performance and emission characteristics in a heavy-duty diesel engine. *Fuel*, Vol. 262 n° November 2019, pp. 116436, feb 2020. (cited in p. 87)
- [4] Dempsey Adam B., Walker N. Ryan, Gingrich Eric and Reitz Rolf D. Comparison of low temperature combustion strategies for advanced compression ignition engines with a focus on controllability. *Combustion Science and Technology*, Vol. 186 n° 2, pp. 210–241, 2014. (cited in pp. 10, 32, and 87)
- [5] Splitter Derek A. and Reitz Rolf D. Fuel reactivity effects on the efficiency and operational window of dual-fuel compression ignition engines. *Fuel*, Vol. 118, pp. 163–175, 2014. (cited in p. 87)
- [6] Klos David T and Kokjohn Sage L. Investigation of the Effect of Injection and Control Strategies on Combustion Instability in Reactivity-Controlled Compression Ignition Engines. *Journal of Engineering for Gas Turbines and Power*, Vol. 138 n° 1, pp. 11502, 2016. (cited in p. 87)
- [7] Schmidt Martin, Kimmich Frank, Straky Harald and Isermann Rolf. Combustion Supervision by Evaluating the Crankshaft Speed and Acceleration. In *SAE Technical Papers*, number 724, mar 2000. (cited in p. 88)
- [8] Lee Byungho, Rizzoni Giorgio, Guezennec Yann, Soliman Ahmed, Cavalletti Mauro and Waters James. Engine Control Using Torque Estimation. In *SAE Technical Papers*, number 724, mar 2001. (cited in p. 88)
- [9] Thor Mikael, Egardt Bo, McKelvey Tomas and Andersson Ingemar. Closed-loop diesel engine combustion phasing control based on crankshaft torque measurements. *Control Engineering Practice*, Vol. 33, pp. 115–124, dec 2014. (cited in pp. 12 and 88)

-
- [10] Guillemin Fabrice, Grondin Olivier, Chauvin Jonathan and Nguyen Emmanuel. Combustion Parameters Estimation Based on Knock Sensor for Control Purpose Using Dedicated Signal Processing Platform. In *SAE Technical Papers*, volume 2008, apr 2008. (cited in p. 88)
- [11] Kim Seonguk and Min Kyoungdoug. Detection of combustion start in the controlled auto ignition engine by wavelet transform of the engine block vibration signal. *Measurement Science and Technology*, Vol. 19 n° 8, pp. 085407, aug 2008. (cited in p. 88)
- [12] Taglialatela-Scafati Ferdinando, Cesario Nicola, Lavorgna Mario, Mancaruso Ezio and Vaglieco Bianca Maria. Diagnosis and Control of Advanced Diesel Combustions using Engine Vibration Signal. In *SAE Technical Papers*, apr 2011. (cited in p. 88)
- [13] Saracino Roberto, Gaballo Maria Rosaria, Mannal Soenke, Motz Stefan, Carlucci Antonio and Benegiamo Marco. Cylinder Pressure-Based Closed Loop Combustion Control: A Valid Support to Fulfill Current and Future Requirements of Diesel Powertrain Systems. In *SAE Technical Papers*, volume 2015, sep 2015. (cited in pp. 12 and 88)
- [14] Willems Frank. Is Cylinder Pressure-Based Control Required to Meet Future HD Legislation? *IFAC-PapersOnLine*, Vol. 51 n° 31, pp. 111–118, 2018. (cited in pp. 12, 34, 55, and 88)
- [15] Sellnau Mark C., Matekunas Frederic A., Battiston Paul A., Chang Chen-Fang and Lancaster David R. Cylinder-Pressure-Based Engine Control Using Pressure-Ratio-Management and Low-Cost Non-Intrusive Cylinder Pressure Sensors. In *SAE Technical Papers*, number 724, mar 2000. (cited in p. 88)
- [16] Strandh Petter, Christensen Magnus, Bengtsson Johan, Johansson Rolf, Vressner Andreas, Tunestål Per and Johansson Bengt. Ion Current Sensing for HCCI Combustion Feedback. In *SAE Technical Paper Series*, oct 2003. (cited in p. 88)
- [17] Badawy Tamer, Shrestha Amit and Henein Naeim. Detection of Combustion Resonance Using an Ion Current Sensor in Diesel Engines. *Journal of Engineering for Gas Turbines and Power*, Vol. 134 n° 5, may 2012. (cited in p. 88)
- [18] Malaczynski Gerard, Roth Gregory and Johnson Donald. Ion-sense-based real-time combustion sensing for closed loop engine control. *SAE International Journal of Engines*, Vol. 6 n° 1, pp. 267–277, apr 2013. (cited in p. 88)
- [19] Ängeby Jakob, Johnsson Anders and Hellström Kristina. Knock Detection Using Multiple Indicators and a Classification Approach. *IFAC-PapersOnLine*, Vol. 51 n° 31, pp. 297–302, 2018. (cited in p. 88)
- [20] Ravaglioli Vittorio, Carra Filippo, Moro Davide, De Cesare Matteo and Stola Federico. Remote Sensing Methodology for the Closed-Loop Control of RCCI Dual Fuel Combustion. In *SAE Technical Papers*, volume 2018-April, pp. 1–10, apr 2018. (cited in pp. 34 and 88)

- [21] Li Yun, Ang Kiam Heong and Chong Gregory C.Y. PID control system analysis and design. *IEEE Control Systems*, Vol. 26 n° 1, pp. 32–41, feb 2006. (cited in p. 89)
- [22] Hellstrom Erik, Larimore Jacob, Jade Shyam, Stefanopoulou Anna G. and Jiang Li. Reducing cyclic variability while regulating combustion phasing in a four-cylinder HCCI engine. *IEEE Transactions on Control Systems Technology*, Vol. 22 n° 3, pp. 1190–1197, 2014. (cited in p. 89)
- [23] Arora Jayant Kumar and Shahbakhti Mahdi. Real-Time Closed-Loop Control of a Light-Duty RCCI Engine During Transient Operations. In *SAE Technical Paper*, mar 2017. (cited in pp. 35, 38, 55, and 89)
- [24] Fang Cheng, Ouyang Minggao, Tunestal Per, Yang Fuyuan and Yang Xiaofan. Closed-loop combustion phase control for multiple combustion modes by multiple injections in a compression ignition engine fueled by gasoline-diesel mixture. *Applied Energy*, Vol. 231 n° May, pp. 816–825, dec 2018. (cited in pp. 12 and 89)
- [25] Ingesson Gabriel, Yin Lianhao, Johansson Rolf and Tunestål Per. Proportional–Integral Controller Design for Combustion-Timing Feedback, From n-Heptane to Iso-Octane in Compression–Ignition Engines. *Journal of Dynamic Systems, Measurement, and Control*, Vol. 140 n° 5, may 2018. (cited in pp. 89 and 147)
- [26] Payri F., Broatch A., Salavert J. M. and Martín J. Investigation of diesel combustion using multiple injection strategies for idling after cold start of passenger-car engines. *Experimental Thermal and Fluid Science*, Vol. 34 n° 7, pp. 857–865, 2010. (cited in pp. 74 and 90)
- [27] Ladommatos N., Abdelhalim S. M., Zhao Hua and Hu Z. The Dilution, Chemical, and Thermal Effects of Exhaust Gas Recirculation on Diesel Engine Emissions - Part 1: Effect of Reducing Inlet Charge Oxygen. In *SAE Technical Papers*, number 412, may 1996. (cited in p. 96)
- [28] Ladommatos N., Abdelhalim S. M., Zhao Hua and Hu Z. The Dilution, Chemical, and Thermal Effects of Exhaust Gas Recirculation on Diesel Engine Emissions - Part 2: Effects of Carbon Dioxide. In *SAE Technical Papers*, number 412, may 1996. (cited in p. 96)
- [29] Kokjohn Sage L., Hanson Reed M., Splitter Derek A. and Reitz Rolf D. Experiments and modeling of dual-fuel HCCI and PCCI combustion using in-cylinder fuel blending. *SAE International Journal of Engines*, Vol. 2 n° 2, pp. 24–39, nov 2010. (cited in pp. 31, 96, and 151)
- [30] Desantes José M., Benajes Jesús, García Antonio and Monsalve-Serrano Javier. The role of the in-cylinder gas temperature and oxygen concentration over low load reactivity controlled compression ignition combustion efficiency. *Energy*, Vol. 78, pp. 854–868, 2014. (cited in pp. 31, 96, 151, and 157)
- [31] DelVescovo Dan, Kokjohn Sage and Reitz Rolf. The Effects of Charge Preparation, Fuel Stratification, and Premixed Fuel Chemistry on Reactivity Controlled Compression Ignition (RCCI) Combustion. *SAE International Journal of Engines*, Vol. 10 n° 4, pp. 1491–1505, 2017. (cited in pp. 32, 96, 112, 127, and 157)

-
- [32] Krishnan Sundar Rajan, Srinivasan Kalyan Kumar and Raihan Mostafa Shameem. The effect of injection parameters and boost pressure on diesel-propane dual fuel low temperature combustion in a single-cylinder research engine. *Fuel*, Vol. 184, pp. 490–502, nov 2016. (cited in p. 98)
- [33] Klos David and Kokjohn Sage L. Investigation of the sources of combustion instability in low-temperature combustion engines using response surface models. *International Journal of Engine Research*, Vol. 16 n° 3, pp. 419–440, apr 2015. (cited in p. 104)
- [34] Singh Ajay, Saxena Mohit Raj and Maurya Rakesh Kumar. Investigation of Nature of Cyclic Combustion Variations in RCCI Engine. In *Lecture Notes in Mechanical Engineering*, pp. 589–598. Springer Science and Business Media Deutschland GmbH, 2021. (cited in p. 104)
- [35] Aquino C.F. Transient A/F Control Characteristics of the 5 Liter Central Fuel Injection Engine. In *SAE Technical Paper Series*, number 810494, feb 1981. (cited in pp. 106, 115, 157, and 170)
- [36] Raut Akshat, Bidarvatan Mehran, Borhan Hoseinali and Shahbakhti Mahdi. Model Predictive Control of an RCCI Engine. In *2018 Annual American Control Conference (ACC)*, pp. 1604–1609. IEEE, jun 2018. (cited in pp. 36, 106, 148, and 157)
- [37] Khodadadi Sadabadi Kaveh and Shahbakhti Mahdi. Dynamic Modelling and Controller Design of Combustion Phasing for an RCCI Engine. In *Volume 2: Mechatronics; Mechatronics and Controls in Advanced Manufacturing; Modeling and Control of Automotive Systems and Combustion Engines; Modeling and Validation; Motion and Vibration Control Applications; Multi-Agent and Networked Systems; Path Pla.* American Society of Mechanical Engineers, oct 2016. (cited in pp. 36, 38, and 106)
- [38] Leith Doug J. and Leithead W. E. Survey of gain-scheduling analysis and design. *International Journal of Control*, Vol. 73 n° 11, pp. 1001–1025, jan 2000. (cited in p. 106)
- [39] Tan Y., Moase W. H., Manzie C., Nešić D. and Mareels I. M.Y. Extremum seeking from 1922 to 2010. *Proceedings of the 29th Chinese Control Conference, CCC'10*, pp. 14–26, 2010. (cited in p. 107)
- [40] Zurbriggen Florian, Hutter Richard and Onder Christopher. Diesel-minimal combustion control of a natural gas-diesel engine. *Energies*, Vol. 9 n° 1, 2016. (cited in p. 107)
- [41] Wang Wenyi, Li Yaoyu and Hu Bin. Real-time efficiency optimization of a cascade heat pump system via multivariable extremum seeking. *Applied Thermal Engineering*, Vol. 176 n° November 2019, pp. 115399, jul 2020. (cited in p. 107)
- [42] Kumar Saurav, Mohammadi Alireza, Quintero David, Rezazadeh Siavash, Gans Nicholas and Gregg Robert D. Extremum Seeking Control for Model-Free Auto-Tuning of Powered Prosthetic Legs. *IEEE Transactions on Control Systems Technology*, Vol. 28 n° 6, pp. 2120–2135, nov 2020. (cited in p. 107)

- [43] Tan Qingyuan, Divekar Prasad S., Tan Ying, Chen Xiang and Zheng Ming. Pressure Sensor Data-Driven Optimization of Combustion Phase in a Diesel Engine. *IEEE/ASME Transactions on Mechatronics*, Vol. 25 n° 2, pp. 694–704, apr 2020. (cited in pp. 107 and 108)
- [44] Krstić Miroslav and Wang Hsin-Hsiung. Stability of extremum seeking feedback for general nonlinear dynamic systems. *Automatica*, Vol. 36 n° 4, pp. 595–601, apr 2000. (cited in p. 107)
- [45] Dochain Denis, Perrier Michel and Guay Martin. Extremum seeking control and its application to process and reaction systems: A survey. *Mathematics and Computers in Simulation*, Vol. 82 n° 3, pp. 369–380, nov 2011. (cited in p. 107)
- [46] Hellstrom Erik, Lee Donghoon, Jiang Li, Stefanopoulou Anna G and Yilmaz Hakan. On-Board Calibration of Spark Timing by Extremum Seeking for Flex-Fuel Engines. *IEEE Transactions on Control Systems Technology*, Vol. 21 n° 6, pp. 2273–2279, nov 2013. (cited in p. 107)
- [47] Zhang Yahui and Shen Tielong. Cylinder pressure based combustion phase optimization and control in spark-ignited engines. *Control Theory and Technology*, Vol. 15 n° 2, pp. 83–91, 2017. (cited in p. 107)
- [48] Novella Ricardo, Pla Benjamin, Bares Pau and Martinez-Hernandez Pablo José. Closed-Loop Combustion Control by Extremum Seeking with the Passive-Chamber Ignition Concept in SI Engines. In *SAE Technical Papers*, volume 2020-April, pp. 1–11, apr 2020. (cited in p. 107)
- [49] Lewander M., Widd A., Johansson B. and Tunestal P. Steady state fuel consumption optimization through feedback control of estimated cylinder individual efficiency. *2012 American Control Conference (ACC)*, pp. 4210–4214, 2014. (cited in p. 107)
- [50] van der Weijst Robert, van Keulen Thijs and Willems Frank. Constrained multi-variable extremum-seeking for online fuel-efficiency optimization of Diesel engines. *Control Engineering Practice*, Vol. 87 n° March, pp. 133–144, jun 2019. (cited in p. 107)
- [51] Benajes Jesús, Molina Santiago, García Antonio and Monsalve-Serrano Javier. Effects of direct injection timing and blending ratio on RCCI combustion with different low reactivity fuels. *Energy Conversion and Management*, Vol. 99, pp. 193–209, 2015. (cited in pp. 32, 109, 157, and 185)
- [52] Atta Khalid Tourkey and Guay Martin. Adaptive amplitude fast proportional integral phasor extremum seeking control for a class of nonlinear system. *Journal of Process Control*, Vol. 83, pp. 147–154, nov 2019. (cited in p. 110)
- [53] Li Changle. *Stratification and Combustion in the Transition from HCCI to PPC*. PhD Thesis, 2018. (cited in p. 112)
- [54] Blanco-Rodriguez David. *Modelling and Observation of Exhaust Gas Concentrations for Diesel Engine Control*. Springer Theses. Springer International Publishing, Cham, 2014. (cited in pp. 114 and 173)

-
- [55] Heywood J.B. *Internal Combustion Engine Fundamentals*. Automotive technology series. McGraw-Hill, 1988. (cited in pp. 6, 71, 118, 119, 150, and 158)
- [56] UNECE. United Nations Economic Commission for Europe, Addendum 48: Regulation No. 49, Revision 6. Concerning the Adoption of Uniform Technical Prescriptions for Wheeled Vehicles, Equipment and Parts which can be fitted and/or be used on Wheeled Vehicles and the Conditions for Reciprocal Recognition of Approvals Granted on the Basis of these Prescriptions, 2013. (cited in p. 119)
- [57] Peyton Jones James C., Spelina Jill M. and Frey Jesse. Optimizing knock thresholds for improved knock control. *International Journal of Engine Research*, Vol. 15 n° 1, pp. 123–132, jan 2014. (cited in pp. 120 and 128)
- [58] Zhang Yahui, Shen Xun, Wu Yuhu and Shen Tielong. On-board knock probability map learning-based spark advance control for combustion engines. *International Journal of Engine Research*, Vol. 20 n° 10, pp. 1073–1088, dec 2019. (cited in p. 120)
- [59] Pla Benjamín, Bares Pau, Jiménez Irina, Guardiola Carlos, Zhang Yahui and Shen Tielong. A fuzzy logic map-based knock control for spark ignition engines. *Applied Energy*, Vol. 280 n° May, pp. 116036, dec 2020. (cited in p. 120)
- [60] Selim Mohamed Y.E. Combustion Noise Measurements and Control from Small Diesel and Dual Fuel Engines. In *SAE Technical Papers*, volume 2004-Septe, sep 2004. (cited in p. 120)
- [61] Kirsten Martin, Pirker Gerhard, Redtenbacher Christoph, Wimmer Andreas and Chmela Franz. Advanced Knock Detection for Diesel/Natural Gas Engine Operation. *SAE International Journal of Engines*, Vol. 9 n° 3, pp. 1571–1583, apr 2016. (cited in p. 120)
- [62] Lounici M.S., Benbellil M.A., Loubar K., Niculescu D.C. and Tazerout M. Knock characterization and development of a new knock indicator for dual-fuel engines. *Energy*, Vol. 141, pp. 2351–2361, dec 2017. (cited in p. 120)
- [63] Chen Lin, Zhang Ren, Pan Jiaying and Wei Haiqiao. Optical study on autoignition and knocking characteristics of dual-fuel engine under CI vs SI combustion modes. *Fuel*, Vol. 266 n° November 2019, pp. 117107, apr 2020. (cited in p. 120)
- [64] Sjöberg Magnus and Dec John E. Effects of Engine Speed, Fueling Rate, and Combustion Phasing on the Thermal Stratification Required to Limit HCCI Knocking Intensity. In *SAE Technical Papers*, may 2005. (cited in p. 120)
- [65] Broatch A., Margot X., Novella R. and Gomez-Soriano J. Combustion noise analysis of partially premixed combustion concept using gasoline fuel in a 2-stroke engine. *Energy*, Vol. 107, pp. 612–624, jul 2016. (cited in p. 120)
- [66] Wang Ying, Guo Chunlan, Wang Peng and Wang Dongxing. Numerical Investigation on Knock Combustion in a Diesel–Dimethyl Ether Dual-Fuel Engine. *Energy & Fuels*, Vol. 33 n° 6, pp. 5710–5718, jun 2019. (cited in p. 120)

- [67] Ott T., Zurbriggen F., Onder C. and Guzzella L. Cylinder Individual Feedback Control of Combustion in a Dual Fuel Engine. *IFAC Proceedings Volumes*, Vol. 46 n° 21, pp. 600–605, 2013. (cited in pp. 34, 37, and 121)
- [68] Ingesson Gabriel, Yin Lianhao, Johansson Rolf and Tunestål Per. A Double-Injection Control Strategy For Partially Premixed Combustion. *IFAC-PapersOnLine*, Vol. 49 n° 11, pp. 353–360, 2016. (cited in pp. 76 and 121)
- [69] Haskara Ibrahim and Wang Yue-Yun. Closed-Loop Combustion Noise Limit Control for Modern Diesel Combustion Modes. *IEEE Transactions on Control Systems Technology*, Vol. 25 n° 4, pp. 1168–1179, jul 2017. (cited in pp. 76 and 121)
- [70] Mashkournia Masoud, Audet Adrian and Koch Charles Robert. Knock Detection and Control in an HCCI Engine Using DWT. In *ASME 2011 Internal Combustion Engine Division Fall Technical Conference*, pp. 391–399. ASMEDC, jan 2011. (cited in p. 121)
- [71] Kyratatos Panagiotis, Brückner Clemens and Boulouchos Konstantinos. Cycle-to-cycle variations in diesel engines. *Applied Energy*, Vol. 171, pp. 120–132, jun 2016. (cited in p. 125)
- [72] Payri Francisco, Lujan Jose, Climent Hector and Pla Benjamín. Effects of the Intake Charge Distribution in HSDI Engines. *SAE Technical Paper Series*, Vol. 1, 2010. (cited in pp. 125 and 161)
- [73] Kassa Mateos, Hall Carrie, Ickes Andrew and Wallner Thomas. Modeling and control of fuel distribution in a dual-fuel internal combustion engine leveraging late intake valve closings. *International Journal of Engine Research*, Vol. 18 n° 8, pp. 797–809, 2017. (cited in pp. 125 and 158)
- [74] Robert Anthony, Truffin Karine, Iafrate Nicolas, Jay Stephane, Colin Olivier and Angelberger Christian. Large-eddy simulation analysis of knock in a direct injection spark ignition engine. *International Journal of Engine Research*, Vol. 20 n° 7, pp. 765–776, sep 2019. (cited in p. 125)
- [75] Kiencke Uwe and Nielsen Lars. *Automotive Control Systems: For Engine, Driveline, and Vehicle*. Springer Berlin Heidelberg, Berlin, Heidelberg, 2005. (cited in pp. 11 and 128)
- [76] Spelina Jill M., Peyton Jones James C. and Frey Jesse. Stochastic simulation and analysis of a classical knock controller. *International Journal of Engine Research*, Vol. 16 n° 3, pp. 461–473, apr 2015. (cited in p. 128)
- [77] Naber Jeffrey, Blough Jason R., Frankowski Dave, Goble Monroe and Szpytman John E. Analysis of Combustion Knock Metrics in Spark-Ignition Engines. In *SAE Technical Papers*, volume 2006, apr 2006. (cited in p. 129)
- [78] Vulli S., Dunne J.F., Potenza R., Richardson D. and King P. Time-frequency analysis of single-point engine-block vibration measurements for multiple excitation-event identification. *Journal of Sound and Vibration*, Vol. 321 n° 3-5, pp. 1129–1143, apr 2009. (cited in p. 129)

Chapter 5

Model-based approach for dual-fuel combustion control

5.1 Introduction

Describing a system by physical equations has always been of high interest in control theory. The model might be used to develop simulations for control strategies thanks to the system mathematical representation, to facilitate the estimation of internal parameters through state observers, or to develop more advanced control methods such as model predictive control (MPC).

Internal combustion engines are nonlinear systems where control strategies such as the ones described in Chapter 4 are widely used because they do not require to develop a complete model of the engine. Furthermore, the engine nonlinearities might be insignificant enough to be tackled by a simple controller such as proportional-integral control. Nonetheless, these strategies might require a substantial experimental calibration effort, particularly when applied to a wide range of operating conditions. The physics-based control-oriented model (COM) approach presents several advantages [1]. First, the model could be used to calibrate conventional control strategies off-line instead of undertaking a considerable experimental calibration campaign for each condition. By doing so, experimental data could be used for system identification and validate a model, and once it is sufficiently representative of the engine operation, no more experiments are theoretically required. A new controller could therefore be designed and evaluated prior to its real implementation [2–5]. Finally, these models might also be integrated directly into enhanced model-based control strategies where the mathematical model allows to get a better insight about the expected behavior of the engine [6–9].

Some models might require some information from a specific variable in order to provide a proper estimate. In the case where this variable is hard to measure, some errors might be observed in the model output and this could result in a less efficient control of the system. In internal combustion engines, this is especially true due to the system dynamics and cylinder-to-cylinder dispersion which might come from various sources (e.g., fueling variations, ageing, hardware design). In single fuel applications, state-of-the-art closed-loop control strategies used to be effective for the compensation of the cylinder-to-cylinder dispersion due to fueling variations [10]. However, dual-fuel engines represent a more complex environment [11,12], especially under diluted operation, where similar individual combustion phasing is not necessarily representative of the same fuel mixture reactivity in all the cylinders due to uneven fuel and air dilution distribution. There is therefore a need to provide tools that give a better insight of the individual cylinder conditions in order to enhance the feedback information for dual-fuel combustion controllers dealing with the fuel dispersion reduction between cylinders. A state observer is a powerful tool to address this kind of task by leveraging the model representation of the system combined with the available information from the sensors [13,14].

This chapter investigates the potential of using models describing the dual-fuel combustion operation to provide tools that could enhance the development of control strategies for such combustion concept. The first section presents a control-oriented model developed to provide an estimation of the combustion phasing in RCCI operation and the second section explores the use of a state observer to estimate the individual cylinder fuel blending ratio. The results are respectively discussed in sections 5.2 and 5.3.

5.2 Combustion phasing control-oriented model for RCCI engines

The combustion phasing is traditionally assumed to be a relevant indicator and target for ensuring an efficient combustion operation. Whether to use it as a feedback for developing control strategies, or to implement it directly in the controller, its estimation through modeling is therefore particularly valuable. Several studies in the literature aimed to develop combustion modeling for control applications in advanced combustion concepts such as HCCI [15–17], and some of them were dedicated to dual-fuel combustion as discussed in Chapter 2.

In this section, a control-oriented model with the objective of predicting the CA50 from the operating conditions in RCCI combustion mode (fully and highly premixed conditions, Chapter 3) is proposed. A modified knock integral model, which makes use of the mixture reactivity and the in-cylinder oxygen concentration, was used to estimate the ignition delay. Then, the CA50 was approximated using a linear equation which characterizes the duration between the start of combustion (SOC) and the CA50.

The model was first calibrated using a set of experimental data from engine B in RCCI conditions, and was finally validated in a load transient test which resulted in a change in the CA50 as well. The model description and the results are provided hereinafter.

5.2.1 Model description

The control-oriented model developed for the premixed dual-fuel combustion is described below. This model aims to propose a simple approach to predict the start of combustion and the CA50 using physical equations based on measurable operating conditions variables. The COM is divided into three parts: the estimation of the in-cylinder conditions at the intake valve closing (IVC), the compression from IVC to SOC, and the combustion process from SOC to CA50.

IVC conditions

The in-cylinder charge conditions at the intake valve closing contribute to the combustion timing of RCCI engines and must therefore be determined [18]. In the proposed model, some simplifications were made, that is, the residual gases from the previous cycle were not considered and the in-cylinder pressure at IVC was approximated from the intake manifold pressure P_{int} by a linear function as suggested by Rausen et al. [19]:

$$p_{ivc} = \beta_0 + \beta_1 P_{int} \quad (5.1)$$

The in-cylinder temperature at IVC was then approximated using the ideal gas law:

$$T_{ivc} = \frac{p_{ivc} \cdot V_{ivc}}{m_{cyl} \cdot R} \quad (5.2)$$

with R the ideal gas constant equal to 287 J/kg.K and V_{ivc} the volume at IVC obtained from geometrical equations (see Chapter 3). The in-cylinder trapped mass m_{cyl} was estimated using a volumetric efficiency map calibrated from experimental

data and was calculated by:

$$m_{cyl} = \frac{\eta_v P_{int} V_{dis}}{R T_{int}} \quad (5.3)$$

where η_v is the volumetric efficiency (i.e., the pumping performance of the inlet port which is normally between 0.8 and values above 0.9 [20]), V_{dis} the cylinder displacement, and T_{int} the intake manifold temperature. More detailed approaches to estimate the conditions at IVC, which take into account the effect of the residual gases, can be found in [4, 19]. These models, however, represent a more complex approach with a higher calibration effort, and were therefore not evaluated in this work.

Compression (from IVC to SOC)

Premixed combustion concepts are characterized by their long ignition delays which promote NO_x and soot reduction. The ignition delay τ_{id} , the time between the fuel injection and its auto-ignition, has been usually correlated with Arrhenius-like equations of the form [20]:

$$\tau_{id} = A p^{-n} \exp\left(\frac{Ea}{RT}\right) \quad (5.4)$$

where A and n are calibration constants, Ea is the activation energy, R is the specific gas constant, and p and T are respectively the mixture pressure and temperature.

Nonetheless, in an engine, the conditions inside the cylinder vary over time as the piston moves from the bottom to the top dead center during the compression stroke. To take into account the effect of these changing conditions, the so called *knock integral model* is traditionally used. In this approach, the start of combustion is considered at the index where this expression reaches the unity as proposed by Livengood and Wu [21]:

$$\int_{t_{soi}}^{t_{soi} + \tau_{id}} \frac{1}{\tau} dt = 1 \quad (5.5)$$

with t_{soi} being the injection timing and τ the instantaneous ignition delay calculation at time t . Various applications of such model, with as many definitions of τ , can be found in the literature [22–25]. In this work, the considered model, in the crank angle domain, was of the following form [26]:

$$\int_{\theta_{ivc}}^{\theta_{soc}} \frac{1}{A N \exp\left(\frac{b}{T(\theta)} p(\theta)^n\right)} d\theta = 1 \quad (5.6)$$

where A , b and n are calibration constants, N is the engine speed, and T and p are respectively the instantaneous in-cylinder temperature and pressure, which are function of the crank angle degree θ . Here, it was decided to start the integral at the IVC because the gasoline is injected during the intake stroke and it was assumed that the reaction rate until the diesel injection should not bias the integral computation under highly premixed conditions.

Dual-fuel combustion ignition delay was found to be sensitive to the mixture reactivity and the in-cylinder oxygen concentration [27, 28]. In highly premixed conditions, these parameters are directly associated to the gasoline fraction in the mixture and the air dilution by the exhaust gas recirculation. The model should therefore encompass these effects. The constant b in (5.6) can be correlated to the activation energy Ea in (5.4) through:

$$b = \frac{Ea}{R} \quad (5.7)$$

As suggested by Khodadadi Sadabadi et al. [26], the activation energy was considered to be related with the fuel cetane number CN :

$$Ea = \frac{c_1}{CN + c_2} \quad (5.8)$$

Being composed of two fuels, a global cetane number, CN_{mix} , was estimated for the mixture from the proportion of each of the fuels and their respective CN :

$$CN_{mix} = GF \cdot CN_g + (1 - GF) \cdot CN_d \quad (5.9)$$

where CN_g was considered to be 15, CN_d is 51, and GF is the gasoline fraction defined by the ratio of the gasoline mass m_g to the total injected fuel including the diesel quantity m_d :

$$GF = \frac{m_g}{m_g + m_d} \quad (5.10)$$

As aforementioned, the available oxygen concentration in the cylinder also plays a significant role in the combustion timing. This parameter is related to the EGR rate, therefore the oxygen concentration at the exhaust $[O_2]_{exh}$, and was accounted here by considering the oxygen concentration at the intake $[O_2]_{int}$ as follows:

$$[O_2]_{int} = [O_2]_{atm} \cdot (1 - EGR) + [O_2]_{exh} \cdot EGR \quad (5.11)$$

where the atmospheric concentration is $[O_2]_{atm} = 21\%$, and EGR is defined as in (3.1).

The effect of a change in the oxygen concentration at the intake was implemented in place of the calibration constant A in (5.6) through a simple linear equation which was found to work properly for the EGR rate levels here considered. The final modified knock integral model (MKIM) used in this work to estimate the ignition delay resulted therefore in the following equation:

$$\int_{\theta_{ivc}}^{\theta_{soc}} \frac{1}{(c_3 + c_4([O_2]_{atm} - [O_2]_{int})) N \exp\left(\frac{c_1}{(CN_{mix} + c_2)RT(\theta)}p(\theta)^n\right)} d\theta = 1 \quad (5.12)$$

where the instantaneous pressure and temperature, p and T , were estimated assuming that the compression was following a polytropic process ($pV^\kappa = constant$):

$$p(\theta) = p_{ivc} \cdot \left(\frac{V_{ivc}}{V(\theta)}\right)^\kappa \quad (5.13)$$

$$T(\theta) = T_{ivc} \cdot \left(\frac{V_{ivc}}{V(\theta)}\right)^{\kappa-1} \quad (5.14)$$

with κ a constant polytropic coefficient and V the instantaneous volume. Note that, here, the modeling approach aims to estimate the combustion phasing as a mean to either provide an off-line calibration tool or to be used in a model-based strategy as a prediction of this metric. Consequently, although the in-cylinder pressure was indeed measured and used to validate the model, here its measurement is not considered inside of the model and explains why an estimation is required.

Combustion (from SOC to CA50)

The combustion phasing, expressed as the CA50, is computed from the heat release rate calculation. Nonetheless, without a measurement of the pressure traces, or in a prediction application, such signal cannot be measured. For that matter, control-oriented models traditionally use Wiebe functions [29], where an estimation of the burn duration has to be expressed [26, 30], to predict the CA50. In this work, it was decided to consider the combustion duration modeling only from the SOC to the CA50 itself and to investigate a simple approach in order to reduce the calibration process. Consequently, by developing and calibrating this model only, the CA50 could then be directly estimated using the SOC estimation provided by (5.12). By computing a multiple variables regression model, taking into account various control variables (e.g., gasoline fraction, equivalence ratio, intake pressure), it was found that the temperature at the start of combustion T_{soc} and the global equivalence ratio ϕ were able to represent the majority of the

training data considered in this work with a coefficient of determination R^2 of 0.71. It is important to note that such value of R^2 is affected by the cycle-to-cycle dispersion of such combustion mode, and consequently this value was considered acceptable. The statistical analysis led therefore to the following expression of the burn duration θ_d :

$$\theta_d = CA50 - SOC = b_0 + b_1 T_{soc} + b_2 \phi \quad (5.15)$$

where b_0 , b_1 and b_2 are calibration constants, T_{soc} is calculated using the instantaneous polytropic temperature T in (5.14) at θ_{soc} , and ϕ is obtained from:

$$\phi = \frac{1}{m_a} (m_g \psi_{s,g} + m_d \psi_{s,d}) \simeq \frac{1}{m_a} (m_g + m_d) \psi_s \quad (5.16)$$

where m_a is the fresh air mass entering the cylinder and ψ_s refers to the air-to-fuel ratio in stoichiometric conditions for each fuel, which might be considered as a single and same value for both of the fuels considered in this work as they exhibit a similar value ($\psi_{s,g} = 14.7$ and $\psi_{s,d} = 14.5$).

5.2.2 Results and discussion

The model previously described was firstly calibrated using a training data set in steady-state operation in order to evaluate the impact of the modeling assumptions on the SOC and CA50 estimation. Finally, the calibration was validated with a test which consisted in a transient operation with a CA50 variation. The experimental SOC and CA50 were evaluated through the apparent heat release rate model as described in Chapter 3.

Steady-state calibration

Various experiments were carried out in order to calibrate the combustion model. These experiments consisted in operating conditions sweeps at a constant engine speed, whose details can be found in Table 5.1. A simple linear regression with the pressure levels measured at IVC, and the intake manifold pressure, allowed to obtain the constants β_0 and β_1 in (5.1). The calibration of the constant n in (5.12) was achieved using a data set where the intake pressure was varied with no EGR and a constant gasoline fraction, and where the activation energy Ea was first considered as a single parameter definition through the constant b in (5.6). An optimization calibration was executed in order to reduce the root mean squared error between the integration value at the experimental θ_{soc} and the desired value at this same θ , being the unity. The same principle was then applied to a test at constant intake pressure and no EGR with a change in the mixture reactivity

Table 5.1: Steady-state operating conditions used for the RCCI control-oriented model calibration (training data set).

Engine speed	1200 rpm
Intake pressure	From 1.1 to 1.7 bar
Intake temperature	From 295 to 310 K
GF	From 25 to 65 %
EGR	From 0 to 20 %

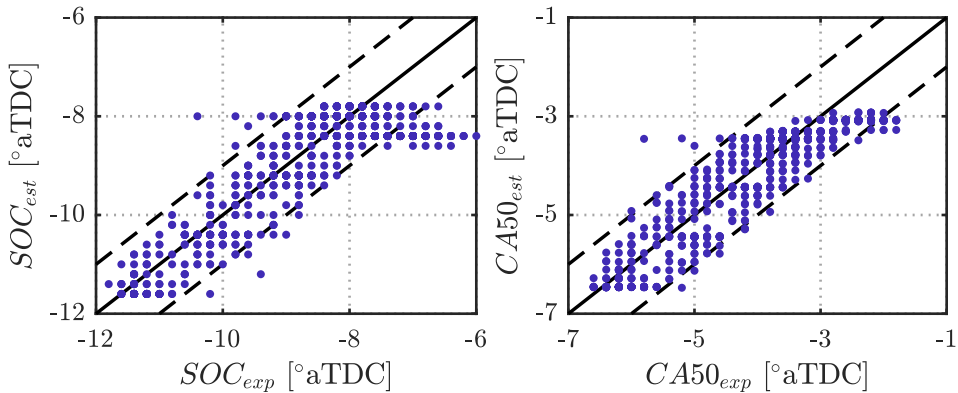
through the gasoline fraction in order to calibrate the constants c_1 and c_2 in (5.8). Similarly, the EGR effect was calibrated at a constant intake pressure and gasoline fraction varying the EGR rate. Finally, the combustion duration model calibration was completed with a linear regression with the duration measured between the experimental SOC and CA50.

Table 5.2 lists the calibration constants obtained after the model calibration with the steady-state data set, and Figure 5.1 shows the resulting SOC and CA50 estimation against the corresponding experimental values. In this figure, the dashed black lines show a ± 1 crank angle degree deviation. The results showed a good agreement with the experimental data, resulting in a mean absolute error of 0.6 CAD and 0.4 CAD for the SOC and the CA50 estimation, respectively. The observed deviation could be explained by:

- the calibration constants which cannot perfectly fit all the operating conditions
- the ability of the model to tackle the cycle-to-cycle variation, as previously highlighted, where the overall cyclic variations of the training data were respectively 0.36 CAD for SOC and 0.27 CAD for CA50
- the modeling assumptions
- the cylinder-to-cylinder species concentration dispersion, because here the data from a single cylinder was used to calibrate the model although the operating conditions were measured for the whole engine
- the injector model, where the required fuel quantity might not be injected due to some bias at the injector or in the injector look-up table which converts the desired fuel mass into injector energizing time.

Table 5.2: Resulting calibration constants values from the steady-state calibration procedure.

IVC conditions (5.1)		Ignition delay (5.12)		Burn duration (5.15)	
β_0	2.62e+03	n	-0.0702	b_0	28.92
β_1	1.18	c_1	2.74e+09	b_1	-0.028
		c_2	778.69	b_2	-2.59
		c_3	8.63e-05		
		c_4	-2.36e-06		

**Figure 5.1:** SOC (left) and CA50 (right) estimation (*est*) from the control-oriented model against experimental values (*exp*) from the training data set using the calibration constants listed in Table 5.2. The dashed black lines represent a ± 1 CAD interval.

Also, it is important to note that the proposed calibration presents some improvement margin by considering a wider range of operating conditions in the calibration of the model. As an example, increasing the EGR rate range should be beneficial. In some conditions, premixed dual-fuel combustion can be performed under significant exhaust gas recirculation rates [31, 32], and the ones considered in this model might not be sufficient for the model calibration to cover higher rates. Nonetheless, the achieved results with this simple approach were considered representative enough to consider this model for the transient validation.

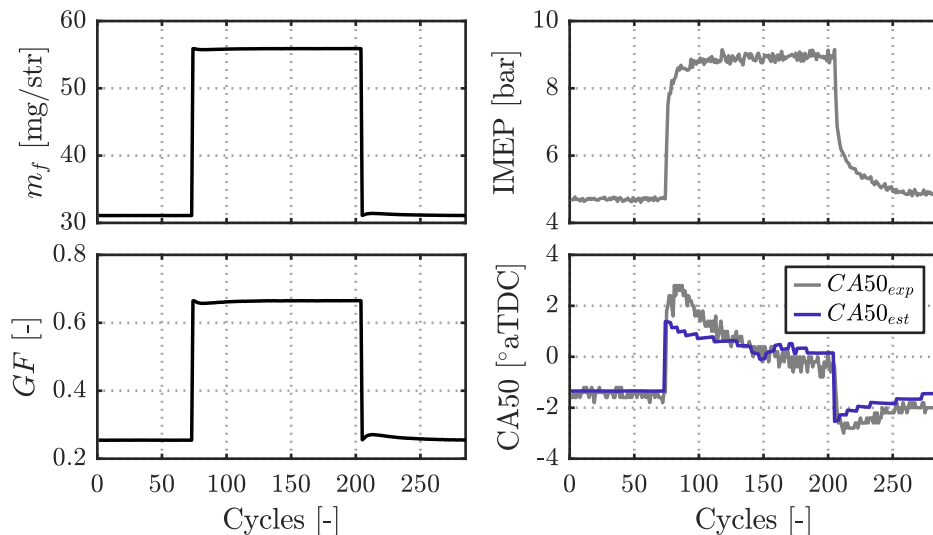


Figure 5.2: Control-oriented model validation in a load transient (top right) data set resulting from a variation in the total fuel quantity (top left) and which includes a gasoline fraction variation as well (bottom left). It is observed that the model exhibits an overall good estimation of the CA50 (bottom right) throughout the test with the calibration listed in Table 5.2.

Transient validation

The model was applied to experimental data from a step in the engine load (IMEP) at a constant engine speed (1200 rpm, equal to the one in the calibration process). The goal was to verify the ability of the model to predict the CA50 under transient operation using the available inputs, and the model calibration constants detailed in the previous section. In this test, a step in the total injected fuel quantity ($m_f = m_g + m_d$) and gasoline fraction (GF) was performed, while the EGR valve and the variable geometry turbocharger positions were kept constant. Figure 5.2 provides the results.

The control-oriented model showed a good prediction of the CA50 at low load, while some error was noticed at the highest IMEP (highest m_f) value during the first 100 cycles. This observation might be explained by the engine dynamics and/or by the aforementioned potential sources of estimation errors in this region of operation (e.g., injector model, calibration constants). Moreover, the lack of real-time measurement of the oxygen concentration at the intake and the simple model used for the EGR effect on the SOC prediction are extremely likely to

contribute to this estimation inaccuracy. Higher calibration effort and in-cylinder species concentration observers such as investigated in [14,33], as well as modeling the port fuel injection dynamics [8,34], could contribute to enhance the model outcomes. Despite the difference obtained during the first cycles after the load transient step, the estimated CA50 exhibited a level similar to the experimental CA50 value even when the latter was slowly decreasing due to the varying operating conditions dynamics (e.g., air-path). The mean absolute error for the complete transient operation was 0.43 CAD, with an error standard deviation of 0.59 CAD and a peak error of around 2 CAD.

This model might be used for off-line control strategies investigation, or to enhance a closed-loop controller by predicting the CA50 from the operating conditions. Nonetheless, it is important to note that a deeper analysis of the RCCI combustion modeling covering a wider range of operating conditions must be performed in order to improve the model estimation capabilities.

5.3 Individual cylinder fuel blend estimation using a state observer

Dual-fuel combustion was found to be sensitive to the operating conditions (e.g., intake pressure and temperature, EGR rate), as well as to the injection strategies such as the blending ratio of the two fuels in the mixture [35–37]. Desantes et al. [28] reported an improvement of 4% in the gross indicated efficiency, maintaining the NO_x and soot emissions under EURO VI limits, in a single cylinder RCCI engine by setting the correct EGR and gasoline fraction. It appears therefore that a proper knowledge about the in-cylinder species concentration is of great interest in order to provide efficient combustion.

In a research environment, the cylinder charge composition used to be estimated thanks to dedicated devices such as the fuel balance for the fuel consumption, or the CO_2 balance technique for the EGR rate using an external gas analyzer. However, in on-board applications only a few sensors are available for estimating the in-cylinder mixture. Moreover, multi-cylinder configurations are prone to cylinder-to-cylinder dispersion which might be explained by an uneven fuel and species concentration distribution. As an example, the injected fuel quantity is usually estimated based on an injector look-up table, function of the injector energizing time and a pressure of reference (e.g., rail pressure for direct injectors). Nonetheless, in direct injection engines, small manufacturing variations, ageing, or nozzle coking, might favour the cylinder-to-cylinder air-fuel ratio (AFR) dis-

persion [38–40]. Meanwhile, in port fuel injection, in addition to the injectors bias, AFR dispersion due to the cylinder-to-cylinder air distribution is also expected [20]. These variations can represent a source of performance drop and an increase in pollutant emissions, and should therefore be tackled.

Over the years, different methods were investigated for individual cylinder air-fuel ratio estimation. Using an Universal Exhaust Gas Oxygen (UEGO) sensor placed at the exhaust, also known as lambda sensor, is one of them. Although usually limited to an average engine AFR every cycle [41, 42], some studies aimed to quantify the contribution of each cylinder to the AFR measured by a single UEGO sensor by modeling the exhaust dynamics [43–46]. In-cylinder pressure can also be used to estimate the composition of the mixture in the cylinder: in [47–49], the authors determined the AFR by an inverse combustion model and in-cylinder pressure measurement.

The majority of the available works were developed for single fuel applications. However, both direct injection dispersion and port fuel variability are observed when dealing with dual-fuel engines [50, 51]. Different studies and techniques can be found for blending ratio (BR) estimation in dual-fuel applications. Most of them are applied to diesel-biodiesel combustion and use either the significant difference in the low heating value (LHV) of both fuels through combustion diagnosis [52, 53], or their different oxygen content with oxygen concentration measurement at the exhaust [54, 55]. Wang et al. [56] studied a blending of diesel and gasoline and based their estimation on a multi-factors fusion relying on the energy released during the combustion, and the ignition delay, obtained from in-cylinder pressure measurements. The factors were used to create mean value experimental maps which were then used to estimate the blending ratio. The cylinder-to-cylinder dispersion was however not evaluated.

In-cylinder pressure sensors offer the potential to individually measure the energy released by the injected fuel quantity in each cylinder by computing the heat released during the combustion [57, 58]. Enhanced by such measurement, the current engine set of sensors might be combined with models in this data-rich environment to provide a better estimate of the in-cylinder conditions by designing adequate sensor data fusion algorithms [14, 59, 60]. This section investigates the use of such approach for estimating the individual cylinder fuel quantity and blending ratio in a dual-fuel engine. By combining conventional sensors, cycle-to-cycle measurement of the energy released by the fuel mixture through the in-cylinder pressure measurement, and pre-calibrated injection look-up tables, the proposed

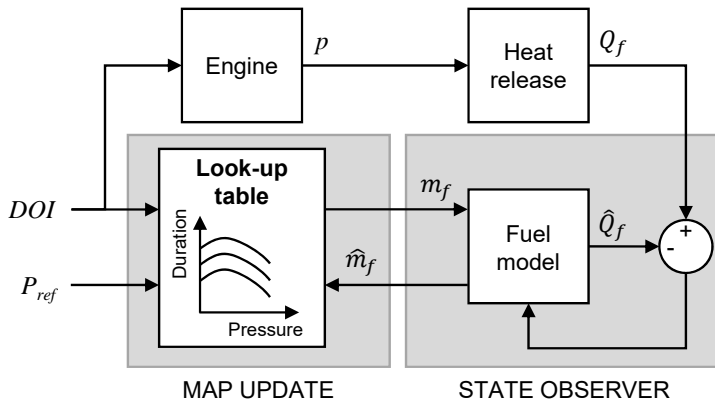


Figure 5.3: Illustration of the concept proposed in this work to estimate the individual cylinder fuel concentration.

method addresses the cylinder-to-cylinder dispersion, estimates the ratio of both fuels and updates the injection maps in order to improve later control of the engine following the idea illustrated in Figure 5.3. The duration of injection (DOI) and a pressure of reference (P_{ref} , e.g., rail in direct injection) provide the expected fuel quantity injected in the cylinder (m_f). The combustion resulting from the injected fuel is measured through the in-cylinder pressure (p) which is used to compute the heat release model and obtain the total energy released by the fuel (Q_f). The energy estimate from the fuel model (\hat{Q}_f) is compared to the measurement to update the state observer, while the resulting fuel quantity estimate (\hat{m}_f) is used to update the injector look-up table. In the present case, a Kalman filter was chosen in the state observer to benefit from the available sensors information and to cope with the dynamics of the studied system, such as port fuel injection wall wetting effect and uneven distribution between cylinders.

The following subsections investigate the cylinder-to-cylinder fuel dispersion in a dual-fuel engine using data from engine B and describe the models used to provide a better estimate of the fuel blending ratio. The proposed estimation method is then evaluated under various conditions and the results are discussed.

5.3.1 Fuel quantity estimation from heat release computation

As it was described in Chapter 3, the heat supplied to the system dQ is described by the difference between a chemical energy source dQ_c (the fuel), and an energy

loss dQ_{ht} (the heat transferred to the walls):

$$dQ = dQ_c - dQ_{ht} \quad (5.17)$$

where the energy balance in the cylinder is obtained from the first law of thermodynamics by the following equation:

$$dQ = \frac{\gamma}{\gamma - 1}pdV + \frac{1}{\gamma - 1}Vdp \quad (5.18)$$

with p the in-cylinder pressure, V the instantaneous volume obtained by geometric crankshaft-piston position, and γ the heat capacity ratio.

The evolution of the chemical energy released dQ_c is directly proportional to the fuel quantity burnt in the cylinder. Considering the combustion efficiency η_c and the low heating value (*LHV*) as known variables, here for a single fuel, the fuel quantity injected inside the cylinder m_f can be estimated through:

$$m_f = \frac{Q_c}{\eta_c LHV} = \frac{1}{\eta_c LHV} \int_{\theta_{ivc}}^{\theta_{evo}} \frac{dQ_c}{d\theta} d\theta \quad (5.19)$$

where θ_{ivc} and θ_{evo} are the crank angle of the intake valve closing and the exhaust valve opening, respectively.

In order to improve the fuel amount estimation, the heat release model which takes into account the heat transferred to the cylinder walls dQ_{ht} and the crank based γ estimation, as described in Chapter 3, was considered here. This whole calculation procedure can then be used individually at each cylinder, hence providing the system with six measurements of injected fuel mass every cycle. Furthermore, aiming at taking advantage of the full potential of the in-cylinder pressure sensor, the trapped mass estimation, required in this model, was performed from the in-cylinder pressure resonance analysis (see Chapter 3). Note that this approach is made possible thanks to the sufficient resonance intensity in the studied combustion mode. Otherwise, methods such as the one proposed by Guardiola et al. [61] might be implemented instead.

Sensitivity analysis Although the fuel burned during the combustion can be estimated with one cycle resolution per cylinder thanks to the heat released computation, this estimation might suffer from some bias due to unknown parameters that vary with the operating conditions. As seen in (5.19), the fuel quantity estimation is directly impacted by the value of the combustion efficiency and the low

heating value. While the low heating value can be considered the same in all the cylinders, it is difficult to evaluate precisely the individual combustion efficiency. For this reason, in this work, it was decided to assume a single η_c for the whole engine.

Nonetheless, it can be assumed that some differences between the cylinders might exist in the compression ratio r_c , because of machining disparity between pistons, in the distribution of the trapped mass and/or masses concentration between cylinders, due to the hardware design, and in the heat transferred to the walls, due to differences in the wall temperature T_w caused by unequal refrigeration in all the cylinders (inner cylinders might be at a higher temperature). These representative factors were therefore selected and numerically biased to evaluate the model deviation to such bias compared to the levels obtained with the initial conditions. Their impact on the calculation of the heat released was evaluated at a 1200 rpm-25% load diesel operating point. The respective biases and results are listed in Table 5.3. The relative bias ε_{Q_c} was calculated in percentage by comparing the results of the biased calculation with the original ones.

It was observed that a bias of 0.2 points in the compression ratio will be translated into a variation in the injected fuel quantity estimation below 1% with the considered heat release computation model. Similarly, a difference in the wall temperature of 30°C and a 20% reduction in fresh air (m_a) would cause an estimation deviation below 1%. Finally, a 10% fluctuation in the bulk temperature (in other words, the trapped mass m_{cyl}) would imply a variation of 3% in the final measurement. The model robustness against these parameters was considered representative of the model accuracy and henceforth, it was assumed to be sufficiently precise for the application presented in this work, that is, the cylinder-to-cylinder dispersion evaluation. The temperature of the walls, the compression ratio, but also the combustion efficiency, were therefore considered the same for all the six cylinders.

It must be noted that high pressure EGR was found to be responsible of an unequal distribution of the air charge, resulting in a different cylinder species concentration between cylinders [62]. However, if all the fuel is burned, the same amount of energy should be measured regardless of the air dilution level in the cylinder. Therefore, this effect is expected to not impact the fuel quantity estimation considerably.

Table 5.3: Sensitivity analysis results on the heat release computation model where ε_{Q_c} is the measured relative error between initial and biased fuel estimation.

Variable	Bias applied	Calculated ε_{Q_c}
r_c	0.2 points	<1%
T_w	30°C	<1%
m_a	20%	<1%
m_{cyl}	10%	~3%

5.3.2 Characterization of the fuel mass dispersion in multi-cylinder dual-fuel engines

Conventional engine control units (ECU) rely on built-in look-up tables using the energizing time of the injector and a pressure difference at the injector nozzle to estimate the injected fuel quantity. This pressure of reference used to be the rail pressure for direct injection (negligible cylinder counter-pressure), and the intake manifold pressure for port fuel injection (with a constant injection pressure). However, even when using the same control settings, each injector could inject a different fuel quantity (e.g., due to manufacturing variations). Several works dealing with injector bias can be found in the literature [38, 39, 63]. Hereafter, an analysis of the injectors dispersion in engine B is provided to characterize the bias at the direct injection (DI) and the port fuel injection (PFI) systems. Note that in this section the definition of the variables was intentionally written with *PFI* and *DI* subscripts, and not by the corresponding fuel, in order to highlight and ease the interpretation of how both systems were addressed. Furthermore, the present method might be applied to other fuels than the ones considered in this work (i.e., gasoline and diesel).

The fuel burned at each cylinder is calculated from the total energy released, as previously described, and a bias is then calculated and analyzed at each cylinder (Θ_{cyl} [%]) by comparing the individual cylinder energy level to the average energy released by the six cylinders:

$$\Theta_{cyl} = \frac{Q_{c,cyl} - \overline{Q_c}}{\overline{Q_c}} \quad \text{with} \quad \overline{Q_c} = \frac{1}{6} \sum_{cyl=1}^6 Q_{c,cyl} \quad (5.20)$$

Direct injection characterization

An analysis of the direct injection of the six cylinders was performed by analyzing data sets of 100 consecutive cycles at various diesel injection settings, in conventional diesel combustion (CDC), in order to isolate the diesel contribution in the energy released computation. In these tests, the rail pressure, the duration of injection (DOI), and the dwell time, were varied to evaluate their effect on the cylinder-to-cylinder dispersion. The injection duration and the rail pressure levels were chosen according to dual-fuel operation over the whole engine map, and the injection timings were adapted to CDC conditions to avoid high pressure rise rates.

Figure 5.4 shows the bias Θ_{cyl} obtained for all the six cylinders at various rail pressure levels, ranging from 600 to 2000 bar, and for four values of DOI of the main injection, namely 700, 900, 1100 and 1300 μs . Note that here, a double injection strategy was used but only the main injection duration was varied. The duration of the pilot injection (400 μs) and the start of both diesel injections (SOI) at 15°bTDC and 5°bTDC respectively, were kept constant. It was observed that for a given cylinder and injection duration, as P_{rail} increases, the bias tends to decrease. It was also noticed that increasing the duration of injection tends to decrease the bias for all the cylinders (in percentage).

In multiple injection strategies, the dwell time, which corresponds to the time between the end of one injection and the start of the following one, might affect the fuel quantity delivered by the rail due to internal fluid dynamics [64,65]. Figure 5.5 shows the bias found at each cylinder for various dwell times (from 0.7 to 1.8 ms) at three levels of rail pressure and constant engine speed of 1200 rpm. Here, the start of the pilot injection (15°bTDC) and the duration of both the pilot injection (400 μs) and the main injection (1100 μs) were kept constant, while only the SOI of the main injection was varied. The variations appreciated in Figure 5.5 were considered small enough to assume that the dwell time should not affect extensively the injection dispersion between cylinders, and therefore the resulting cylinder-to-cylinder fuel distribution estimation.

As the injection dispersion is supposed to depend only on the injection duration and the rail pressure, but not on the operating conditions, one way to take into account the cylinder-to-cylinder dispersion in the control unit is to measure the injection rate at each injector under different injection settings and to obtain which correction should be applied to each injector. Such method is usually performed by car/truck manufacturers when installing the injectors in a new engine. Each injector is firstly tested and then a specific coefficient is applied in the ECU to

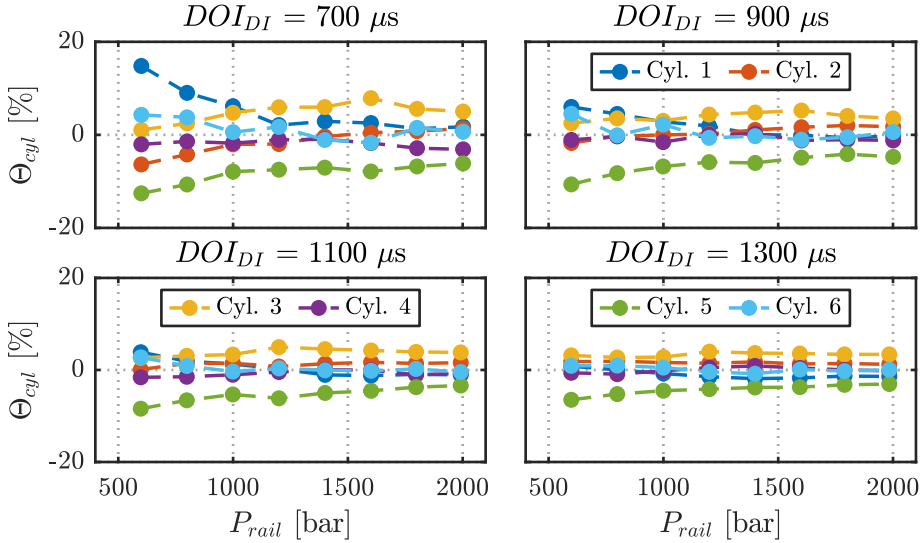


Figure 5.4: Energy bias at each cylinder for different injection durations (DOI_{DI}) and rail pressures (P_{rail}) compared to the average energy released by all the cylinders evaluated over 100 cycles. The longer the injection duration, and the higher the injection pressure, the lower is the cylinder-to-cylinder dispersion.

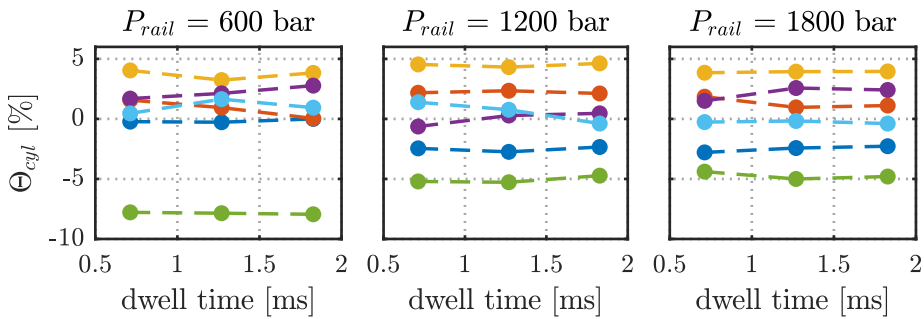


Figure 5.5: Energy release bias at each cylinder at different dwell time and rail pressure levels compared to the mean energy released by all the cylinders over 100 cycles (the reader is referred to Figure 5.4 for the cylinder color legend description).

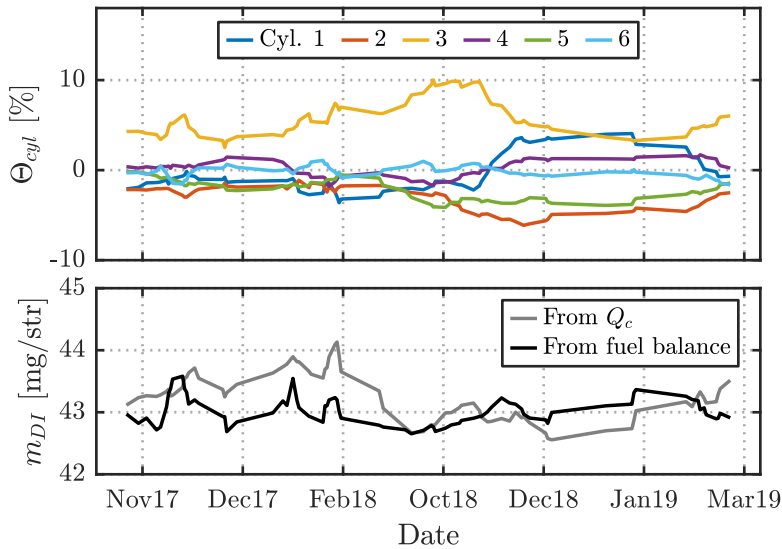


Figure 5.6: Energy release bias at each cylinder at a reference diesel operating point over time (top), and estimated fuel quantity from the energy released computation in grey and the fuel balance measurement in black (bottom).

compensate such dispersion. However, some phenomena, such as ageing or coking due to particulate matter produced by the combustion over time, can interfere with such calibration. As an example, Figure 5.6 shows an analysis of several tests with engine B during 17 months at the same operating point (1200 rpm and 25% load with the same injection settings). The evolution of the injectors bias in the top plot shows that over time, the bias at each injector is not necessarily constant and might vary depending on factors such as the injector's clogging. The bottom plot of this figure shows the fuel mass estimation from the average energy released from all the six cylinders (with a combustion efficiency assumed to be constant and equal to 0.98), together with the value given by the fuel balance in mg/str. Overall, in this figure, it was observed that although both the fuel balance and the fuel estimation are providing a relatively constant and similar injected fuel quantity measurement, each injector's contribution was found to vary over time as shown in the top plot. Such variation might be explained by ageing or deposits accumulation that affect each cylinder differently, and illustrates the need to consider each injector individually.

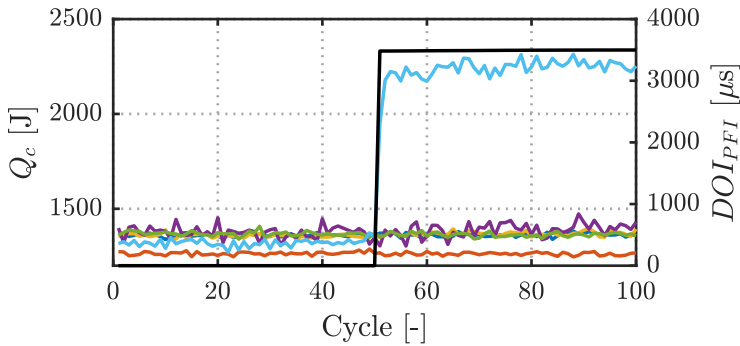


Figure 5.7: Illustration of the port fuel injection duration variation (black line) in a single cylinder for measuring the impact on the other cylinders using the energy released computation (the reader is referred to Figure 5.6 for the cylinder color legend description).

Port fuel injection characterization

Similarly to the direct fuel injection, the port fuel injection variability was also studied. In the case of such injection system, due to intake manifold design, air flow dynamics, or port fuel injectors location, some fuel coming from one injector may actually not end up inside of the corresponding cylinder. An experiment that aims to investigate if such phenomena could be an additional source of cylinder-to-cylinder dispersion is illustrated in Figure 5.7. In this test, the pilot and the main diesel injections were maintained both in duration (800 and 920 μs respectively) and timing (15°bTDC and 5°bTDC respectively) at a constant injection pressure of 600 bar. The port fuel injection timing was fixed at 340°bTDC . Then, the duration of the gasoline injection of only one injector was varied, from 0 up to 3500 μs , and the energy released Q_c was calculated in all the cylinders. The amount of energy for each gasoline duration level was then averaged at each cylinder. The procedure was repeated for each cylinder and the results are listed in Table 5.4.

Each row of Table 5.4 corresponds to the cylinder where a variation in the injection duration was performed, and each column summarizes the variation measured in the energy released at each cylinder. As expected, the diagonal matrix (in bold) shows that the highest variation in the energy released Q_c is measured at the cylinder where the injection duration was increased. However, it can also be noticed that other cylinders exhibit some variation. For instance, in the case where the change in DOI is applied to cylinder 4, both cylinders 5 and 6 reveal a significant Q_c variation, reaching around 10% of the variation of cylinder 4 in cylinder 5. This observation demonstrates that dual-fuel engines equipped with port fuel

Table 5.4: Results of the cylinder-to-cylinder dispersion characterization from the port fuel injection system in engine B with gasoline injection duration variations as illustrated in Figure 5.7.

ΔDOI Cylinder	Variation ΔQ_c [J]						Total
	1	2	3	4	5	6	
1	1034	18	7	25	-3	5	1086
2	25	902	16	2	-1	11	955
3	24	33	887	26	16	0	986
4	24	8	6	774	80	62	954
5	10	-2	7	-34	900	26	907
6	1	0	5	-23	-7	952	928

injectors are prone to multiple cylinder-to-cylinder dispersion sources which must be considered when evaluating this combustion concept. In this case, it is shown that part of the fuel injected from one injector might be transferred and burned in another cylinder. Finally, note that the total energy variation calculated in the last column of Table 5.4 is not the same in all the cylinders. Aside from the eventual heat release computation errors, this observation might indicate that each injector could be providing a different amount of fuel for the same injection settings, e.g., due to different conditions at the nozzle such as intake pressure.

According to the previous results, it was decided to vary the conditions at the port fuel injector nozzle and to evaluate if any effect on the fuel distribution could also be observed. Figure 5.8 shows the cylinder-to-cylinder dispersion when keeping constant the diesel injection settings (i.e., rail pressure, duration and timing) and varying only the gasoline injection duration, starting with no gasoline and ending up to 4000 μs in all the cylinders, with simultaneous variation of the intake pressure conditions. It was found that the cylinder-to-cylinder port fuel injection distribution exhibits a significant sensitivity to the intake conditions as illustrated by the bias Θ_{cyl} . This figure shows that throughout the varying conditions, each cylinder might be affected differently, consolidating the previous conclusions about the necessity to include such dispersion source in the modeling of the individual cylinder fuel distribution.

5.3.3 Individual cylinder fuel distribution estimation method

In order to determine the final individual cylinder fuel distribution, it was decided to use a double feature strategy: a fuel observer is combined with an on-board

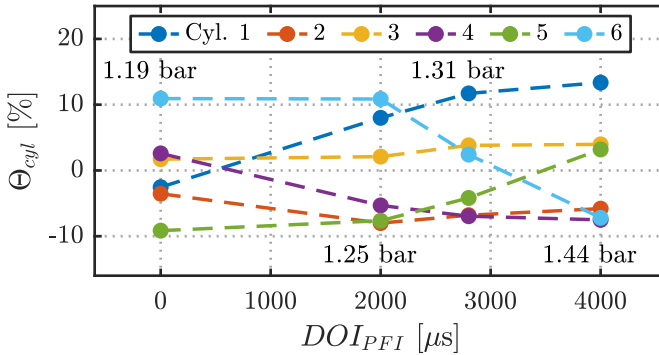


Figure 5.8: Energy release bias at each cylinder in dual-fuel combustion varying the port fuel injection duration and the intake pressure. The intake pressure is indicated in *bar* for each condition.

update of the injection look-up tables as previously suggested in Figure 5.3. First, the observer is used to evaluate the cylinder-to-cylinder dispersion bias caused by the operating conditions and the hardware setup. Its aim is twofold: it uses additional sensors, namely lambda or fuel balance (in test bench applications) to update the combustion efficiency, and it combines the estimation of the overall energy delivered by the fuel with the direct injection to determine the port fuel quantity injected in the cylinder. Finally, the look-up tables are slowly updated with the injector bias encountered with the observer to improve their feedforward action.

Observer design

As previously observed, both of the injection systems are prone to cylinder-to-cylinder injection dispersion. In the direct diesel injection system, the bias at each direct injector can be caused by slow dynamics (e.g., ageing, deposits accumulation) and could therefore be smoothly covered by individual look-up tables update over time when the engine is run in pure diesel conditions, e.g., in low load operation [66]. That is, each direct injector has its own injection look-up table that provides an estimation of the fuel quantity injected according to the injection settings, i.e., rail pressure and injection duration. These individual look-up tables get then updated with the evolving cylinder-to-cylinder dispersion measured by the energy released at each cylinder to compensate for any deviation. In dual-fuel operation, however, when a difference between the expected energy released (i.e., from the fuel quantities estimated by the look-up tables) and the one measured

during the combustion (i.e., from the heat release computation) is observed, it is not certain from which injection system, and to what extent, this difference comes from. Consequently, dual-fuel operation requires one of the two injection systems to be previously characterized. Being less prone to external disturbances, the direct diesel injection was therefore selected as an input to the observer in dual-fuel operation by considering the fuel quantity value provided by the look-up tables correct. As a result, when using both injection systems, any fuel quantity difference between the estimation and the measurement was assigned to an error in the port fuel injection estimation. Also, note that in this work the diesel injection bias and correction was considered as a single value for each injector. This means that the fuel distribution between the pilot and the main injection was not addressed here and the look-up table provides a single fuel quantity estimation for the total diesel injection duration (pilot + main) instead of addressing each injection separately. Although this decision neglects the eventual effects of the split ratio on the injected quantity [67–69], this choice was made because only the total diesel quantity matters in the fuel distribution method presented here. Furthermore, an additional assumption in the method would have been necessary to choose to which diesel injection, and to what extent, assign the correction of the look-up table to compensate for the difference measured at the energy released in diesel operation. Consequently, it was decided to simplify the approach by addressing the diesel injections as a whole.

Due to the port fuel injection sensitivity to the local conditions around the nozzle, and because of the air distribution and the injector location which might favor cross injection between cylinders, it was decided to simplify the system by using a single look-up table for all the cylinders. At every engine cycle k , from the injection duration and the intake manifold pressure, this look-up table provides a single fuel quantity estimation considered to be injected individually by each of the port fuel injectors. The final gasoline quantity really reaching each cylinder, however, might be higher or lower than the fuel coming from the injector due to the cross injection as observed in section 5.3.2. This phenomena was considered in the method by using six states which aim to cope with the gasoline quantity distribution between cylinders. These states, here named $\boldsymbol{\vartheta}_{PFI}^k$, are factors that are applied to the value provided by the single open-loop (OL) look-up table for the port fuel injection quantity ($m_{PFI,OL}$). Note that in the equations describing the observer design, the bold type is used for multiple cylinder vector notation ($\boldsymbol{\vartheta}_{PFI} = [\vartheta_{PFI,1} \dots \vartheta_{PFI,6}]^T$). The product of the fuel quantity provided by the PFI look-up table, considered the same for all the cylinders, with this factor for each individual cylinder corresponds therefore to the final quantity of gasoline

reaching every cylinder intake port. As an example, if 20% of the fuel injected by the port fuel injector from cylinder 4 ends in the intake port of cylinder 5, and no fuel from the cylinder 5 injector is distributed to another cylinder, $\vartheta_{PFI,4}$ would be equal to 0.8 and $\vartheta_{PFI,5}$ to 1.2. Inherently, in steady state conditions, $\sum \vartheta_{PFI} = 6$ due to mass conservation. This state was assumed to be a constant bias from one cycle to the other such as:

$$\vartheta_{PFI}^k = \vartheta_{PFI}^{k-1} \quad (5.21)$$

Additionally, six states were used for the port fuel injection dynamics resulting from the fuel film at the intake walls (also known as *wall wetting*, where m_{ff} stands for *fuel film mass*) [34, 70]:

$$m_{ff}^k = (1 - \beta) m_{ff}^{k-1} + (1 - \alpha) m_{PFI,OL}^{k-1} \vartheta_{PFI}^{k-1} \quad (5.22)$$

where α and β are calibration constants which, in the case at hand, were assumed to be the same for the six cylinders. These constants characterize the evolution of the fuel film mass at the intake port. In this equation, the product of $m_{PFI,OL}^{k-1}$ with ϑ_{PFI}^{k-1} represents the quantity of fuel reaching each cylinder intake port when addressing the cross injection distribution in port fuel injection, as previously explained. As a result, in (5.22), the fuel film mass in the intake port at cycle k is made of the fuel film mass from the previous cycle that has not entered the cylinder (left part of the sum), and the fuel from the port fuel injection quantity that does not directly enter the cylinder and is kept instead on the intake port walls (right part of the sum). The fuel quantity entering the cylinder coming from the port fuel injection is therefore expressed as:

$$m_{PFI}^k = \alpha m_{PFI,OL}^k \vartheta_{PFI}^k + \beta m_{ff}^k \quad (5.23)$$

The measured energy released is associated to the injected fuel quantity through the combustion efficiency. The cylinder-to-cylinder dispersion being addressed by the aforementioned states, the combustion efficiency was assumed to have a similar impact in all the cylinders and a single state, constant from one cycle to the other, was therefore considered:

$$\eta_c^k = \eta_c^{k-1} \quad (5.24)$$

In addition, the lambda sensor can provide an overall fuel quantity estimation when combined with the air flow measurement. It was therefore decided to include this feature in the observer design considering a first order system for the time response of the lambda sensor (e.g., gas transport delay) with the following state:

$$\lambda^k = \mu \lambda^{k-1} + (1 - \mu) \frac{1}{\psi_s} \frac{m_a^{k-1}}{m_f^{k-1}} \quad (5.25)$$

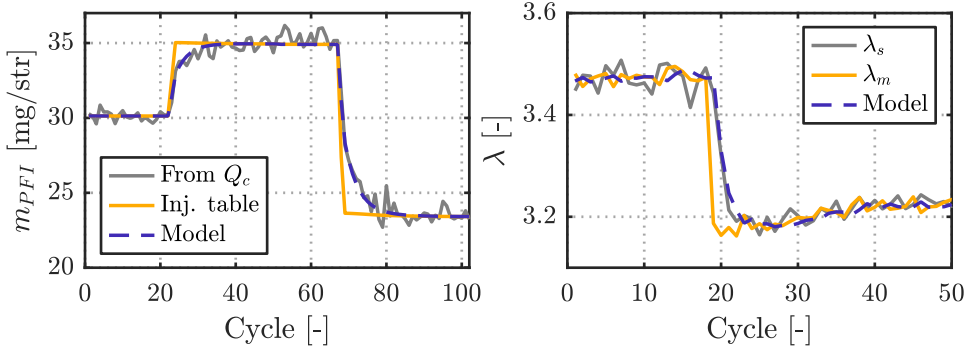


Figure 5.9: Modeling of the dynamics at the port fuel injection for considering the wall wetting effect (left), and at the λ measurement for gas transport delay (right). λ_m represents the value of lambda computed from the air and fuel masses measured at every cycle, right part of (5.25), and λ_s is the value measured by the lambda sensor.

with μ the constant characterizing the time response of the sensor and ψ_s the stoichiometric air-to-fuel ratio assumed to be the same for both the fuels used in this study and equal to 14.6. A graphical representation of the respective dynamics from m_{ff} and λ , and their modeling after calibration of the constants α , β and μ , is illustrated in Figure 5.9.

The total injected fuel mass m_f is obtained using the energy released and the diesel quantity provided by the injection look-up tables, assuming that the respective low heating values are known:

$$m_f^{k-1} = \frac{1}{6} \sum \left(m_{DI}^{k-1} + \left[\frac{Q_c^{k-1}}{\eta_c^{k-1}} - m_{DI}^{k-1} LHV_{DI} \right] \frac{1}{LHV_{PFI}} \right) \quad (5.26)$$

The measurements of the system consist in the heat released at each cylinder, which is defined by:

$$\begin{aligned} Q_c^k &= \left[Q_{DI}^k + Q_{PFI}^k \right] \eta_c^k \\ &= \left[m_{DI}^k LHV_{DI} + m_{PFI}^k LHV_{PFI} \right] \eta_c^k \\ &= \left[m_{DI}^k LHV_{DI} + \left(\alpha m_{PFI,OL}^k \vartheta_{PFI}^k + \beta m_{ff}^k \right) LHV_{PFI} \right] \eta_c^k \end{aligned} \quad (5.27)$$

and the measurement provided by the lambda sensor λ_s at the exhaust:

$$\lambda_s^k = \lambda^k \quad (5.28)$$

The state space representation of the system in its discrete form of one cycle step is:

$$x_k = f(x_{k-1}, u_k) + g_k \quad (5.29)$$

$$y_k = h(x_k, u_k) + s_k \quad (5.30)$$

where x are the states, y the outputs, u the inputs, and g and s are the process and observation noises modeled as a Gaussian distribution with zero mean and covariance matrices G and S , respectively.

The present system is therefore described by the following states x , measurements y , and inputs u :

$$x = \begin{pmatrix} \vartheta_{PFI,1} \\ \vdots \\ \vartheta_{PFI,6} \\ m_{ff,1} \\ \vdots \\ m_{ff,6} \\ \eta_c \\ \lambda \end{pmatrix}, y = \begin{pmatrix} Q_{c,1} \\ \vdots \\ Q_{c,6} \\ \lambda_s \end{pmatrix}, u = \begin{pmatrix} m_a \\ m_{DI,1} \\ \vdots \\ m_{DI,6} \\ m_{PFI,OL} \end{pmatrix} \quad (5.31)$$

Note that in test bench applications, in addition to lambda, the measurement provided by the fuel balances, gasoline and diesel, can be considered by including them in the measurements vector. Here, m_{DI} is considered as an input in order to attribute the difference between the expected energy released and the measured one to the gasoline bias as previously explained. In this case, each cylinder has its own diesel fuel quantity input because, as opposed to the port fuel injection, every cylinder is provided with a dedicated look-up table.

A Kalman filter (KF) was chosen to estimate the states of the system described in (5.31), where the state vector is defined by:

$$\hat{x}_{k|k-1} = f(\hat{x}_{k-1}, u_k) \quad (5.32)$$

$$e_k = y_k - h(\hat{x}_{k|k-1}, u_k) \quad (5.33)$$

$$\hat{x}_k = \hat{x}_{k|k-1} + K_k e_k \quad (5.34)$$

The Kalman filter is characterized for minimizing the expected estimation error by solving an iterative Riccati matrix equation and updating the value of the Kalman

gain (K), following:

$$P_{k|k-1} = F_k P_{k-1} F_k^T + G_k \quad (5.35)$$

$$K_k = P_{k|k-1} H_k^T (H_k P_{k|k-1} H_k^T + S_k)^{-1} \quad (5.36)$$

$$P_k = (I - K_k H_k) P_{k|k-1} \quad (5.37)$$

where the covariance matrices G_k and S_k are constant and diagonal, and F_k and H_k are the state transition and observation matrices of the system representing (5.29) and (5.30), respectively. In the considered system, these equations are non-linear and an extended Kalman filter (EKF) was therefore used by linearizing them around the current estimate such as:

$$F_k = \left. \frac{\partial f}{\partial x} \right|_{\hat{x}_{k-1}, u_k} \quad (5.38)$$

$$H_k = \left. \frac{\partial h}{\partial x} \right|_{\hat{x}_{k|k-1}} \quad (5.39)$$

The Kalman filter outcome is function of its noises calibration in the covariance matrices. A trade-off between observer stability and convergence for the investigated application needs to be taken when applying the state observer to the considered system [71].

Adaptive look-up tables

In parallel to the state observer, the investigated fuel distribution strategy proposes to update the look-up tables dedicated to the injection systems in order to cover eventual bias over time due to manufacturing discrepancies or ageing. Both direct and port fuel injection look-up tables are updated. However, here the diesel injection is considered as an input of the observer, therefore, the individual diesel look-up tables can only be updated when the engine is running in pure diesel operation. The updating method is based on a principle which was used in timing control applications for spark ignition engines [72, 73]. Particularly, it was decided to learn from the value provided by the model and update the look-up table with a Gaussian filter in order to adapt the complete grid of the table. Compared to a nearest grid nodes update strategy, this method ensures improved smoothness of the complete map and could provide better results when operating in a region which has not been run previously. Each grid node value Z_{ij} is considered part of a map whose axes are (X_i, Y_j) with $i = 1, 2, \dots, n$ and $j = 1, 2, \dots, m$ and is calculated as follows:

$$Z_{ij}^k = Z_{ij}^{k-1} + (z_k - \hat{z}_k) \frac{\Omega(X_i, Y_j)}{\Omega(x_k, y_k)} \delta \quad (5.40)$$

where $(z_k - \hat{z}_k)$ represents the error between the output of the model and the estimate based on the actual look-up table, and x_k and y_k are in this case the map coordinates of the operating point at cycle k . Here, $\Omega(X_i, Y_j)$ is the weight factor applied to each grid node of the map, which is determined by a Gaussian function resulting from the distance between the operating point (x_k, y_k) and each grid node:

$$\Omega = \frac{1}{\sqrt{2\pi}\sigma_x} \exp\left(-\frac{(x_k - X_i)^2}{2\sigma_x^2}\right) \cdot \frac{1}{\sqrt{2\pi}\sigma_y} \exp\left(-\frac{(y_k - Y_j)^2}{2\sigma_y^2}\right) \quad (5.41)$$

where σ_x and σ_y are the standard deviations for each coordinates and act as smoothing factors for the learned-map. Finally, in (5.40), $\Omega(x_k, y_k)$ is used to normalize the weight factor, and δ corresponds to the learning rate that will be later named as δ_{DI} for the direct injection, or δ_{PFI} for the port fuel injection update.

Figure 5.10 illustrates the implementation of the complete fuel distribution estimation algorithm. The final estimation is composed of two blocks: a first one, including the look-up tables which are slowly updated, and another one, with the Kalman filter, that is able to update the combustion efficiency and the port fuel dispersion in a cycle-by-cycle basis.

5.3.4 Results and discussion

Experimental data sets were recorded with engine B for the validation of the proposed estimation strategy (a graphical representation of the operating conditions can be found in Figure 5.11):

- Test A: this test aims to evaluate the update capability of the adaptive look-up tables algorithm. For this purpose, a conventional diesel combustion case was selected. The test consists in rail pressure sweeps from 600 to 2000 bar at a constant engine speed of 1200 rpm, constant total injection duration of 1500 μs , and SOI of 15°bTDC and 5°bTDC for pilot and main injections, respectively. The low-pressure EGR and VGT valves positions were maintained constant throughout the test.
- Test B: this experiment simulates an injector fault or leakage. To this end, the port fuel injection duration was increased in only one cylinder (see black dashed line in the middle top plot of Figure 5.11). Although the duration in cylinder 1 was changed in practice, the algorithm was still fed with the same duration in all the cylinders, hence simulating that the injector provides more fuel than the expected, and allowing therefore to appreciate the observer

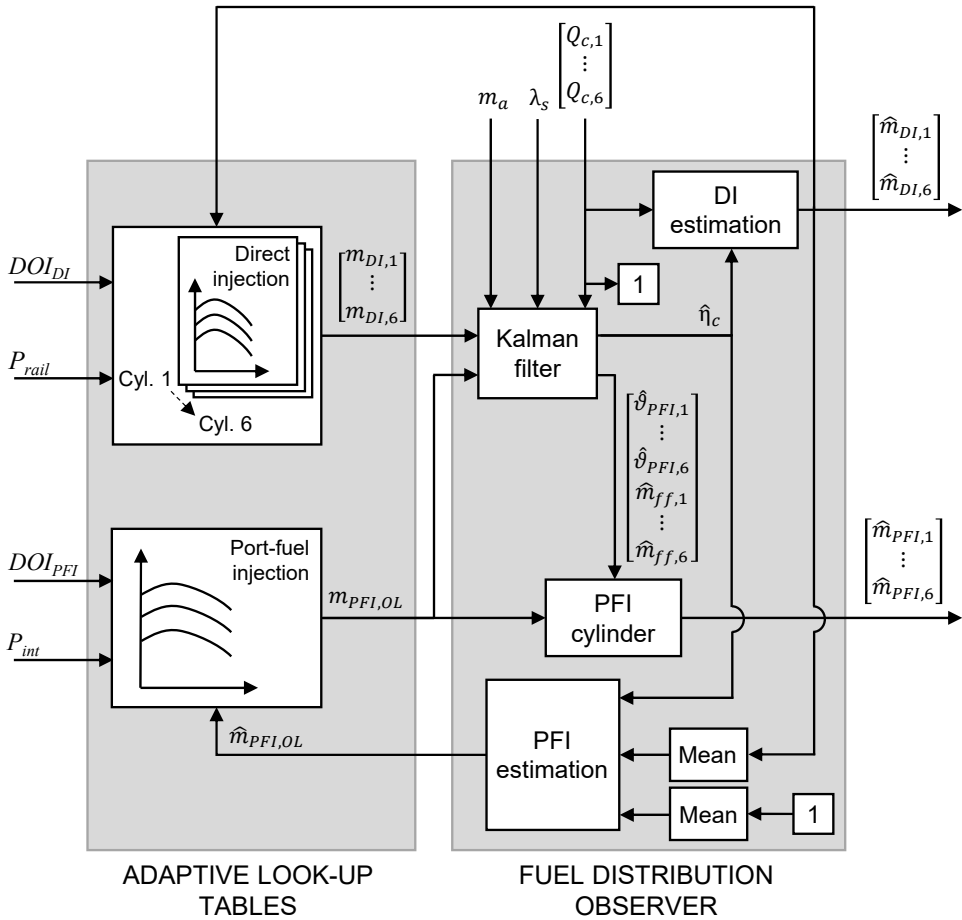


Figure 5.10: On-board fuel distribution estimation layout: update of the injection look-up tables and fuel observer for estimating the respective fuel quantities in every cylinder using the energy released during the combustion.

response to this scenario. The overall objective is to force a cylinder-to-cylinder dispersion in order to compare the behavior of the proposed strategy with conventional methods response, such as relying only on the original look-up table estimation. No EGR was performed in this test and the VGT position was kept constant, as well as were the engine speed (1200 rpm), the injection pressure (600 bar) and both the injection duration (1600 μ s) and the timing of the diesel injections (55°bTDC and 40°bTDC for pilot and main injection, respectively).

- Test C: here the data is composed of injection duration sweeps in both the diesel and the gasoline injections. The goal of this test is to show the full ability of the proposed observer strategy, associated to the adaptive look-up tables algorithm, to estimate the fuel distribution between cylinders. The data were collected at a constant engine speed of 1200 rpm, and the pilot and the main diesel injections were maintained at a constant SOI of 30°bTDC and 15°bTDC, respectively. The rail pressure was also kept constant at 600 bar. The VGT and the EGR valve positions were maintained unchanged during the test and only low pressure EGR was used in order to ensure a proper mixing and distribution of the charge between the cylinders.

The results obtained in each test are hereafter detailed and discussed.

Test A - Adaptive look-up tables algorithm validation

In this test, the learning capability of the adaptive look-up tables algorithm was evaluated. The update of the injector map aims to cope with an eventual injector deviation over time. This process is considered slow and the algorithm must then be applied a long time to converge to its final state if the starting error is important. To simulate this, the proposed method was applied to the same data several times, referred to as *iterations* in the following discussions. Figure 5.12 shows the response of the fuel estimation method when applied to test A (diesel combustion case). The top plot presents the fuel quantity estimation from various sources: the original look-up table which was intentionally biased, the average value from the individual updated look-up tables after the 1st and the 2nd iteration of the test (each diesel injector has its own look-up table), and the mean energy released by all the cylinders measured with the heat release model described in section 5.3.1. The purpose of this test is only to give an insight into the adaptive behavior of the method which works in parallel with the fuel observer. Consequently, the combustion efficiency was here set to a constant of 0.98, and the lambda measurement (therefore the observer) was not used in this context. Such assumption might provide an error in the final fuel mass estimation, but it is still representative of

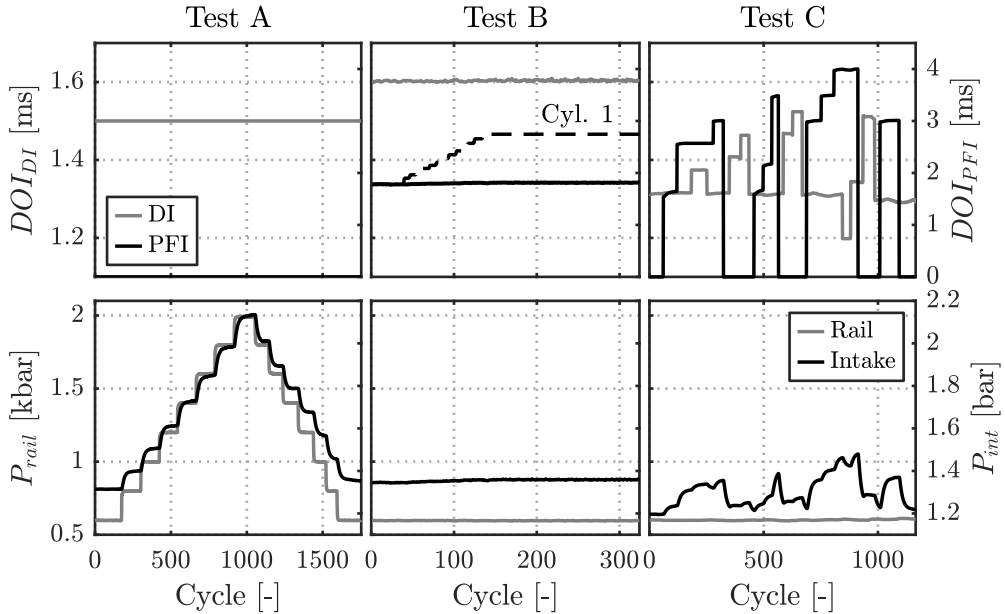


Figure 5.11: Operating conditions (DOI_{DI} , DOI_{PFI} , P_{rail} and P_{int}) of the experimental data sets used for the fuel distribution estimation method validation in test A (left), test B (middle) and test C (right). In test B, the port fuel injection duration from cylinder 1 was intentionally varied to a different value compared to the other cylinders.

the cylinder-to-cylinder dispersion and the ability of the algorithm to update the look-up tables. Note that for illustration purposes it was decided to show the average estimate only in the top plot instead of the six cylinder signals. Nonetheless, the cylinder-to-cylinder dispersion is addressed with the standard deviation in the bottom plot.

The adaptive look-up tables update rate is controlled by tuning the constant δ_{DI} , see (5.40), which was here equal to 0.02. In the first iteration, it can be observed that due to an important error in the original look-up tables, the estimated fuel mass in the top plot exhibited a significant bias, especially for the high fuel quantity levels. It is then appreciated that this error got slowly corrected every cycle to reach the levels given by the measured energy, which are considered as the correct estimate, with a mean absolute error of 1.18 mg in the 2nd iteration. It is important to note that a trade-off exists between converging the look-up table to the measured levels, and updating it too frequently. The learning rate δ_{DI} needs to be adjusted accordingly to, for instance, avoid the map update to respond

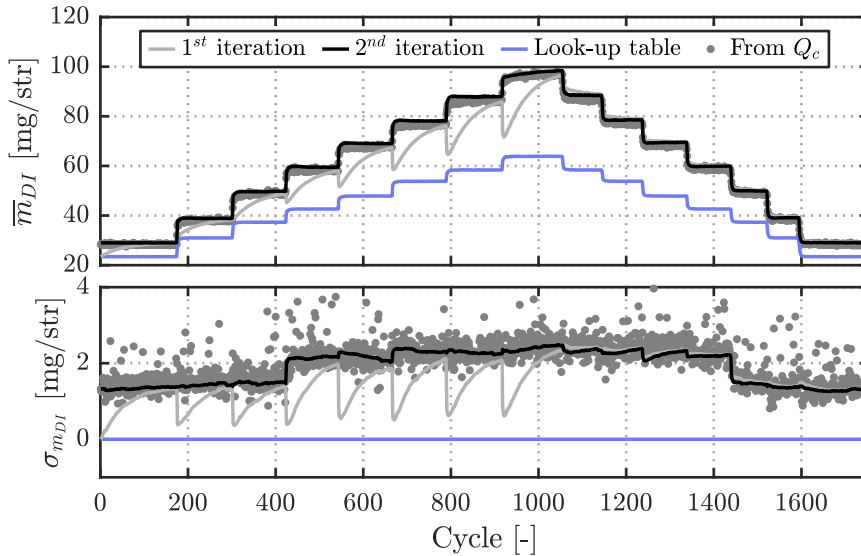


Figure 5.12: Evaluation of the adaptive look-up tables update algorithm applied to test A. Mean injected fuel quantity estimation from various sources (top) and corresponding standard deviation for cylinder-to-cylinder dispersion evaluation (bottom). It is appreciated that after the 2nd iteration the estimation provided by the injectors look-up tables converged to the value measured by the heat release computation in every cylinder.

quickly to a single cycle energy level measurement which may cause the map to never really converge. As previously mentioned, the bias at the direct injection is believed to be evolving slowly over time [39] and to be therefore compensated by such approach. Here, the learning rate value was chosen mainly for illustration purposes but the concept remains.

Bottom plot of Figure 5.12 shows the cylinder-to-cylinder dispersion evaluation through the standard deviation σ of all the cylinders estimations from the aforementioned sources. In the original look-up table case, such value is constant and equals zero because the same look-up table, which was not updated, was used for all the cylinders. In the case of the 1st and the 2nd iteration, it can be appreciated that thanks to the individual look-up tables update, the final standard deviation tends to converge to the standard deviation measured from Q_c (represented with grey dots). Such observation shows that each injector table was properly updated according to the energy levels obtained at the corresponding cylinder.

As previously mentioned, in the proposed strategy, the diesel injection look-up

tables update is performed only under pure diesel combustion, while in dual-fuel combustion, only the single port fuel injection map is updated. The update of the latter uses the same principle than illustrated in Figure 5.12, at the exception that in this case the individual diesel injection maps provide an estimate of the diesel quantity for each cylinder which is considered as correct. As a result, the difference between the measured energy released from the in-cylinder pressure acquisition and the estimated one from the look-up tables is used to update the PFI look-up table.

Test B - Cylinder-to-cylinder port fuel dispersion evaluation

The main objective of the proposed observer is to be able to estimate the blending ratio of the fuels in every cylinder. Detecting and addressing the cylinder-to-cylinder fuel mass dispersion is therefore at the core of the method. In Figure 5.13, the energy levels estimated through various methods are compared in test B. Being a dual-fuel combustion case, the diesel quantity, which was kept constant throughout the test, was previously calibrated using the fuel balance measurement and considered to be the same in all the cylinders. Although this might result in a slight starting error in the energy content estimation because the cylinder-to-cylinder dispersion highlighted in section 5.3.2 was not addressed, it was considered irrelevant for the goal of this test. Indeed, here, the experiment aims to show the ability of the different methods to detect a cylinder-to-cylinder dispersion in the port fuel injection quantity. For this purpose, a significant increase of the injection duration in cylinder 1 was intentionally performed, while all the other cylinders were kept at the same injection duration. However, in order to fully evaluate the diagnosis ability of each method, it was necessary to simulate that the DOI_{PFI} in cylinder 1 was equal to the other cylinders. Otherwise, the estimate in cylinder 1 would obviously be higher from the look-up table. The system was consequently fed with a fake duration for this specific cylinder, hence providing the look-up table with the same duration for all the cylinders, although more fuel was injected and higher energy levels were released in cylinder 1, as this would happen in the case of an injector leakage. The studied estimation methods were: relying on the original look-up table only (in blue), using the look-up table update algorithm for the port fuel injection table (in orange), and finally combining the state observer (Kalman filter) to the former method (in black). The top plot shows the energy level estimated by the different methods in cylinder 1 (the dark grey line is the measured value from the heat release computation), while the bottom plot presents the results obtained in cylinder 2 for comparison purposes.

As expected, it was observed that when the port fuel injection duration in cylinder 1 was increased, the fuel estimation in blue provided by the original look-

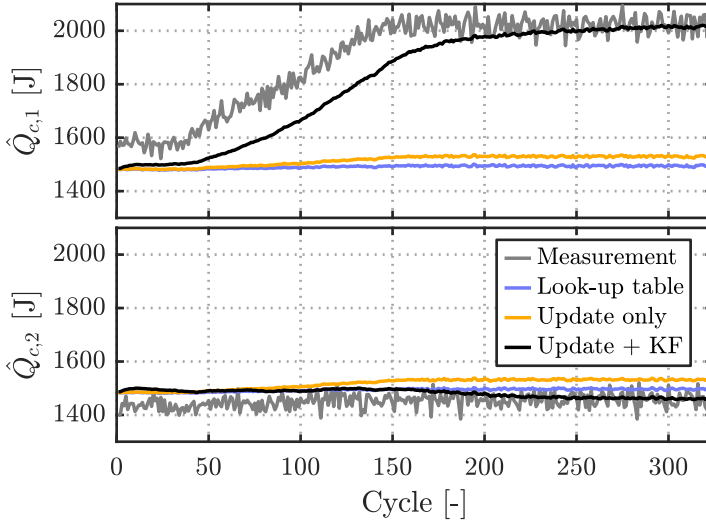


Figure 5.13: Cylinder-to-cylinder port fuel dispersion detection in test B, in cylinder 1 (top) and cylinder 2 (bottom), from various estimation sources: look-up table alone without update, with update, and combined with the Kalman filter. The estimated values are compared to the estimation provided by the heat release calculation, referred here as *measurement*.

up table (in other words, the energy content) remained constant. This resulted in an error of approximately 500 J ($\sim 25\%$) at the end of the fuel step compared to the measured level (remember that for the look-up table estimation, the duration at cylinder 1 is considered constant and equal to the rest of the cylinders although it is increased in practice, see Figure 5.11 and description of test B). Cylinder 2 exhibited an error of only 30 J which was justified by the fact that in this cylinder the estimate provided by the look-up table was closer to the real value. This case highlights the inability of a conventional look-up table estimation strategy to detect any cylinder-to-cylinder dispersion due to the lack of feedback information from the system.

In order to improve the estimate, it was decided to also use the feedback from the heat release computation and apply the look-up table update algorithm on the port fuel injection table, similarly to what was performed in test A with the diesel case. Here, the table update rate δ_{PFI} was tuned at 0.05. When the update of the port fuel injection look-up table was enabled, due to the feedback principle (see Figure 5.10), it was noticed that, as the PFI quantity was increased in cylinder 1,

the look-up table provided a higher estimate of the injected fuel quantity. This resulted therefore in a higher energy released estimate, as illustrated in orange in the figure. However, by considering a single look-up table for all the port fuel injectors, the final table update can only represent the mean energy released by all the cylinders and the individual cylinder quantity cannot be estimated, which was expected. This is observed with the remaining 480 J error at the end of the fuel step in cylinder 1, although an error reduction of 20 J was obtained compared to the previous case without the look-up table update. Moreover, as shown in the bottom plot, in this specific case, note that this method would even result in a higher error for cylinder 2. Likewise the previous method, each cylinder receives the same fuel mass estimation even after the update, consequently, due to the increase in the energy measurement from cylinder 1, and the single port fuel injection table strategy, cylinder 2 was believed to receive more fuel as well.

Finally, in addition to the look-up table update, the observer described in section 5.3.3 was applied. By doing so, the states participated to the final estimation of the fuel distribution through the energy level measurement in each cylinder. As seen in both plots, this method allows to detect and compensate the energy deviation in cylinder 1 and cylinder 2 with an almost zero mean error after 250 cycles. Using the energy released in each cylinder as a measurement, the fuel distribution between cylinders can be tracked thanks to ϑ_{PFI} , while the update algorithm is constantly correcting $m_{PFI,OL}$ (see Figure 5.10). Hence, thanks to the use of the Kalman filter, both individual cylinder fuel content estimation and cylinder-to-cylinder dispersion can be addressed compared to the traditional methods relying on look-up tables only.

Test C - Fuel distribution observer validation

Finally, the proposed individual fuel distribution estimation method was evaluated in the conditions of test C. This test consists in diesel and gasoline injection duration sweeps, including diesel and dual-fuel combustion operation. In this case, both the observer and the look-up tables update algorithms were used, and the results are provided in Figure 5.14. For the sake of clarity, this figure only shows a section of the complete test, which was previously defined in the right part of Figure 5.11. The outcomes of this test were analyzed through the following quantities: the standard deviation of the energy released by all the cylinders as an indicator of the cylinder-to-cylinder dispersion evaluation, the energy level at cylinder 1 as an illustration example of the estimation evolution, and the combustion efficiency and the lambda values for showing the states estimation provided by the Kalman filter. The suggested noises and calibration constants values that were applied for

Table 5.5: Noises and constants used in the estimation method. The values given for the states and the outputs correspond respectively to the standard deviation of the process and the observation from the Kalman filter (\sqrt{G} and \sqrt{S}).

Variable	Type	Equation	Value	Unit
$\vartheta_{PFI,cyl}$	State	(5.21)	2e-3	-
$m_{ff,cyl}$	State	(5.22)	0	mg
η_c	State	(5.24)	3e-4	-
λ	State	(5.25)	0.04	-
$Q_{c,cyl}$	Output	(5.27)	120	J
λ_s	Output	(5.28)	0.05	-
α	Constant	(5.22)	0.50	-
β	Constant	(5.22)	0.25	-
μ	Constant	(5.25)	0.50	-
δ_{DI}	Constant	(5.40)	0.02	-
δ_{PFI}	Constant	(5.40)	0.05	-

obtaining the results in Figure 5.14 are listed in Table 5.5.

Similarly to the diesel case in test A, the method was applied several times on the data for appreciating the injection tables update. In the first iteration, errors in the respective diesel and gasoline look-up tables were observed, providing a biased estimate of the energy released in the engine. This is illustrated by the difference in the standard deviation in the top left plot and the error at cylinder 1 in the bottom left plot (the levels obtained from the estimation method are shown in solid lines, while the measurements are indicated with dark grey dots). Moreover, not only the error at the look-up table could be a reason for explaining the measured energy difference, but also the port fuel distribution between cylinders as concluded in section 5.3.2. Therefore, by updating ϑ_{PFI} , the cylinder-to-cylinder fuel dispersion was addressed, which allowed to reduce the error as shown in the standard deviation plot. After the second iteration, the individual cylinder fuel concentration appeared to match the measurement levels. Note that the proposed algorithm updates the diesel look-up tables only under pure diesel conditions. Consequently, if the diesel injection settings are changed during a dual-fuel combustion operation, the eventual error coming from the diesel injection estimate will be compensated by the gasoline in the Kalman filter and lead to a misleading es-

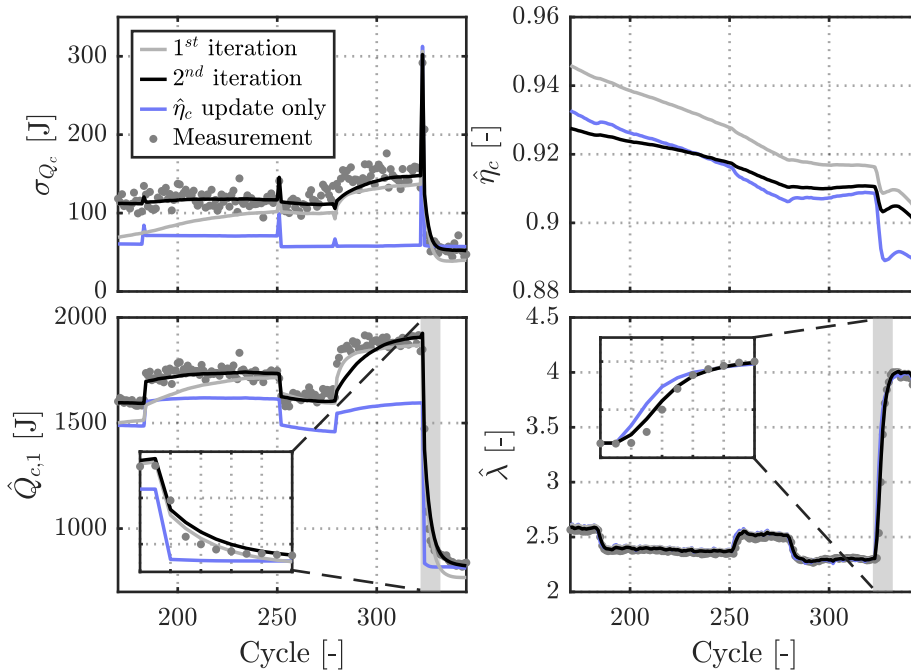


Figure 5.14: Fuel distribution estimation strategy (observer and look-up tables update) applied to test C. In this figure only a section of the total test is illustrated showing the standard deviation of the energy released by all the cylinders (top left), the energy content estimated at cylinder 1 (bottom left), the combustion efficiency (top right) and the lambda estimation (bottom right).

timing of the fuel blend. Nonetheless, the cylinder-to-cylinder dispersion should still be representative of the system.

As observed in the top right plot of Figure 5.14, the combustion efficiency level was decreased to a value of around 0.91, at the second iteration, to obtain similar lambda levels in this section of test C. This value is low compared to a conventional range observed in CDC (between 0.97 and 0.99). Excluding the effect of the Kalman filter's noises calibration on the estimation, various reasons might be considered to explain such observation: in this study, the combustion efficiency is not evaluated using the exhaust gas emissions concentration (e.g., HC and CO), but represents the energy conversion from the injected fuel. Consequently, the considered fuel low heating values play an important role in the update of such variable as the estimation of the energy released is directly proportional to the LHV, see (5.19). Furthermore, premixed dual-fuel combustion was also found to

provide lower combustion efficiency levels in general [74, 75]. Finally, the combustion model errors in the energy released estimation might contribute to the levels obtained in the present work.

Together with the output from the proposed strategy (1st and 2nd iteration in Figure 5.14, which include both observer and adaptive look-up tables actions), the results from a simplified method are shown in a blue line. This estimation corresponds to the results of updating only the combustion efficiency to match the lambda level, meaning that the port fuel distribution and the dynamics at the fuel film and lambda were not considered. This simplified method aims to show the importance of the different states considered in this study, as illustrated in the zoom section in the bottom plots of Figure 5.14. Each zoom corresponds to the colored area in their respective plot. It can be observed that thanks to the fuel film mass m_{ff} in (5.22), the energy released dynamics when changing the fuel quantities are better captured compared to a straightforward estimation from the look-up tables. Furthermore, the gas transport delay in the lambda measurement in (5.25) allows to improve its estimation which results in a smoother update of the combustion efficiency. Similarly to the conclusions from test B, it is observed that not considering the fuel distribution by means of ϑ_{PFI} results in a higher inaccuracy in the fuel concentration and distribution estimation, showing the significance of addressing the port fuel injection dispersion in such hardware setup.

Figure 5.15 illustrates the final estimation of the total injected fuel quantity m_f and blending ratio (gasoline fraction GF in this case) from the proposed strategy in the complete test C:

$$m_f = m_{PFI} + m_{DI} = m_g + m_d \quad (5.42)$$

$$GF = \frac{m_{PFI}}{m_f} = \frac{m_g}{m_f} \quad (5.43)$$

Each color represents the individual cylinder fuel estimation after the second iteration, while the black line represents the levels obtained from the fuel balances measurements. It can be noticed that depending on the combustion mode and the operating conditions, the cylinder-to-cylinder dispersion is different in both terms of magnitude and order, where the same cylinder does not always provide the same dispersion, which agrees with the observations made in section 5.3.2. Moreover, the trend and the levels achieved by the estimation method showed a good agreement with the amounts measured by the fuel balances (note that the fuel balance only provides a single value representative of the average fuel quantity injected in

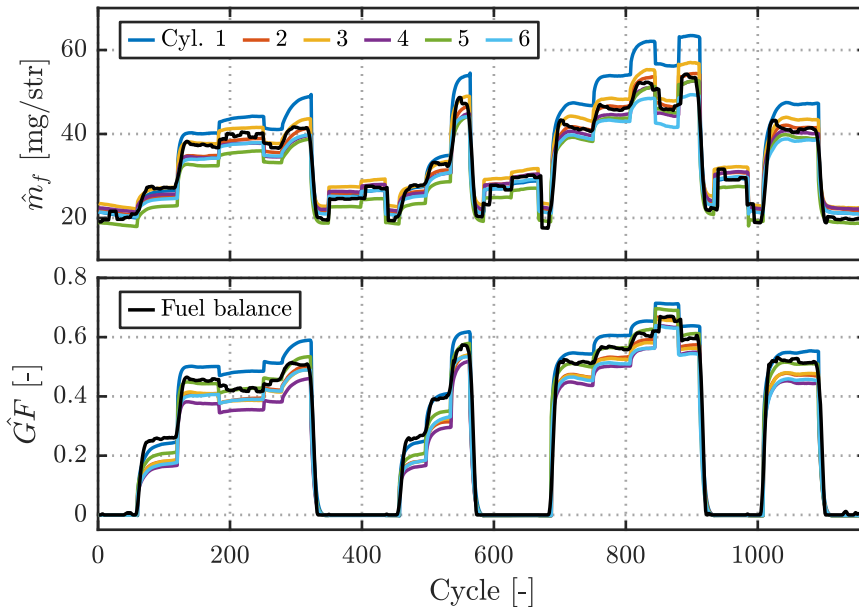


Figure 5.15: Individual cylinder fuel concentration (top) and blending ratio (bottom) estimation from the proposed method at the end of the 2nd iteration in test C with the levels measured by the fuel balances.

the whole engine).

Figure 5.16 aims to analyze the cylinder-to-cylinder dispersion evaluation obtained in test C. To this end, a section of the results in Figure 5.15 was selected and the results of cylinder 2 and 4 are compared. Together with m_f and GF , the CA50 is shown as an indicator for the combustion phasing evaluation. In this part of the test, the duration of the diesel injection was held constant and only the duration of the gasoline injection was increased. An increase in the total fuel mass and in the gasoline fraction was therefore expected. Such statement was confirmed in both \hat{m}_f and \hat{GF} plots on the left side of this figure. Around cycle 100, according to the estimation given by the method, the total fuel amount was similar in both cylinders, but cylinder 2 exhibited a slightly higher gasoline fraction. This observation may be verified by the CA50 level where cylinder 2 had a later combustion compared to cylinder 4. Indeed, it was observed that an increase in the low reactivity fuel fraction tends to delay the combustion as a result of the decrease in the fuel mixture reactivity [35, 76]. This is further observed around cycle 150 where both cylinders were still exhibiting a very similar total fuel amount, with a

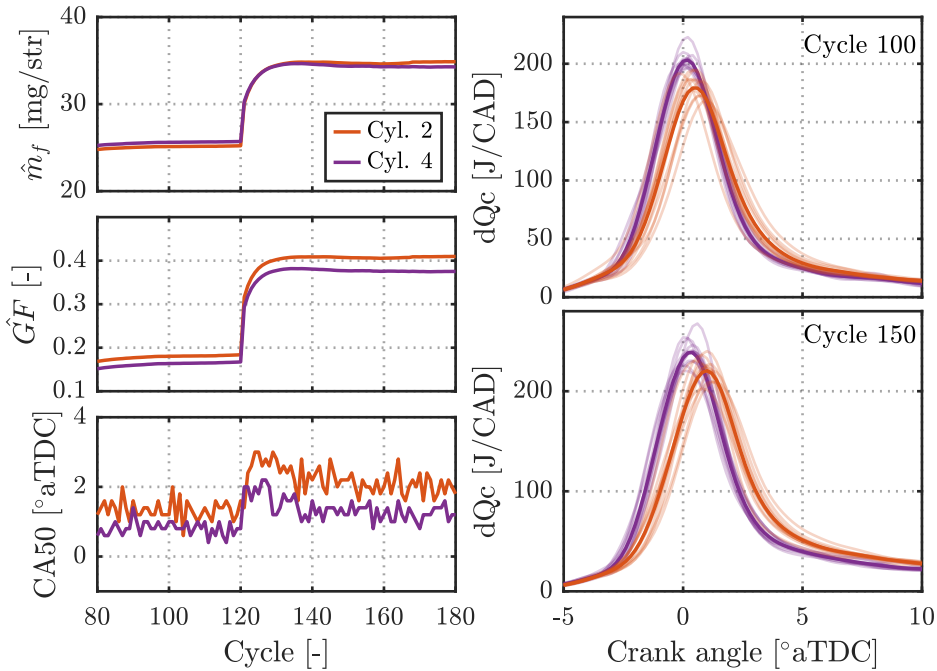


Figure 5.16: Zoom on a section of the test presented in Figure 5.15 for studying the dispersion between cylinder 2 (red) and cylinder 4 (purple): total fuel amount estimation (top left), gasoline fraction estimation (middle left), CA50 measurement (bottom left). The heat release computation from two selected cycle areas is shown in the right part where 10 consecutive cycles are shown in semi-transparent lines, and an average cycle is illustrated in a full line.

higher gasoline concentration and a more delayed combustion in cylinder 2. These observations are further investigated in the right side of Figure 5.16 where the heat release rate of these two specific cycles are shown. In particular, 10 consecutive cycles centered on cycles 100 and 150 from both cylinders are illustrated to show the cycle-to-cycle variation in these sections, and an average trace for both cylinders is also shown. Although the effect is less noticeable around cycle 100 as the cycle-to-cycle variation from both cylinders overlap each other, a lower combustion rate in cylinder 2 is globally observed in both cycles conditions. Considering that only low-pressure EGR was used in this test to ensure a proper mixing and distribution of the intake charge, such observation is encouraging to state that the proposed strategy was able to provide an insight into the individual cylinder fuel distribution.

Dual-fuel engines are complex systems and the results obtained through these various experiments have shown the importance of considering an injection correction at each cylinder through feedback control for improving performance, engine stability, and presumably pollutant emissions in advanced combustion concepts such as premixed dual-fuel. The proposed method was oriented to on-road applications but could be improved by sensor data fusion together with fuel balance measurement and individual UEGO sensor at each cylinder exhaust in a research environment, which would result in a better estimate of the fuel concentration under both steady and transient operation. The outcomes of this strategy have shown encouraging results to be used as a tool to enhance the cylinder-to-cylinder dispersion tackling in dual-fuel combustion controllers.

5.4 Conclusions

This chapter explored the use of physical models to provide tools that could be used to enhance control strategies investigation in dual-fuel engines.

A control-oriented model was first developed and introduced for RCCI combustion. By means of a modified knock integral model and combustion modeling, the start of combustion and the combustion phasing (expressed as the CA50) were estimated, showing a good agreement with experimental data. The validation data consisted in a transient operation where the CA50 estimate was observed to reproduce the experimental levels with a mean absolute error of about 0.43 CAD, with an error standard deviation of 0.59 CAD and a peak error of around 2 CAD. This model might be applied for off-line control strategies investigation and calibration, or on-line for improving combustion control using the model output as a feedforward information or as the core of a model-based controller.

Finally, due to the significance of the cylinder species concentration knowledge to improve engine performance and emissions, an algorithm to enhance the individual cylinder fuel distribution estimation in a multi-cylinder dual-fuel engine was investigated. First, the cylinder-to-cylinder fuel dispersion was analyzed and characterized in both direct and port fuel injection. It was found that, although receiving the same injection settings, each cylinder exhibited a different amount of energy released during the combustion, which highlighted the variations in the injected fuel quantity from one cylinder to the other. In order to address such phenomena, and therefore improve the estimation of the fuel entering each cylinder, a strategy based on individual injection look-up tables and a state observer was proposed. The state observer, based on a Kalman filter, was used to tackle the system

dynamics (e.g., fuel film in the port fuel injection system) and the fuel distribution dispersion. By combining the measurement of the fuel quantity estimated from the computation of the energy released, the injection look-up tables, and the sensors embedded in the engine, this method was able to provide an estimate of the total fuel quantity and the blending ratio of the two fuels in every cylinder. Compared to the conventional value provided by traditional single look-up table applications or fuel balance measurement, this strategy showed encouraging results to be implemented in a combustion controller and enhance therefore the engine operation. In parallel to the state observation, an on-line learning algorithm was developed for the individual injection look-up tables in order to correct injector drift over time to improve later control of the engine, which could ease the implementation of such dual-fuel concept in commercial applications.

The outcomes of this chapter highlighted the possibilities allowed by model-based methods in combustion engines. Either for off-line or on-line applications, models are powerful tools with predictive capabilities that can enable a more accurate control of the engine and, therefore, significantly contribute to the engine stability and emissions reduction.

References

- [1] Tang Jian, Zhu Guoming G. and Men Yifan. Review of engine control-oriented combustion models. *International Journal of Engine Research*, feb 2021. (cited in p. 147)
- [2] Shaver G M, Gerdes J C and Roelle M. Physics-based closed-loop control of phasing, peak pressure and work output in HCCI engines utilizing variable valve actuation. *Proceedings of the American Control Conference*, Vol. 1, pp. 150–155, 2004. (cited in p. 147)
- [3] Van Alstine Daniel G, Kocher Lyle E, Koeberlein Ed, Stricker Karla and Shaver Gregory M. Control-oriented premixed charge compression ignition combustion timing model for a diesel engine utilizing flexible intake valve modulation. *International Journal of Engine Research*, Vol. 14 n° 3, pp. 211–230, jun 2013. (cited in p. 147)
- [4] Kondipati Naga Nithin Teja, Arora Jayant Kumar, Bidarvatan Mehran and Shahbakhti Mahdi. Modeling, design and implementation of a closed-loop combustion controller for an RCCI engine. In *2017 American Control Conference (ACC)*, pp. 4747–4752. IEEE, may 2017. (cited in pp. 36, 38, 147, and 150)
- [5] Ingesson Gabriel, Yin Lianhao, Johansson Rolf and Tunestål Per. Proportional–Integral Controller Design for Combustion–Timing Feedback, From n-Heptane to Iso-Octane in Compression–Ignition Engines. *Journal of Dynamic Systems, Measurement, and Control*, Vol. 140 n° 5, may 2018. (cited in pp. 89 and 147)

-
- [6] Hall Carrie M., Shaver Gregory M., Chauvin Jonathan and Petit Nicolas. Control-oriented modelling of combustion phasing for a fuel-flexible spark-ignited engine with variable valve timing. *International Journal of Engine Research*, Vol. 13 n° 5, pp. 448–463, oct 2012. (cited in p. 148)
- [7] Turesson Gabriel. *Model-Based Optimization of Combustion-Engine Control*. PhD Thesis, 2018. (cited in p. 148)
- [8] Raut Akshat, Bidarvatan Mehran, Borhan Hoseinali and Shahbakhti Mahdi. Model Predictive Control of an RCCI Engine. In *2018 Annual American Control Conference (ACC)*, pp. 1604–1609. IEEE, jun 2018. (cited in pp. 36, 106, 148, and 157)
- [9] Norouzi Armin, Heidarifar Hamed, Shahbakhti Mahdi, Koch Charles Robert and Borhan Hoseinali. Model Predictive Control of Internal Combustion Engines: A Review and Future Directions. *Energies*, Vol. 14 n° 19, pp. 6251, oct 2021. (cited in pp. 11 and 148)
- [10] Willems Frank, Doosje Erik, Engels Frank and Seykens Xander. Cylinder pressure-based control in heavy-duty EGR diesel engines using a virtual heat release and emission sensor. *SAE Technical Papers*, pp. 1–17, 2010. (cited in p. 148)
- [11] Strandh Petter, Bengtsson Johan, Johansson Rolf, Tunestål Per and Johansson Bengt. Cycle-to-Cycle Control of a Dual-Fuel HCCI Engine. In *SAE Technical Paper*, volume 2004, mar 2004. (cited in pp. 34, 37, and 148)
- [12] Willems Frank, Kupper Frank, Ramesh Sudarshan, Indrajuna Armando and Doosje Erik. Coordinated Air-Fuel Path Control in a Diesel-E85 RCCI Engine. In *SAE Technical Paper*, pp. 1–11, apr 2019. (cited in pp. 36, 38, and 148)
- [13] Arsie I., Pianese C. and Rizzo G. A non linear observer for fuel film dynamics into the intake manifold of a spark ignition engine. *IEEE/ASME International Conference on Advanced Intelligent Mechatronics, AIM*, pp. 251–256, 1999. (cited in p. 148)
- [14] Guardiola Carlos, Pla Benjamín, Bares Pau and Stefanopoulou Anna. Cylinder charge composition observation based on in-cylinder pressure measurement. *Measurement: Journal of the International Measurement Confederation*, Vol. 131, pp. 559–568, 2019. (cited in pp. 148, 157, and 158)
- [15] Widd Anders, Tunestål P. and Johansson R. Physical modeling and control of homogeneous charge compression ignition (HCCI) engines. *IEEE Conference on Decision and Control*, pp. 5615–5620, 2008. (cited in p. 148)
- [16] Shahbakhti Mahdi and Koch Charles Robert. Physics Based Control Oriented Model for HCCI Combustion Timing. *Journal of Dynamic Systems, Measurement, and Control*, Vol. 132 n° 2, pp. 021010, 2010. (cited in pp. 34 and 148)
- [17] Ravi Nikhil, Roelle Matthew J., Liao Hsien Hsin, Jungkunz Adam F., Chang Chen Fang, Park Sungbae and Gerdes J. Christian. Model-based control of HCCI engines using exhaust recompression. *IEEE Transactions on Control Systems Technology*, Vol. 18 n° 6, pp. 1289–1302, 2010. (cited in p. 148)

- [18] Wu Yifeng, Hanson Reed and Reitz Rolf D. Investigation of Combustion Phasing Control Strategy During Reactivity Controlled Compression Ignition (RCCI) Multicylinder Engine Load Transitions. *Journal of Engineering for Gas Turbines and Power*, Vol. 136 n° 9, pp. 091511, 2014. (cited in p. 149)
- [19] Rausen D. J., Stefanopoulou A. G., Kang J.-M., Eng J. A. and Kuo T.-W. A Mean-Value Model for Control of Homogeneous Charge Compression Ignition (HCCI) Engines. *Journal of Dynamic Systems, Measurement, and Control*, Vol. 127 n° 3, pp. 355, 2005. (cited in pp. 149 and 150)
- [20] Heywood J.B. *Internal Combustion Engine Fundamentals*. Automotive technology series. McGraw-Hill, 1988. (cited in pp. 6, 71, 118, 119, 150, and 158)
- [21] Livengood J. C. and Wu P. C. Correlation of autoignition phenomena in internal combustion engines and rapid compression machines. *Symposium (International) on Combustion*, Vol. 5 n° 1, pp. 347–356, 1955. (cited in p. 150)
- [22] Bengtsson J., Gafvert M. and Strandh P. Modeling of HCCI diesel engine combustion for control analysis. *2004 43rd IEEE Conference on Decision and Control (CDC) (IEEE Cat. No.04CH37601)*, Vol. 2, pp. 1682–1687, 2004. (cited in p. 150)
- [23] Chiang Chia Jui and Stefanopoulou Anna G. Sensitivity analysis of combustion timing and duration of homogeneous charge compression ignition (HCCI) engines. *Proceedings of the 2006 American Control Conference*, pp. 1857–1862, 2006. (cited in p. 150)
- [24] Mayhew Christopher G., Knierim Karl Lukas, Chaturvedi Nalin A., Park Sungbae, Ahmed Jasim and Kojic Aleksandar. Reduced-order modeling for studying and controlling misfire in four-stroke HCCI engines. *Proceedings of the IEEE Conference on Decision and Control*, n° 1, pp. 5194–5199, 2009. (cited in p. 150)
- [25] DelVescovo Dan, Kokjohn Sage and Reitz Rolf. The Development of an Ignition Delay Correlation for PRF Fuel Blends from PRF0 (n-Heptane) to PRF100 (iso-Octane). *SAE International Journal of Engines*, Vol. 9 n° 1, pp. 520–535, 2016. (cited in p. 150)
- [26] Khodadadi Sadabadi K., Shahbakhti M., Bharath A. N. and Reitz R. D. Modeling of combustion phasing of a reactivity-controlled compression ignition engine for control applications. *International Journal of Engine Research*, Vol. 17 n° 4, pp. 421–435, 2016. (cited in pp. 36, 150, 151, and 152)
- [27] Kokjohn Sage L., Hanson Reed M., Splitter Derek A. and Reitz Rolf D. Experiments and modeling of dual-fuel HCCI and PCCI combustion using in-cylinder fuel blending. *SAE International Journal of Engines*, Vol. 2 n° 2, pp. 24–39, nov 2010. (cited in pp. 31, 96, and 151)
- [28] Desantes José M., Benajes Jesús, García Antonio and Monsalve-Serrano Javier. The role of the in-cylinder gas temperature and oxygen concentration over low load reactivity controlled compression ignition combustion efficiency. *Energy*, Vol. 78, pp. 854–868, 2014. (cited in pp. 31, 96, 151, and 157)

-
- [29] Ghojel J. I. Review of the development and applications of the Wiebe function: A tribute to the contribution of Ivan Wiebe to engine research. *International Journal of Engine Research*, Vol. 11 n° 4, pp. 297–312, 2010. (cited in p. 152)
- [30] Shahbakhti Mahdi and Koch Charles Robert. Control oriented modeling of combustion phasing for an HCCI engine. *Proceedings of the American Control Conference*, n° Ivc, pp. 3694–3699, 2007. (cited in pp. 34 and 152)
- [31] Benajes Jesus, Garcia Antonio, Monsalve-Serrano Javier and Boronat Vicente. Achieving clean and efficient engine operation up to full load by combining optimized RCCI and dual-fuel diesel-gasoline combustion strategies. *Energy Conversion and Management*, Vol. 136, pp. 142–151, 2017. (cited in pp. 32 and 155)
- [32] Li Jing, Yang Wenming and Zhou Dezhi. Review on the management of RCCI engines. *Renewable and Sustainable Energy Reviews*, Vol. 69 n° May 2016, pp. 65–79, 2017. (cited in pp. 10, 32, and 155)
- [33] Lujan Jose, Pla Benjamin, Bares Pau and Aramburu Alexandra. Optimal Sensor Placement for High Pressure and Low Pressure EGR Estimation. In *SAE Technical Papers*, number 2021, pp. 1–11, apr 2021. (cited in p. 157)
- [34] Aquino C.F. Transient A/F Control Characteristics of the 5 Liter Central Fuel Injection Engine. In *SAE Technical Paper Series*, number 810494, feb 1981. (cited in pp. 106, 115, 157, and 170)
- [35] Benajes Jesús, Molina Santiago, García Antonio and Monsalve-Serrano Javier. Effects of direct injection timing and blending ratio on RCCI combustion with different low reactivity fuels. *Energy Conversion and Management*, Vol. 99, pp. 193–209, 2015. (cited in pp. 32, 109, 157, and 185)
- [36] Wang Yifeng, Yao Mingfa, Li Tie, Zhang Weijing and Zheng Zunqing. A parametric study for enabling reactivity controlled compression ignition (RCCI) operation in diesel engines at various engine loads. *Applied Energy*, Vol. 175, pp. 389–402, 2016. (cited in pp. 32 and 157)
- [37] DelVescovo Dan, Kokjohn Sage and Reitz Rolf. The Effects of Charge Preparation, Fuel Stratification, and Premixed Fuel Chemistry on Reactivity Controlled Compression Ignition (RCCI) Combustion. *SAE International Journal of Engines*, Vol. 10 n° 4, pp. 1491–1505, 2017. (cited in pp. 32, 96, 112, 127, and 157)
- [38] Payri F., Luján J. M., Guardiola C. and Rizzoni G. Injection diagnosis through common-rail pressure measurement. *Proceedings of the Institution of Mechanical Engineers, Part D: Journal of Automobile Engineering*, Vol. 220 n° 3, pp. 347–357, 2006. (cited in pp. 158 and 162)
- [39] D’Ambrosio S. and Ferrari A. Diesel Injector Coking: Optical-Chemical Analysis of Deposits and Influence on Injected Flow-Rate, Fuel Spray and Engine Performance. *Journal of Engineering for Gas Turbines and Power*, Vol. 134 n° 6, pp. 062801, 2012. (cited in pp. 158, 162, and 178)

- [40] Zhang Wenbin, Zhang Zhou, Ma Xiao, Awad Omar I., Li Yanfei, Shuai Shijin and Xu Hongming. Impact of injector tip deposits on gasoline direct injection engine combustion, fuel economy and emissions. *Applied Energy*, Vol. 262 n° July 2019, pp. 114538, mar 2020. (cited in p. 158)
- [41] Franceschi E. M., Muske Kenneth R., Peyton Jones James C. and Makki Imad. An Adaptive Delay-Compensated PID Air Fuel Ratio Controller. *SAE Technical Paper*, Vol. 2007 n° 724, 2007. (cited in p. 158)
- [42] Ebrahimi B., Tafreshi R., Masudi H., Franchek M.A., Mohammadpour J. and Grigoriadis K. A Systematic Air-fuel Ratio Control Strategy for Lean-burn SI Engines. *IFAC Proceedings Volumes*, Vol. 45 n° 30, pp. 296–301, 2012. (cited in p. 158)
- [43] Chauvin J., Petit N., Rouchon P., Moulin P. and Corde G. Six Degrees Crankshaft Individual Air Fuel Ratio Estimation of Diesel Engines for Cylinder Balancing Purpose. In *SAE Technical Paper Series*, volume 1, apr 2006. (cited in p. 158)
- [44] Suzuki Kenji, Shen Tielong, Kako Junichi and Oguri Yasufumi. Individual A/F control with fuel-gas ratio estimation for multi-cylinder IC engines. *Proceedings of the American Control Conference*, pp. 5094–5099, 2007. (cited in p. 158)
- [45] Cavina Nicolò, Corti Enrico and Moro Davide. Closed-loop individual cylinder air-fuel ratio control via UEGO signal spectral analysis. *Control Engineering Practice*, Vol. 18 n° 11, pp. 1295–1306, 2010. (cited in p. 158)
- [46] Wang Tianbo, Chang Siqin, Liu Liang, Zhu Jianhui and Xu Yaxuan. Individual cylinder air–fuel ratio estimation and control for a large-bore gas fuel engine. *International Journal of Distributed Sensor Networks*, Vol. 15 n° 2, feb 2019. (cited in p. 158)
- [47] Tunestål Per and Hedrick J. Karl. Cylinder air/fuel ratio estimation using net heat release data. *Control Engineering Practice*, Vol. 11 n° 3, pp. 311–318, 2003. (cited in p. 158)
- [48] Di Leo Rocco. Methodologies for air-fuel ratio and trapped mass estimation in diesel engines using the in-cylinder pressure measurement. *Energy Procedia*, Vol. 82, pp. 957–964, 2015. (cited in p. 158)
- [49] Finesso Roberto and Spessa Ezio. A control-oriented approach to estimate the injected fuel mass on the basis of the measured in-cylinder pressure in multiple injection diesel engines. *Energy Conversion and Management*, Vol. 105, pp. 54–70, 2015. (cited in p. 158)
- [50] Bach Florian, Hampe Clemens, Wagner Uwe, Spicher Ulrich and Sauer Christina. Low Temperature Gasoline Combustion With Diesel Micro-Pilot Injection in a Six-Cylinder Heavy Duty Engine. In *ASME 2012 Internal Combustion Engine Division Fall Technical Conference*, pp. 349–359. American Society of Mechanical Engineers, sep 2012. (cited in p. 158)
- [51] Kassa Mateos, Hall Carrie, Ickes Andrew and Wallner Thomas. Modeling and control of fuel distribution in a dual-fuel internal combustion engine leveraging late intake valve closings. *International Journal of Engine Research*, Vol. 18 n° 8, pp. 797–809, 2017. (cited in pp. 125 and 158)

-
- [52] Beatrice Carlo, Guido Chiara, Napolitano Pierpaolo, Iorio Silvana Di and Giacomo Nicola Del. Assessment of biodiesel blending detection capability of the on-board diagnostic of the last generation automotive diesel engines. *Fuel*, Vol. 90 n° 5, pp. 2039–2044, may 2011. (cited in p. 158)
- [53] Junfeng Zhao and Junmin Wang. Energy-based and oxygen-based biodiesel blend level estimation methods for diesel engines. In *2012 American Control Conference (ACC)*, pp. 4975–4980. IEEE, jun 2012. (cited in p. 158)
- [54] Snyder David B., Adi Gayatri H., Bunce Michael P., Satkoski Christopher A. and Shaver Gregory M. Fuel blend fraction estimation for fuel-flexible combustion control: Uncertainty analysis. *Control Engineering Practice*, Vol. 18 n° 4, pp. 418–432, apr 2010. (cited in p. 158)
- [55] Mirheidari Saleh, Franchek Matthew, Grigoriadis Karolos, Mohammadpour Javad, Wang Yue-Yun and Haskara Ibrahim. Real-time and robust estimation of biodiesel blends. *Fuel*, Vol. 92 n° 1, pp. 37–48, feb 2012. (cited in p. 158)
- [56] Wang Jinli, Yang Fuyuan and Ouyang Minggao. Dieseline fueled flexible fuel compression ignition engine control based on in-cylinder pressure sensor. *Applied Energy*, Vol. 159, pp. 87–96, dec 2015. (cited in p. 158)
- [57] Asad Usman and Zheng Ming. Fast heat release characterization of a diesel engine. *International Journal of Thermal Sciences*, Vol. 47 n° 12, pp. 1688–1700, 2008. (cited in pp. 71 and 158)
- [58] Tunestål Per. Self-tuning gross heat release computation for internal combustion engines. *Control Engineering Practice*, Vol. 17 n° 4, pp. 518–524, 2009. (cited in pp. 71 and 158)
- [59] Hasegawa Yusuke, Akazaki Shusuke, Maki Hidetaka, Nishimura Youichi and Hirota Toshiaki. Individual Cylinder Air-Fuel Ratio Feedback Control Using an Observer. *SAE Technical Paper*, n° 940376, 1994. (cited in p. 158)
- [60] Moulin Philippe, Corde Gilles, Castagné Michel and Rousseau Grégory. Cylinder Individual AFR Estimation based on a Physical Model and using Kalman Filters. In *SAE Technical Paper*, number 724, mar 2004. (cited in p. 158)
- [61] Guardiola C., Pla B., Bares P. and Peyton Jones J.C. Integration of intermittent measurement from in-cylinder pressure resonance in a multi-sensor mass flow estimator. *Mechanical Systems and Signal Processing*, Vol. 131, pp. 152–165, sep 2019. (cited in p. 160)
- [62] Payri Francisco, Lujan Jose, Climent Hector and Pla Benjamín. Effects of the Intake Charge Distribution in HSDI Engines. *SAE Technical Paper Series*, Vol. 1, 2010. (cited in pp. 125 and 161)
- [63] Macian V., Lujan J.M., Guardiola Carlos and Yuste Pedro. DFT-based controller for fuel injection unevenness correction in turbocharged diesel engines. *IEEE Transactions on Control Systems Technology*, Vol. 14 n° 5, pp. 819–827, sep 2006. (cited in p. 162)

- [64] Catania Andrea E., Ferrari Alessandro, Manno Michele and Spessa Ezio. Experimental Investigation of Dynamics Effects on Multiple-Injection Common Rail System Performance. *Journal of Engineering for Gas Turbines and Power*, Vol. 130 n° 3, pp. 032806, 2008. (cited in p. 163)
- [65] Han Dong, Li Ke, Duan Yaozong, Lin He and Huang Zhen. Numerical study on fuel physical effects on the split injection processes on a common rail injection system. *Energy Conversion and Management*, Vol. 134, pp. 47–58, feb 2017. (cited in p. 163)
- [66] Paykani Amin, Garcia Antonio, Shahbakhti Mahdi, Rahnama Pourya and Reitz Rolf D. Reactivity controlled compression ignition engine: Pathways towards commercial viability. *Applied Energy*, Vol. 282 n° PA, pp. 116174, jan 2021. (cited in pp. 33 and 168)
- [67] Li Tie, Nishida Keiya, Zhang Yuyin, Yamakawa Masahisa and Hiroyasu Hiroyuki. An Insight Into Effect of Split Injection on Mixture Formation and Combustion of DI Gasoline Engines. In *SAE Technical Papers*. SAE International, jun 2004. (cited in p. 169)
- [68] Kim Jaeheun, Kakami Shinichi, Nishida Keiya and Ogata Yoichi. Effects of ratio and dwell of split injection on fuel spray and mixture formation process under evaporating, non-reacting condition. In *SAE Technical Papers*, number December, dec 2019. (cited in p. 169)
- [69] Dhanji Meghnaa and Zhao Hua. Investigations of split injection properties on the spray characteristics using a solenoid high-pressure injector. *International Journal of Engine Research*, Vol. 23 n° 2, pp. 262–284, feb 2022. (cited in p. 169)
- [70] Coppin Thomas and Maamri Nezha. Fuel estimation and air-to-fuel ratio control for Flexfuel spark-ignition engines. In *2010 IEEE International Conference on Control Applications*, number 2, pp. 555–560. IEEE, sep 2010. (cited in p. 170)
- [71] Blanco-Rodriguez David. *Modelling and Observation of Exhaust Gas Concentrations for Diesel Engine Control*. Springer Theses. Springer International Publishing, Cham, 2014. (cited in pp. 114 and 173)
- [72] Tamaki Shunpei, Sakayanagi Yoshihiro, Sekiguchi Kazuma, Ibuki Tatsuya, Tahara Kohei and Sampei Mitsuji. On-line Feedforward Map Generation for Engine Ignition Timing Control. *IFAC Proceedings Volumes*, Vol. 47 n° 3, pp. 5691–5696, 2014. (cited in p. 173)
- [73] Gao Jinwu, Zhang Yahui and Shen Tielong. An On-Board Calibration Scheme for Map-Based Combustion Phase Control of Spark-Ignition Engines. *IEEE/ASME Transactions on Mechatronics*, Vol. 22 n° 4, pp. 1485–1496, aug 2017. (cited in p. 173)
- [74] Kokjohn S L, Hanson R M, Splitter D A and Reitz R D. Fuel reactivity controlled compression ignition (RCCI): a pathway to controlled high-efficiency clean combustion. *International Journal of Engine Research*, Vol. 12 n° 3, pp. 209–226, 2011. (cited in pp. 31, 77, and 184)

- [75] Benajes Jesús, Molina Santiago, García Antonio, Belarte Eduardo and Vanvolsem Michel. An investigation on RCCI combustion in a heavy duty diesel engine using in-cylinder blending of diesel and gasoline fuels. *Applied Thermal Engineering*, Vol. 63 n° 1, pp. 66–76, 2014. (cited in pp. 32 and 184)
- [76] Hanson Reed, Kokjohn Sage, Splitter Derek and Reitz Rolf D. Fuel Effects on Reactivity Controlled Compression Ignition (RCCI) Combustion at Low Load. *SAE International Journal of Engines*, Vol. 4 n° 1, pp. 394–411, 2011. (cited in pp. 31 and 185)

Chapter 6

Conclusions and future work

With the urgent need to reduce anthropogenic greenhouse gases emissions and to limit their impact on human health, researchers and manufacturers have committed to investigate and develop cleaner technologies. Transportation relies to a large extent on the combustion of fossil fuels with the use of internal combustion engines. In this sense, over the years, new concepts have emerged such as the low temperature combustion which provides ultra-low emissions of NO_x and soot while maintaining high thermal efficiency. This dissertation presented the investigations carried out to address the challenges encountered in the control of the premixed dual-fuel combustion concept. This work was based on processing and leveraging the feedback from the in-cylinder pressure sensor signal in order to develop real-time controllers and models for a more efficient operation of such combustion mode. The conclusions from the results reported in this thesis are summarized below along with suggestions for future work.

Feedback controllers

Based on the measurement of the in-cylinder pressure signal, various feedback control strategies were investigated and implemented in real-time to satisfy the following purposes:

- **Combustion control:** using proportional-integral actions, the in-cylinder pressure signal feedback was used to control the engine load and combustion phasing at a target value while maintaining the pressure rise rate level to a safe threshold by adjusting the fuel quantities (i.e., both diesel and gasoline) and the diesel injection timing. External disturbances were found to be effectively rejected by the controller to maintain the desired operation.

Furthermore, encouraging results were observed in a significant load transient where the load reference tracking was fulfilled within few cycles and the mechanical constraints limitation was not exceeded.

While this solution represents a quick approach to provide an accurate control of the combustion, it is usually limited to specific engine operating regions, especially with a single calibration. A more detailed characterization of the input-output pairing, especially under transient conditions due to the air dynamics, with a fine tuning of the proportional-integral calibration gains and eventual gain-scheduling approach, might provide a wider application range of such control strategy.

- **Combustion optimization:** the extremum seeking technique was explored to optimize the dual-fuel combustion operation. A cost function was designed to track the best engine efficiency- NO_x emissions reduction trade-off. The developed controller successfully actuated over the gasoline fraction and the diesel injection timing to comply with the objectives set by the definition of the considered cost function.

The combustion phasing and the NO_x emissions were found to be sensitive to the selected control variables in all the mixture stratification strategies. Considering such statement, it is believed that the proposed controller could be enhanced by additional constraints and a combustion switching-mode feature that would seek for the best engine operation with a smooth transition between combustion modes.

- **Combustion operation limitation:** due to the high combustion rates observed in premixed dual-fuel combustion, and their harmful potential for the engine, it was decided to analyze the cylinder pressure oscillations in various injection strategies. The pressure oscillations were observed to vary with the mixture stratification level where some conditions could result in significant amplitudes. For this reason, it was decided to develop a controller that would keep the pressure oscillations amplitude below a defined threshold. Due to the stochastic behavior of cycles with high amplitudes, a knock-like controller was implemented with the gasoline fraction and the diesel injection timing as the control variables. The controller was found to be able to control the probability of high amplitude events to the desired threshold in all the combustion modes, thus ensuring a safer operation of the engine.

The definition of operational limits such as MPRR or MAPO is traditionally set empirically. In the present case, the MAPO was used as the limitation index and its level was chosen according to observations made at each mixture stratification level. A deeper characterization of the pressure resonance

in various premixed dual-fuel combustion engines design could enhance the development of appropriate controllers to adapt the limitation to the combustion mode. Furthermore, in this work the gasoline fraction and the injection timing control were evaluated separately. Consequently, the controller might be upgraded by including both control variables and providing the priority to the one with the highest sensitivity over the combustion in real-time.

Modeling

A control-oriented model was explored as a way of improving the development of control strategies in premixed dual-fuel combustion. Modeling is especially interesting to cost-effectively design and investigate new controllers by substituting the real engine by its mathematical representation, or to be integrated directly into the controller definition. In the present case, the model aimed to estimate the start of combustion and the combustion phasing of RCCI combustion using the available operating conditions. A modified knock integral model was designed to estimate the start of combustion (SOC), while a simplified burn duration model was used to estimate the combustion phasing (CA50 in this case). Encouraging results were observed in the SOC and CA50 estimation even under load and mixture reactivity transient operation, showing the potential of such approach to enhance combustion control research activities.

This model was limited to RCCI combustion with an early injection strategy. A wider range of operating conditions should be evaluated to develop this kind of models, taking into account the various injection strategies considered in such combustion concept: fully, highly and partially premixed. The internal cylinder reactions are complex and the mixture reactivity sensitivity to the start of injection (from early to late injection) could be implemented in the model to improve and expand the estimation capability. Furthermore, such model might be experimented in a model-based controller to verify its ability to enhance the control of the dual-fuel combustion. Indeed, such control implementation has been proven to be effective in various combustion strategies, as well as in dual-fuel operation as reported in Chapter 2.

State estimation

The cylinder-to-cylinder dispersion observed in multi-cylinder engines might be responsible of performance drop and pollutant emissions increase. These variations can be explained by uneven cylinder conditions (e.g., pressure and temperature) and species concentration (e.g., EGR and fuel due to ageing or discrepancies). In

dual-fuel engines, the ratio of both of the fuels in the cylinder plays a significant role in combustion efficiency and control. Nevertheless, a hardware configuration with port fuel injectors might exhibit additional fuel distribution dispersion between cylinders. Conventional injection control based on look-up tables does not have a direct feedback from the real fuel concentration and consequently fails to ensure the desired fuel blending ratio in each cylinder. A detailed analysis and characterization of the respective injection systems (direct and port fuel injection) was performed. It was observed that the cylinder-to-cylinder dispersion in each system was sensitive to different factors and should therefore be approached accordingly. In an attempt to address this issue, a pressure-based observer was developed. The in-cylinder pressure signal was used to compute the heat released by the combustion in each cylinder, and by combining these results with the set of sensors installed on the engine, the fuel quantity and blending ratio were evaluated. Additionally, a learning algorithm aiming to update the injection look-up tables was implemented to deal with injector drift over time. The method was evaluated off-line with various sets of data. Both the adaptive look-up table algorithm and the fuel observer showed their capability to address the assumed injector bias and the fuel distribution between cylinders where an estimation of the individual fuel blending ratio was obtained.

The proposed technique showed the significance of using feedback from the available set of sensors for ensuring the highest efficiency operation in such complex combustion concepts and engine hardware configurations. Nevertheless, in this work, this method was exclusively evaluated off-line. Its implementation in an on-line real-time controller could help to validate its potential for improving cylinder balancing and verify if a gain in performance and emissions reduction could be obtained thanks to it.

Final remarks

The work provided in this thesis has highlighted and confirmed the potential of the in-cylinder pressure signal for a more accurate and efficient control of new combustion concepts such as premixed dual-fuel. Either by considering its feedback alone, or by leveraging its information into models, the various sources of controllability and variability issues were found to be addressed by such techniques.

Although the future of internal combustion engines for the transportation sector is under debate, solutions and methods to improve ongoing research concepts that might end in on-road applications are necessary. Marginally used in series appli-

cations, the in-cylinder pressure sensor is a source of high value information and could ease the transition to more efficient engines. This thesis attempted to provide tools that could be applied on premixed dual-fuel platforms where a special emphasis on the various injection strategies and mixture stratification was made. From fulfilling the desired performance and ensuring a safe operation, to optimizing the combustion with emissions reduction, the methods are manifold and the development of accurate and cost-effective combustion diagnostic and control concepts could participate into reaching these goals sooner.

References

Alphabetic Order of Authors

- Abdul-Manan Amir F.N.** Uncertainty and differences in GHG emissions between electric and conventional gasoline vehicles with implications for transport policy making. *Energy Policy*, Vol. 87, pp. 1–7, dec 2015. (cited in p. 5)
- Acar Canan and Dincer Ibrahim.** The potential role of hydrogen as a sustainable transportation fuel to combat global warming. *International Journal of Hydrogen Energy*, Vol. 45 n° 5, pp. 3396–3406, jan 2020. (cited in p. 9)
- ACEA.** ACEA, Making the Transition to Zero-Emission Mobility - 2020 progress report, 2020. <https://www.acea.auto/publication/making-the-transition-to-zero-emission-mobility-2020-progress-report/>. (cited in p. 4)
- ACEA.** ACEA, Making the Transition to Zero-Emission Mobility - 2021 progress report, 2021. <https://www.acea.auto/publication/2021-progress-report-making-the-transition-to-zero-emission-mobility/>. (cited in pp. 2, 4, and 5)
- Adler Joerg.** Ceramic Diesel Particulate Filters. *International Journal of Applied Ceramic Technology*, Vol. 2 n° 6, pp. 429–439, nov 2005. (cited in p. 8)
- Agarwal Avinash Kumar, Singh Akhilendra Pratap and Maurya Rakesh Kumar.** Evolution, challenges and path forward for low temperature combustion engines. *Progress in Energy and Combustion Science*, Vol. 61, pp. 1–56, 2017. (cited in p. 10)
- Ahmadi Pouria, Torabi Seyed Hosein, Afsaneh Hadi, Sadegheih Yousef, Ganjehsarabi Hadi and Ashjaee Mehdi.** The effects of driving patterns and PEM fuel cell degradation on the lifecycle assessment of hydrogen fuel cell vehicles. *International Journal of Hydrogen Energy*, Vol. 45 n° 5, pp. 3595–3608, jan 2020. (cited in p. 9)
- Albin Thivaharan.** *Nonlinear Model Predictive Control of Combustion Engines*. 2021. (cited in p. 12)
- Aliramezani Masoud, Koch Charles Robert and Shahbakhti Mahdi.** Modeling, diagnostics, optimization, and control of internal combustion engines via modern machine learning techniques: A review and future directions. *Progress in Energy and Combustion Science*, Vol. 88, jan 2022. (cited in p. 11)

- Alkemade Ulrich G. and Schumann Bernd.** Engines and exhaust after treatment systems for future automotive applications. *Solid State Ionics*, Vol. 177 n° 26-32 SPEC. ISS., pp. 2291–2296, 2006. (cited in p. 8)
- Alriksson Malin, Rente Tanja and Denbratt Ingemar.** Low Soot, Low NO_x in a Heavy Duty Diesel Engine Using High Levels of EGR. In *SAE Technical Papers*, volume 2006, pp. 75–2006, oct 2005. (cited in p. 10)
- Ambaye Teklit Gebregiorgis, Vaccari Mentore, Bonilla-Petriciolet Adrián, Prasad Shiv, van Hullebusch Eric D. and Rtimi Sami.** Emerging technologies for biofuel production: A critical review on recent progress, challenges and perspectives. *Journal of Environmental Management*, Vol. 290 n° March, pp. 112627, jul 2021. (cited in p. 9)
- Ängeby Jakob, Johnsson Anders and Hellström Kristina.** Knock Detection Using Multiple Indicators and a Classification Approach. *IFAC-PapersOnLine*, Vol. 51 n° 31, pp. 297–302, 2018. (cited in p. 88)
- Antonopoulos Antonis and Hountalas Dimitrios.** Identification and Correction of the Error Induced by the Sampling Method Used to Monitor Cylinder Pressure of Reciprocating Internal Combustion Engines. In *SAE Technical Papers*, apr 2012. (cited in p. 59)
- Aquino C.F.** Transient A/F Control Characteristics of the 5 Liter Central Fuel Injection Engine. In *SAE Technical Paper Series*, number 810494, feb 1981. (cited in pp. 106, 115, 157, and 170)
- Arora Jayant Kumar and Shahbakhti Mahdi.** Real-Time Closed-Loop Control of a Light-Duty RCCI Engine During Transient Operations. In *SAE Technical Paper*, mar 2017. (cited in pp. 35, 38, 55, and 89)
- Arsie I., Pianese C. and Rizzo G.** A non linear observer for fuel film dynamics into the intake manifold of a spark ignition engine. *IEEE/ASME International Conference on Advanced Intelligent Mechatronics, AIM*, pp. 251–256, 1999. (cited in p. 148)
- Asad Usman, Divekar Prasad, Zheng Ming and Tjong Jimi.** Low Temperature Combustion Strategies for Compression Ignition Engines: Operability limits and Challenges. *SAE Technical Paper Series*, Vol. 1, 2013. (cited in p. 77)
- Asad Usman and Zheng Ming.** Fast heat release characterization of a diesel engine. *International Journal of Thermal Sciences*, Vol. 47 n° 12, pp. 1688–1700, 2008. (cited in pp. 71 and 158)
- Atta Khalid Tourkey and Guay Martin.** Adaptive amplitude fast proportional integral phasor extremum seeking control for a class of nonlinear system. *Journal of Process Control*, Vol. 83, pp. 147–154, nov 2019. (cited in p. 110)
- Bach Florian, Hampe Clemens, Wagner Uwe, Spicher Ulrich and Sauer Christina.** Low Temperature Gasoline Combustion With Diesel Micro-Pilot Injection in a Six-Cylinder Heavy Duty Engine. In *ASME 2012 Internal Combustion Engine Division Fall Technical Conference*, pp. 349–359. American Society of Mechanical Engineers, sep 2012. (cited in p. 158)

- Badami M., Mallamo F., Millo F. and Rossi E. E.** Influence of Multiple Injection Strategies on Emissions, Combustion Noise and BSFC of a DI Common Rail Diesel Engine. In *SAE Technical Papers*, volume 2002, mar 2002. (cited in p. 7)
- Badawy Tamer, Shrestha Amit and Henein Naeim.** Detection of Combustion Resonance Using an Ion Current Sensor in Diesel Engines. *Journal of Engineering for Gas Turbines and Power*, Vol. 134 n° 5, may 2012. (cited in p. 88)
- Bahri Bahram, Shahbakhti Mahdi, Kannan Kaushik and Aziz Azhar Abdul.** Identification of ringing operation for low temperature combustion engines. *Applied Energy*, Vol. 171, pp. 142–152, jun 2016. (cited in p. 77)
- Bares P., Selmanaj D., Guardiola C. and Onder C.** A new knock event definition for knock detection and control optimization. *Applied Thermal Engineering*, Vol. 131, pp. 80–88, feb 2018. (cited in p. 61)
- Bares Moreno Pau.** *In-cylinder pressure resonance analysis for trapped mass estimation in automotive engines.* PhD Thesis, Universitat Politècnica de València, 2017. (cited in p. 63)
- Basina L. N. Aditya, Irdmouza Behrouz K., Velni Javad Mohammadpour, Borhan Hoseinali, Naber Jeffrey D. and Shahbakhti Mahdi.** Data-driven Modeling and Predictive Control of Maximum Pressure Rise Rate in RCCI Engines. In *2020 IEEE Conference on Control Technology and Applications (CCTA)*, pp. 94–99. IEEE, aug 2020. (cited in pp. 36 and 39)
- Batool Sadaf, Naber Jeffrey D. and Shahbakhti Mahdi.** Multi-mode Low Temperature Combustion (LTC) and Mode Switching Control. In *Energy, Environment, and Sustainability*, pp. 43–93. Springer Nature, 2022. (cited in p. 37)
- Bauer Christian, Hofer Johannes, Althaus Hans-Jörg, Del Duce Andrea and Simons Andrew.** The environmental performance of current and future passenger vehicles: Life cycle assessment based on a novel scenario analysis framework. *Applied Energy*, Vol. 157, pp. 871–883, nov 2015. (cited in p. 4)
- Beatrice Carlo, Guido Chiara, Napolitano Pierpaolo, Iorio Silvana Di and Giacomo Nicola Del.** Assessment of biodiesel blending detection capability of the on-board diagnostic of the last generation automotive diesel engines. *Fuel*, Vol. 90 n° 5, pp. 2039–2044, may 2011. (cited in p. 158)
- Bekdemir Cemil, Baert Rik, Willems Frank and Somers Bart.** Towards Control-Oriented Modeling of Natural Gas-Diesel RCCI Combustion. In *SAE Technical Paper*, apr 2015. (cited in pp. 36 and 38)
- Benajes J., Novella R., De Lima D. and Thein K.** Impact of injection settings operating with the gasoline Partially Premixed Combustion concept in a 2-stroke HSDI compression ignition engine. *Applied Energy*, Vol. 193 n° x, pp. 515–530, may 2017. (cited in p. 29)

- Benajes Jesus, Garcia Antonio, Monsalve-Serrano Javier and Boronat Vicente.** Achieving clean and efficient engine operation up to full load by combining optimized RCCI and dual-fuel diesel-gasoline combustion strategies. *Energy Conversion and Management*, Vol. 136, pp. 142–151, 2017. (cited in pp. 32 and 155)
- Benajes Jesús, Molina Santiago, García Antonio, Belarte Eduardo and Vanvolsem Michel.** An investigation on RCCI combustion in a heavy duty diesel engine using in-cylinder blending of diesel and gasoline fuels. *Applied Thermal Engineering*, Vol. 63 n° 1, pp. 66–76, 2014. (cited in pp. 32 and 184)
- Benajes Jesús, Molina Santiago, García Antonio and Monsalve-Serrano Javier.** Effects of direct injection timing and blending ratio on RCCI combustion with different low reactivity fuels. *Energy Conversion and Management*, Vol. 99, pp. 193–209, 2015. (cited in pp. 32, 109, 157, and 185)
- Benajes Jesús, Molina Santiago, García Antonio and Monsalve-Serrano Javier.** Effects of low reactivity fuel characteristics and blending ratio on low load RCCI (reactivity controlled compression ignition) performance and emissions in a heavy-duty diesel engine. *Energy*, Vol. 90, pp. 1261–1271, 2015. (cited in p. 31)
- Benajes Jesús, Pastor José V., García Antonio and Boronat Vicente.** A RCCI operational limits assessment in a medium duty compression ignition engine using an adapted compression ratio. *Energy Conversion and Management*, Vol. 126, pp. 497–508, 2016. (cited in pp. 32 and 49)
- Benajes Jesús, Pastor José V., García Antonio and Monsalve-Serrano Javier.** The potential of RCCI concept to meet EURO VI NO_x limitation and ultra-low soot emissions in a heavy-duty engine over the whole engine map. *Fuel*, Vol. 159, pp. 952–961, 2015. (cited in p. 32)
- Bendu Harisankar and Murugan S.** Homogeneous charge compression ignition (HCCI) combustion: Mixture preparation and control strategies in diesel engines. *Renewable and Sustainable Energy Reviews*, Vol. 38, pp. 732–746, oct 2014. (cited in pp. 10, 30, and 87)
- Bengtsson J., Gafvert M. and Strandh P.** Modeling of HCCI diesel engine combustion for control analysis. *2004 43rd IEEE Conference on Decision and Control (CDC) (IEEE Cat. No.04CH37601)*, Vol. 2, pp. 1682–1687, 2004. (cited in p. 150)
- Bengtsson J., Strandh P., Johansson R., Tunestål P. and Johansson B.** Closed-loop combustion control of homogeneous charge compression ignition(HCCI) engine dynamics. *International Journal of Adaptive Control and Signal Processing*, Vol. 18 n° 2, pp. 167–179, mar 2004. (cited in p. 74)
- Bengtsson Johan, Strandh Petter, Johansson Rolf, Tunestal Per and Johansson Bengt.** Model predictive control of homogeneous charge compression ignition (HCCI) engine dynamics. *Computer Aided Control System Design, 2006 IEEE International Conference on Control Applications, 2006 IEEE International Symposium on Intelligent Control, 2006 IEEE*, pp. 1675–1680, 2006. (cited in pp. 12, 34, and 37)

- Bengtsson Johan, Strandh Petter, Johansson Rolf, Tunestål Per and Johansson Bengt.** Multi-Output Control of a Heavy Duty HCCI Engine Using Variable Valve Actuation and Model Predictive Control. In *SAE Technical Paper Series*, apr 2006. (cited in p. 34)
- Bessonette Paul W., Schleyer Charles H., Duffy Kevin P., Hardy William L. and Liechty Michael P.** Effects of Fuel Property Changes on Heavy-Duty HCCI Combustion. In *SAE Technical Papers*, volume 2007, pp. 776–790, apr 2007. (cited in p. 30)
- Bidarvatan M., Shahbakhti M., Jazayeri S. A. and Koch C. R.** Cycle-to-cycle modeling and sliding mode control of blended-fuel HCCI engine. *Control Engineering Practice*, Vol. 24 n° 1, pp. 79–91, 2014. (cited in pp. 34 and 37)
- Bieker Georg.** A global comparison of the life-cycle greenhouse gas emissions of combustion engine and electric passenger cars, 2021. <https://theicct.org/publications/global-LCA-passenger-cars-jul2021>. (cited in p. 4)
- Blanco-Rodriguez David.** *Modelling and Observation of Exhaust Gas Concentrations for Diesel Engine Control*. Springer Theses. Springer International Publishing, Cham, 2014. (cited in pp. 114 and 173)
- Blumreiter Julie and Edwards Chris.** Overcoming Pressure Waves to Achieve High Load HCCI Combustion. In *SAE Technical Papers*, volume 1. SAE International, apr 2014. (cited in p. 76)
- Boronat Colomer Vicente.** *Dual-Fuel Dual-Mode combustion strategy to achieve high thermal efficiency, low NOx and smoke emissions in compression ignition engines*. PhD Thesis, Universitat Politècnica de València, 2018. (cited in pp. 32 and 51)
- Bouter Anne, Hache Emmanuel, Ternel Cyprien and Beauchet Sandra.** Comparative environmental life cycle assessment of several powertrain types for cars and buses in France for two driving cycles: “worldwide harmonized light vehicle test procedure” cycle and urban cycle. *The International Journal of Life Cycle Assessment*, Vol. 25 n° 8, pp. 1545–1565, aug 2020. (cited in p. 4)
- Brijesh P. and Sreedhara S.** Exhaust emissions and its control methods in compression ignition engines: A review. *International Journal of Automotive Technology*, Vol. 14 n° 2, pp. 195–206, apr 2013. (cited in p. 7)
- Broatch A., Margot X., Novella R. and Gomez-Soriano J.** Combustion noise analysis of partially premixed combustion concept using gasoline fuel in a 2-stroke engine. *Energy*, Vol. 107, pp. 612–624, jul 2016. (cited in p. 120)
- Broatch Alberto, Guardiola Carlos, Bares Pau and Denia Francisco D.** Determination of the resonance response in an engine cylinder with a bowl-in-piston geometry by the finite element method for inferring the trapped mass. *International Journal of Engine Research*, Vol. 17 n° 5, pp. 534–542, jun 2016. (cited in p. 62)
- Brunt Michael F. J. and Pond Christopher R.** Evaluation of Techniques for Absolute Cylinder Pressure Correction. *SAE Technical Paper*, n° 412, 1997. (cited in p. 59)

- Brunt Michael F.J., Pond Christopher R. and Biundo John.** Gasoline Engine Knock Analysis using Cylinder Pressure Data. In *SAE Technical Papers*, number 724, feb 1998. (cited in p. 63)
- Brynolf Selma, Taljegard Maria, Grahn Maria and Hansson Julia.** Electrofuels for the transport sector: A review of production costs. *Renewable and Sustainable Energy Reviews*, Vol. 81 n° February 2017, pp. 1887–1905, jan 2018. (cited in p. 9)
- Burul Dora and Algesten David.** Scania - Life cycle assessment of distribution vehicles: Battery electric vs diesel driven, 2021. <https://www.scania.com/group/en/home/newsroom/press-releases/press-release-detail-page.html/3999115-scania-publishes-life-cycle-assessment-of-battery-electric-vehicles>. (cited in p. 4)
- Carlucci A. P., Laforgia D., Motz S., Saracino R. and Wenzel S. P.** Advanced closed loop combustion control of a LTC diesel engine based on in-cylinder pressure signals. *Energy Conversion and Management*, Vol. 77, pp. 193–207, 2014. (cited in p. 12)
- Catania Andrea E., Ferrari Alessandro, Manno Michele and Spessa Ezio.** Experimental Investigation of Dynamics Effects on Multiple-Injection Common Rail System Performance. *Journal of Engineering for Gas Turbines and Power*, Vol. 130 n° 3, pp. 032806, 2008. (cited in p. 163)
- Caton Jerald A.** Combustion phasing for maximum efficiency for conventional and high efficiency engines. *Energy Conversion and Management*, Vol. 77, pp. 564–576, jan 2014. (cited in p. 73)
- Cavina Nicolò, Corti Enrico and Moro Davide.** Closed-loop individual cylinder air-fuel ratio control via UEGO signal spectral analysis. *Control Engineering Practice*, Vol. 18 n° 11, pp. 1295–1306, 2010. (cited in p. 158)
- Çebi Emrah Cihan, Rottenkolber Gregor and Uyar Erol.** In-Cylinder Pressure Based Real-Time Estimation of Engine-Out Particulate Matter Emissions of a Diesel Engine. In *SAE 2011 World Congress and Exhibition*, apr 2011. (cited in p. 55)
- Chang Kyoungjoon, Lavoie George A., Babajimopoulos Aristotelis, Filipi Zoran and Assanis Dennis N.** Control of a Multi-Cylinder HCCI Engine During Transient Operation by Modulating Residual Gas Fraction to Compensate for Wall Temperature Effects. In *SAE Technical Papers*, apr 2007. (cited in p. 37)
- Chauvin J., Petit N., Rouchon P., Moulin P. and Corde G.** Six Degrees Crankshaft Individual Air Fuel Ratio Estimation of Diesel Engines for Cylinder Balancing Purpose. In *SAE Technical Paper Series*, volume 1, apr 2006. (cited in p. 158)
- Chen Lin, Zhang Ren, Pan Jiaying and Wei Haiqiao.** Optical study on autoignition and knocking characteristics of dual-fuel engine under CI vs SI combustion modes. *Fuel*, Vol. 266 n° November 2019, pp. 117107, apr 2020. (cited in p. 120)
- Chesterton Andrew.** How many cars are there in the world? <https://www.carsguide.com.au/car-advice/how-many-cars-are-there-in-the-world-70629>. Accessed 22 March 2022. (cited in p. 2)

- Chiang C. J. and Stefanopoulou A. G.** Dynamics of homogeneous charge compression ignition (HCCI) engines with high dilution. *Proceedings of the American Control Conference*, Vol. 15 n° 2, pp. 2979–2984, 2007. (cited in p. 33)
- Chiang Cha Jui, Stefanopoulou Anna G. and Janković Mrdjan.** Nonlinear observer-based control of load transitions in homogeneous charge compression ignition engines. *IEEE Transactions on Control Systems Technology*, Vol. 15 n° 3, pp. 438–448, 2007. (cited in p. 37)
- Chiang Chia Jui and Stefanopoulou Anna G.** Sensitivity analysis of combustion timing and duration of homogeneous charge compression ignition (HCCI) engines. *Proceedings of the 2006 American Control Conference*, pp. 1857–1862, 2006. (cited in p. 150)
- Christensen Magnus, Johansson Bengt, Annéus Per and Mauss Fabian.** Supercharged Homogeneous Charge Compression Ignition. In *SAE Technical Paper Series*, number 724, feb 1998. (cited in p. 30)
- Cloudt Robert and Willems Frank.** Integrated Emission Management strategy for cost-optimal engine-aftertreatment operation. *SAE International Journal of Engines*, Vol. 4 n° 1, pp. 1784–1797, apr 2011. (cited in p. 8)
- Conway Graham, Joshi Ameya, Leach Felix, García Antonio and Senecal Peter Kelly.** A review of current and future powertrain technologies and trends in 2020. *Transportation Engineering*, Vol. 5 n° June, pp. 100080, sep 2021. (cited in p. 5)
- Coppin Thomas and Maamri Nezha.** Fuel estimation and air-to-fuel ratio control for Flexfuel spark-ignition engines. In *2010 IEEE International Conference on Control Applications*, number 2, pp. 555–560. IEEE, sep 2010. (cited in p. 170)
- Cummins C. Lyle.** Early IC and Automotive Engines. In *SAE Technical Papers*, pp. 1960–1971, feb 1976. (cited in p. 6)
- Dahl Daniel, Andersson Mats and Denbratt Ingemar.** The Origin of Pressure Waves in High Load HCCI Combustion: A High-Speed Video Analysis. *Combustion Science and Technology*, Vol. 183 n° 11, pp. 1266–1281, nov 2011. (cited in p. 63)
- D’Ambrosio S. and Ferrari A.** Diesel Injector Coking: Optical-Chemical Analysis of Deposits and Influence on Injected Flow-Rate, Fuel Spray and Engine Performance. *Journal of Engineering for Gas Turbines and Power*, Vol. 134 n° 6, pp. 062801, 2012. (cited in pp. 158, 162, and 178)
- de Ojeda William, Zoldak Philip, Espinosa Raul and Kumar Raj.** Development of a Fuel Injection Strategy for Partially Premixed Compression Ignition Combustion. *SAE International Journal of Engines*, Vol. 2 n° 1, apr 2009. (cited in p. 29)
- Dec John E.** Advanced compression-ignition engines—understanding the in-cylinder processes. *Proceedings of the Combustion Institute*, Vol. 32 n° 2, pp. 2727–2742, 2009. (cited in p. 29)
- Dec John E. and Sjöberg Magnus.** Isolating the Effects of Fuel Chemistry on Combustion Phasing in an HCCI Engine and the Potential of Fuel Stratification for Ignition Control. In *SAE Technical Papers*, volume 2004, mar 2004. (cited in p. 30)

- Dec John E. and Yang Yi.** Boosted HCCI for High Power without Engine Knock and with Ultra-Low NOx Emissions - using Conventional Gasoline. *SAE International Journal of Engines*, Vol. 3 n° 1, apr 2010. (cited in p. 10)
- DelVescovo Dan, Kokjohn Sage and Reitz Rolf.** The Development of an Ignition Delay Correlation for PRF Fuel Blends from PRF0 (n-Heptane) to PRF100 (iso-Octane). *SAE International Journal of Engines*, Vol. 9 n° 1, pp. 520–535, 2016. (cited in p. 150)
- DelVescovo Dan, Kokjohn Sage and Reitz Rolf.** The Effects of Charge Preparation, Fuel Stratification, and Premixed Fuel Chemistry on Reactivity Controlled Compression Ignition (RCCI) Combustion. *SAE International Journal of Engines*, Vol. 10 n° 4, pp. 1491–1505, 2017. (cited in pp. 32, 96, 112, 127, and 157)
- Dempsey Adam B., Walker N. Ryan, Gingrich Eric and Reitz Rolf D.** Comparison of low temperature combustion strategies for advanced compression ignition engines with a focus on controllability. *Combustion Science and Technology*, Vol. 186 n° 2, pp. 210–241, 2014. (cited in pp. 10, 32, and 87)
- Dernotte Jeremie, Dec John and Ji Chunsheng.** Investigation of the Sources of Combustion Noise in HCCI Engines. *SAE International Journal of Engines*, Vol. 7 n° 2, pp. 730–761, apr 2014. (cited in pp. 62 and 77)
- Desantes José M., Benajes Jesús, García Antonio and Monsalve-Serrano Javier.** The role of the in-cylinder gas temperature and oxygen concentration over low load reactivity controlled compression ignition combustion efficiency. *Energy*, Vol. 78, pp. 854–868, 2014. (cited in pp. 31, 96, 151, and 157)
- Dhanji Meghnaa and Zhao Hua.** Investigations of split injection properties on the spray characteristics using a solenoid high-pressure injector. *International Journal of Engine Research*, Vol. 23 n° 2, pp. 262–284, feb 2022. (cited in p. 169)
- Di Leo Rocco.** Methodologies for air-fuel ratio and trapped mass estimation in diesel engines using the in-cylinder pressure measurement. *Energy Procedia*, Vol. 82, pp. 957–964, 2015. (cited in p. 158)
- Díaz Jaime Martín.** *Aportación al diagnóstico de la combustión en motores diesel de inyección directa*. PhD Thesis, Universitat Politècnica de València, 2007. (cited in p. 57)
- Dimitriou Pavlos and Tsujimura Taku.** A review of hydrogen as a compression ignition engine fuel. *International Journal of Hydrogen Energy*, Vol. 42 n° 38, pp. 24470–24486, sep 2017. (cited in p. 9)
- Divekar Prasad, Han Xiaoye, Tan Qingyuan, Asad Usman, Yanai Tadanori, Chen Xiang, Tjong Jimi and Zheng Ming.** Mode Switching to Improve Low Load Efficiency of an Ethanol-Diesel Dual-Fuel Engine. *SAE Technical Paper*, 2017. (cited in p. 36)
- Dochain Denis, Perrier Michel and Guay Martin.** Extremum seeking control and its application to process and reaction systems: A survey. *Mathematics and Computers in Simulation*, Vol. 82 n° 3, pp. 369–380, nov 2011. (cited in p. 107)

- Docquier Nicolas and Candel Sébastien.** Combustion control and sensors: a review. *Progress in Energy and Combustion Science*, Vol. 28 n° 2, pp. 107–150, jan 2002. (cited in p. 12)
- Doosje Erik, Willems Frank and Baert Rik.** Experimental demonstration of RCCI in heavy-duty engines using diesel and natural gas. *SAE Technical Papers*, Vol. 1, 2014. (cited in p. 32)
- Draper C.S.** The physical effects of detonation in a closed cylindrical chamber. *NACA Report*, n° 493, 1935. (cited in pp. 60, 61, 62, and 63)
- Díaz Sonsoles, Bernard Marie Rajon, Bernard Yoann, Bieker Georg, Lee Kaylin, Mock Peter, Mulholland Eamonn, Ragon Pierre-Louis, Rodriguez Felipe, Tietge Uwe and Wappelhorst Sandra.** European vehicle market statistics 2021/22, 2021. <https://theicct.org/wp-content/uploads/2021/12/ICCT-EU-Pocketbook-2021-Web-Dec21.pdf>. (cited in p. 4)
- Ebrahimi B., Tafreshi R., Masudi H., Franchek M.A., Mohammadpour J. and Grigoriadis K.** A Systematic Air-fuel Ratio Control Strategy for Lean-burn SI Engines. *IFAC Proceedings Volumes*, Vol. 45 n° 30, pp. 296–301, 2012. (cited in p. 158)
- Ebrahimi Khashayar and Koch Charles.** Model Predictive Control for Combustion Timing and Load Control in HCCI Engines. In *SAE Technical Papers*, volume 2015-April, apr 2015. (cited in p. 12)
- Ebrahimi Khashayar and Koch Charles Robert.** HCCI combustion timing control with Variable Valve Timing. In *2013 American Control Conference*, pp. 4429–4434. IEEE, jun 2013. (cited in p. 34)
- EEA.** European Environment Agency, Average CO₂ emissions from new cars and new vans increased again in 2019. <https://www.eea.europa.eu/highlights/average-co2-emissions-from-new-cars-vans-2019>. Accessed 22 March 2022. (cited in p. 4)
- EEA.** European Environment Agency, New registrations of electric vehicles in Europe. <https://www.eea.europa.eu/ims/new-registrations-of-electric-vehicles>. Accessed 22 March 2022. (cited in p. 4)
- Egeskog Andrea, Hagdahl Karl-Henrik, Krewer Christoffer, Råde Ingrid and Bolin Lisa.** Volvo Cars, with the participation of the IVL Swedish Environmental Research Institute - Carbon footprint report: Battery electric XC40 Recharge and the XC40 ICE, 2020. https://group.volvocars.com/news/sustainability/2020/ /media/ccs/Volvo_carbonfootprintreport.pdf. (cited in p. 4)
- Eichlleder Helmut, Wallner Thomas, Freymann Raymond and Ringler Jürgen.** The Potential of Hydrogen Internal Combustion Engines in a Future Mobility Scenario. In *SAE Technical Papers*, number 724, jun 2003. (cited in p. 9)
- Eng J. A.** Characterization of Pressure Waves in HCCI Combustion. In *SAE Technical Papers*, number 724, oct 2002. (cited in pp. 30, 62, and 76)

- Epping Kathi, Aceves Salvador, Bechtold Richard and Dec John E.** The Potential of HCCI Combustion for High Efficiency and Low Emissions. In *SAE Technical Papers*, number 724, jun 2002. (cited in pp. 10 and 30)
- Eriksson Lars and Nielsen Lars.** *Modeling and Control of Engines and Drivelines*. John Wiley & Sons, Ltd, Chichester, UK, feb 2014. (cited in p. 12)
- Eriksson Lars and Thomasson Andreas.** Cylinder state estimation from measured cylinder pressure traces - A Survey. *IFAC-PapersOnLine*, Vol. 50 n° 1, pp. 11029–11039, jul 2017. (cited in p. 55)
- EUR-Lex.** Regulation (EU) 2019/1242 of the European Parliament and of the Council of 20 June 2019 setting CO₂ emission performance standards for new heavy-duty vehicles and amending Regulations (EC) No 595/2009 and (EU) 2018/956 of the European Parliament and of the Council and Council Directive 96/53/EC. <https://eur-lex.europa.eu/eli/reg/2019/1242/oj>. Accessed 22 March 2022. (cited in p. 4)
- European Commission.** Emissions in the automotive sector. https://ec.europa.eu/growth/sectors/automotive/environment-protection/emissions_en. Accessed 22 March 2022. (cited in p. 7)
- European Commission.** Reducing CO₂ emissions from passenger cars - before 2020. https://ec.europa.eu/clima/policies/transport/vehicles/cars_en. Accessed 22 March 2022. (cited in p. 4)
- Fang Cheng, Ouyang Minggao, Tunestal Per, Yang Fuyuan and Yang Xiaofan.** Closed-loop combustion phase control for multiple combustion modes by multiple injections in a compression ignition engine fueled by gasoline-diesel mixture. *Applied Energy*, Vol. 231 n° May, pp. 816–825, dec 2018. (cited in pp. 12 and 89)
- Fathi Morteza, Jahanian Omid and Shahbakhti Mahdi.** Modeling and controller design architecture for cycle-by-cycle combustion control of homogeneous charge compression ignition (HCCI) engines – A comprehensive review. *Energy Conversion and Management*, Vol. 139, pp. 1–19, 2017. (cited in pp. 12 and 34)
- Fayaz H., Saidur R., Razali N., Anuar F.S., Saleman A.R. and Islam M.R.** An overview of hydrogen as a vehicle fuel. *Renewable and Sustainable Energy Reviews*, Vol. 16 n° 8, pp. 5511–5528, oct 2012. (cited in p. 9)
- Ferrari A., Novara C., Paolucci E., Vento O., Violante M. and Zhang T.** Design and rapid prototyping of a closed-loop control strategy of the injected mass for the reduction of CO₂, combustion noise and pollutant emissions in diesel engines. *Applied Energy*, Vol. 232 n° October, pp. 358–367, dec 2018. (cited in p. 12)
- Finesso Roberto and Spessa Ezio.** A control-oriented approach to estimate the injected fuel mass on the basis of the measured in-cylinder pressure in multiple injection diesel engines. *Energy Conversion and Management*, Vol. 105, pp. 54–70, 2015. (cited in p. 158)

- Formentin Simone, Corno Matteo, Waschl Harald, Alberer Daniel and Savaresi Sergio M.** NO_x Estimation in Diesel Engines via In-Cylinder Pressure Measurement. *IEEE Transactions on Control Systems Technology*, Vol. 22 n° 1, pp. 396–403, jan 2014. (cited in p. 55)
- Franceschi E. M., Muske Kenneth R., Peyton Jones James C. and Makki Imad.** An Adaptive Delay-Compensated PID Air Fuel Ratio Controller. *SAE Technical Paper*, Vol. 2007 n° 724, 2007. (cited in p. 158)
- Freire Ordóñez Diego, Shah Nilay and Guillén-Gosálbez Gonzalo.** Economic and full environmental assessment of electrofuels via electrolysis and co-electrolysis considering externalities. *Applied Energy*, Vol. 286 n° July 2020, pp. 116488, mar 2021. (cited in p. 9)
- Galloni Enzo.** Dynamic knock detection and quantification in a spark ignition engine by means of a pressure based method. *Energy Conversion and Management*, Vol. 64, pp. 256–262, dec 2012. (cited in p. 61)
- Gan Suyin, Ng Hoon Kiat and Pang Kar Mun.** Homogeneous Charge Compression Ignition (HCCI) combustion: Implementation and effects on pollutants in direct injection diesel engines. *Applied Energy*, Vol. 88 n° 3, pp. 559–567, mar 2011. (cited in p. 30)
- Gao Jinwu, Zhang Yahui and Shen Tielong.** An On-Board Calibration Scheme for Map-Based Combustion Phase Control of Spark-Ignition Engines. *IEEE/ASME Transactions on Mechatronics*, Vol. 22 n° 4, pp. 1485–1496, aug 2017. (cited in p. 173)
- García Antonio, Carlucci Paolo, Monsalve-Serrano Javier, Valletta Andrea and Martínez-Boggio Santiago.** Energy management optimization for a power-split hybrid in a dual-mode RCCI-CDC engine. *Applied Energy*, Vol. 302 n° August, pp. 117525, nov 2021. (cited in p. 10)
- García Antonio, Monsalve-Serrano Javier, Sari Rafael, Dimitrakopoulos Nikolaos, Tunér Martín and Tunestål Per.** Performance and emissions of a series hybrid vehicle powered by a gasoline partially premixed combustion engine. *Applied Thermal Engineering*, Vol. 150 n° January, pp. 564–575, mar 2019. (cited in p. 10)
- García Antonio, Monsalve-Serrano Javier, Villalta David and Guzmán-Mendoza María.** Methanol and OME_x as fuel candidates to fulfill the potential EURO VII emissions regulation under dual-mode dual-fuel combustion. *Fuel*, Vol. 287 n° September 2020, pp. 119548, mar 2021. (cited in p. 10)
- Ghojel J. I.** Review of the development and applications of the Wiebe function: A tribute to the contribution of Ivan Wiebe to engine research. *International Journal of Engine Research*, Vol. 11 n° 4, pp. 297–312, 2010. (cited in p. 152)
- Guan Bin, Zhan Reggie, Lin He and Huang Zhen.** Review of state of the art technologies of selective catalytic reduction of NO_x from diesel engine exhaust. *Applied Thermal Engineering*, Vol. 66 n° 1-2, pp. 395–414, may 2014. (cited in p. 8)
- Guardiola C., Martín J., Pla B. and Bares P.** Cycle by cycle NO_x model for diesel engine control. *Applied Thermal Engineering*, Vol. 110, pp. 1–2, 2017. (cited in p. 55)

- Guardiola C., Pla B., Bares P. and Peyton Jones J.C.** Integration of intermittent measurement from in-cylinder pressure resonance in a multi-sensor mass flow estimator. *Mechanical Systems and Signal Processing*, Vol. 131, pp. 152–165, sep 2019. (cited in p. 160)
- Guardiola Carlos, Pla Benjamín, Bares Pau and Stefanopoulou Anna.** Cylinder charge composition observation based on in-cylinder pressure measurement. *Measurement: Journal of the International Measurement Confederation*, Vol. 131, pp. 559–568, 2019. (cited in pp. 148, 157, and 158)
- Guillemin Fabrice, Grondin Olivier, Chauvin Jonathan and Nguyen Emmanuel.** Combustion Parameters Estimation Based on Knock Sensor for Control Purpose Using Dedicated Signal Processing Platform. In *SAE Technical Papers*, volume 2008, apr 2008. (cited in p. 88)
- Guzzella Lino and Onder Christopher H.** *Introduction to Modeling and Control of Internal Combustion Engine Systems*. Springer Berlin Heidelberg, Berlin, Heidelberg, 2010. (cited in p. 11)
- Guzzella Lino and Sciarretta Antonio.** *Vehicle Propulsion Systems*, volume 91. Springer Berlin Heidelberg, Berlin, Heidelberg, 2013. (cited in p. 5)
- Hadler Jens, Rudolph Falko, Dorenkamp Richard, Stehr Hartmut, Hilzendeger Juergen and Kranzusch Sebastian.** Volkswagen’s new 2.0 l TDI engine for the most stringent emission standards - Part 1. *MTZ worldwide*, Vol. 69 n° 5, pp. 12–18, 2008. (cited in p. 12)
- Hall Carrie and Kassa Mateos.** Advances in combustion control for natural gas–diesel dual fuel compression ignition engines in automotive applications: A review. *Renewable and Sustainable Energy Reviews*, Vol. 148 n° August 2020, sep 2021. (cited in p. 34)
- Hall Carrie M., Shaver Gregory M., Chauvin Jonathan and Petit Nicolas.** Control-oriented modelling of combustion phasing for a fuel-flexible spark-ignited engine with variable valve timing. *International Journal of Engine Research*, Vol. 13 n° 5, pp. 448–463, oct 2012. (cited in p. 148)
- Han Dong, Li Ke, Duan Yaozong, Lin He and Huang Zhen.** Numerical study on fuel physical effects on the split injection processes on a common rail injection system. *Energy Conversion and Management*, Vol. 134, pp. 47–58, feb 2017. (cited in p. 163)
- Hänggi Severin, Elbert Philipp, Bütler Thomas, Cabalzar Urs, Teske Sinan, Bach Christian and Onder Christopher.** A review of synthetic fuels for passenger vehicles. *Energy Reports*, Vol. 5, pp. 555–569, nov 2019. (cited in p. 9)
- Hannula Ilkka and Reiner David M.** Near-Term Potential of Biofuels, Electrofuels, and Battery Electric Vehicles in Decarbonizing Road Transport. *Joule*, Vol. 3 n° 10, pp. 2390–2402, oct 2019. (cited in p. 9)
- Hanson Reed, Curran Scott, Wagner Robert, Kokjohn Sage, Splitter Derek and Reitz Rolf D.** Piston Bowl Optimization for RCCI Combustion in a Light-Duty Multi-Cylinder Engine. *SAE International Journal of Engines*, Vol. 5 n° 2, pp. 286–299, 2012. (cited in p. 32)

- Hanson Reed, Kokjohn Sage, Splitter Derek and Reitz Rolf D.** Fuel Effects on Reactivity Controlled Compression Ignition (RCCI) Combustion at Low Load. *SAE International Journal of Engines*, Vol. 4 n° 1, pp. 394–411, 2011. (cited in pp. 31 and 185)
- Hanson Reed and Reitz Rolf.** Transient RCCI Operation in a Light-Duty Multi-Cylinder Engine. *SAE International Journal of Engines*, Vol. 6 n° 3, pp. 1694–1705, 2013. (cited in pp. 35 and 38)
- Hanson Reed M., Kokjohn Sage L., Splitter Derek A. and Reitz Rolf D.** An experimental investigation of fuel reactivity controlled PCCI combustion in a heavy-duty engine. *SAE Technical Papers*, Vol. 3 n° 1, pp. 700–716, 2010. (cited in p. 31)
- Haraldsson Göran, Tunestål Per, Johansson Bengt and Hyvönen Jari.** HCCI Combustion Phasing in a Multi Cylinder Engine Using Variable Compression Ratio. In *SAE Technical Papers*, number 724, oct 2002. (cited in p. 30)
- Haraldsson Goran, Tunestal Per, Johansson Bengt and Hyvonen Jari.** HCCI Combustion Phasing with Closed-Loop Combustion Control Using Variable Compression Ratio in a Multi Cylinder Engine. In *SAE Technical Papers*, may 2003. (cited in p. 55)
- Haraldsson Göran, Tunestål Per, Johansson Bengt and Hyvönen Jari.** HCCI Closed-Loop Combustion Control Using Fast Thermal Management. In *SAE Technical Paper Series*. SAE International, mar 2004. (cited in p. 34)
- Haraldsson Göran, Tunestal Per, Johansson Bengt and Hyvönen Jari.** Transient Control of a Multi Cylinder HCCI Engine During a Drive Cycle. In *SAE Technical Paper Series*, apr 2005. (cited in p. 34)
- Hasan M.M. and Rahman M.M.** Homogeneous charge compression ignition combustion: Advantages over compression ignition combustion, challenges and solutions. *Renewable and Sustainable Energy Reviews*, Vol. 57, pp. 282–291, may 2016. (cited in p. 10)
- Hasegawa Yusuke, Akazaki Shusuke, Maki Hidetaka, Nishimura Youichi and Hirota Toshiaki.** Individual Cylinder Air-Fuel Ratio Feedback Control Using an Observer. *SAE Technical Paper*, n° 940376, 1994. (cited in p. 158)
- Haskara Ibrahim and Wang Yue-Yun.** Closed-Loop Combustion Noise Limit Control for Modern Diesel Combustion Modes. *IEEE Transactions on Control Systems Technology*, Vol. 25 n° 4, pp. 1168–1179, jul 2017. (cited in pp. 76 and 121)
- Hellstrom Erik, Larimore Jacob, Jade Shyam, Stefanopoulou Anna G. and Jiang Li.** Reducing cyclic variability while regulating combustion phasing in a four-cylinder HCCI engine. *IEEE Transactions on Control Systems Technology*, Vol. 22 n° 3, pp. 1190–1197, 2014. (cited in p. 89)
- Hellstrom Erik, Lee Donghoon, Jiang Li, Stefanopoulou Anna G and Yilmaz Hakan.** On-Board Calibration of Spark Timing by Extremum Seeking for Flex-Fuel Engines. *IEEE Transactions on Control Systems Technology*, Vol. 21 n° 6, pp. 2273–2279, nov 2013. (cited in p. 107)

- Hellweg Stefanie and Mila i Canals L.** Emerging approaches, challenges and opportunities in life cycle assessment. *Science*, Vol. 344 n° 6188, pp. 1109–1113, jun 2014. (cited in p. 4)
- Hempson J. G. G.** The Automobile Engine 1920-1950. In *SAE Technical Papers*, feb 1976. (cited in p. 6)
- Heywood J.B.** *Internal Combustion Engine Fundamentals*. Automotive technology series. McGraw-Hill, 1988. (cited in pp. 6, 71, 118, 119, 150, and 158)
- Husted H., Kruger D., Fattic G., Ripley G. and Kelly E.** Cylinder Pressure-Based Control of Pre-Mixed Diesel Combustion. In *SAE Technical Papers*, volume 2007, apr 2007. (cited in p. 55)
- IEA.** IEA (2020), Transport Biofuels, IEA, Paris. <https://www.iea.org/reports/transport-biofuels>. Accessed 22 March 2022. (cited in p. 9)
- IEA.** IEA (2020), Trucks and Buses, IEA, Paris. <https://www.iea.org/reports/trucks-and-buses>. Accessed 22 March 2022. (cited in p. 5)
- IEA.** IEA (2021), Global EV Outlook 2021, IEA, Paris. <https://www.iea.org/reports/global-ev-outlook-2021>. Accessed 22 March 2022. (cited in p. 5)
- IEA.** IEA, Data and statistics: World CO2 emissions by energy source. <https://www.iea.org/data-and-statistics/data-browser/?country=WORLD&fuel=CO2%20emissions&indicator=CO2BySource>. Accessed 22 March 2022. (cited in p. 2)
- IEA.** IEA, Global electric passenger car stock, 2010-2020, IEA, Paris. <https://www.iea.org/data-and-statistics/charts/global-electric-passenger-car-stock-2010-2020>. Accessed 22 March 2022. (cited in pp. 4 and 5)
- IEA.** IEA, World Energy Outlook 2020, Achieving net-zero emissions by 2050, IEA, Paris. <https://www.iea.org/reports/world-energy-outlook-2020/achieving-net-zero-emissions-by-2050>. Accessed 22 March 2022. (cited in p. 4)
- Imtenan S., Varman M., Masjuki H.H., Kalam M.A., Sajjad H., Arbab M.I. and Rizwanul Fattah I.M.** Impact of low temperature combustion attaining strategies on diesel engine emissions for diesel and biodiesels: A review. *Energy Conversion and Management*, Vol. 80 n° x, pp. 329–356, apr 2014. (cited in p. 10)
- Inagaki Kazuhisa, Fuyuto Takayuki, Nishikawa Kazuaki, Nakakita Kiyomi and Sakata Ichiro.** Dual-Fuel PCI Combustion Controlled by In-Cylinder Stratification of Ignitability. In *SAE Technical Paper Series*, volume 1, apr 2006. (cited in pp. 30 and 31)
- Indrajuana Armando, Bekdemir Cemil, Feru Emanuel and Willems Frank.** Towards Model-Based Control of RCCI-CDF Mode-Switching in Dual Fuel Engines. In *SAE Technical Paper*, pp. 1–13, apr 2018. (cited in pp. 36 and 38)

- Indrajuana Armando, Bekdemir Cemil, Luo Xi and Willems Frank.** Robust Multivariable Feedback Control of Natural Gas-Diesel RCCI Combustion. *IFAC-PapersOnLine*, Vol. 49 n° 11, pp. 217–222, 2016. (cited in pp. 36 and 38)
- Ingesson Gabriel, Yin Lianhao, Johansson Rolf and Tunestal Per.** Simultaneous Control of Combustion Timing and Ignition Delay in Multi-Cylinder Partially Premixed Combustion. *SAE International Journal of Engines*, Vol. 8 n° 5, pp. 2089–2098, 2015. (cited in p. 12)
- Ingesson Gabriel, Yin Lianhao, Johansson Rolf and Tunestål Per.** A Double-Injection Control Strategy For Partially Premixed Combustion. *IFAC-PapersOnLine*, Vol. 49 n° 11, pp. 353–360, 2016. (cited in pp. 76 and 121)
- Ingesson Gabriel, Yin Lianhao, Johansson Rolf and Tunestål Per.** Proportional–Integral Controller Design for Combustion-Timing Feedback, From n-Heptane to Iso-Octane in Compression–Ignition Engines. *Journal of Dynamic Systems, Measurement, and Control*, Vol. 140 n° 5, may 2018. (cited in pp. 89 and 147)
- IPCC.** IPCC, 2007: Climate Change 2007: Synthesis Report. Contribution of Working Groups I, II and III to the Fourth Assessment Report of the Intergovernmental Panel on Climate Change [Core Writing Team, Pachauri, R.K and Reisinger, A. (eds.)]. IPCC, Geneva, Switzerland, 104 pp. <https://www.ipcc.ch/report/ar4/syr/>. (cited in p. 1)
- IPCC.** IPCC, 2014: Climate Change 2014: Synthesis Report. Contribution of Working Groups I, II and III to the Fifth Assessment Report of the Intergovernmental Panel on Climate Change [Core Writing Team, R.K. Pachauri and L.A. Meyer (eds.)]. IPCC, Geneva, Switzerland, 151 pp. <https://www.ipcc.ch/report/ar5/syr/>. (cited in pp. 1, 2, and 3)
- IPCC.** IPCC, 2021: Summary for Policymakers. In: Climate Change 2021: The Physical Science Basis. Contribution of Working Group I to the Sixth Assessment Report of the Intergovernmental Panel on Climate Change [Masson-Delmotte, V., P. Zhai, A. Pirani, S. L. Connors, C. Péan, S. Berger, N. Caud, Y. Chen, L. Goldfarb, M. I. Gomis, M. Huang, K. Leitzell, E. Lonnoy, J.B.R. Matthews, T. K. Maycock, T. Waterfield, O. Yelekçi, R. Yu and B. Zhou (eds.)]. Cambridge University Press. In Press. <https://www.ipcc.ch/report/ar6/wg1/>. (cited in p. 1)
- Irdmoussa B K, Rizvi Syed Z, Velni J Mohammadpour, Naber J D and Shahbakhti M.** Data-driven Modeling and Predictive Control of Combustion Phasing for RCCI Engines. *2019 American Control Conference (ACC)*, pp. 1617–1622, 2019. (cited in pp. 36 and 39)
- Isermann Rolf.** *Engine Modeling and Control*. Springer Berlin Heidelberg, Berlin, Heidelberg, 2014. (cited in p. 12)
- Jambo Siti Azmah, Abdulla Rahmath, Mohd Azhar Siti Hajar, Marbawi Hartinie, Gansau Jualang Azlan and Ravindra Pogaku.** A review on third generation bioethanol feedstock. *Renewable and Sustainable Energy Reviews*, Vol. 65, pp. 756–769, nov 2016. (cited in p. 9)

- Johansson Thomas, Johansson Bengt, Tunestål Per and Aulin Hans.** HCCI Operating Range in a Turbo-charged Multi Cylinder Engine with VVT and Spray-Guided DI. In *SAE Technical Paper Series*, apr 2009. (cited in p. 75)
- Johnson Timothy and Joshi Ameya.** Review of Vehicle Engine Efficiency and Emissions. *SAE International Journal of Engines*, Vol. 11 n° 6, pp. 1307–1330, apr 2018. (cited in p. 6)
- Jorques Moreno Carlos, Stenlaas Ola and Tunestal Per.** Cylinder Pressure-Based Virtual Sensor for In-Cycle Pilot Mass Estimation. *SAE International Journal of Engines*, Vol. 11 n° 6, pp. 1167–1182, apr 2018. (cited in p. 55)
- Jorques Moreno Carlos, Stenlaas Ola and Tunestal Per.** In-Cycle Closed-Loop Combustion Control for Pilot Misfire Compensation. In *SAE Technical Papers*, number 2020, pp. 1–13, sep 2020. (cited in p. 12)
- Junfeng Zhao and Junmin Wang.** Energy-based and oxygen-based biodiesel blend level estimation methods for diesel engines. In *2012 American Control Conference (ACC)*, pp. 4975–4980. IEEE, jun 2012. (cited in p. 158)
- Jung Insoo, Jin Jaemin, Lee Dongchul, Lee Seunghyun, Yang Seungwook and Min Kyoungdoug.** Closed-Loop Control Method for Monitoring and Improving the Diesel Combustion Noise. In *SAE Technical Papers*, volume 2016-June, jun 2016. (cited in p. 12)
- Kalghatgi Gautam.** Is it really the end of internal combustion engines and petroleum in transport? *Applied Energy*, Vol. 225 n° February, pp. 965–974, sep 2018. (cited in p. 5)
- Kanda Tomohiro, Hakozaki Takazo, Uchimoto Tatsuya, Hatano Jyunichi, Kitayama Naoto and Sono Hiroshi.** PCCI Operation with Early Injection of Conventional Diesel Fuel. In *SAE Technical Papers*, volume 2005, apr 2005. (cited in p. 29)
- Karim Ghazi A.** A review of combustion processes in the dual fuel engine—The gas diesel engine. *Progress in Energy and Combustion Science*, Vol. 6 n° 3, pp. 277–285, jan 1980. (cited in p. 30)
- Kassa Mateos, Hall Carrie, Ickes Andrew and Wallner Thomas.** Modeling and control of fuel distribution in a dual-fuel internal combustion engine leveraging late intake valve closings. *International Journal of Engine Research*, Vol. 18 n° 8, pp. 797–809, 2017. (cited in pp. 125 and 158)
- Kazuhiro Nagatsu, Atsushi Inoue, Kota Matsumoto, Takashi Kaminaga, Toru Miyamoto and Takashi Youso.** Control device for compression ignition-type engine. U.S. Patent No. 9,719,441 B2., 2017. (cited in p. 12)
- Khandal S.V., Banapurmath N.R. and Gaitonde V.N.** Performance studies on homogeneous charge compression ignition (HCCI) engine powered with alternative fuels. *Renewable Energy*, Vol. 132 n° x, pp. 683–693, mar 2019. (cited in p. 10)

- Khodadadi Sadabadi K., Shahbakhti M., Bharath A. N. and Reitz R. D.** Modeling of combustion phasing of a reactivity-controlled compression ignition engine for control applications. *International Journal of Engine Research*, Vol. 17 n° 4, pp. 421–435, 2016.
(cited in pp. 36, 150, 151, and 152)
- Khodadadi Sadabadi Kaveh and Shahbakhti Mahdi.** Dynamic Modelling and Controller Design of Combustion Phasing for an RCCI Engine. In *Volume 2: Mechatronics; Mechatronics and Controls in Advanced Manufacturing; Modeling and Control of Automotive Systems and Combustion Engines; Modeling and Validation; Motion and Vibration Control Applications; Multi-Agent and Networked Systems; Path Pla.* American Society of Mechanical Engineers, oct 2016.
(cited in pp. 36, 38, and 106)
- Kiencke Uwe and Nielsen Lars.** *Automotive Control Systems: For Engine, Driveline, and Vehicle.* Springer Berlin Heidelberg, Berlin, Heidelberg, 2005.
(cited in pp. 11 and 128)
- Kim Jaeheun, Kakami Shinichi, Nishida Keiya and Ogata Yoichi.** Effects of ratio and dwell of split injection on fuel spray and mixture formation process under evaporating, non-reacting condition. In *SAE Technical Papers*, number December, dec 2019.
(cited in p. 169)
- Kim Seonguk and Min Kyoungdoug.** Detection of combustion start in the controlled auto ignition engine by wavelet transform of the engine block vibration signal. *Measurement Science and Technology*, Vol. 19 n° 8, pp. 085407, aug 2008.
(cited in p. 88)
- Kirsten Martin, Pirker Gerhard, Redtenbacher Christoph, Wimmer Andreas and Chmela Franz.** Advanced Knock Detection for Diesel/Natural Gas Engine Operation. *SAE International Journal of Engines*, Vol. 9 n° 3, pp. 1571–1583, apr 2016.
(cited in p. 120)
- Klos David and Kokjohn Sage L.** Investigation of the sources of combustion instability in low-temperature combustion engines using response surface models. *International Journal of Engine Research*, Vol. 16 n° 3, pp. 419–440, apr 2015.
(cited in p. 104)
- Klos David T and Kokjohn Sage L.** Investigation of the Effect of Injection and Control Strategies on Combustion Instability in Reactivity-Controlled Compression Ignition Engines. *Journal of Engineering for Gas Turbines and Power*, Vol. 138 n° 1, pp. 11502, 2016.
(cited in p. 87)
- Kokjohn S L, Hanson R M, Splitter D A and Reitz R D.** Fuel reactivity controlled compression ignition (RCCI): a pathway to controlled high-efficiency clean combustion. *International Journal of Engine Research*, Vol. 12 n° 3, pp. 209–226, 2011.
(cited in pp. 31, 77, and 184)
- Kokjohn Sage, Hanson Reed, Splitter Derek, Kaddatz John and Reitz Rolf.** Fuel Reactivity Controlled Compression Ignition (RCCI) Combustion in Light- and Heavy-Duty Engines. *SAE International Journal of Engines*, Vol. 4 n° 1, pp. 360–374, apr 2011.
(cited in p. 32)

- Kokjohn Sage L., Hanson Reed M., Splitter Derek A. and Reitz Rolf D.** Experiments and modeling of dual-fuel HCCI and PCCI combustion using in-cylinder fuel blending. *SAE International Journal of Engines*, Vol. 2 n° 2, pp. 24–39, nov 2010. (cited in pp. 31, 96, and 151)
- Kondipati Naga Nithin Teja, Arora Jayant Kumar, Bidarvatan Mehran and Shahbakhti Mahdi.** Modeling, design and implementation of a closed-loop combustion controller for an RCCI engine. In *2017 American Control Conference (ACC)*, pp. 4747–4752. IEEE, may 2017. (cited in pp. 36, 38, 147, and 150)
- Krishnamoorthi M., Malayalamurthi R., He Zhixia and Kandasamy Sabariswaran.** A review on low temperature combustion engines: Performance, combustion and emission characteristics. *Renewable and Sustainable Energy Reviews*, Vol. 116 n° September, pp. 109404, dec 2019. (cited in p. 10)
- Krishnan Sundar Rajan, Srinivasan Kalyan Kumar and Raihan Mostafa Shameem.** The effect of injection parameters and boost pressure on diesel-propane dual fuel low temperature combustion in a single-cylinder research engine. *Fuel*, Vol. 184, pp. 490–502, nov 2016. (cited in p. 98)
- Krstić Miroslav and Wang Hsin-Hsiung.** Stability of extremum seeking feedback for general nonlinear dynamic systems. *Automatica*, Vol. 36 n° 4, pp. 595–601, apr 2000. (cited in p. 107)
- Kubesh John and Brehob Diana D.** Analysis of Knock in a Dual-Fuel Engine. In *SAE Technical Papers*, oct 1992. (cited in p. 31)
- Kumar Pravin and Rehman A.** Bio-diesel in homogeneous charge compression ignition (HCCI) combustion. *Renewable and Sustainable Energy Reviews*, Vol. 56, pp. 536–550, apr 2016. (cited in p. 10)
- Kumar Saurav, Mohammadi Alireza, Quintero David, Rezazadeh Siavash, Gans Nicholas and Gregg Robert D.** Extremum Seeking Control for Model-Free Auto-Tuning of Powered Prosthetic Legs. *IEEE Transactions on Control Systems Technology*, Vol. 28 n° 6, pp. 2120–2135, nov 2020. (cited in p. 107)
- Kyrtatos Panagiotis, Brückner Clemens and Boulouchos Konstantinos.** Cycle-to-cycle variations in diesel engines. *Applied Energy*, Vol. 171, pp. 120–132, jun 2016. (cited in p. 125)
- Ladommatos N., Abdelhalim S. M., Zhao Hua and Hu Z.** The Dilution, Chemical, and Thermal Effects of Exhaust Gas Recirculation on Diesel Engine Emissions - Part 1: Effect of Reducing Inlet Charge Oxygen. In *SAE Technical Papers*, number 412, may 1996. (cited in p. 96)
- Ladommatos N., Abdelhalim S. M., Zhao Hua and Hu Z.** The Dilution, Chemical, and Thermal Effects of Exhaust Gas Recirculation on Diesel Engine Emissions - Part 2: Effects of Carbon Dioxide. In *SAE Technical Papers*, number 412, may 1996. (cited in p. 96)

- Lago Sari Rafael.** *Dual Mode Dual Fuel Combustion: Implementation on a Real Medium Duty Engine Platform.* PhD Thesis, Universitat Politècnica de València, 2021.
(cited in pp. 33 and 51)
- Lapuerta M., Armas O. and Hernández J.J.** Diagnosis of DI Diesel combustion from in-cylinder pressure signal by estimation of mean thermodynamic properties of the gas. *Applied Thermal Engineering*, Vol. 19 n° 5, pp. 513–529, may 1999.
(cited in pp. 69 and 70)
- Lee Byeongsoek, Oh Heechang, Han Seungkook, Woo Soohyung and Son Jinwook.** Development of High Efficiency Gasoline Engine with Thermal Efficiency over 42%. In *SAE Technical Papers*, volume 2017-October, oct 2017.
(cited in p. 6)
- Lee Byungho, Rizzoni Giorgio, Guezennec Yann, Soliman Ahmed, Cavalletti Mauro and Waters James.** Engine Control Using Torque Estimation. In *SAE Technical Papers*, number 724, mar 2001.
(cited in p. 88)
- Lee Kangyoon, Kwon Minsu, Sunwoo Myoungcho and Yoon Maru.** An in-cylinder pressure referencing method based on a variable polytropic coefficient. *SAE Technical Papers*, n° 2007-01-3535, 2007.
(cited in p. 59)
- Lehrheuer Bastian, Pischinger Stefan, Wick Maximilian, Andert Jakob, Berneck Dirk, Ritter Dennis, Albin Thivaharan and Thewes Matthias.** A Study on In-Cycle Combustion Control for Gasoline Controlled Autoignition. In *SAE Technical Papers*, volume 2016-April, apr 2016.
(cited in p. 12)
- Lehtveer Mariliis, Brynolf Selma and Grahn Maria.** What Future for Electrofuels in Transport? Analysis of Cost Competitiveness in Global Climate Mitigation. *Environmental Science & Technology*, Vol. 53 n° 3, pp. 1690–1697, feb 2019.
(cited in p. 9)
- Leith Doug J. and Leithead W. E.** Survey of gain-scheduling analysis and design. *International Journal of Control*, Vol. 73 n° 11, pp. 1001–1025, jan 2000.
(cited in p. 106)
- Leonhardt Steffen, Muller N. and Isermann Rolf.** Methods for engine supervision and control based on cylinder pressure information. *IEEE/ASME Transactions on Mechatronics*, Vol. 4 n° 3, pp. 235–245, 1999.
(cited in p. 12)
- Lešnik Luka, Kegl Breda, Torres-Jiménez Eloísa and Cruz-Peragón Fernando.** Why we should invest further in the development of internal combustion engines for road applications. *Oil & Gas Science and Technology – Revue d’IFP Energies nouvelles*, Vol. 75 n° 1, sep 2020.
(cited in p. 5)
- Lewander M., Widd A., Johansson B. and Tunestal P.** Steady state fuel consumption optimization through feedback control of estimated cylinder individual efficiency. *2012 American Control Conference (ACC)*, pp. 4210–4214, 2014.
(cited in p. 107)
- Lewander Magnus, Ekholm Kent, Johansson Bengt, Tunestål Per, Milovanovic Nebojsa, Keeler Nathan, Harcombe Tony and Bergstrand Pär.** Investigation of the combustion characteristics with focus on partially premixed combustion in a heavy duty engine. *SAE International Journal of Fuels and Lubricants*, Vol. 1 n° 1, pp. 1063–1074, jun 2009.
(cited in p. 29)

- Li Changle.** *Stratification and Combustion in the Transition from HCCI to PPC.* PhD Thesis, 2018. (cited in p. 112)
- Li Jing, Ling Xiang, Liu Deng, Yang Wenming and Zhou Dezhi.** Numerical study on double injection techniques in a gasoline and biodiesel fueled RCCI (reactivity controlled compression ignition) engine. *Applied Energy*, Vol. 211 n° August 2017, pp. 382–392, feb 2018. (cited in p. 31)
- Li Jing, Yang Wenming and Zhou Dezhi.** Review on the management of RCCI engines. *Renewable and Sustainable Energy Reviews*, Vol. 69 n° May 2016, pp. 65–79, 2017. (cited in pp. 10, 32, and 155)
- Li Ruixue C. and Zhu Guoming G.** A real-time pressure wave model for knock prediction and control. *International Journal of Engine Research*, Vol. 22 n° 3, pp. 986–1000, mar 2021. (cited in p. 77)
- Li Tie, Nishida Keiya, Zhang Yuyin, Yamakawa Masahisa and Hiroyasu Hiroyuki.** An Insight Into Effect of Split Injection on Mixture Formation and Combustion of DI Gasoline Engines. In *SAE Technical Papers*. SAE International, jun 2004. (cited in p. 169)
- Li Tie and Ogawa Hideyuki.** Analysis of the trade-off between soot and nitrogen oxides in diesel-Like combustion by chemical kinetic calculation. *SAE International Journal of Engines*, Vol. 5 n° 2, pp. 94–101, aug 2012. (cited in p. 10)
- Li Xuping, Anderson Paul, Jhong Huei-Ru Molly, Paster Mark, Stubbins James F. and Kenis Paul J. A.** Greenhouse Gas Emissions, Energy Efficiency, and Cost of Synthetic Fuel Production Using Electrochemical CO₂ Conversion and the Fischer–Tropsch Process. *Energy & Fuels*, Vol. 30 n° 7, pp. 5980–5989, jul 2016. (cited in p. 9)
- Li Yaopeng, Jia Ming, Chang Yachao, Xu Zhen, Xu Guangfu, Liu Hong and Wang Tianyou.** Principle of determining the optimal operating parameters based on fuel properties and initial conditions for RCCI engines. *Fuel*, Vol. 216 n° October 2017, pp. 284–295, mar 2018. (cited in p. 31)
- Li Yu, Li Hailin, Guo Hongsheng, Li Yongzhi and Yao Mingfa.** A numerical investigation on methane combustion and emissions from a natural gas-diesel dual fuel engine using CFD model. *Applied Energy*, Vol. 205 n° February, pp. 153–162, nov 2017. (cited in p. 6)
- Li Yun, Ang Kiam Heong and Chong Gregory C.Y.** PID control system analysis and design. *IEEE Control Systems*, Vol. 26 n° 1, pp. 32–41, feb 2006. (cited in p. 89)
- Lim Jae Hyung and Reitz Rolf D.** High Load (21 Bar IMEP) Dual Fuel RCCI Combustion Using Dual Direct Injection. *Journal of Engineering for Gas Turbines and Power*, Vol. 136 n° 10, pp. 101514, 2014. (cited in p. 32)
- Livengood J. C. and Wu P. C.** Correlation of autoignition phenomena in internal combustion engines and rapid compression machines. *Symposium (International) on Combustion*, Vol. 5 n° 1, pp. 347–356, 1955. (cited in p. 150)

- Lounici M.S., Benbellil M.A., Loubar K., Niculescu D.C. and Tazerout M.** Knock characterization and development of a new knock indicator for dual-fuel engines. *Energy*, Vol. 141, pp. 2351–2361, dec 2017. (cited in p. 120)
- Lu Xingcai, Han Dong and Huang Zhen.** Fuel design and management for the control of advanced compression-ignition combustion modes. *Progress in Energy and Combustion Science*, Vol. 37 n° 6, pp. 741–783, 2011. (cited in pp. 12 and 30)
- Lujan Jose, Pla Benjamin, Bares Pau and Aramburu Alexandra.** Optimal Sensor Placement for High Pressure and Low Pressure EGR Estimation. In *SAE Technical Papers*, number 2021, pp. 1–11, apr 2021. (cited in p. 157)
- Ma Fanhua, Wang Yu, Wang Junjun, Ding Shangfen, Wang Yefu and Zhao Shuli.** Effects of Combustion Phasing, Combustion Duration, and Their Cyclic Variations on Spark-Ignition (SI) Engine Efficiency. *Energy & Fuels*, Vol. 22 n° 5, pp. 3022–3028, sep 2008. (cited in p. 73)
- Macian V., Lujan J.M., Guardiola Carlos and Yuste Pedro.** DFT-based controller for fuel injection unevenness correction in turbocharged diesel engines. *IEEE Transactions on Control Systems Technology*, Vol. 14 n° 5, pp. 819–827, sep 2006. (cited in p. 162)
- Malaczynski Gerard, Roth Gregory and Johnson Donald.** Ion-sense-based real-time combustion sensing for closed loop engine control. *SAE International Journal of Engines*, Vol. 6 n° 1, pp. 267–277, apr 2013. (cited in p. 88)
- Martin Jonathan and Boehman André.** Mapping the combustion modes of a dual-fuel compression ignition engine. *International Journal of Engine Research*, may 2021. (cited in p. 34)
- Mashkournia Masoud, Audet Adrian and Koch Charles Robert.** Knock Detection and Control in an HCCI Engine Using DWT. In *ASME 2011 Internal Combustion Engine Division Fall Technical Conference*, pp. 391–399. ASMEDC, jan 2011. (cited in p. 121)
- Mayhew Christopher G., Knierim Karl Lukas, Chaturvedi Nalin A., Park Sungbae, Ahmed Jasim and Kojic Aleksandar.** Reduced-order modeling for studying and controlling misfire in four-stroke HCCI engines. *Proceedings of the IEEE Conference on Decision and Control*, n° 1, pp. 5194–5199, 2009. (cited in p. 150)
- McBride Bonnie J.** *NASA Glenn coefficients for calculating thermodynamic properties of individual species.* National Aeronautics and Space Administration, John H. Glenn Research Center, 2002. (cited in p. 69)
- Michał Krzyżanowski, Birgit Kuna-Dibbert and Jürgen Schneider.** *Health effects of transport-related air pollution.* WHO Regional Office Europe, 2005. (cited in p. 7)
- Millo F. and Ferraro C. V.** Knock in S.I. Engines: A Comparison between Different Techniques for Detection and Control. In *SAE Technical Papers*, number 724, oct 1998. (cited in p. 61)
- Mirheidari Saleh, Franchek Matthew, Grigoriadis Karolos, Mohammadpour Javad, Wang Yue-Yun and Haskara Ibrahim.** Real-time and robust estimation of biodiesel blends. *Fuel*, Vol. 92 n° 1, pp. 37–48, feb 2012. (cited in p. 158)

- Mohan Balaji, Yang Wenming and Chou Siaw Kiang.** Fuel injection strategies for performance improvement and emissions reduction in compression ignition engines—A review. *Renewable and Sustainable Energy Reviews*, Vol. 28 n° x, pp. 664–676, dec 2013. (cited in p. 7)
- Molina S., Garcia A., Pastor J. M., Belarte E. and Balloul I.** Operating range extension of RCCI combustion concept from low to full load in a heavy-duty engine. *Applied Energy*, Vol. 143, pp. 211–227, 2015. (cited in p. 32)
- Moulin Philippe, Corde Gilles, Castagné Michel and Rousseau Grégory.** Cylinder Individual AFR Estimation based on a Physical Model and using Kalman Filters. In *SAE Technical Paper*, number 724, mar 2004. (cited in p. 158)
- Munawer Muhammad Ehsan.** Human health and environmental impacts of coal combustion and post-combustion wastes. *Journal of Sustainable Mining*, Vol. 17 n° 2, pp. 87–96, 2018. (cited in p. 7)
- Naber Jeffrey, Blough Jason R., Frankowski Dave, Goble Monroe and Szpytman John E.** Analysis of Combustion Knock Metrics in Spark-Ignition Engines. In *SAE Technical Papers*, volume 2006, apr 2006. (cited in p. 129)
- Nates R.J. and Yates A. D. B.** Knock Damage Mechanisms in Spark-Ignition Engines. In *SAE Technical Papers*, number 412, oct 1994. (cited in p. 61)
- Nazemi M. and Shahbakhti M.** Modeling and analysis of fuel injection parameters for combustion and performance of an RCCI engine. *Applied Energy*, Vol. 165, pp. 135–150, mar 2016. (cited in p. 31)
- Nigam Poonam Singh and Singh Anoop.** Production of liquid biofuels from renewable resources. *Progress in Energy and Combustion Science*, Vol. 37 n° 1, pp. 52–68, feb 2011. (cited in p. 9)
- Noehre Christof, Andersson Magnus, Johansson Bengt and Hultqvist Anders.** Characterization of Partially Premixed Combustion. In *SAE Technical Papers*, number 724, pp. 776–790, oct 2006. (cited in p. 29)
- Norouzi Armin, Heidarifar Hamed, Shahbakhti Mahdi, Koch Charles Robert and Borhan Hoseinali.** Model Predictive Control of Internal Combustion Engines: A Review and Future Directions. *Energies*, Vol. 14 n° 19, pp. 6251, oct 2021. (cited in pp. 11 and 148)
- Novella Ricardo, Pla Benjamin, Bares Pau and Martinez-Hernandez Pablo José.** Closed-Loop Combustion Control by Extremum Seeking with the Passive-Chamber Ignition Concept in SI Engines. In *SAE Technical Papers*, volume 2020-April, pp. 1–11, apr 2020. (cited in p. 107)
- OICA.** OICA, retrieved from Statista: Number of passenger cars and commercial vehicles in use worldwide from 2006 to 2015 in (1,000 units). <https://www.statista.com/statistics/281134/number-of-vehicles-in-use-worldwide/>. Accessed 22 March 2022. (cited in p. 2)

- Olsson Jan-Ola, Tunestål Per, Haraldsson Göran and Johansson Bengt.** A Turbo Charged Dual Fuel HCCI Engine. In *SAE Technical Papers*, number 724, may 2001. (cited in pp. 10 and 31)
- Olsson Jan-ola, Tunestål Per and Johansson Bengt.** Closed-Loop Control of an HCCI Engine. In *SAE Technical Paper*, mar 2001. (cited in pp. 12, 34, 35, and 37)
- Ott T., Zurbriggen F., Onder C. and Guzzella L.** Cylinder Individual Feedback Control of Combustion in a Dual Fuel Engine. *IFAC Proceedings Volumes*, Vol. 46 n° 21, pp. 600–605, 2013. (cited in pp. 34, 37, and 121)
- Oumer A.N., Hasan M.M., Baheta Aklilu Tesfamichael, Mamat Rizalman and Abdullah A.A.** Bio-based liquid fuels as a source of renewable energy: A review. *Renewable and Sustainable Energy Reviews*, Vol. 88 n° October 2017, pp. 82–98, may 2018. (cited in p. 9)
- P. Forster, Ramaswamy V., Artaxo P., Berntsen T., Betts R., Fahey D.W., Haywood J., Lean J., Lowe D.C., Myhre G., Nganga J., Prinn R., Raga G., Schulz M. and Dorland R. Van.** Changes in Atmospheric Constituents and in Radiative Forcing. In: *Climate Change 2007: The Physical Science Basis. Contribution of Working Group I to the Fourth Assessment Report of the Intergovernmental Panel on Climate Change* [Solomon, S., D. Qin, M. Manning, Z. Chen, M. Marquis, K.B. Averyt, M. Tignor and H.L. Miller (eds.)]. Cambridge University Press, Cambridge, United Kingdom and New York, NY, USA. <https://www.ipcc.ch/site/assets/uploads/2018/02/ar4-wg1-chapter2-1.pdf>. (cited in p. 1)
- Pachiannan Tamilselvan, Zhong Wenjun, Rajkumar Sundararajan, He Zhixia, Leng Xianying and Wang Qian.** A literature review of fuel effects on performance and emission characteristics of low-temperature combustion strategies. *Applied Energy*, Vol. 251 n° 301, pp. 113380, oct 2019. (cited in pp. 10 and 11)
- Paykani Amin, Garcia Antonio, Shahbakhti Mahdi, Rahnama Pourya and Reitz Rolf D.** Reactivity controlled compression ignition engine: Pathways towards commercial viability. *Applied Energy*, Vol. 282 n° PA, pp. 116174, jan 2021. (cited in pp. 33 and 168)
- Paykani Amin, Kakaee Amir-Hasan, Rahnama Pourya and Reitz Rolf D.** Progress and recent trends in reactivity-controlled compression ignition engines. *International Journal of Engine Research*, Vol. 17 n° 5, pp. 481–524, jun 2016. (cited in p. 77)
- Payri F., Benajes J., Margot X. and Gil A.** CFD modeling of the in-cylinder flow in direct-injection Diesel engines. *Computers & Fluids*, Vol. 33 n° 8, pp. 995–1021, sep 2004. (cited in p. 6)
- Payri F., Broatch A., Salavert J. M. and Martín J.** Investigation of diesel combustion using multiple injection strategies for idling after cold start of passenger-car engines. *Experimental Thermal and Fluid Science*, Vol. 34 n° 7, pp. 857–865, 2010. (cited in pp. 74 and 90)

- Payri F., Broatch A., Tormos B. and Marant V.** New methodology for in-cylinder pressure analysis in direct injection diesel engines - Application to combustion noise. *Measurement Science and Technology*, Vol. 16 n° 2, pp. 540–547, 2005. (cited in p. 59)
- Payri F., Luján J. M., Guardiola C. and Rizzoni G.** Injection diagnosis through common-rail pressure measurement. *Proceedings of the Institution of Mechanical Engineers, Part D: Journal of Automobile Engineering*, Vol. 220 n° 3, pp. 347–357, 2006. (cited in pp. 158 and 162)
- Payri F., Luján J. M., Martín J. and Abbad A.** Digital signal processing of in-cylinder pressure for combustion diagnosis of internal combustion engines. *Mechanical Systems and Signal Processing*, Vol. 24 n° 6, pp. 1767–1784, 2010. (cited in p. 59)
- Payri F., Luján JM, Guardiola C. and Pla B.** A Challenging Future for the IC Engine: New Technologies and the Control Role. *Oil & Gas Science and Technology – Revue d’IFP Energies nouvelles*, Vol. 70 n° 1, pp. 15–30, jun 2015. (cited in p. 11)
- Payri F., Molina S., Martín J. and Armas O.** Influence of measurement errors and estimated parameters on combustion diagnosis. *Applied Thermal Engineering*, Vol. 26 n° 2-3, pp. 226–236, 2006. (cited in p. 71)
- Payri F., Olmeda P., Guardiola C. and Martín J.** Adaptive determination of cut-off frequencies for filtering the in-cylinder pressure in diesel engines combustion analysis. *Applied Thermal Engineering*, Vol. 31 n° 14-15, pp. 2869–2876, oct 2011. (cited in p. 59)
- Payri Francisco, Lujan Jose, Climent Hector and Pla Benjamín.** Effects of the Intake Charge Distribution in HSDI Engines. *SAE Technical Paper Series*, Vol. 1, 2010. (cited in pp. 125 and 161)
- Pearson Richard J., Eisaman Matthew D., Turner James W. G., Edwards Peter P., Jiang Zheng, Kuznetsov Vladimir L., Littau Karl A., di Marco Leon and Taylor S. R. Gordon.** Energy Storage via Carbon-Neutral Fuels Made From CO₂, Water, and Renewable Energy. *Proceedings of the IEEE*, Vol. 100 n° 2, pp. 440–460, feb 2012. (cited in p. 9)
- Persson H, Pfeiffer R, Hultqvist A, Johansson B and Ström H.** Cylinder-to-Cylinder and Cycle-to-Cycle Variations at HCCI Operation With Trapped Residuals. In *SAE Technical Paper Series*, volume 2005, apr 2005. (cited in p. 30)
- Peyton Jones James C., Spelina Jill M. and Frey Jesse.** Optimizing knock thresholds for improved knock control. *International Journal of Engine Research*, Vol. 15 n° 1, pp. 123–132, jan 2014. (cited in pp. 120 and 128)
- Pipitone Emiliano and Beccari Alberto.** Determination of TDC in internal combustion engines by a newly developed thermodynamic approach. *Applied Thermal Engineering*, Vol. 30 n° 14-15, pp. 1914–1926, oct 2010. (cited in p. 57)
- Pla Benjamín, Bares Pau, Jiménez Irina, Guardiola Carlos, Zhang Yahui and Shen Tielong.** A fuzzy logic map-based knock control for spark ignition engines. *Applied Energy*, Vol. 280 n° May, pp. 116036, dec 2020. (cited in p. 120)

- Pla Benjamin, De La Morena Joaquin, Bares Pau and Jiménez Irina.** Knock Analysis in the Crank Angle Domain for Low-Knocking Cycles Detection. In *SAE Technical Papers*, volume 2020-April, pp. 1–11, apr 2020. (cited in p. 61)
- Ponti Fabrizio.** In-Cylinder Pressure Measurement: Requirements for On-Board Engine Control. *Journal of Engineering for Gas Turbines and Power*, Vol. 130 n° 3, pp. 032803, 2008. (cited in p. 59)
- Powell J. David.** Engine Control Using Cylinder Pressure: Past, Present, and Future. *Journal of Dynamic Systems, Measurement, and Control*, Vol. 115 n° 2B, pp. 343–350, jun 1993. (cited in p. 12)
- Praveena V. and Martin M. Leenus Jesu.** A review on various after treatment techniques to reduce NOx emissions in a CI engine. *Journal of the Energy Institute*, Vol. 91 n° 5, pp. 704–720, oct 2018. (cited in p. 8)
- Rausen D. J., Stefanopoulou A. G., Kang J.-M., Eng J. A. and Kuo T.-W.** A Mean-Value Model for Control of Homogeneous Charge Compression Ignition (HCCI) Engines. *Journal of Dynamic Systems, Measurement, and Control*, Vol. 127 n° 3, pp. 355, 2005. (cited in pp. 149 and 150)
- Raut A., Irdmoussa B.K. and Shahbakhti M.** Dynamic modeling and model predictive control of an RCCI engine. *Control Engineering Practice*, Vol. 81 n° June, pp. 129–144, dec 2018. (cited in pp. 36 and 38)
- Raut Akshat, Bidarvatan Mehran, Borhan Hoseinali and Shahbakhti Mahdi.** Model Predictive Control of an RCCI Engine. In *2018 Annual American Control Conference (ACC)*, pp. 1604–1609. IEEE, jun 2018. (cited in pp. 36, 106, 148, and 157)
- Ravaglioli Vittorio, Carra Filippo, Moro Davide, De Cesare Matteo and Stola Federico.** Remote Sensing Methodology for the Closed-Loop Control of RCCI Dual Fuel Combustion. In *SAE Technical Papers*, volume 2018-April, pp. 1–10, apr 2018. (cited in pp. 34 and 88)
- Ravi Nikhil, Roelle Matthew J., Liao Hsien Hsin, Jungkunz Adam F., Chang Chen Fang, Park Sungbae and Gerdes J. Christian.** Model-based control of HCCI engines using exhaust recompression. *IEEE Transactions on Control Systems Technology*, Vol. 18 n° 6, pp. 1289–1302, 2010. (cited in p. 148)
- Reif Konrad.** *Diesel Engine Management*. Springer Fachmedien Wiesbaden, Wiesbaden, 2014. (cited in p. 57)
- Reitz Rolf D.** Directions in internal combustion engine research. *Combustion and Flame*, Vol. 160 n° 1, pp. 1–8, 2013. (cited in p. 29)
- Reitz Rolf D. and Duraisamy Ganesh.** Review of high efficiency and clean reactivity controlled compression ignition (RCCI) combustion in internal combustion engines. *Progress in Energy and Combustion Science*, Vol. 46, pp. 12–71, 2015. (cited in p. 32)
- Reşitoğlu İbrahim Aslan, Altinişik Kemal and Keskin Ali.** The pollutant emissions from diesel-engine vehicles and exhaust aftertreatment systems. *Clean Technologies and Environmental Policy*, Vol. 17 n° 1, pp. 15–27, jan 2015. (cited in p. 8)

- Ritchie Hannah.** Cars, planes, trains: where do CO₂ emissions from transport come from? <https://ourworldindata.org/co2-emissions-from-transport#licence>. Accessed 22 March 2022. (cited in p. 4)
- Ritchie Hannah and Roser Max.** CO₂ and Greenhouse Gas Emissions. *Our World in Data*, 2020. <https://ourworldindata.org/co2-and-other-greenhouse-gas-emissions>. (cited in pp. 1, 2, and 3)
- Ritchie Hannah and Roser Max.** Energy. *Our World in Data*, 2020. <https://ourworldindata.org/energy>. (cited in p. 5)
- Robert Anthony, Truffin Karine, Iafate Nicolas, Jay Stephane, Colin Olivier and Angelberger Christian.** Large-eddy simulation analysis of knock in a direct injection spark ignition engine. *International Journal of Engine Research*, Vol. 20 n° 7, pp. 765–776, sep 2019. (cited in p. 125)
- Rogers David R.** *Engine Combustion: Pressure Measurement and Analysis*. SAE international Warrendale, PA, 2010. (cited in pp. 12, 56, and 63)
- Russell April and Epling William S.** Diesel Oxidation Catalysts. *Catalysis Reviews*, Vol. 53 n° 4, pp. 337–423, oct 2011. (cited in p. 8)
- Salvi B.L. and Subramanian K.A.** Sustainable development of road transportation sector using hydrogen energy system. *Renewable and Sustainable Energy Reviews*, Vol. 51, pp. 1132–1155, nov 2015. (cited in p. 9)
- Saracino Roberto, Gaballo Maria Rosaria, Mannal Soenke, Motz Stefan, Carlucci Antonio and Benegiamo Marco.** Cylinder Pressure-Based Closed Loop Combustion Control: A Valid Support to Fulfill Current and Future Requirements of Diesel Powertrain Systems. In *SAE Technical Papers*, volume 2015, sep 2015. (cited in pp. 12 and 88)
- Saxena Samveg and Bedoya Iván D.** Fundamental phenomena affecting low temperature combustion and HCCI engines, high load limits and strategies for extending these limits. *Progress in Energy and Combustion Science*, Vol. 39 n° 5, pp. 457–488, oct 2013. (cited in p. 10)
- Schemme Steffen, Samsun Remzi Can, Peters Ralf and Stolten Detlef.** Power-to-fuel as a key to sustainable transport systems – An analysis of diesel fuels produced from CO₂ and renewable electricity. *Fuel*, Vol. 205, pp. 198–221, oct 2017. (cited in p. 9)
- Schmidt Martin, Kimmich Frank, Straky Harald and Isermann Rolf.** Combustion Supervision by Evaluating the Crankshaft Speed and Acceleration. In *SAE Technical Papers*, number 724, mar 2000. (cited in p. 88)
- Scholl David, Davis Craig, Russ Stephen and Barash Terry.** The Volume Acoustic Modes of Spark-Ignited Internal Combustion Chambers. In *SAE Technical Papers*, number 724, feb 1998. (cited in p. 62)
- Selim Mohamed Y.E.** Combustion Noise Measurements and Control from Small Diesel and Dual Fuel Engines. In *SAE Technical Papers*, volume 2004-Septe, sep 2004. (cited in p. 120)

- Sellnau Mark C., Matekunas Frederic A., Battiston Paul A., Chang Chen-Fang and Lancaster David R.** Cylinder-Pressure-Based Engine Control Using Pressure-Ratio-Management and Low-Cost Non-Intrusive Cylinder Pressure Sensors. In *SAE Technical Papers*, number 724, mar 2000. (cited in p. 88)
- Senecal P.K. and Leach Felix.** Diversity in transportation: Why a mix of propulsion technologies is the way forward for the future fleet. *Results in Engineering*, Vol. 4 n° October, pp. 100060, dec 2019. (cited in p. 5)
- Shahbakhti Mahdi and Koch Charles Robert.** Control oriented modeling of combustion phasing for an HCCI engine. *Proceedings of the American Control Conference*, n° Ivc, pp. 3694–3699, 2007. (cited in pp. 34 and 152)
- Shahbakhti Mahdi and Koch Charles Robert.** Physics Based Control Oriented Model for HCCI Combustion Timing. *Journal of Dynamic Systems, Measurement, and Control*, Vol. 132 n° 2, pp. 021010, 2010. (cited in pp. 34 and 148)
- Shahlari Arsham J., Hocking Chris, Kurtz Eric and Ghandhi Jaal.** Comparison of compression ignition engine noise metrics in low-temperature combustion regimes. *SAE International Journal of Engines*, Vol. 6 n° 1, pp. 541–552, apr 2013. (cited in p. 77)
- Shaver G M, Gerdes J C and Roelle M.** Physics-based closed-loop control of phasing, peak pressure and work output in HCCI engines utilizing variable valve actuation. *Proceedings of the American Control Conference*, Vol. 1, pp. 150–155, 2004. (cited in p. 147)
- Shim Euijoon, Park Hyunwook and Bae Choongsik.** Comparisons of advanced combustion technologies (HCCI, PCCI, and dual-fuel PCCI) on engine performance and emission characteristics in a heavy-duty diesel engine. *Fuel*, Vol. 262 n° November 2019, pp. 116436, feb 2020. (cited in p. 87)
- Siano Daniela, Panza Maria Antonietta and D’Agostino Danilo.** Knock detection based on MAPO analysis, AR model and discrete wavelet transform applied to the in-cylinder pressure data: Results and comparison. *SAE International Journal of Engines*, Vol. 8 n° 1, pp. 1–13, oct 2015. (cited in p. 55)
- Singh Ajay, Saxena Mohit Raj and Maurya Rakesh Kumar.** Investigation of Nature of Cyclic Combustion Variations in RCCI Engine. In *Lecture Notes in Mechanical Engineering*, pp. 589–598. Springer Science and Business Media Deutschland GmbH, 2021. (cited in p. 104)
- Singh Akhilendra Pratap and Agarwal Avinash Kumar.** Combustion characteristics of diesel HCCI engine: An experimental investigation using external mixture formation technique. *Applied Energy*, Vol. 99, pp. 116–125, nov 2012. (cited in p. 87)
- Sinigaglia Tiago, Lewiski Felipe, Santos Martins Mario Eduardo and Mairesse Siluk Julio Cezar.** Production, storage, fuel stations of hydrogen and its utilization in automotive applications—a review. *International Journal of Hydrogen Energy*, Vol. 42 n° 39, pp. 24597–24611, sep 2017. (cited in p. 9)

- Sjöberg Magnus and Dec John E.** Effects of Engine Speed, Fueling Rate, and Combustion Phasing on the Thermal Stratification Required to Limit HCCI Knocking Intensity. In *SAE Technical Papers*, may 2005. (cited in p. 120)
- Snyder David B., Adi Gayatri H., Bunce Michael P., Satkoski Christopher A. and Shaver Gregory M.** Fuel blend fraction estimation for fuel-flexible combustion control: Uncertainty analysis. *Control Engineering Practice*, Vol. 18 n° 4, pp. 418–432, apr 2010. (cited in p. 158)
- Solouk Ali and Shahbakhti Mahdi.** Energy Optimization and Fuel Economy Investigation of a Series Hybrid Electric Vehicle Integrated with Diesel/RCCI Engines. *Energies*, Vol. 9 n° 12, pp. 1020, dec 2016. (cited in p. 10)
- Spelina Jill M., Peyton Jones James C. and Frey Jesse.** Stochastic simulation and analysis of a classical knock controller. *International Journal of Engine Research*, Vol. 16 n° 3, pp. 461–473, apr 2015. (cited in p. 128)
- Splitter Derek, Hanson Reed, Kokjohn Sage and Reitz Rolf D.** Reactivity Controlled Compression Ignition (RCCI) Heavy-Duty Engine Operation at Mid-and High-Loads with Conventional and Alternative Fuels. In *SAE 2011 World Congress and Exhibition*, volume 1, apr 2011. (cited in p. 31)
- Splitter Derek, Hanson Reed, Kokjohn Sage, Wissink Martin and Reitz Rolf D.** Injection Effects in Low Load RCCI Dual-Fuel Combustion. In *SAE Technical Paper*, sep 2011. (cited in p. 31)
- Splitter Derek, Wissink Martin, DelVescovo Dan and Reitz Rolf D.** RCCI Engine Operation Towards 60% Thermal Efficiency. *SAE Technical Paper Series*, Vol. 1 n° X, 2013. (cited in p. 32)
- Splitter Derek, Wissink Martin, Kokjohn Sage and Reitz Rolf D.** Effect of Compression Ratio and Piston Geometry on RCCI Load Limits and Efficiency. *SAE Technical Paper*, 2012. (cited in p. 32)
- Splitter Derek A. and Reitz Rolf D.** Fuel reactivity effects on the efficiency and operational window of dual-fuel compression ignition engines. *Fuel*, Vol. 118, pp. 163–175, 2014. (cited in p. 87)
- Stanglmaier Rudolf H and Roberts Charles E.** Homogeneous Charge Compression Ignition (HCCI): Benefits, Compromises, and Future Engine Applications. In *SAE Technical Paper*, number 724, 1999. (cited in pp. 10 and 30)
- Stępień Zbigniew.** A Comprehensive Overview of Hydrogen-Fueled Internal Combustion Engines: Achievements and Future Challenges. *Energies*, Vol. 14 n° 20, oct 2021. (cited in p. 9)
- Strandh Petter, Bengtsson Johan, Johansson Rolf, Tunestål Per and Johansson Bengt.** Cycle-to-Cycle Control of a Dual-Fuel HCCI Engine. In *SAE Technical Paper*, volume 2004, mar 2004. (cited in pp. 34, 37, and 148)

- Strandh Petter, Christensen Magnus, Bengtsson Johan, Johansson Rolf, Vressner Andreas, Tunestål Per and Johansson Bengt.** Ion Current Sensing for HCCI Combustion Feedback. In *SAE Technical Paper Series*, oct 2003. (cited in p. 88)
- Sui Wenbo, González Jorge Pulpeiro and Hall Carrie M.** Combustion Phasing Modelling of Dual Fuel Engines. *IFAC-PapersOnLine*, Vol. 51 n° 31, pp. 319–324, 2018. (cited in p. 36)
- Suzuki Kenji, Shen Tielong, Kako Junichi and Oguri Yasufumi.** Individual A/F control with fuel-gas ratio estimation for multi-cylinder IC engines. *Proceedings of the American Control Conference*, pp. 5094–5099, 2007. (cited in p. 158)
- Taglialatela F., Moselli G. and Lavorgna M.** Engine knock detection and control using in-cylinder pressure signal and soft computing techniques. In *SAE Technical Papers*, volume 2005-Septe, sep 2005. (cited in p. 55)
- Taglialatela-Scafati Ferdinando, Cesario Nicola, Lavorgna Mario, Mancaruso Ezio and Vaglieco Bianca Maria.** Diagnosis and Control of Advanced Diesel Combustions using Engine Vibration Signal. In *SAE Technical Papers*, apr 2011. (cited in p. 88)
- Tamaki Shunpei, Sakayanagi Yoshihiro, Sekiguchi Kazuma, Ibuki Tatsuya, Tahara Kohei and Sampei Mitsuji.** On-line Feedforward Map Generation for Engine Ignition Timing Control. *IFAC Proceedings Volumes*, Vol. 47 n° 3, pp. 5691–5696, 2014. (cited in p. 173)
- Tan Qingyuan, Divekar Prasad S., Tan Ying, Chen Xiang and Zheng Ming.** Pressure Sensor Data-Driven Optimization of Combustion Phase in a Diesel Engine. *IEEE/ASME Transactions on Mechatronics*, Vol. 25 n° 2, pp. 694–704, apr 2020. (cited in pp. 107 and 108)
- Tan Y., Moase W. H., Manzie C., Nešić D. and Mareels I. M.Y.** Extremum seeking from 1922 to 2010. *Proceedings of the 29th Chinese Control Conference, CCC'10*, pp. 14–26, 2010. (cited in p. 107)
- Tang Jian, Zhu Guoming G. and Men Yifan.** Review of engine control-oriented combustion models. *International Journal of Engine Research*, feb 2021. (cited in p. 147)
- Tang Qinglong, Liu Haifeng, Li Mingkun, Yao Mingfa and Li Zhongshan.** Study on ignition and flame development in gasoline partially premixed combustion using multiple optical diagnostics. *Combustion and Flame*, Vol. 177, pp. 98–108, mar 2017. (cited in p. 6)
- Thor Mikael, Egardt Bo, McKelvey Tomas and Andersson Ingemar.** Closed-loop diesel engine combustion phasing control based on crankshaft torque measurements. *Control Engineering Practice*, Vol. 33, pp. 115–124, dec 2014. (cited in pp. 12 and 88)
- Thring R. H.** Homogeneous-Charge Compression-Ignition (HCCI) Engines. In *SAE Technical Paper Series*, sep 1989. (cited in p. 10)

- Tietge Uwe, Mock Peter and Dornoff Jan.** CO₂ emissions from new passenger cars in Europe: Car manufacturers' performance in 2019, 2020. <https://theict.org/publications/co2-new-passenger-cars-europe-aug2020>. (cited in p. 4)
- Torregrosa A.J., Broatch A., Novella R., Gomez-Soriano J. and Mónico L.F.** Impact of gasoline and Diesel blends on combustion noise and pollutant emissions in Premixed Charge Compression Ignition engines. *Energy*, Vol. 137, pp. 58–68, oct 2017. (cited in p. 29)
- TransportPolicy.** EU: Heavy-duty: Emissions. <https://www.transportpolicy.net/standard/eu-heavy-duty-emissions/>. Accessed 22 March 2022. (cited in p. 8)
- Tree Dale R. and Svensson Kenth I.** Soot processes in compression ignition engines. *Progress in Energy and Combustion Science*, Vol. 33 n° 3, pp. 272–309, jun 2007. (cited in p. 10)
- Tunestål Per.** Model Based TDC Offset Estimation from Motored Cylinder Pressure Data. *IFAC Proceedings Volumes*, Vol. 42 n° 26, pp. 241–247, 2009. (cited in p. 57)
- Tunestål Per.** Self-tuning gross heat release computation for internal combustion engines. *Control Engineering Practice*, Vol. 17 n° 4, pp. 518–524, 2009. (cited in pp. 71 and 158)
- Tunestål Per and Hedrick J. Karl.** Cylinder air/fuel ratio estimation using net heat release data. *Control Engineering Practice*, Vol. 11 n° 3, pp. 311–318, 2003. (cited in p. 158)
- Turesson Gabriel.** *Model-Based Optimization of Combustion-Engine Control*. PhD Thesis, 2018. (cited in p. 148)
- Twigg Martyn V.** Progress and future challenges in controlling automotive exhaust gas emissions. *Applied Catalysis B: Environmental*, Vol. 70 n° 1-4, pp. 2–15, jan 2007. (cited in p. 8)
- UNECE.** United Nations Economic Commission for Europe, Addendum 48: Regulation No. 49, Revision 6. Concerning the Adoption of Uniform Technical Prescriptions for Wheeled Vehicles, Equipment and Parts which can be fitted and/or be used on Wheeled Vehicles and the Conditions for Reciprocal Recognition of Approvals Granted on the Basis of these Prescriptions, 2013. (cited in p. 119)
- Van Alstine Daniel G, Kocher Lyle E, Koeberlein Ed, Stricker Karla and Shaver Gregory M.** Control-oriented premixed charge compression ignition combustion timing model for a diesel engine utilizing flexible intake valve modulation. *International Journal of Engine Research*, Vol. 14 n° 3, pp. 211–230, jun 2013. (cited in p. 147)
- van der Weijst Robert, van Keulen Thijs and Willems Frank.** Constrained multi-variable extremum-seeking for online fuel-efficiency optimization of Diesel engines. *Control Engineering Practice*, Vol. 87 n° March, pp. 133–144, jun 2019. (cited in p. 107)
- Verhelst S.** Recent progress in the use of hydrogen as a fuel for internal combustion engines. *International Journal of Hydrogen Energy*, Vol. 39 n° 2, pp. 1071–1085, jan 2014. (cited in p. 9)

- Vressner Andreas, Lundin Andreas, Christensen Magnus, Tunestål Per and Johansson Bengt.** Pressure Oscillations During Rapid HCCI Combustion. In *SAE Technical Papers*, volume 2003, oct 2003. (cited in p. 61)
- Vulli S., Dunne J.F., Potenza R., Richardson D. and King P.** Time-frequency analysis of single-point engine-block vibration measurements for multiple excitation-event identification. *Journal of Sound and Vibration*, Vol. 321 n° 3-5, pp. 1129–1143, apr 2009. (cited in p. 129)
- Wang Jinli, Yang Fuyuan and Ouyang Minggao.** Dieseline fueled flexible fuel compression ignition engine control based on in-cylinder pressure sensor. *Applied Energy*, Vol. 159, pp. 87–96, dec 2015. (cited in p. 158)
- Wang Tianbo, Chang Siqin, Liu Liang, Zhu Jianhui and Xu Yaxuan.** Individual cylinder air–fuel ratio estimation and control for a large-bore gas fuel engine. *International Journal of Distributed Sensor Networks*, Vol. 15 n° 2, feb 2019. (cited in p. 158)
- Wang Wenyi, Li Yaoyu and Hu Bin.** Real-time efficiency optimization of a cascade heat pump system via multivariable extremum seeking. *Applied Thermal Engineering*, Vol. 176 n° November 2019, pp. 115399, jul 2020. (cited in p. 107)
- Wang Yifeng, Yao Mingfa, Li Tie, Zhang Weijing and Zheng Zunqing.** A parametric study for enabling reactivity controlled compression ignition (RCCI) operation in diesel engines at various engine loads. *Applied Energy*, Vol. 175, pp. 389–402, 2016. (cited in pp. 32 and 157)
- Wang Ying, Guo Chunlan, Wang Peng and Wang Dongxing.** Numerical Investigation on Knock Combustion in a Diesel–Dimethyl Ether Dual-Fuel Engine. *Energy & Fuels*, Vol. 33 n° 6, pp. 5710–5718, jun 2019. (cited in p. 120)
- Wang Zhe, Zhu Qilun and Prucka Robert.** A Review of Spark-Ignition Engine Air Charge Estimation Methods. In *SAE Technical Papers*, volume 2016-April, apr 2016. (cited in p. 70)
- Wang Zhi, Liu Hui and Reitz Rolf D.** Knocking combustion in spark-ignition engines. *Progress in Energy and Combustion Science*, Vol. 61, pp. 78–112, jul 2017. (cited in p. 61)
- Wärtsilä.** Wärtsilä 31SG, the world’s most efficient 4-stroke engine. <https://www.wartsila.com/insights/article/wartsila-31sg-the-worlds-most-efficient-4-stroke-engine>. Accessed 22 March 2022. (cited in p. 6)
- Weaver Christopher S and Turner Sean H.** Dual Fuel Natural Gas/Diesel Engines: Technology, Performance, and Emissions. In *SAE Technical Papers*, mar 1994. (cited in p. 30)
- Whitaker Jeanette, Ludley Katherine E., Rowe Rebecca, Taylor Gail and Howard David C.** Sources of variability in greenhouse gas and energy balances for biofuel production: A systematic review. *GCB Bioenergy*, Vol. 2 n° 3, pp. 99–112, jun 2010. (cited in p. 9)

- WHO.** World Health Organization (WHO), Coronavirus disease (COVID-19) pandemic. <https://www.who.int/emergencies/diseases/novel-coronavirus-2019>. Accessed 22 March 2022. (cited in p. 2)
- Wick Maximilian, Bedei Julian, Gordon David, Wouters Christian, Lehrheuer Bastian, Nuss Eugen, Andert Jakob and Koch Charles Robert.** In-cycle control for stabilization of homogeneous charge compression ignition combustion using direct water injection. *Applied Energy*, Vol. 240 n° January, pp. 1061–1074, apr 2019. (cited in p. 55)
- Widd Anders, Tunestål P. and Johansson R.** Physical modeling and control of homogeneous charge compression ignition (HCCI) engines. *IEEE Conference on Decision and Control*, pp. 5615–5620, 2008. (cited in p. 148)
- Willems Frank.** Is Cylinder Pressure-Based Control Required to Meet Future HD Legislation? *IFAC-PapersOnLine*, Vol. 51 n° 31, pp. 111–118, 2018. (cited in pp. 12, 34, 55, and 88)
- Willems Frank, Doosje Erik, Engels Frank and Seykens Xander.** Cylinder pressure-based control in heavy-duty EGR diesel engines using a virtual heat release and emission sensor. *SAE Technical Papers*, pp. 1–17, 2010. (cited in p. 148)
- Willems Frank, Kupper Frank, Ramesh Sudarshan, Indrajuaana Armando and Doosje Erik.** Coordinated Air-Fuel Path Control in a Diesel-E85 RCCI Engine. In *SAE Technical Paper*, pp. 1–11, apr 2019. (cited in pp. 36, 38, and 148)
- Wissink Martin, Wang Zhi, Splitter Derek, Shahlari Arsham and Reitz Rolf D.** Investigation of Pressure Oscillation Modes and Audible Noise in RCCI, HCCI, and CDC. In *SAE Technical Papers*, volume 2, apr 2013. (cited in pp. 62, 76, and 77)
- Wissink Martin L, Lim Jae Hyung, Splitter Derek A, Hanson Reed M. and Reitz Rolf D.** Investigation of Injection Strategies To Improve High Efficiency RCCI combustion with diesel and gasoline direct injection. *Asme Icef2012-92107*, pp. 1–12, 2012. (cited in p. 31)
- Worret R., Bernhardt S., Schwarz F. and Spicher U.** Application of Different Cylinder Pressure Based Knock Detection Methods in Spark Ignition Engines. In *SAE Technical Papers*, number 724, may 2002. (cited in p. 55)
- Woschni G.** A Universally Applicable Equation for the Instantaneous Heat Transfer Coefficient in the Internal Combustion Engine. *SAE Technical Paper*, 1967. (cited in p. 71)
- Wu Yifeng, Hanson Reed and Reitz Rolf D.** Investigation of Combustion Phasing Control Strategy During Reactivity Controlled Compression Ignition (RCCI) Multicylinder Engine Load Transitions. *Journal of Engineering for Gas Turbines and Power*, Vol. 136 n° 9, pp. 091511, 2014. (cited in p. 149)
- Wu Yifeng and Reitz Rolf D.** Effects of Exhaust Gas Recirculation and Boost Pressure on Reactivity Controlled Compression Ignition Engine at High Load Operating Conditions. *Journal of Energy Resources Technology*, Vol. 137 n° 3, pp. 032210, may 2015. (cited in p. 31)

- Wu Zhixin, Wang Michael, Zheng Jihu, Sun Xin, Zhao Mingnan and Wang Xue.** Life cycle greenhouse gas emission reduction potential of battery electric vehicle. *Journal of Cleaner Production*, Vol. 190, pp. 462–470, jul 2018. (cited in p. 8)
- Yang Fuyuan, Wang Jinli, Gao Guojing and Ouyang Minggao.** In-cycle diesel low temperature combustion control based on SOC detection. *Applied Energy*, Vol. 136, pp. 77–88, dec 2014. (cited in p. 12)
- Yang Tianhao, Yin Lianhao, Ingesson Gabriel, Tunestal Per, Johansson Rolf and Long Wuqiang.** Simultaneous control of soot emissions and pressure rise rate in gasoline PPC engine. In *1st Annual IEEE Conference on Control Technology and Applications, CCTA 2017*, volume 2017-Janua, pp. 572–577. IEEE, aug 2017. (cited in p. 76)
- Yang Z., Winward E. and Stobart R.K.** Improve Cylinder-to-Cylinder Consistency and Reduce Cycle-to-Cycle Variations of a Diesel Engine Using Closed-loop Control of Fuel Path Input Variables. *IFAC-PapersOnLine*, Vol. 49 n° 11, pp. 239–244, 2016. (cited in p. 12)
- Yao Mingfa, Zheng Zhaolei and Liu Haifeng.** Progress and recent trends in homogeneous charge compression ignition (HCCI) engines. *Progress in Energy and Combustion Science*, Vol. 35 n° 5, pp. 398–437, 2009. (cited in pp. 10, 30, and 77)
- Zhang Wenbin, Zhang Zhou, Ma Xiao, Awad Omar I., Li Yanfei, Shuai Shijin and Xu Hongming.** Impact of injector tip deposits on gasoline direct injection engine combustion, fuel economy and emissions. *Applied Energy*, Vol. 262 n° July 2019, pp. 114538, mar 2020. (cited in p. 158)
- Zhang Yahui and Shen Tielong.** Cylinder pressure based combustion phase optimization and control in spark-ignited engines. *Control Theory and Technology*, Vol. 15 n° 2, pp. 83–91, 2017. (cited in p. 107)
- Zhang Yahui, Shen Xun, Wu Yuhu and Shen Tielong.** On-board knock probability map learning-based spark advance control for combustion engines. *International Journal of Engine Research*, Vol. 20 n° 10, pp. 1073–1088, dec 2019. (cited in p. 120)
- Zhao H. and Ladommatos N.** Optical diagnostics for soot and temperature measurement in diesel engines. *Progress in Energy and Combustion Science*, Vol. 24 n° 3, pp. 221–255, jan 1998. (cited in p. 6)
- Zhen Xudong, Wang Yang, Xu Shuaiqing, Zhu Yongsheng, Tao Chengjun, Xu Tao and Song Mingzhi.** The engine knock analysis – An overview. *Applied Energy*, Vol. 92, pp. 628–636, apr 2012. (cited in pp. 62 and 77)
- Zheng Ming, Reader Graham T. and Hawley J.Gary.** Diesel engine exhaust gas recirculation—a review on advanced and novel concepts. *Energy Conversion and Management*, Vol. 45 n° 6, pp. 883–900, apr 2004. (cited in p. 7)
- Zurbruggen Florian, Hutter Richard and Onder Christopher.** Diesel-minimal combustion control of a natural gas-diesel engine. *Energies*, Vol. 9 n° 1, 2016. (cited in p. 107)